UNIVERSIDAD COMPLUTENSE DE MADRID

FACULTAD DE CIENCIAS QUÍMICAS

Departamento de Ciencia de los Materiales e Ingeniería Metalúrgica

TESIS DOCTORAL

Profundización en los mecanismos de corrosión de las aleaciones de magnesio: estrategias para mejorar la resistencia a la corrosión

MEMORIA PARA OPTAR AL GRADO DE DOCTOR

PRESENTADA POR

Alejandro Samaniego Miracle

Director

Sebastián Feliu Batlle

Madrid, 2014

UNIVERSIDAD COMPLUTENSE DE MADRID

FACULTAD DE CIENCIAS QUÍMICAS

DEPT. CIENCIA DE LOS MATERIALES E INGENIERÍA METALÚRGICA

Profundización en los Mecanismos de Corrosión de las Aleaciones de Magnesio. Estrategias para Mejorar la Resistencia a la Corrosión.

Tesis Doctoral

ALEJANDRO SAMANIEGO MIRACLE

DIRECTOR

DR. SEBASTIÁN FELIU BATLLE (CENIM-CSIC)

TUTOR

DR. RAÚL ARRABAL DURÁN (UCM)

CSIC
CONSEJO SUPERIOR DE INVESTIGACIONES CIENTÍFICAS

CENIM
Centro Nacional de Investigaciones Metalúrgicas

MINISTERIO DE ECONOMÍA Y COMPETITIVIDAD

A mis padres que día a día hacen todo lo posible para que pueda lograr mis sueños. Gracias por haberme apoyado en todo momento, por vuestros consejos, valores y por la motivación constante que me aportáis en todo lo que hago.

A mi hermano, por ser un ejemplo del cual aprendo cada día.

A mi novia María, gracias por tu paciencia y comprensión. Gracias por sacrificar tu tiempo para que yo pueda cumplir con el mío. Esta tesis lleva mucho de ti, gracias por estar a mi lado.

En primer lugar, me gustaría dar las gracias a todas las personas que trabajan en el CENIM por su acogida y apoyo. Con vosotros estos últimos cuatro años han pasado volando, y eso solo ha sido posible gracias a vuestro trato. Me gustaría extender este agradecimiento de forma especial a los miembros del departamento de Ingeniería de Superficies, Corrosión, y Durabilidad con los que he tenido la posibilidad de compartir mí día a día durante la realización de esta tesis.

Asimismo, quisiera expresar mi enorme gratitud a mi director de tesis, el Dr. Sebastián Feliu Batlle, por su paciencia, enseñanzas y apoyo constante en el desarrollo de la tesis, así como por anteponer mi desarrollo y aprendizaje frente a su propio beneficio personal. ¡Gracias Sebastián por sacar lo mejor de mí, tanto en el ámbito profesional como en el personal! No quisiera olvidarme de su padre, el Dr. Sebastián Feliu Matas, quien con su experiencia y paciencia, ha sabido transmitirme muchos conocimientos y más ilusión. También, me gustaría dar las gracias al Dr. Raúl Arrabal, por su ayuda durante la tesis y por hacerme saber que siempre podía acudir a él cuando lo necesitara.

No podría haberlo hecho sin la financiación aportada por el Ministerio de Economía y Competitividad a través del proyecto MAT 2009-13530 y la gestión realizada por el CSIC durante mi tesis y mis estancias en el extranjero. En especial, me gustaría agradecer la gestión realizada por Isabel Ocaña.

Quisiera hacer una mención especial a mis compañeros del CENIM; Amir, Violeta, Juan Carlos, Blanca, Rodrigo, Emilio, Santi, Belén, Cristina, Lucía, María Lorenza, María, Laura, Dani, Irene, Oscar, Iván, Heydis, Diana, Blanca, Joaquín, Teresa, Ana, David, Manuel, Fede y Mónica. ¡¡Gracias!! ¡¡Compartir este tiempo con vosotros ha sido sensacional!!

A mis compañeros de máster y del CENIM, Alberto y Sara, y a Chus, Víctor, Nacho, Miliki, Antonio, Iñaki y Alfonso por su ayuda y apoyo durante la experimentación.

Toda mi gratitud por el tiempo y el buen trato recibido durante mis estancias en el extranjero al Dr. Nick Birbilis (Monash University) y al Dr. Gerald Frankel (Fontana Corrosion Center, OSU), así como a todos aquellos que han amenizado mi experiencia en esos países. Kateryna, Xiao-Bo, Rajeev, Nazatul, Jermain, Nico, Ben, Will, Sara y Dan. Thanks to all folks!! Was great sharing some time with you!!

Finalmente, quiero expresar mi agradecimiento de forma muy especial a mis padres, a mi hermano, a mi novia María y a mis abuelos; los que están y los que se han ido. Gracias por vuestro cariño, comprensión y apoyo incondicional en todo momento. Sin vosotros, no lo hubiera conseguido.

Contenido

Esta Memoria se ha editado siguiendo el formato de compilación de artículos científicos ya publicados, según la reglamentación de la Universidad Complutense de Madrid (www.ucm.es). Los artículos científicos se han insertado en la memoria en formato Word, manteniendo el texto, organización, numeraciones y bibliografía en el idioma original de las publicaciones. Junto con estos artículos ya publicados se han insertado como trabajo adicional tres artículos que actualmente se encuentran en revisión y todavía no han sido publicados. El resto de la memoria se ha redactado en castellano de acuerdo a la normativa oficial. Asimismo, se ha optado por enumerar de forma independiente la bibliografía general de esta memoria de aquella incluida en los artículos publicados, a fin de poder facilitar la lectura.

Summary

Magnesium (Mg) alloys posses a combination of low density, high specific strength and good castability, which makes them promising lightweight structural materials. However, since magnesium is one of the most chemically active metals, its corrosion resistance is one of the key points that limit its use in real conditions.

This thesis is divided into three chapters. The first focuses on the corrosion mechanism of pure magnesium and the negative difference effect (NDE). The second is formed by an in-depth study of the native oxide surface films and the corrosion products layers formed on the AZ31 and AZ61 magnesium alloys, along with their influence on corrosion. The third chapter comprises several studies where different strategies to reduce the corrosion rate of magnesium and its alloys were analyzed.

Chapter I: Corrosion Mechanisms of Magnesium and the Negative Difference Effect (NDE).

Despite the large number of papers published on the corrosion mechanisms of magnesium and its alloys, there are still some issues that have not been sufficiently clarified. Magnesium experiences what in literature is called negative difference effect (NDE). This effect is characterized by an increase in the amount of hydrogen generated at anodic polarization; which is contradictory to the expected behaviour based on the classic electrochemical theory. The NDE phenomenon should be totally understood in order to fully assess the utilities of Mg as an electrode or as a structural material, the latter related to corrosion.

Several mechanisms for the source of superfluous hydrogen evolution (HE) have been discussed. So far, the mechanism suggesting the presence of monovalent magnesium (Mg^+) stands out as being responsible for the additional hydrogen evolution. Although the existence of Mg^+ was supposedly demonstrated in 1953 by Roy Petty, this intermediate could not be directly detected by any analytical technique, and its existence has not yet been confirmed. For this reason, recent publications suggested that Mg^+ is not responsible for NDE. In order to clarify this effect, several experiments were performed which suggested it is impossible to proving the existence of Mg^+ by the experiments proposed by Petty in 1953. An alternative mechanism based on the

variation of the exchange current density during polarization of magnesium was proposed to explain the so-called NDE. Lastly, additional studies were performed by adding noble (Fe) and active elements (Li and Ca) to pure magnesium, where this theory could be valid.

To summarize, it must be concluded that the existence of Mg^+ was not established by Petty et al in 1953. Therefore the mechanisms involving Mg^+ to explain NDE is highly improbable. An alternative mechanism was proposed to explain this effect which was supported by the latter experiments.

Chapter II: Characterization of the native oxide surface film and corrosion products layers of AZ31 and AZ61 alloys.

-Characterization of the native oxide surface films: The corrosion mechanisms of AZ31 and AZ61 alloys were also studied because of their great scientific and technological interest produced over the last two decades. A clear influence of the surface condition and the aluminium concentration of the alloys on the outermost oxide layers of the alloys was observed. It was found that a mechanical polishing of AZ61 tends to form a surface oxide film, that is more protective than that formed on AZ31 or on the samples in 'as received' conditions. This higher protection was associated to the higher amount of aluminium present in the AZ61 alloy, which stabilized the pre-existing native oxide film formed on the polished surface of this alloy.

- Corrosion products layer of AZ31 and AZ61 magnesium alloys: here, we studied the protective effect of the corrosion products formed during immersion in NaCl solutions. We observed a higher concentration of carbonate content in the corrosion product layers formed on the AZ31 alloy, than on those formed on AZ61. This enrichment was associated with the increase of the corrosion resistance with the immersion time observed on the alloy AZ31 which was not detected on AZ61. This different behaviour was associated to the presence of β phase in the AZ61 alloy, which resulted in the formation of micro-galvanic couples that caused a localized increase of pH, favouring the formation of magnesium hydroxide species as regards to the formation of carbonates.

Chapter III: Strategies to reduce the corrosion rate of magnesium and its alloys.

- Heat treatments at low temperatures: in order to increase the protective effect of the surface films spontaneously formed on the alloys AZ31 and AZ61, heat treatment at moderate temperatures and times (200 ° C, 5-60 min) were performed in both surface conditions (polished and 'as received' conditions). These studies highlighted the following results:

On polished surfaces, aluminium enrichment was observed on the surface of the AZ61 alloy, which was related to the increase of the corrosion resistance observed on this alloy. This effect was less notable in the AZ31 magnesium alloy with lower aluminium content.

In 'as received' conditions, heat treatments provoked an adverse effect on the corrosion resistant of alloy AZ31 where an enrichment of surface precipitates (Al_2O_3 and ZnO) was detected. This enrichment was not detected on AZ61 and no significant changes on the corrosion resistance of the alloy were observed after heat treatments.

The differences observed by comparing the two surface conditions were associated to the different nature of the surface layers formed in each of the studied surface states.

- Protective surface oxides on AZ31 via lutetium additions: here, we attempted to modify the surface oxides formed on AZ31 alloy by adding low content alloying elements (<1%) with higher oxygen affinity than magnesium. The elements added individually on the alloys were Lu, Y, Sc, Ca and Nd. However, at present, only the data of Lu additions has been fully prepared. This study concluded that low-level Lu additions to AZ31 did not lead to the replacement of magnesium in the developed surface oxide/hydroxide. Nonetheless, a beneficial effect reducing the corrosion rate of the as-cast alloy, up to 80%, was observed in 0.1% NaCl solutions. It was also observed that Lu combined with Al and Mn and formed Al-Mn-Lu particles (~2 μm in diameter) without significantly changing the cathodic activity of these particles relative to the magnesium matrix. Lastly it was concluded that heat treatment (400ºC) for up to 300 minutes had a negative impact on the corrosion. of as cast AZ31 with low-level additions of Lu

- $NaHCO_3$ surface conversion treatments on AZ31 and AZ61 alloys: in order to maximize the protective effect of carbonates formed on the surface of these alloys, surface conversion treatments were performed using a saturated sodium bicarbonate solution. A beneficial effect on the treatment was observed on AZ61 when samples were treated during 10 and 60 minutes in the conversion bath. This effect was associated to a strong enrichment of aluminium hydroxide detected on the surface of the samples, combined with the absence of cracks in the conversion film formed during these times of immersion. No beneficial effect was observed on AZ31 or on AZ61 at other immersion times.

- Adding arsenic to pure magnesium: Finally, we attempted to reduce the corrosion rate of pure magnesium by adding small amounts of arsenic. In previous studies about inhibitors, it was observed that arsenate anions (AsO_4^{3-}) slowed the recombination of the hydrogen formed in the cathode reaction and reduced corrosion. Using these findings as a starting point, an alloy with 0.37 wt. % of arsenic (As) was produced. Cathodic kinetics significantly decreased which was associated with the presence of arsenic in the alloy. Corrosion rate decreased ~ 400% and the morphology of corrosion changed when samples were exposed to 0.1 M NaCl solutions.

Resumen

El magnesio y sus aleaciones presentan una combinación de baja densidad, alta resistencia específica y buena moldeabilidad, que los convierte en prometedores materiales estructurales. Sin embargo, dado que el magnesio es uno de los metales químicamente más activos, su resistencia frente a la corrosión es uno de los puntos clave que limitan su utilización en condiciones reales de servicio.

Esta tesis se ha dividido en tres capítulos bien diferenciados. El primero de ellos se centra en el mecanismo de corrosión del magnesio puro y el efecto diferencial negativo (NDE). En el segundo capítulo se presenta un profundo estudio sobre las películas de óxidos superficiales espontáneamente formadas sobre las aleaciones AZ31 y AZ61, junto con un análisis de sus productos de corrosión y su influencia sobre la corrosión. El tercer capítulo está formado por varios estudios donde se analizan diferentes estrategias para disminuir la velocidad de corrosión del magnesio y sus aleaciones.

Capítulo I: Profundización en los Mecanismos de Corrosión del Magnesio y el Efecto Diferencial Negativo (NDE).

A pesar de la gran cantidad de trabajos publicados sobre los mecanismos de corrosión del magnesio y sus aleaciones, todavía existen aspectos que no han sido suficientemente clarificados. El magnesio experimenta lo que en la literatura se ha denominado "negative difference effect" (NDE) o en castellano "efecto diferencial negativo". Este efecto se caracteriza por un aumento de la cantidad de hidrógeno generado al polarizar anódicamente, lo cual es contradictorio al comportamiento esperable según la teoría electroquímica clásica. Para poder evaluar de forma completa el uso de magnesio como electrodo o como material estructural, es necesario comprender el efecto diferencial negativo en profundidad, ya que está relacionado con el mecanismo de corrosión de este metal.

Con el fin de explicar el efecto diferencial negativo se han propuesto multitud de teorías y mecanismos. Hasta el momento, destaca el mecanismo que sugiere la presencia de un intermedio de reacción con menor estado de oxidación al habitual (Mg^{+}), como

responsable de la generación adicional de hidrógeno. Pese a que la existencia de Mg^+ fue supuestamente demostrada en 1953 por Roy Petty, este intermedio no se ha podido detectar de forma directa mediante ninguna técnica analítica, y su existencia no ha podido ser corroborada. Por esta razón, publicaciones recientes sugieren que el Mg^+ no es el responsable del NDE. Con el fin de aumentar la comprensión de este efecto, se realizó un estudio donde se demostró la imposibilidad de demostrar la existencia de Mg^+ mediante los experimentos propuestos por Petty en 1953. Posteriormente, se propuso un mecanismo alternativo para explicar el denominado NDE, basado en la variación de la corriente de intercambio de la reacción de hidrógeno al polarizar el magnesio. Por último, se realizaron estudios adicionando elementos más activos (Li y Ca) y más nobles (Fe) sobre magnesio puro, donde se pudo comprobar el ajuste de los datos obtenidos con la teoría previamente propuesta.

En resumen, se pudo concluir que la existencia de magnesio monovalente no pudo ser demostrada por Petty y colaboradores en 1953. Por lo tanto el mecanismo que involucra esta especie como responsable del NDE es altamente improbable. Se propuso un mecanismo alternativo para explicar este efecto que pudo ser corroborado en estudios posteriores.

Capítulo II: Caracterización de la película de óxidos superficiales y de la capa de productos de corrosión de las aleaciones AZ31 y AZ61.

- Influencia de los óxidos superficiales sobre la corrosión de las aleaciones AZ31 y AZ61: Se escogieron las aleaciones del sistema Mg-Al-Zn como materiales de estudio por el creciente interés científico y tecnológico que han despertado durante las dos últimas décadas. Se observó una clara influencia del estado superficial y de la concentración de aluminio en la aleación sobre los óxidos formados en las capas más externas. Se encontró que el pulido mecánico de las muestras de la aleación con un mayor contenido en aluminio, tiende a formar una película de óxidos sobre la superficie cuyo efecto protector es muy superior al formado cuando el contenido de aluminio en la aleación es inferior, o al formado en las muestras en estado de recepción.

- Influencia de los productos de corrosión sobre la corrosión de las aleaciones AZ31 y AZ61: se realizó un estudio sobre el efecto protector de los productos de corrosión formados durante la inmersión de estas dos aleaciones en soluciones de cloruro sódico, En comparación con la aleación AZ61, Se observó un incremento importante en la concentración de carbonatos en los productos de corrosión formados sobre la aleación

AZ31. Asociado con el enriquecimiento en carbonatos en la capa superficial de productos de corrosión, se detectó un aumento en la resistencia a la corrosión con el tiempo de inmersión, que no tuvo lugar al estudiar la aleación AZ61. La presencia de fase β en la aleación AZ61, originó la formación de micro-pares galvánicos que provocaron un aumento del pH localizado, favoreciendo la formación de especies ricas en hidróxido de magnesio, respecto a la formación de carbonatos.

Capítulo III: Estrategias para reducir la velocidad de corrosión del magnesio y sus aleaciones.

- Tratamientos térmicos a bajas temperaturas: Para intentar aumentar el efecto protector de estas películas superficiales formadas espontáneamente sobre las aleaciones de trabajo, se realizó un tratamiento térmico a temperaturas moderadas y tiempos cortos (200ºC, 5-60 minutos), en ambas condiciones superficiales (pulido y estado de recepción). De estos estudios destacaron los siguientes resultados:

En estado pulido, se observó un enriquecimiento superficial en el contenido de aluminio, con un notable efecto positivo en la resistencia a la corrosión de la aleación con alto contenido en aluminio, AZ61, cuyo efecto fue muy inferior en la aleación AZ31.

En estado de recepción, se observó un efecto negativo del tratamiento térmico sobre la aleación AZ31, donde se detectó un enriquecimiento superficial importante en el contenido de precipitados de óxidos de aluminio y de zinc. En contraste, en la aleación AZ61 no se observaron cambios significativos con el tratamiento.

Las diferencias observadas comparando las dos condiciones superficiales fueron asociadas a la diferente naturaleza de las capas superficiales formadas en cada uno de los dos estados superficiales estudiados.

- Microadiciones de lutecio en AZ31: Así mismo, se intentaron modificar los óxidos superficiales formados sobre la aleación AZ31 mediante la adición de bajos contenidos (< 1%) de elementos aleantes con mayor afinidad por el oxígeno que el magnesio. Los elementos, añadidos de manera individual sobre la aleación fueron el Lu, Y, Sc, Ca y Nd. Sin embargo, por el momento solo han sido publicados los datos sobre la adición de

Lu, donde se concluyó que un 0.21% en peso de este elemento, no es una cantidad suficiente para sustituir el Mg en el óxido superficial. Pese a todo, en soluciones de NaCl al 0.1%, se observó un efecto beneficioso sobre la velocidad de corrosión de la aleación de colada, al reducirla hasta en un 80%. Se observó que el lutecio se combina con aluminio y manganeso formando partículas Al-Mn-Lu sin alterar la actividad catódica de estas partículas respecto a la matriz. Por último se concluyo que tratamientos térmicos a 400ºC durante tiempos de hasta 300 minutos, tuvieron un impacto negativo en la velocidad de corrosión de la aleación AZ31-0.21%Lu.

-Tratamiento de conversión superficial sobre aleaciones AZ31 y AZ61: Intentando aprovechar el efecto protector de los carbonatos formados en la superficie de estas aleaciones, se realizó un tratamiento de conversión superficial, utilizando una solución de bicarbonato sódico saturado. Se observó un efecto beneficioso del tratamiento al mantener las muestras de AZ61 durante 10 y 60 minutos en el baño de conversión, debido a la aparición de un fuerte enriquecimiento en el contenido de hidróxidos de aluminio sobre la superficie, combinada con la ausencia de grietas presentes en la película de conversión formada. No se observó un efecto beneficioso al aplicar este tratamiento sobre la aleación AZ31 o sobre la aleación AZ61 para otros tiempos de inmersión inversión en el baño de conversión.

- Adición de arsénico sobre magnesio: Por último, se intentó reducir la velocidad de corrosión de magnesio puro mediante la adición de pequeñas cantidades de arsénico. En estudios previos sobre inhibidores, se observó que aniones arseniato (AsO_4^{3-}) fueron capaces de ralentizar la recombinación del hidrógeno formado en la reacción catódica y disminuir la corrosión. Utilizando estas observaciones como punto de partida, se produjo una aleación con un 0.37 % en peso de arsénico (As), detectando una disminución muy significativa de la reacción catódica, asociada a la presencia de arsénico, que originó una disminución de más de un 400% en la velocidad de corrosión de la aleación en soluciones de NaCl 0.1 M.

Introducción

El Magnesio es un elemento metálico alcalinotérreo que por sus propiedades y abundancia presenta un enorme potencial como material estructural [1, 2]. Aunque su uso ha sufrido altibajos a lo largo de la historia, en los últimos años ha experimentado un importante auge, convirtiéndose en el tercer elemento metálico estructural más utilizado, solo superado por el aluminio y el hierro (acero) [3].

Entre sus propiedades destaca su gran ligereza (ρ =1,7 g/cm^3, de la del aluminio o de la del hierro), que combinada con sus propiedades mecánicas convierten al magnesio en uno de los materiales metálicos con mayor resistencia específica. Otras características atractivas de este metal son su media/alta conductividad térmica y eléctrica, su no-toxicidad, su comportamiento no magnético o su capacidad de ser mecanizado por métodos convencionales. Su estructura cristalina es hexagonal compacta (hcp), lo que condiciona sus propiedades mecánicas. Entre sus mayores inconvenientes como material estructural, destacan su baja resistencia a la corrosión y su limitada resistencia mecánica, además del riesgo de explosión durante la fundición y el mecanizado, debido a su elevada reactividad. Las principales propiedades del magnesio metálico se ilustran en la Tabla 1-1.

En cuanto a su disponibilidad, el magnesio es el cuarto elemento más abundante de la tierra [4], siendo el octavo elemento en abundancia de la corteza terrestre (2.2%) y el tercero en el agua del mar (representa el 0.13 % del agua del mar, lo que equivale a 1.3 kg/m^3), por lo que es prácticamente inagotable [5]. En la corteza terrestre, se encuentra en minerales como la dolomita ($MgCO_3$ $CaCO_3$), la magnesita ($MgCO_3$) o la brucita ($Mg(OH)_2$, siendo el más abundante la dolomita.

El magnesio fue reconocido como elemento químico en 1755 por el inglés Joseph Black; sin embargo, no fue aislado hasta 1808 cuando Humpry Davy, mediante el uso de la electrolisis en pila de Volta sobre un mezcla pastosa de magnesia y sulfuro de mercurio, consiguió aislar este elemento metálico [5, 6].

Tabla 1-1. *Propiedades generales del magnesio puro [1].*

Radio atómico	150 pm
Densidad (25ºC)	1,738 gcm-3
Módulo de Young	45 GPa
Tensión de rotura	80-180 MPa
Deformación a rotura	1-12%
Resistencia a tracción (extruido)	165-205 MPa
Resistencia a tracción (laminado)	180-220 MPa
Conductividad eléctrica específica a temperatura ambiente	22,4 mΩ-1mm-2
Potencial normal de reducción	-2,37 V_{SHE}
Temperatura de fusión	650 ºC
Temperatura de ebullición	1090 ºC
Presión de vapor (a 20 ºC)	189 kPa
Calor de fusión	195 kJkg-1
Capacidad específica térmica	1,05 kJkg-1K-1
Coeficiente de expansión lineal	26x10-6 K-1
Contracción (durante el cambio de estado líquido-sólido)	4,20%
Contracción (durante el enfriamiento en estado sólido)	5%

El proceso productivo fue mejorando y así, veinte años más tarde, en 1828, el químico francés Antoine Bussy logró obtener el metal con mayor pureza al reducir cloruro de magnesio en forma anhidra con potasio. Dos años más tarde Liebig, aprovechando los resultados de Bussy, consiguió aislar varios gramos de magnesio puro y determinar algunas de sus propiedades. Sin embargo, su producción a escala industrial no se produjo hasta 1862, por el método de Saint–Claire Deville, basado en la extracción de magnesio a partir del $MgCl_2$ descrita por el científico alemán Robert Bunsen en 1852 [5, 6].

La obtención industrial de magnesio a mayor escala comenzó en Alemania en 1886 con una producción de tan solo 10 toneladas/año a nivel mundial, que en 1915 se vio incrementada a 350 toneladas/año. Posteriormente, debido a la I Guerra Mundial, la producción anual se incrementó de manera abrupta alcanzando las 3000 toneladas/año. Sin embargo, al término de la guerra volvió a caer hasta las 350 toneladas/año. Años más tarde, debido a la influencia de la II Guerra Mundial la producción volvió a crecer

alcanzando las 320000 toneladas/año, diez veces más que antes de iniciarse el conflicto. Tras la II Guerra Mundial la producción de magnesio cayó drásticamente. Sin embargo, desde la década de 1950 su consumo y aplicación han estado creciendo a un ritmo lento pero constante. En los últimos años, los aspectos medioambientales han ganando importancia, lo que ha provocado un aumento en el uso y desarrollo de aleaciones de magnesio como material estructural, ya que su uso en aeronáutica y automoción pueden rebajar de manera significativa las emisiones de gases contaminantes. Así por ejemplo, mediante el uso de estas aleaciones en diferentes componentes de automóviles como llantas, cajas de cambios, estructuras de asientos o embragues se puede reducir el consumo de combustible de manera muy significativa lo cual aumenta la eficiencia del transporte y reduce las emisiones. Se ha calculado que por cada 10 kg de acero sustituidos por 4 kg de magnesio, hay una reducción de 100 kg de gases emitidos a lo largo de la vida del vehículo [7]. Además se puede reciclar más del 50% de la aleación primaria consumiendo únicamente un 3% de la energía que utilizada durante su producción por electrolisis [6]. Por esta razón la producción mundial de magnesio ha pasado de 284.000 t en el año 2000 a 808.000 t en 2008, siendo la producción anual en el año 2013 de 910.000 t [8-10]. La demanda ha aumentado de manera constante en estos últimos años aunque ha sufrido un pequeño descenso en el año 2009 debido a la crisis mundial vivida [11]. En la actualidad más de un 35% del magnesio producido se destina a aleaciones con fines estructurales.

Actualmente, los países con mayores reservas de minerales de magnesio son China, Corea, Rusia y Australia, mientras que los principales productores son Estados Unidos, China, Turquía, Rusia y Canadá [12]. El magnesio se extrae principalmente por distintos métodos basados en dos procedimientos generales: la electrólisis ígnea de $MgCl_2$ anhidro fundido (representa el 80% del Mg producido) y la reducción térmica de MgO. Con respecto a la extracción por electrólisis ígnea, se pueden distinguir la electrólisis del MgO disuelto en fluoruro y el método de electrólisis de $MgCl_2$ fundido que a su vez puede clasificarse en función del procedimiento para obtener el $MgCl_2$. En cuanto a los procesos de reducción térmica, pueden clasificarse en función de la naturaleza del reductor utilizado (reducción por carbono, por silicio y por CaC_2). La Figura 1.1 muestra un esquema de los diferentes método de producción [5]. En cualquier caso, todos los procesos de extracción de magnesio son altamente energéticos.

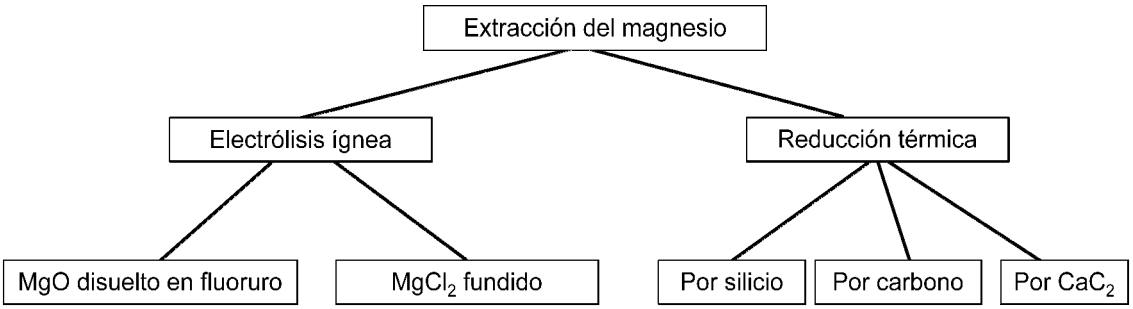

Figura 1.1. *Métodos de producción de magnesio [5].*

Respecto al procesado, las aleaciones de Mg se pueden procesar tanto por moldeo como por forja (Figura 1.1). Sin embargo, el magnesio tiene excelentes propiedades de moldeo y presenta limitaciones a la deformación plástica, debido a su estructura hexagonal compacta. Aunque las aleaciones de magnesio forjadas pueden presentar ventajas frente a las aleaciones de moldeo, tales como una menor porosidad y/o mejores propiedades mecánicas [6, 13], en la actualidad el 98% de los componentes estructurales de magnesio son fabricados por diferentes procesos de moldeo [3]. El mayor coste de las aleaciones de forja frente al de las aleaciones de moldeo, junto con la evolución de los procesos de moldeo que permiten minimizar problemas asociados a esta técnica, han relevado el procesado por forja a un porcentaje de fabricación muy inferior.

Los diferentes tipos de procesado por forja o moldeo pueden observarse en la figura 1.2 [3].

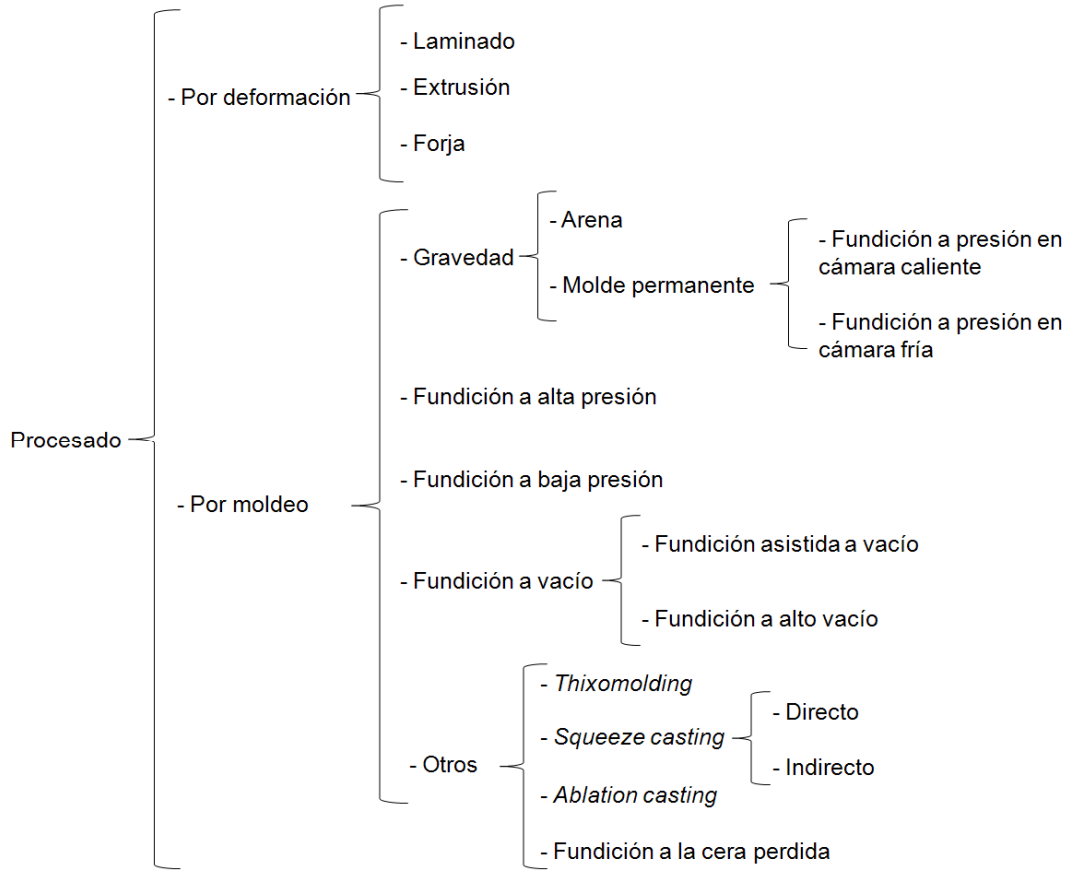

Figura 1.2. *Tipos de procesado de magnesio [3].*

Propiedades mecánicas

Desde el punto de vista mecánico, el magnesio presenta limitaciones significativas debidas a su estructura cristalina hexagonal compacta (hcp). El magnesio exhibe una baja tenacidad y ductilidad a temperatura ambiente, así como una limitada resistencia a la fluencia. Su relación c/a es de 1,624, por debajo de la ideal 1,633, lo que dificulta el deslizamiento en el plano dominante basal (0001)<11$\bar{2}$0> [14]. Además, para el deslizamiento basal, el número total de sistemas de deslizamiento es tres y ninguno de ellos es capaz de contribuir a la deformación plástica en la dirección normal al plano basal (Figura 1.3) [14]. Por lo tanto, el magnesio no puede satisfacer la condición de Von Mises o Taylor de deformación homogénea con la única activación del deslizamiento basal, lo que explica su baja ductilidad a temperatura ambiente. Además,

la limitación en los modos de deformación en el magnesio da lugar a una fuerte respuesta anisótropa, fuertemente relacionado con su textura.

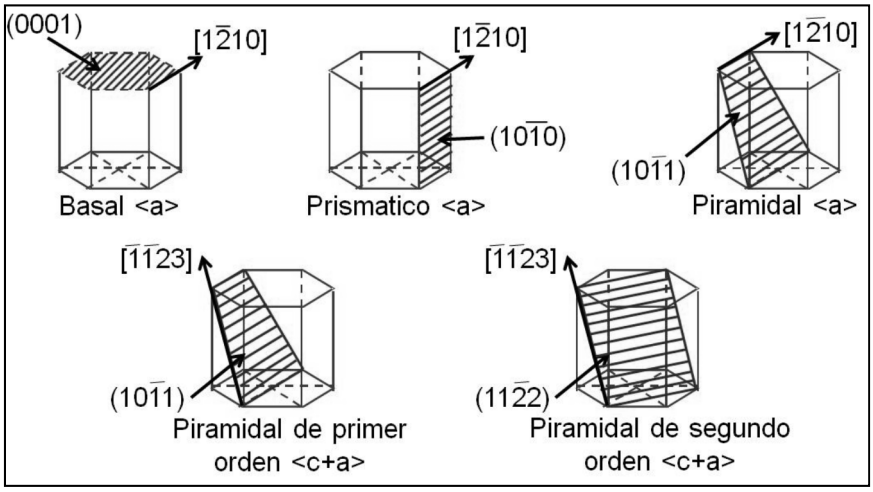

Figura 1.3. *Estructura cristalina y sistemas de deslizamiento en el magnesio puro [15].*

Los parámetros de red del magnesio puro aumentan con el aumento de la temperatura, favoreciendo su conformación en caliente. A alta temperatura, la activación del deslizamiento piramidal <c+a> y otros deslizamientos no basales, así como la activación de procesos de deslizamiento de fronteras de grano y la recristalización dinámica, producen una menor cizalladura crítica resuelta (CRSS), aumentando la ductilidad y disminuyendo la resistencia mecánica con la temperatura [14]. Como consecuencia, el magnesio presenta una baja resistencia mecánica a alta temperatura y problemas de fluencia.

Utilización del magnesio.

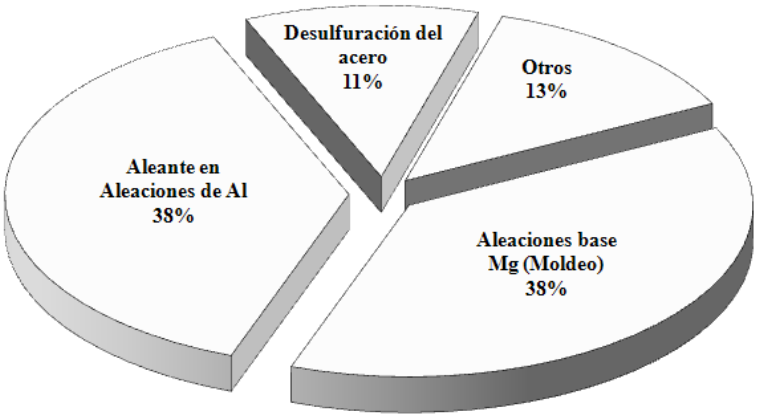

Figura 1.4. *Uso del magnesio primario producido en 2011 [16].*

De todo el magnesio primario producido anualmente, en 2011, aproximadamente un 38% fue utilizado tanto como elemento de aleación para las aleaciones de aluminio, como para la producción de aleación de moldeo base magnesio (Figura 1.4) [16]. En torno a un 11 % se utilizó en la desulfuración del acero, aunque su porcentaje de uso podría disminuir al ser sustituido por carburo de calcio [8]. Del 13% restante producido, alrededor de un 4% se utilizó en la en la producción de titanio por el proceso Kroll, aunque se espera que su uso en este sentido aumente, ya que el titanio es usado cada vez más en la industria aeroespacial. También se utiliza en la producción de aleaciones por forja y en otras aplicaciones como ánodos de sacrificio, bombas incendiarias o fuegos artificiales. En la actualidad el uso del magnesio como material estructural se ha incrementado, convirtiendo al magnesio y sus aleaciones en el tercer elemento metálico estructuras por detrás del aluminio y el hierro [3].

Aplicaciones estructurales

El magnesio ha sido utilizado en la industria del automóvil desde hace más de 90 años. En 1921, Dow Chemical produjo el primer pistón de magnesio para el modelo “indi 500” [17], sin embargo su uso no se extendió demasiado por problemas de conformado y de corrosión. En 1971, su aplicación en automóviles experimentó un fuerte aumento gracias al uso de aleaciones de magnesio en los motores refrigerados por aire y las cajas de cambios utilizadas en el modelo “escarabajo” de Volkswagen [18]. Gracias a la búsqueda de materiales ligeros para mejorar el rendimiento y reducir las emisiones de

gases de efecto invernadero, en la actualidad se utilizan aleaciones de magnesio en cantidad de componentes tanto en el interior, como en el chasis o en los sistemas de potencia. Así por ejemplo, las aleaciones de magnesio se utilizan en estructura de asientos, estructuras de radios, bastidores de suelo, tapa de llenado de combustible, llantas, brazos de pedal de freno o cajas de transmisión, entre otros [3].

Pese a todos los posibles beneficios aportados por el magnesio como material estructural en aviones, en la actualidad, el magnesio no es utilizado como material estructural por grandes compañías como Boeing o Airbus debido a restricciones legislativas relacionadas con su relativa baja temperatura de inflamación. Afortunadamente, estas consideraciones están siendo revisadas en la actualidad y posiblemente el uso del magnesio en aviones comerciales quede menos restringido en el futuro [3, 19]. Pese a todo, las aleaciones de magnesio tienen grandes aplicaciones en helicópteros donde es posible encontrarlo formando cajas de cambios u otros componentes no estructurales [20].

Las aleaciones de magnesio también se utilizan en material deportivo o en la industria electrónica, donde forman las estructuras de las cámaras de video, ordenadores, teléfonos móviles, radares y multitud de componentes más [21]. Por otro lado, la industria de la herramienta eléctrica depende cada vez más de componentes de magnesio de fundición para ofrecer diseños más ligeros y duraderos que son más fáciles de manejar [22].

Comportamiento a la corrosión del magnesio y sus aleaciones

En la actualidad la utilización de las aleaciones de Mg como material estructural está limitada debido a la rápida corrosión que sufren como consecuencia de la alta reactividad de este metal [23-25]. Esta reactividad se ve reflejada en su bajo potencial estándar de reducción, –2,38 V con respecto al electrodo del hidrogeno (V_{SHE}) [25]; uno de los más bajos de todos los metales de ingeniería (Tabla 1.2).

Teniendo en cuenta la serie de potenciales de reducción estándar, el magnesio presenta un comportamiento anódico respecto a la mayoría de los metales y aleaciones. Esta cualidad puede aprovecharse para utilizarlo como ánodo de sacrificio [26]; sin embargo,

en aplicaciones estructurales es un problema que debe reducirse al máximo, por lo que se están realizando grandes esfuerzos de investigación.

Tabla 1.2. *Serie electroquímica de los elementos más representativos.*

Media reacción	E^o (V_{SHE})
$Li^+(aq) + e^- \rightarrow Li(s)$	−3,05
$Na^+(aq) + e^- \rightarrow Na(s)$	−2,71
$Mg^{2+}(aq) + 2e^- \rightarrow Mg(s)$	−2,38
$Be^{2+}(aq) + 2e^- \rightarrow Be(s)$	−1,85
$Al^{3+}(aq) + 3e^- \rightarrow Al(s)$	−1,68
$Ti^{2+}(aq) + 2e^- \rightarrow Ti(s)$	−1,63
$Ti^{3+}(aq) + 3e^- \rightarrow Ti(s)$	−1,21
$Mn^{2+}(aq) + 2e^- \rightarrow Mn(s)$	−1,18
$Zn^{2+}(aq) + 2e^- \rightarrow Zn(s)$	−0,76
$Cr^{3+}(aq) + 3e^- \rightarrow Cr(s)$	−0,74
$Fe^{2+}(aq) + 2e^- \rightarrow Fe(s)$	−0,44
$Ni^{2+}(aq) + 2e^- \rightarrow Ni(s)$	−0,25
$Ag^+(aq) + e^- \rightarrow Ag(s)$	0,8
$Hg^{2+}(aq) + 2e^- \rightarrow Hg(l)$	0,85
$Au^{3+}(aq) + 3e^- \rightarrow Au(s)$	1,52
$Au^+(aq) + e^- \rightarrow Au(s)$	1,83

Pese a que su potencial estándar de reducción es -2,38 V_{SHE}, en soluciones acuosas su potencial de corrosión se encuentra alrededor de –1,5 V_{SHE} [25]. Esto se asocia a la formación en la superficie de capas parcialmente protectoras de una mezcla de MgO e $Mg(OH)_2$ que eleva el potencial a valores menos negativos. La estructura de estas capas se ha descrito como una mono capa de una mezcla de $MgO/Mg(OH)_2$ [27, 28], una monocapa de $MgO_x(OH)_y$ nH_2O [29] o una bicapa formada por una capa interna de MgO y una capa externa de $Mg(OH)_2$ [30]. Respecto a su composición, se ha propuesto que inicialmente se forma una película de MgO que posteriormente se hidrata formando $Mg(OH)_2$ [31, 32].

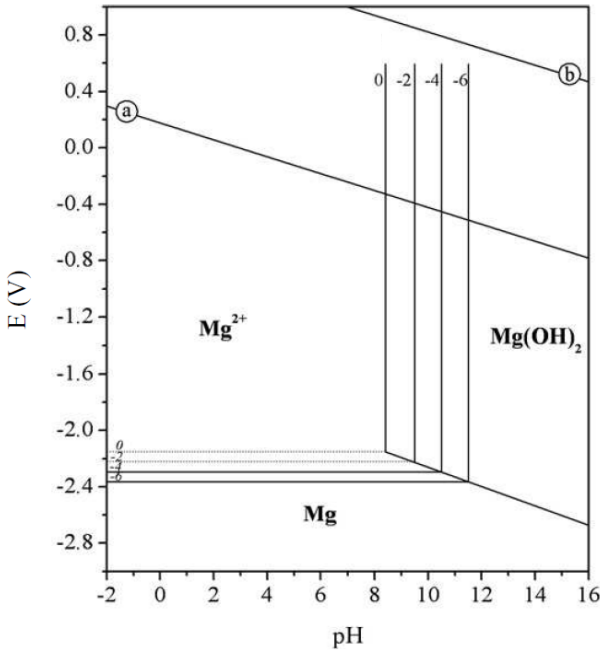

Figura 1.5. *Diagrama de Porubaix de magnesio en condiciones estándar [33].*

El diagrama de Pourbaix, representado en la figura 1.5, muestra la termodinámica asociada a la reactividad del magnesio en medios acuosos. Debido a su bajo potencial de corrosión en este tipo de medios (~ –1,5 V_{SHE}), la corrosión de magnesio se produce muy por debajo de la región de estabilidad del agua, situadas entre las líneas (a) y (b) del diagrama. Por lo tanto, la reacción catódica esperada es la reducción del agua que produce aniones hidróxido (OH^-) e hidrógeno gas (H_2):

$$H_2O + 1e^- \rightarrow 1/2\ H_2 + OH^- \quad \text{(Medio neutro o básico)}$$
$$H+ + 1e^- \rightarrow 1/2\ H_2 \quad \text{(Medio ácido)}$$

La concentración de oxígeno no parece afectar a la corrosión de magnesio en medios acuosos [25, 34, 35], aunque sí es un factor importante en la corrosión atmosférica de este metal [27, 36, 37]. En este diagrama también se observan las diferentes regiones de estabilidad de las especies de magnesio, resaltando una zona de "inmunidad" por debajo de -2,38 V_{SHE} y una zona de pasividad a pHs por encima de 10,5. Cabe destacar que las zonas de estabilidad pueden variar en función de la concentración de las especies en el equilibrio, tal y como se indica mediante las líneas discontinuas del diagrama.

Mecanismo de corrosión

Como se ha comentado anteriormente, en ambientes acuosos, la reacción catódica es la reducción de agua, por lo que la corrosión del magnesio en inmersión no es sensible a la concentración de oxígeno en el medio [25]. Sin embargo, la presencia de oxígeno es un factor importante en la corrosión atmosférica del Mg [37-40].

Pese a que lleva estudiándose más de un siglo, el mecanismo de corrosión del magnesio y sus aleaciones no está totalmente clarificado y actualmente se están realizando grandes esfuerzos de investigación para comprenderlo. El magnesio experimenta lo que en la literatura se ha denominado "negative difference effect" (NDE) o en castellano "efecto diferencial negativo" [41]. Este efecto se caracteriza por un aumento de la cantidad de hidrógeno generado al aplicar una polarización anódica, lo cual es contradictorio al comportamiento esperable según la teoría electroquímica general [42, 43]. Para explicar este comportamiento se han propuesto multitud de teorías que serán tratadas en profundidad en el primer capítulo de esta tesis.

Factores que influyen en el comportamiento a la corrosión

La corrosión de las aleaciones de magnesio depende tanto de factores metalúrgicos, como la concentración de impurezas, elementos aleantes, fases secundarias o la microestructura, como de factores ambientales tales como la temperatura, el pH, la concentración de iones cloruro y/o la humedad relativa [25, 35]. A continuación se hace una breve descripción de la influencia de cada uno de estos factores:

a) Factores metalúrgicos

- Impurezas y límites de tolerancia: Las impurezas más perjudiciales en el magnesio son el hierro, el níquel y el cobre porque tienen bajos límites de solubilidad en solución sólida y presentan una baja sobretensión para la descarga de hidrógeno. Debido a esto, actúan como cátodos, favoreciendo fenómenos de micro-corrosión galvánica al formar zonas de gran actividad catódica que aumentan la corrosión [35]. Para una concentración similar, el Ni es más dañino que el Fe, que a su vez, es más dañino que el Cu [25, 35].

Tal y como se muestra en la figura 1.6., por lo general hay un límite de tolerancia de impurezas a partir del cual se acelera la corrosión. Las velocidades de corrosión se multiplican por un factor de entre 10 y 100 cuando la concentración de estas impurezas aumenta por encima de su límite de tolerancia [44]. Estos límites están influenciados por la presencia de elementos adicionales en la aleación [45]. Así, por ejemplo, el límite de tolerancia de hierro en las aleaciones Mg-Al está fuertemente ligado a la concentración de Mn [2].

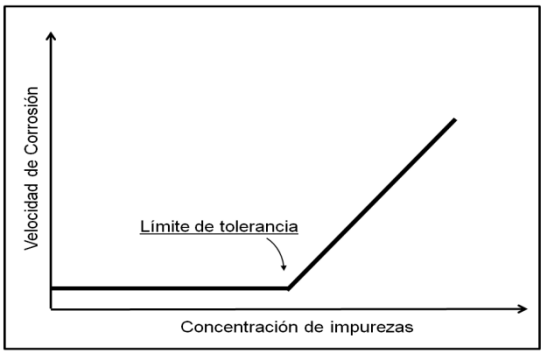

Figura 1.6. *Variación de la velocidad de corrosión en función de la concentración de impurezas.*

En este sentido, Hanawalt [35] encontró que Fe, Ni, Cu y Co tienen efectos muy perjudiciales sobre la corrosión en agua salada a concentraciones por debajo de 0,2 %; que Ag, Ca, Zn tienen una influencia poco significativa a concentraciones de entre 0,5 a 5 %, y que Sn, Cd, Mn, Si y Na tienen poca influencia en concentraciones de hasta 5 %.

Gracias a estos estudios, el contenido de impurezas en las aleaciones producidas en la actualidad ha disminuido enormemente y se intentan mantener por debajo su límite de tolerancia, lo que ha generado una mejora significativa en el comportamiento a la corrosión de las aleaciones de magnesio.

- Microestructura y fases secundarias: La adición de elementos aleantes para mejorar las propiedades mecánicas favorece la formación de compuestos intermetálicos, que influyen tanto en las propiedades mecánicas como en la resistencia a la corrosión del material. La naturaleza y composición de estos compuestos intermetálicos y fases secundarias depende de la composición de la aleación. La influencia en la corrosión de estas fases depende en gran medida de su comportamiento electroquímico respecto a la matriz que se puede cuantificar por su diferencia de potencial respecto a la misma. Por

lo tanto, aquellas fases electroquímicamente más nobles que la matriz actuarán como cátodos, formando micro-pares galvánicos que aceleran la disolución de la matriz. En función de su composición, los compuestos intermetálicos pueden tener un impacto más o menos negativo en la corrosión de la aleación. Así, por ejemplo, el Al_3Fe, formado en aleaciones con alto contenido de aluminio y hierro, es el intermetálico más perjudicial en las aleaciones de magnesio, debido a la elevada diferencia de potencial existente con la matriz de magnesio. Sin embargo al añadir manganeso a la aleación se forman intermetálicos Al-Mn-Fe que son menos perjudiciales que Al_3Fe.

Además de la presencia de fases secundarias y compuestos intermetálicos, también existen otros parámetros que juegan un papel importante en el comportamiento a la corrosión de las aleaciones de magnesio, como por ejemplo, el tamaño de grano o la microestructura [45-47]. Varios autores han reportado que la influencia de las fases secundarias puede variar en función de su distribución. Así, por ejemplo, varios estudios sugieren que la presencia de fases secundarias de microestructura fina, continua y homogénea puede ejercer un efecto barrera frente a la corrosión disminuyendo la corrosión, mientras que cuando se encuentran de manera discreta ejercen un efecto perjudicial sobre la misma [48-51].

En general, la adición de elementos aleantes favorece la formación de fases secundarias o compuestos intermetálicos catódicos respecto a la matriz de Mg que aceleran su corrosión. Hasta hace poco tiempo, se pensaba que ningún elemento aleante era capaz de producir una aleación con magnesio cuya velocidad de corrosión fuera menor que la del magnesio puro en un medio tan agresivo como solución de NaCl al 3,5% en masa [25, 52-54]. Esto se debe a que el magnesio es muy mal cátodo, ya que presenta una de las menores corrientes de intercambio para de la generación de hidrógeno [55]. Por lo tanto, cuando se combina con otros elementos capaces de soportar la reacción catódica, la corrosión aumenta en gran medida. Recientemente, fue publicado que el arsénico es capaz de reducir la corrosión del magnesio puro al reducir la reacción catódica sobre este metal, tal y como se explica en uno de los artículos presentados en esta tesis [24].

b) Influencia del medio

Como para otros metales, el medio es un factor fundamental a la hora de determinar la resistencia a la corrosión de las aleaciones de magnesio. Factores como el pH, la humedad relativa, la temperatura o la concentración de iones agresivos, son críticos a la

hora de estudiar la resistencia a la corrosión de las aleaciones de magnesio. Así por ejemplo, en medios básicos las alecciones de magnesio presentan cierta protección adicional debido a la mayor estabilidad de la capa de $Mg(OH)_2$ formada, tal como indica el diagrama de Pourbaix (figura 1.6), lo que favorece que, la corrosión normalmente comience en forma de picaduras [42].

Humedad relativa: desempeña un papel importante en la corrosión del magnesio y sus aleaciones ya que el comportamiento a la corrosión atmosférica difiere considerablemente del comportamiento en solución (100% humedad). La reacción catódica principal en solución, es la reducción del agua [25], mientras que durante corrosión atmosférica, el oxígeno juega un papel importante en esta reacción [38, 40, 56]. El magnesio y sus aleaciones tienen buena resistencia a la corrosión atmosférica, alcanzando en algunos casos resistencias similares a las aleaciones de aluminio [57]. En una atmósfera húmeda, el magnesio tiende a recubrirse de una capa de $Mg(OH)_2$ razonablemente protectora. Sin embargo el ataque aumenta considerablemente por encima del 90% de humedad relativa [39, 58].

Temperatura: en general la velocidad de corrosión aumenta con la temperatura [2, 59].

Concentración de especies en el medio: como es habitual en corrosión, la presencia de aniones agresivos, como los cloruros, tiene un efecto muy perjudicial en la corrosión, ya que rompen las películas protectoras y facilitan la corrosión localizada por picaduras [25, 57].

En corrosión atmosférica, la presencia de NaCl y/o CO_2 afecta al mecanismo de corrosión de las aleaciones de magnesio. Se ha observado una alta susceptibilidad a la corrosión en presencia de NaCl y ausencia de CO_2, con corrosión localizada y formación de hidróxido de magnesio como el producto de corrosión principal [60-62]. En presencia de CO_2, el mecanismo de corrosión aparece en forma de corrosión generalizada con desarrollo de una capa gris de oxido sobre la superficie. En este caso, el aumento de la resistencia a la corrosión ha sido atribuido a la formación de carbonatos de magnesio en la superficie que bloquean el proceso [60-62].

Tipos de corrosión

Las aleaciones de magnesio presentan diferentes morfologías de corrosión dependiendo de la composición, de la microestructura y de la naturaleza del medio al que están expuestas [25, 35, 45]. Así, por ejemplo, la corrosión atmosférica es mayoritariamente uniforme mientras que en inmersión aparece corrosión filiforme [24, 46, 63]. Se pueden distinguir más de 9 tipos de corrosión en base a la morfología del ataque. Sin embargo, por su peculiaridad y características particulares en el magnesio destacan las siguientes:

a) Corrosión galvánica: este tipo de corrosión ocurre cuando el magnesio está en contacto con otros metales menos activos que él o existen segundas fases o impurezas en la aleación que actúan como cátodos, aumentado la corrosión. La corrosión galvánica aumenta con la conductividad del medio, la diferencia de potencial entre el ánodo y cátodo, la relación área cátodo/ánodo y la menor distancia entre ánodo y cátodo.

b) Corrosión por picadura: al igual que en otros metales, este tipo de ataque solo se produce cuando el material opera a un potencial de corrosión ($E_{corr)}$, superior al potencial de picadura (E_{pic}), ya que por debajo de este valor, la picadura pierde su actividad. En el magnesio, este tipo de ataque, normalmente se inicia en forma de picaduras irregulares, las cuales crecen y terminan cubriendo toda la superficie [64]. El mecanismo parece diferente al de la picadura autocatalítica que se da en aceros inoxidables y la tendencia mayoritaria es a una picadura menos profunda debida al aumento de pH y la posterior formación de la película protectora de hidróxido de magnesio que dificulta el avance de la picadura [52, 65, 66]. Pese a todo, en determinadas situaciones, normalmente debido a la influencia de la microestructura de la aleación, se pueden observar picaduras más profundas. Como es habitual, este tipo de corrosión depende del tipo de anión agresivo y su concentración, de la composición del material metálico, el pH, la temperatura y la geometría de la superficie.

c) Corrosión filiforme: este tipo de corrosión es común en las aleaciones de magnesio inmersas en soluciones acuosas [24, 25]. Sin embargo, al ser insensibles a la concentración de oxígeno en solución, el mecanismo por el que se produce debe ser diferente a la aeración diferencial, comúnmente utilizado para explicar este proceso [67]. En este sentido, estudios utilizando técnicas de exploración de electrodo vibrante (SVET) revelaron que el borde de ataque del filamento es anódico mientras que el área corroída detrás del filamento de avance es un cátodo activo [46, 68].

d) Corrosión en resquicio: Al igual que ocurre durante la corrosión filiforme, el mecanismo por el cual aparece este tipo de corrosión debe estar relacionado con un mecanismo diferente a la aireación diferencial. En este sentido, se ha propuesto que la corrosión en resquicio puede deberse a hidrólisis del magnesio y los cambios de pH asociados [45].

Aleaciones de Magnesio

Como se ha comentado anteriormente, el magnesio presenta limitadas propiedades mecánicas, por lo que para poder utilizarlo en aplicaciones ingenieriles es necesario combinarlo con otros metales formando aleaciones. De forma muy general, las aleaciones de magnesio se pueden dividir en dos grandes grupos: el primero de ellos formados por aleaciones con un alto contenido de aluminio (2-10%) y otros elementos, que presentan buenas propiedades mecánicas a temperaturas inferiores a 120ºC y un coste moderado. El segundo grupo de aleaciones está formado por otro tipo de elementos aleantes, como tierras raras, plata o zinc, sin contenido de aluminio; son más costosas pero capaces de mantener sus propiedades mecánicas a temperaturas más elevadas.

Las aleaciones de magnesio se identifican según la norma ASTM, donde la denominación de cada aleación consta de cuatro partes. En primer lugar, se indican los dos principales elementos de aleación mediantes dos letras, seguido por una segunda parte constituida por dos números enteros relacionados con el porcentaje en peso de cada uno de ellos en la aleación. A continuación se añade una letra, relacionada con el porcentaje de los elementos no principales de aleación. Por último, se indican las condiciones de fabricación mediante una letra y uno o dos números enteros. En la tabla 1.3 se esquematiza la nomenclatura de las aleaciones de magnesio. Es habitual designar las aleaciones únicamente mediante las dos primeras partes. Así por ejemplo, la aleación con un 3 % de aluminio y un 1 % de Zinc se denomina como AZ31.

Tabla 1.3. *Designación aleaciones de magnesio*

Primera Parte	Segunda Parte	Tercera Parte	Cuarta Parte
Indica los dos principales elementos de aleación	Indica la cantidad de los dos elementos principales de aleación	Distingue entre las aleaciones con iguales porcentajes de elementos principales pero diferente contenido de elementos secundarios	Indica las condiciones de fabricación.

Existen multitud de familias y tipos de aleaciones en función de las propiedades que se busquen para la aleación. De este modo, las aleaciones con altos contenidos en ytrio junto con tierras raras, como por ejemplo la aleación WE54-T6, se caracterizan por su resistencia a la fluencia y su capacidad de endurecimiento por precipitación, mientras que las aleaciones con altos contenidos en aluminio y manganeso se caracterizan por su buena ductilidad. La Figura 1.7 muestra un esquema de la tendencia para mejorar las propiedades mecánicas de las aleaciones de magnesio como material estructural.

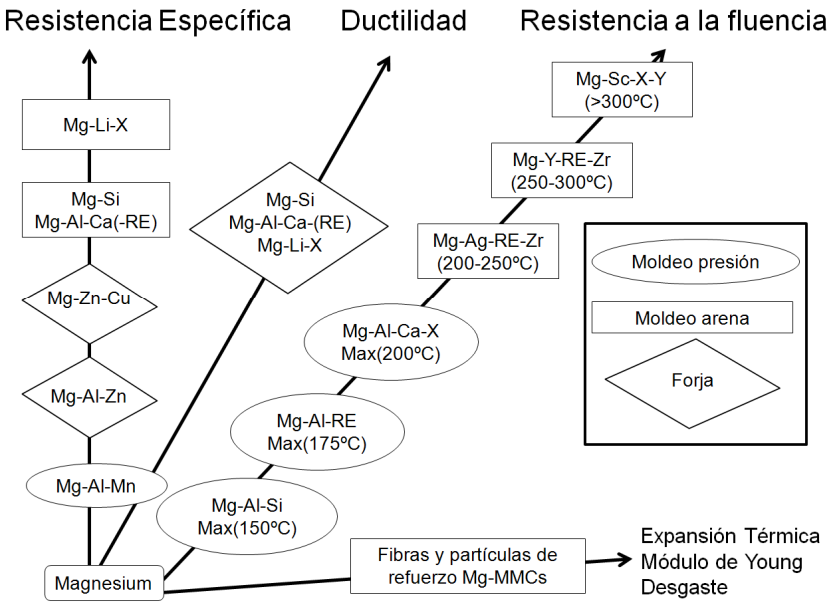

Figura 1.7. *Evolución aleaciones de magnesio [1].*

En los estudios realizados durante esta tesis doctoral se ha utilizado magnesio puro y aleaciones de magnesio del sistema Mg-Al-Zn. Estas aleaciones son las más utilizadas como aleaciones de moldeo. Presentan una combinación óptima de resistencia y ductilidad junto con una buena resistencia a la corrosión y bajo coste [5]. Gracias a la

presencia del Zn, su resistencia mecánica es mayor que las aleaciones del sistema Mg-Al, por lo que su campo de aplicación es más amplio. Aunque presentan buenas propiedades de moldeo, son susceptibles de mostrar microporosidad. Sus propiedades mecánicas y su resistencia a la corrosión son generalmente buenas y pueden utilizarse hasta temperaturas de 110–120 ºC, por encima de las cuales presentan problemas de fluencia [5].

Los principales elementos de aleación son aluminio y zinc y su influencia en la aleación se describen a continuación:

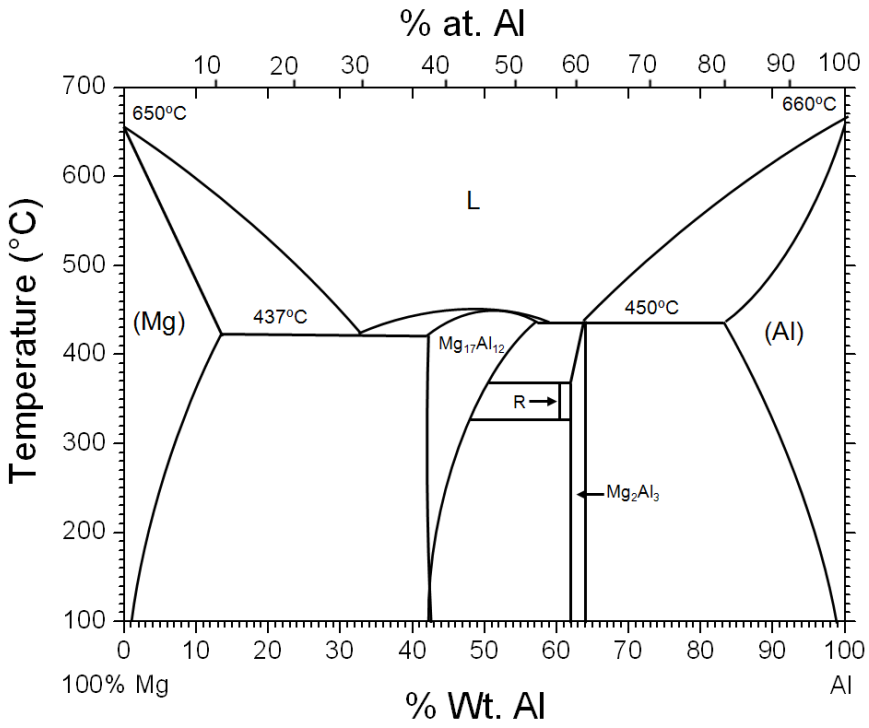

Figura 1.8. *Diagrama de fases binario Mg-Al [69].*

-<u>Aluminio:</u> se adiciona para aumentar la resistencia mecánica y la moldeabilidad. El diagrama de fases binario Mg-Al está representado en la figura 1.8. Se observa que la máxima solubilidad del aluminio en magnesio es de 12,7% a 437 ºC y que disminuye con la temperatura hasta alcanzar un 2% a temperatura ambiente. Por encima de su límite de solubilidad se produce la precipitación de $Mg_{17}Al_{12}$ (fase β); compuesto intermetálico frágil que puede deteriorar la ductilidad y la tenacidad de la aleación, así como disminuir la resistencia a la corrosión de la misma. Si se añade en cantidades específicas puede tener un efecto beneficioso en la resistencia a la corrosión [70], sin

embargo, existen dos efectos asociados a la presencia de aluminio en la aleación con resultados contrapuestos:

En primer lugar, se ha reportado que un aumento en el contenido de aluminio en la fase α, sin precipitación de fase β, mejora la resistencia a la corrosión [71-73]. De hecho, para aleaciones del sistema AZ (Mg–Al–Zn), el contenido en aluminio de la matriz puede variar desde el centro de grano hasta su borde, alcanzando valores de 2 a12% respectivamente [74]. Esto, puede originar que la corrosión comience en el interior de los granos α con menor contenido en aluminio en lugar de en el límite de grano como suele ser habitual [75]. También se ha reportado que concentraciones superiores a 4% de Al en las aleaciones de Mg aumentan significativamente la resistencia a la corrosión debido a la influencia de Al en la película pasiva MgO [70, 76-78]. Por último, parece que el límite de tolerancia del hierro disminuye al aumentar el contenido en aluminio [79].

Por otro lado, la presencia de fase β puede tener un efecto perjudicial en la resistencia a la corrosión. Si esta segunda fase se encuentra de manera discontinua en los límites de grano, forma micropares galvánicos que aceleran la corrosión [45, 80]. Sin embargo, si la cantidad de esta fase β es suficiente como para formar una estructura continua, puede ejercer un efecto barrera que disminuye la velocidad de corrosión [45, 47].

- **Cinc:** se añade principalmente para disminuir el tamaño de grano y aumentar la plasticidad y la resistencia a la tracción de las aleaciones de magnesio. También se ha reportado un efecto positivo en la corrosión al aumentar el nivel de tolerancia de impurezas como Fe, Cu y Ni de las aleaciones Mg-Al [23].

- Manganeso: se añade para mejorar la resistencia a la corrosión de las aleaciones de Mg-Al y Mg-Al-Zn ya que el Mn se combina con Al formando compuestos del tipo MnAl, $MnAl_6$ o $MnAl_4$, los cuales disminuyen el efecto perjudicial del aluminio. Además, estás fases también minimizan el efecto perjudicial de las impurezas de hierro que quedan contenidas en los compuestos Mn-Al [81, 82].

En la figura 1.9 puede observarse el diagrama de fases para las aleaciones del grupo AZ, conteniendo un porcentaje del 1% de Zn, 0.3% de Mn y una cantidad variable de Al. Cabe destacar la presencia de fases AlMn, muy características de estas aleaciones y de fase β, habitual en las aleaciones con alto contenido de aluminio.

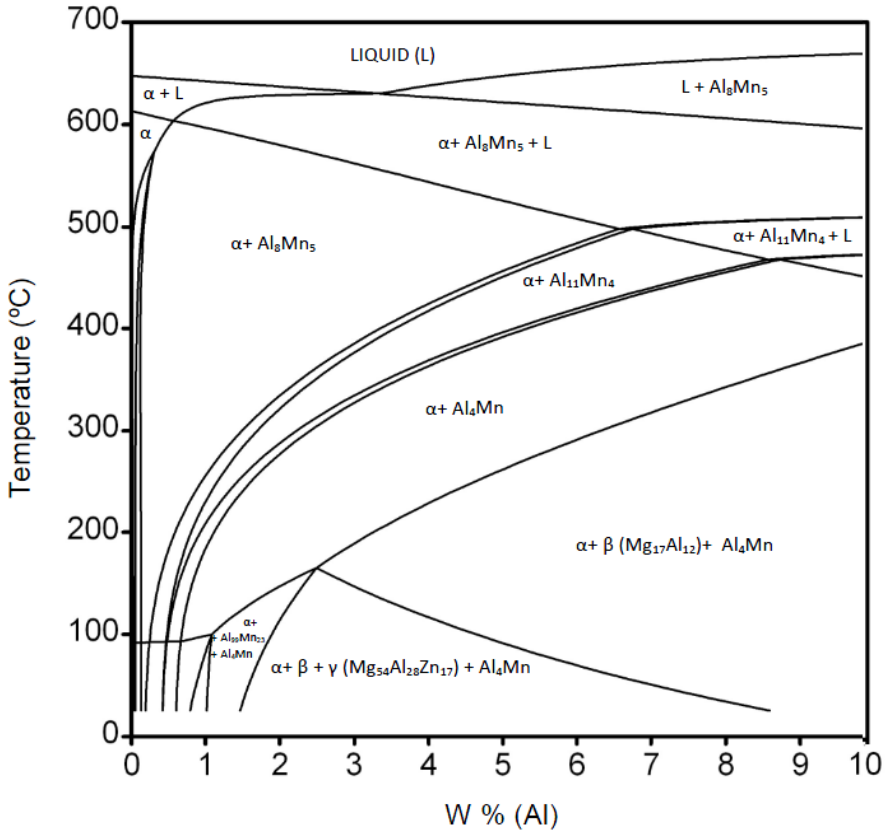

Figura 1.9. *Diagrama de fases en la bajo contenido en aluminio para el sistema AZ, con un contenido del 0,3% en Mn y un 1% de Zinc.*

Protección contra la corrosión

A lo largo de los años se han utilizado multitud de estrategias para intentar proteger las aleaciones de magnesio de la corrosión. Los actuales métodos utilizados en la lucha contra la corrosión, así como las estrategias desarrolladas y estudiadas durante esta tesis serán tratados en mayor profundidad en el tercer capítulo de esta tesis.

Materiales y Técnicas Experimentales

Preparación de materiales

En los estudios realizados en esta tesis, se utilizaron tanto materiales comerciales suministrados por Magnesium Elecktron ltd., como aleaciones de fabricación propia producidas en el departamento de Ciencia de Materiales de Monash University, en Melbourne, Australia.

Las aleaciones comerciales presentan la composición mostrada en la siguiente tabla.

Tabla 2.1. *Composición, expresada en % en casa de las aleaciones comerciales suministradas por Magnesium Elecktron ltd.*

Aleación	Al (%)	Zn(%)	Mn(%)	Si(%)	Fe(%)	Ca(%)
AZ31	3.1	0.73	0.25	0.02	0.005	0.0014
AZ61	6.2	0.74	0.23	0.04	0.004	0.0013

Las aleaciones de fabricación propia, fueron producidas mediante técnicas de fusión y colada empleando un horno de inducción en una atmósfera protectora de argón (Figura 2.1). Las aleaciones se prepararon a partir de una aleación comercial AZ31, junto con elementos aleantes adicionales en estado puro o aleaciones madre, así como magnesio, aluminio y cinc puro para ajustar la composición deseada.

El proceso utilizado durante la fundición se describe a continuación:

1. Antes de la fusión, la cámara del horno de inducción fue vaciada de aire utilizando gas argón (al menos 3 ciclos).
2. La masa fundida de aleación se llevó a una temperatura de 730 ºC dentro de un crisol de acero suave revestido con grafito. Se mantuvo a esta temperatura

durante 30 minutos, periodo durante el cual se agitó intermitentemente al menos tres veces para asegurar la mezcla homogénea de la aleación.

3. A continuación, la masa fundida se vertió en un molde de acero pre-calentado (a 250 º C) y se dejó enfriar a temperatura ambiente dentro de la cámara.

Las composiciones precisas de las aleaciones ensayadas se muestran en la tabla 2.2. La composición se confirmó mediante el uso de espectroscopia de emisión atómica inducida por plasma (ICP-AES) llevada a cabo en el servicio de análisis de Coburg, VIC, Australia.

Tabla 2.2. *Composición de las aleaciones de fabricación propia por colada expresada en porcentaje en masa.*

Aleación	Mg(%)	Al(%)	Zn(%)	Mn(%)	Lu(%)	Fe(%)
AZ31-Lu	95,5	3,05	0,91	0,36	0,21	0,002

Figura 2.1 *horno de inducción junto con sistema de atmósfera contralada utilizado para la fabricación de las aleaciones.*

Técnicas experimentales

Durante la realización de esta tesis doctoral se utilizaron multitud de técnicas de análisis y caracterización; tanto para evaluar la velocidad de corrosión como para caracterizar la microestructura y la influencia de los tratamiento realizados. En el siguiente gráfico se presentan de forma esquemática las técnicas utilizadas:

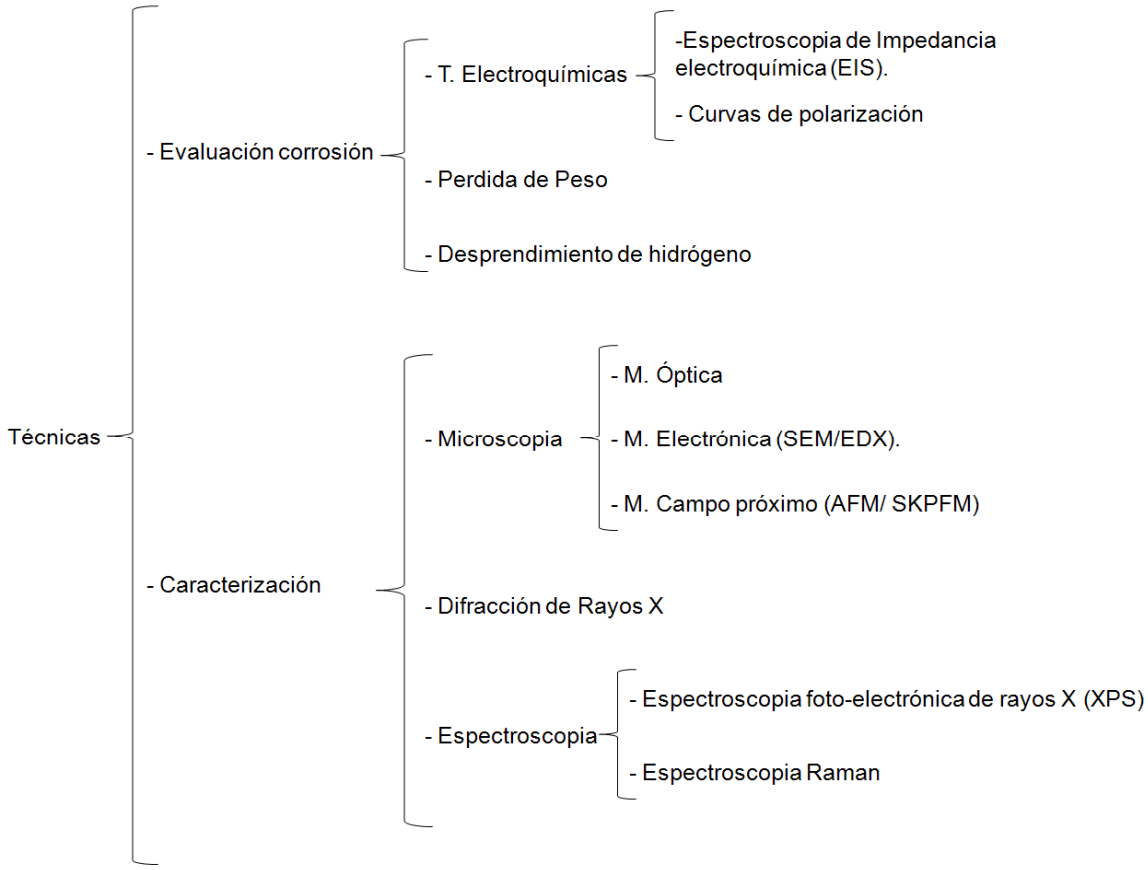

Figura 2.2. *Técnicas experimentales utilizadas durante esta tesis doctoral.*

La mayor parte de los estudios realizados durante esta tesis, tratan sobre el efecto de capas pasivas formadas sobre aleaciones de magnesio y están basados en los resultados obtenidos mediante la utilización conjunta de la espectroscopia de impedancia electroquímica (EIS) y la espectroscopia fotoelectrónica de rayos X (XPS) junto con los datos obtenidos mediante microscopía electrónica de barrido (SEM/EDX). Estudios previos han demostrado que la utilización conjunta de EIS y XPS pueden proporcionar información muy valiosa sobre las características de las películas de óxidos formadas

sobre las superficies de las aleaciones. Los fundamentos teóricos de estas tres técnicas principales se describen a continuación. Los parámetros experimentales y la descripción de las condiciones de trabajo de estas técnicas, así como del resto de las técnicas utilizadas, se describen en la parte experimental de cada uno de los artículos presentados en el capítulo de resultados.

Espectroscopia Fotoelectrónica de rayos X (XPS o ESCA).

Esta técnica se utiliza para el análisis superficial de materiales y se basa en la emisión de electrones internos de átomos del elemento a analizar al irradiar la superficie con rayos X. Debido al efecto fotoeléctrico, la incidencia de un fotón de energía hυ provoca la emisión de fotoelectrones con una energía de ligadura característica que viene dada por la siguiente ecuación:

$$EB = h\upsilon - EK - W \quad (1)$$

donde hυ es la energía de los fotones incidentes, EK, la energía cinética del fotoelectrón producido, W, la función de trabajo del espectrómetro y EB, la energía de ligadura. La energía de ligadura identifica al electrón de forma específica y es característica de cada elemento y nivel atómico. Tal y como se muestra en la figura 2.3b, una vez se ha emitido el fotoelectrón, el átomo se relaja, emitiendo un fotón o un electrón Auger [83].

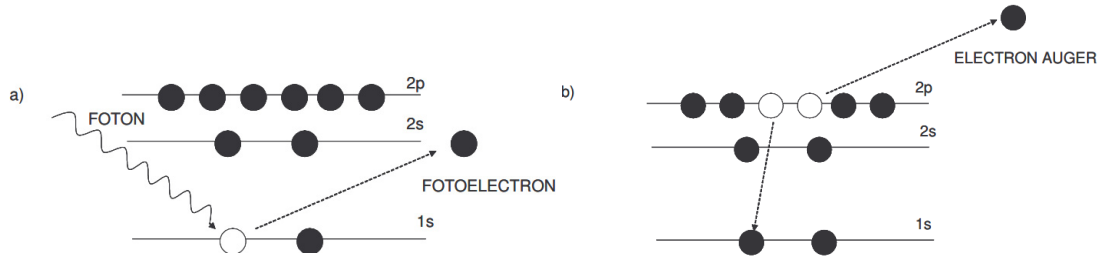

Figura 2.3. *Descripción proceso foto-electrónico.*

Todos los fotoelectrones cuya energía es menor que la energía del rayo X incidente pueden ser emitidos. Sin embargo, la energía de los electrones excitados es muy baja, por lo que solo los electrones originados en las capas más superficiales pueden ser detectados. Los electrones originados en capas más internas pierden su intensidad

debido a interacciones inelásticas, y pasan a formar parte del fondo del espectro. Para minimizar las pérdidas de energía, el análisis XPS debe realizarse en condiciones de ultra-alto vacio (10^{-8} torr).

La técnica XPS permite el análisis cuantitativo y cualitativo de todos los elementos químicos, excepto del hidrógeno. Además, esta técnica puede aplicarse tanto a materiales conductores como no conductores. La energía de ligadura de los picos asociados a la emisión de fotoelectrones está muy bien definida permitiendo identificar el estado de oxidación de cationes y aniones. Así, átomos del mismo elemento pero con diferente estado de oxidación, diferentes enlaces o posiciones no equivalentes en una red cristalina, presentan cambios apreciables en la energía de ligadura, típicamente entre 1-3 eV, que permiten su diferenciación. Respecto al análisis cuantitativo, normalmente se asume una distribución Gaussiana de la energía del fotoelectrón por lo que se puede realizar un ajuste sobre el espectro experimental para cuantificar los elementos analizados. La intensidad de la señal de un elemento es proporcional a la fracción molar de dicho elemento, lo que permite la cuantificación composicional del mismo, mediante la siguiente ecuación:

$$C_x = \frac{Ix/Sx}{\sum Ii/Si} \quad (2)$$

Donde C_x es la concentración atómica, I_x el área relativa del fotoelectrón del elemento x y S_x es el factor de sensibilidad tabulado para dicho elemento [83, 84].

Como se indicó anteriormente, debido a las interacciones inelásticas, mediante XPS únicamente se analiza un espesor de muestra de alrededor de 3 nm, por lo que es una técnica muy eficaz para el análisis y caracterización de superficies. Pese a que el espesor analizado por XPS es de tan solo 3 nm, se puede calcular el espesor de la capa de óxidos sobre la superficie analizada mediante la siguiente expresión:

$$d_o\ (nm) = \lambda_{oxido} \sin\theta \ln[(I_{oxido} \times \lambda_{metal} \times N_{metal})/ (I_{metal} \times \lambda_{oxido} \times N_{oxido})+1] \quad (3)$$

donde d_O es el espesor de la capa de óxidos (en nm); θ es el ángulo de salida de los fotoelectrones e I_{oxido} y I_{metal} son las intensidades de las componentes del material en estado metálico y como óxido del espectro XPS de alta resolución, λ_{metal} y λ_{oxido} son los

caminos inelásticos medios de los fotoelectrones en el substrato y en la capa de óxido y N_{metal} y N_{oxido} son las densidades del elemento en estado metálico y como óxido.

Por otro lado, mediante XPS, también puede obtenerse un perfil de composición en profundidad. Este puede obtenerse tanto por métodos destructivos como por métodos no destructivos. Mediante métodos destructivos pueden analizarse profundidades mayores, desde 30 nm en adelante, mientras que mediante métodos no destructivos pueden analizarse espesores de entre 5-10 nm.

Entre los métodos destructivos, destaca el bombardeo con iones argón, donde la superficie es bombardeada con iones de alta energía. Parte de la energía de estos iones es transferida a los átomos de la superficie, lo que hace que abandonen la superficie. Por lo tanto, la superficie se erosiona controladamente y, posteriormente, se analiza. En principio, este método permite obtener un perfil de composición con resolución de mono-capas. Hay que tener cuidado al utilizar este método ya que el estado químico de los átomos puede ser alterado durante el bombardeo e incluso puede provocar cambios en la composición superficial.

También se puede obtener un perfil composicional en profundidad mediante métodos no destructivos. La intensidad de los electrones emitidos desde una profundidad determinada "d" viene gobernada por la relación de Lambert-Beer:

$$I = I_o \exp(-d/\lambda \operatorname{sen}\theta) \quad (4)$$

donde I_0 es la intensidad de un sustrato puro de espesor infinito y θ es el ángulo de salida de los electrones emitidos, relativo a la superficie de la muestra. Por otro lado, la profundidad de análisis es función de la energía cinética de los electrones y el camino inelástico medio de un electrón (λ) varía con su energía $E^{0.5}$ y su volumen atómico. Cambiando el ángulo de salida de los electrones emitidos, se pueden obtener distintos perfiles en profundidad. Así a 90º, se obtiene información para una profundidad de 3 λ, mientras que a 15º el análisis se refiere a la composición química de la superficie más externa. El espectro adquirido de esta manera, está fuertemente influenciado por la geometría empleada durante la medida.

La mayor limitación de esta técnica, es la incapacidad de focalizar el haz incidente de rayos X, lo que origina una mala resolución lateral, siendo el análisis una media de un área de 1 mm^2. Sin embargo, la tecnología va evolucionando y los últimos

espectrómetros XPS en modo "imaging" consiguen una resolución lateral menor de <3 μm.

Espectroscopia de Impedancia Electroquímica (EIS).

Esta técnica se basa en la determinación de los parámetros cinéticos de las reacciones a partir del análisis de los procesos de relajación de las reacciones electródicas desplazadas del equilibrio por una señal sinusoidal aplicada sobre el potencial, de una amplitud fija y pequeña, para no alterar irreversiblemente el sistema. Normalmente la amplitud utilizada es de10 mV. Al variar la frecuencia (ω) de la señal, se obtiene una respuesta sinusoidal en corriente pero con diferente amplitud y ángulo de fase:

$$E = E_0 \operatorname{sen}\omega t \quad (1)$$

$$i = i_0 \operatorname{sen}(\omega t + \phi) \quad (2)$$

$$Z(\omega) = \frac{V(t)}{I(t)} \quad (3)$$

Siendo E_0 e i_0 las amplitudes máximas de la señal de entrada y de su respuesta en corriente, respectivamente, mientras que ϕ es la diferencia de fase de dichas señales. La impedancia es una magnitud vectorial, con una dirección o argumento, ϕ, que relaciona la señal de potencial aplicada y la corriente de respuesta y cuyo modulo, $|Z|$, queda definido por el cociente de las amplitudes de la señal de voltaje y la señal de corriente. Generalmente se representa mediante una notación compleja, de forma que, la impedancia viene definida por una parte real, relacionada con componentes resistivos, y otra imaginaria relacionada con condensadores e inductores. En el caso de los condensadores, la respuesta capacitiva de la onda resultarte presenta 90º respecto a la onda de voltaje aplicada.

$$|Z| = [(Z')^2 + (Z'')^2]^{1/2} \quad (4)$$

$$\phi = \arctan(Z''/Z') \quad (5)$$

$$|Z| = E_0/i_0 \quad (6)$$

La perturbación del estado estacionario de un sistema consistente en una resistencia y un condensador causa que el sistema se relaje a un nuevo estado estacionario. El tiempo de relajación necesario para este proceso, es conocido como la constante de tiempo y viene dado por:

$$\tau = RC \quad (7)$$

Donde R es la resistencia en Ohmios y C la capacidad en faradios. En general, la respuesta en impedancia es dependiente de la frecuencia. Para transformar la respuesta de la impedancia del dominio del tiempo al dominio de frecuencia, se utiliza la transformada de Laplace. Normalmente la respuesta en impedancia es medida en un amplio intervalo de frecuencias. Del análisis de la respuesta de impedancia en el dominio de frecuencia, se obtiene la información de las propiedades eléctrica del sistema analizado. Procesos rápido, con bajos tiempos de relajación, ocurren a altas frecuencias, mientras que procesos lentos, con altos tiempos de relajación, ocurren a bajas frecuencias.

Normalmente los datos de EIS, son representados por diagramas en planos complejos, basados en el diagrama de Argand (Figura 2.4), que permite definir de manera completa la impedancia al especificar el modulo $|Z|$ y el argumento. Alternativamente se pueden especificar las magnitudes de sus componentes real, Z', e imaginaria, Z''. Las dos notaciones son equivalentes.

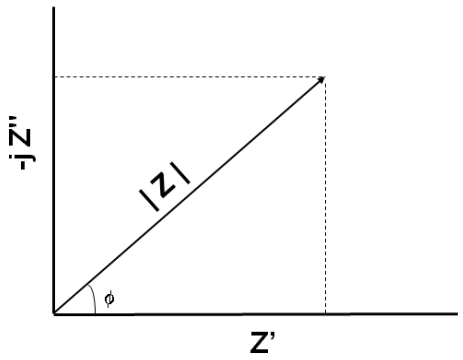

Figura 2.4. *Representación del vector impedancia en el plano complejo. Diagrama de Argand.*

Al aplicar la señal sinusoidal en un rango determinado de frecuencias, se obtiene un valor diferente a cada frecuencia para las componentes real e imaginaria de la impedancia, lo que define un vector impedancia para cada frecuencia. Al representar el vector impedancia para cada frecuencia en un mismo diagrama de Argand, se obtiene un diagrama de Nyquist. (Figura 2.5), del cual se puede obtener mucha información de manera relativamente sencilla.

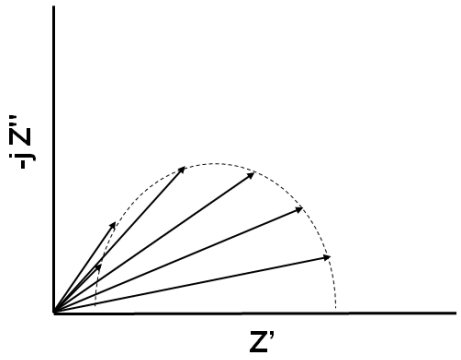

Figura 2.5. *Diagrama de Nyquist*.

También es muy habitual utilizar los diagramas de Bode donde se representa el módulo de la impedancia y el ángulo de fase en función de la frecuencia.

Los datos obtenidos mediante impedancia pueden ser analizados mediante modelos matemáticos exactos basados en teorías físicas que predicen teóricamente los espectros de impedancia o utilizando modelos empíricos de circuitos equivalentes que ajustan con el diagrama obtenido experimentalmente. En ambos casos, los parámetros son calculados teóricamente y comparados con el obtenido experimentalmente. En muchos sistemas prácticos, el sistema es demasiado complejo como para poder describirlo matemáticamente mediante un modelo, por lo que es bastante común, ajustar el espectro mediante un circuito equivalente, representativo de los procesos físicos que tienen lugar sobre el electrodo analizado

Debido a que los materiales de electrodo habitualmente presentan defectos o inhomogeneidades, las propiedades del material pueden variar de los valores teóricos esperados. Por lo tanto, es habitual que los circuitos equivalente ideales puedan ser inadecuados y haya que recurrir a elementos de fase constante. Los procesos de difusión también quedan descritos por elementos específicos.

Los elementos de los circuidos más importantes son las resistencias (R), los condensadores (C), los inductores (L), los elementos de fase constante (CPE) y los elementos relacionados con la difusión. Las resistencias representan la resistencia que los portadores de carga encuentran en el interior del material o en un proceso sobre la interfase. Los condensadores representan la acumulación de especies cargadas, análogos a los procesos que pueden ocurrir en un material dieléctrico o en una interfase debida a la capacidad de la doble capa. Los inductores están generalmente asociados a especias adsorbidas y a la deposición de capas superficiales sobre el electrodo. Los elementos de difusión se utilizan cuando existen

procesos relacionados con la difusión. Por último, los elementos de fase constante sirven para representar un comportamiento dieléctrico no ideal. Los CPE vienen representados como:

$$Z_{(CPE)} = 1/[Y_0(j\omega)^n] \quad (8)$$

Donde Y_0 es una constante, y n es un parámetro matemático con valores entre 0 y 1. En el caso de que n = 1, el CPE se comporta como un condensador ideal cuya capacidad es Y_0. Si n =0, el elemento de fase constante se comporta como una resistencia. Normalmente el valor de n es menor que 1. Existen multitud de factores que pueden ocasionar un comportamiento dieléctrico no ideal, como por ejemplo inhomogeneidades en la composición, en la estequiometria, defectos superficiales, límites de grano, rugosidad, porosidad, etc. En el caso particular de que n= 0.5, el CPE presenta un comportamiento análogo al comportamiento de un elemento de Warburg que describe un comportamiento semi-infinito lineal del proceso de difusión.

La espectroscopia de impedancia electroquímica es una técnica muy potente, a través de la cual se pueden obtener datos relacionados con variables complejas como el transporte de masa, velocidad de reacción, de corrosión, propiedades dieléctricas o detectar la presencia de defectos. Es una técnica muy versátil que puede ser utilizada tanto en materiales conductores, semi-conductores o aislantes. Ha sido ampliamente utilizada para analizar pinturas, y recubrimientos, así como para caracterizar óxidos superficiales. Pese a su potencial, también presenta inconvenientes importantes como la dificultad de interpretar los datos experimentales obtenidos. Así, por ejemplo, es posible realizar ajustes perfectos con circuitos equivalentes que no tienen un significado físico real y por lo tanto carecen de sentido. Por otro lado, las medidas a bajas frecuencias, requieren mucho tiempo de medida, lo que requiere una estabilidad del sistema suficientemente grande y es posible que se produzcan artefactos con relativa facilidad.

Microscopía electrónica de Barrido (SEM) y Espectroscopia de energía dispersiva (EDX)

En este tipo de microscopia, los electrones son producidos y acelerados por un cañón de electrones. Estos electrones son focalizados por lentes condensadores en un haz con un diámetro de entre 2-10 nm, que incide sobre la superficie a analizar. Debido a la

interacción del haz de electrones con los átomos de la muestra, se generan electrones retro-dispersados y electrones secundarios, así como rayox X o electrones Auger. De forma general, para generar imágenes, los microscopios electrónicos de barridos trabajan en modo emisivo mediante el análisis de electrones secundarios o retro-dispersados. El sistema de barrido provoca que el haz se mueva una serie de puntos discretos a lo largo de una línea y al terminar prosiga con otra, de manera que se obtiene un barrido rectangular de la muestra. El SEM se caracteriza por conseguir un buen contraste topográfico. Dependiendo de la topografía de la muestra o de la composición, se pueden obtener diferentes intensidades que permiten obtener las imágenes deseadas. Como los electrones secundarios tienen muy baja energía, solo aquellos emitidos a tan solo unos nanómetros de profundidad son detectados, sin embargo el área analizada es mucho mayor que la del haz incidente. Mediante el barrido del haz de electrones sobre la superficie, se produce una imagen representativa de la superficie analizada. Las imágenes de SEM se caracterizan por su alto grado de contraste y su gran profundidad de foco.

El uso del SEM, comúnmente es acompañado por EDX que permite el análisis semi-cuantitativo de la muestra analizada. Cuando el haz de electrones incide sobre la superficie, se produce la excitación de los átomos de la muestra. Al producirse la relajación de los átomos excitados por el haz de electrones, se producen rayos X característicos de los elementos excitados que pueden ser identificados. La región volumétrica que emite estos rayos X, tiene forma de cono invertido y es mucho más grande que el haz incidente de electrones. Los rayos X son comúnmente analizados mediante técnicas de energías dispersivas. Sobre el detector, los rayos X generan una corriente eléctrica cuya magnitud es proporcional a la energía de los rayos X incidentes. La señal es posteriormente amplificada y analizada.

Objetivos y plan de trabajo

Esta tesis se ha dividido en tres capítulos bien diferenciados, con objetivos diferentes.

El primero de ellos, se centra sobre el mecanismo de corrosión del magnesio que, pese a llevar estudiándose más de un siglo, actualmente sigue siendo una fuente de controversia en la comunidad científica. Esta controversia debe ser aclarada, ya que para poder proteger las aleaciones de magnesio de una manera adecuada es necesario entender el mecanismo a través del cual se produce la corrosión. El objetivo principal de este capítulo de la tesis es clarificar aspectos relacionados con el mecanismo de corrosión del magnesio y el denominado efecto diferencial negativo ("negative difference effect" (NDE)). Para ello, se realizó una extensa revisión bibliográfica, analizando los diferentes mecanismos propuestos y la evolución de los mismos con el tiempo. A continuación se realizó un estudio para clarificar las evidencias sobre la existencia de la especie Mg^{+}, base del mecanismo más citado hasta la actualidad. En estos estudios se evidenció la imposibilidad de demostrar su existencia mediante los métodos utilizados en estudios anteriores.

Posteriormente, se publicó una teoría alternativa para poder explicar el efecto diferencial negativo (NDE). Por último, se realizó un estudio para intentar clarificar el origen físico de la ley que explica los datos experimentales. Por lo que el plan de trabajo de este capítulo puede esquematizarse como:

1. Revisión bibliográfica de los mecanismos de corrosión.
2. Estudio sobre las evidencias del magnesio monovalente (Mg^{+}). Repetición de las experiencias realizadas por Petty en 1953 en conjunto con técnicas analíticas modernas.
3. Obtención de nuevos datos experimentales y proposición de un mecanismo alternativo para explicar el NDE.
4. Estudio de la influencia de elementos aleantes específicos (Li, Ca, Fe) sobre NDE.

El segundo capítulo de la tesis se centra en el estudio sobre la capa de óxidos superficies espontáneamente formados sobre las aleaciones AZ31 y AZ61 y de sus productos de corrosión. Los objetivos fueron los siguientes:

1. Estudiar la composición química de las nanocapas de óxidos que se forman espontáneamente en la superficie de las aleaciones AZ31 y AZ61, en su estado de recepción y después de pulido, con el objetivo de encontrar posibles relaciones entre el contenido de los elementos aleantes del material base, el espesor de la delgada película de óxido formada y la cantidad de aluminio segregado en la superficie más externa.

2. Analizar la influencia de las condiciones superficiales en la química de las nanocapas formadas en la superficie externa de las aleaciones magnesio aluminio.

3. Contribuir a un mejor entendimiento de la influencia de las condiciones superficiales iniciales, particularmente la química de las nanocapas en la posterior resistencia a la corrosión de las aleaciones Mg-Al en solución de NaCl 0.6M

4. Analizar la influencia de los productos de corrosión durante la inmersión de estas dos aleaciones en soluciones de cloruro sódico, y conseguir un mayor entendimiento sobre su influencia en la corrosión.

El tercer capítulo de la tesis consta de varios sub-apartados donde el objetico común es intentar reducir la velocidad de corrosión del magnesio y sus aleaciones. Se utilizaron diferentes estrategias/tratamientos con este fin, que en su mayoría se caracterizan por ser tratamientos baratos y rápidos y se enumeran a continuación:

1. Se realizó un tratamiento térmico a temperaturas moderadas y tiempos cortos (200ºC, 5-60 minutos), en ambas condiciones superficiales (pulido y estado de recepción), con el fin de maximizar el efecto protector de estas películas superficiales formadas espontáneamente sobre las aleaciones AZ31 y AZ61.

2. Se intentaron modificar los óxidos superficiales formados sobre la aleación AZ31 mediante la adición de bajos contenidos de elementos aleantes (<1%), con mayor afinidad hacia el oxígeno que el magnesio y de esta manera

obtener una capa de óxidos superficiales protectora con un rango mayor de estabilidad.

3. Se realizó un tratamiento de conversión superficial, utilizando un baño de bicarbonato sódico con la intención de formar una capa protectora de carbonatos sobre la superficie. Los objetivos adicionales de este estudio fueron.

    a. Optimizar las condiciones del tratamiento de conversión para obtener mejores protecciones.
    b. Contribuir a un mejor entendimiento de los factores que influyen sobre este tipo de capa de conversión.

4. Se adicionó un 0.37 % en peso de arsénico (As) sobre magnesio puro con el fin de estudiar su influencia en la reacción de corrosión y en la micro-estructura de la aleación.

Resultados y Discusión

Los resultados obtenidos durante esta tesis doctoral se muestran a continuación en forma de publicaciones. Por su temática, esta sección se ha divido en tres capítulos independientes, los cuales están sub-divididos en:

i) Introducción.
ii) Resultados (artículos).
iii) Discusión general de capítulo.

Capítulo I

Profundización en los Mecanismos de Corrosión del Magnesio y el Efecto Diferencial Negativo (NDE).

Introducción

Pocos metales presentan un comportamiento electroquímico tan curioso como lo hace el magnesio. Una característica de este metal es la elevada generación de hidrógeno gaseoso que se desprende de su superficie al estar sometido a una polarización anódica. Cabe recordar que, acorde a la teoría electroquímica clásica [85], la reacción catódica debería disminuir al polarizar anódicamente, puesto que la generación de hidrógeno se asocia a una reacción catódica, por lo que el comportamiento esperable sería una disminución y no un aumento de esta reacción. Desde el siglo XIX [86], se ha intentado dar una explicación plausible a los datos experimentales observados. Sin embargo, hasta la fecha, no se ha conseguido constatar un mecanismo capaz de explicar todos los datos experimentales asociados a este fenómeno.

En 1908, Turrentine [87] fue el primero en proponer que esta generación adicional de hidrógeno, acompañada con una pérdida de masa mayor que la teóricamente predicha por la ley de Faraday, podría deberse a que la oxidación de magnesio se lleve a cabo en dos etapas; una electroquímica y otra química. De esta manera, propuso la existencia de una especie intermedia, con menor estado de oxidación (Mg^{+}) formada en una primera reacción electroquímica. Al consumirse únicamente un electrón en esta primera reacción, se podrían explicar las pérdidas de masa adicionales detectadas al polarizar anódicamente. En una segunda etapa, el Mg^{+}, reaccionaría de una manera directa con las moléculas de agua a su alrededor, produciendo hidrógeno gaseoso y cationes Mg^{2+}. Este mecanismo se podría esquematizar mediante las siguientes reacciones:

$$Mg \rightarrow Mg^{+} + e^{-} \quad (1)\ (\text{R. Electroquímica})$$
$$2Mg^{+} + 2H^{+} \rightarrow 2Mg^{2+} + H_2 \quad (2)\ (\text{R. Directa})$$

De este modo, al polarizar anódicamente, se produciría una mayor generación de cationes Mg^{+}, que reaccionarían con el agua produciendo un aumento en la generación de hidrógeno gaseoso, como se observa experimentalmente. Pese a que está teoría se propuso en 1908, no se publicaron evidencias sobre la presencia de esta especie intermedia hasta 1953 [88]. Sin embargo, está teoría no es la única que se ha propuesto para explicar este fenómeno que posteriormente se ha denominado “Negative diferente effect”, o efecto diferencial negativo (NDE). Así, este efecto ha causado una fuerte controversia en la comunidad científica relacionada con este tema, y a lo largo de los años, se han producido intensos debates al respecto. A partir de los años cincuenta y

hasta los años 80, se han propuesto varias teorías. Por ejemplo, en el año 1963, se propuso que el efecto diferencial negativo podría deberse al desprendimiento de partículas catódicas respecto a la matriz de magnesio ("Chunk effect") [89], cuya pérdida de masa no podría contabilizarse electroquímicamente y que podrían ser las responsables de la producción adicional del hidrógeno generado. Adicionalmente, King describió el concepto de pseudo-pasividad [90, 91] y junto con Robinson, consideraron la ruptura de las capas protectoras durante la disolución del metal como las responsables del NDE [92]. Según su teoría, el magnesio reacciona de manera violenta con el agua (similar a como lo hace el sodio [92]), si se produce el contacto directo metal/solución y no a través de las capas superficiales espontáneamente formadas sobre magnesio. De esta forma, al polarizar anódicamente, se estarían modificando las capas superficiales y se estaría aumentando el área de contacto directo entre el metal y la solución, provocando un aumento de la disolución del metal y por consiguiente un aumento en la cantidad de hidrógeno generado [90].

Por otro lado, Perrault, al considerar el potencial de corrosión de magnesio en medios acuosos, concluyó que únicamente podría alcanzarse si en la reacción de corrosión interviniese el hidruro de magnesio como especie intermedia [93]. Por lo tanto, propuso que el NDE se debe a la presencia de hidruro como intermedio de reacción [94]. Otras teorías también fueron propuestas como la que involucra la presencia de magnesio coloidal [95]. Aunque en 1972, Hull sugirió que después de polarizar anódicamente magnesio, la única especie reductora en el anolito era la correspondiente a hidrógeno molecular disuelto [96], en 1997, Atrens y Song [97], concluyeron que el efecto diferencial negativo (NDE), se debe a la presencia de Mg^{+}, como intermedio de reacción. De esta forma, este debate volvió a abrirse y en los últimos años, se han realizado múltiples publicaciones al respecto. Teorías como la que involucran a electrones hidratados o la hidrólisis del agua como responsables de este efecto también han sido propuestas recientemente [98, 99].

Durante esta tesis se realizaron diversos estudios sobre este tema, donde se ha intentado esclarecer y explicar los hechos experimentales. Entre otras cosas, se ha evidenciado la imposibilidad de demostrar la presencia de Mg^{+} mediante los experimentos reportados por Petty en 1954 [88] y se ha propuesto un mecanismo alternativo para poder explicar el efecto diferencial negativo, que recientemente ha sido confirmado en varios estudios [4, 100-102].

Resultados Capítulo I.

Los resultados obtenidos durante la elaboración de esta tesis doctoral, relacionados con este tema, se muestran en esta sección en forma de publicaciones. Los artículos publicados fueron los siguientes:

Evolution of Hydrogen at Dissolving Magnesium Surfaces. G.S. Frankel, A. Samaniego and N. Birbilis. Corrosion Science 70 (2013) 104-111.
http://dx.doi.org/10.1016/j.corsci.2013.01.017

On the Evidence for Univalent Mg. A. Samaniego, B.L. Hurley, G.S. Frankel. Journal of Electroanalytical Chemistry, In Press, Corrected Proof, Available online 2 May 2014.
http://dx.doi.org/10.1016/j.jelechem.2014.04.013

En revisión para el número especial sobre Mg de la revista CORROSION:

Hydrogen Evolution During Anodic Polarization of Mg Alloyed with Li, Ca, or Fe. A. Samaniegoa, N. Birbilis, X. Xia and G.S. Frankel.

On the Evidence for Univalent Mg

A. Samaniego[a,b], B. L. Hurley[a], and G.S. Frankel[a]

a. Fontana Corrosion Center, The Ohio State University, Columbus, OH, USA
b. National Centre for Metallurgical Research (CENIM-CSIC). Department of Materials Engineering, Corrosion and Durability, Madrid, Spain

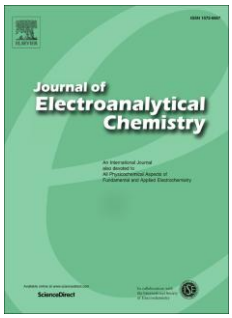

Journal of Electroanalytical Chemistry, In Press, Corrected Proof, Available online 2 May 2014

Abstract

The mechanism of magnesium dissolution in aqueous solutions and the enhanced reduction of water to form hydrogen observed at a magnesium electrode at increasing anodic potentials has received much recent attention. One explanation for this phenomenon is the assumption that a fraction of dissolving Mg enters the solution as univalent Mg (Mg^+), where it is subsequently oxidized by water. A commonly-cited report for the existence of Mg^+ is the 1954 paper by Petty et al., in which indirect analytical techniques were used. In this paper, the experiment performed by Petty et al. was reproduced and supplemented with modern *in situ* Raman spectroscopy. A saturated sulfate solution exposed to a magnesium electrode at open circuit will reduce to form sulfur dioxide, which can serve as a reducing agent. The presence of sulfur dioxide would, therefore, create reducing conditions, which had been attributed to Mg^+ by Petty et al. Furthermore, it was found that the reduction of sulfate at a pure magnesium electrode, similar to the reduction of water, is enhanced at increasing anodic potentials. This effect was not observed at a Pt electrode in the same potential range in a saturated sulfate solution. As a result, it must be concluded that the existence of Mg^+ was not established by Petty et al.

Keywords: Magnesium, univalent magnesium, corrosion, hydrogen evolution, negative difference effect

Introduction

Few metals present corrosion behavior as curious as that of magnesium in aqueous solutions. Since the nineteenth century, the electrochemistry of magnesium has been studied in an effort to achieve a better understanding of the complexity behind experimental observations. The atypical electrochemical behavior of magnesium was first disclosed by Beetz in 1866 [1] who reported "non faradaical mass loss" accompanied by a high amount of hydrogen gas evolved from the electrode during anodic polarization [2-4].

In the last two centuries, researchers have proposed a variety of theories for the anomalous electrochemical behavior noted above. These include the anodically induced separation of metal particles from the metal surface ("chunk effect") [4, 5], the formation of aqueous H atoms [6], the formation of aqueous hydride ions [7, 8], protective film disruption [2, 9, 10], decreasing pH attributed to the hydrolysis of Mg ions [11], hydrated electrons [12], or enhanced catalytic activity at a dissolving Mg surface [13-15]. In 1908, Turrentine was the first to propose the existence of an intermediate species of magnesium with lower valence than the expected divalent Mg^{2+} (i.e. Mg^{+}) to explain the above effect, which he referred to as "reversed electrolysis" at a Mg electrode [16]. However, no evidence of Mg^{+} was reported until 1954 when the PhD dissertation by Roy L. Petty and a subsequent publication described "evidence of unipositive magnesium" [17, 18]. Petty described several experiments using weight loss measurements and other experiments using measured current values.

Petty's most convincing evidence of the existence of unipositive magnesium was found in experiments in which a solution was flowed past a dissolving Mg anode into a separate cell that contained an oxidizing agent [18]. Petty claimed that reduction of the oxidized species observed in the second cell must have occurred in association with the oxidation of aqueous Mg^{+} because the oxidizing agent did not make contact with the Mg anode and no other source or electrons was present in the second cell. Implicit in this explanation is the notion that univalent Mg must be stable in solution for a considerable time without being oxidized by water. As these experiments were performed in 1954 and the available analytical techniques were more limited, the claim was supported only by visual observations. Nonetheless, since 1954, Petty´s evidence of Mg^{+} has had a substantial impact on studies related to the corrosion of magnesium. The presence of Mg^{+} has been proposed in E-pH diagrams [7, 19], corrosion mechanisms [20], and electrochemical studies [21]. In fact, since 1954, Thomson Reuter's Web of

Science indicates that as of January, 2014, Petty's original article [17] has been cited 95 times, with citations evenly distributed over the range from 1954-2013 [22]. Beginning in 1997, citations to this work have increased from authors who attributed the existence of Mg^+ as the cause of the so-called "negative difference effect" (NDE), which can be described as the increased rate of hydrogen evolution on magnesium under anodic polarization [23-26]. This idea has spread widely without any direct experimental evidence of the presence of Mg^+ other than that of Petty.

Given that the experiments reported by Petty in 1954 remain the best evidence of Mg^+, they were repeated in this work using modern techniques that permitted a more rigorous examination of the results. Raman spectroscopy was employed to analyze the products of these experiments and to allow *in situ* analysis of species generated during polarization. Additional experiments using Petty's parameters but substituting platinum for magnesium were also undertaken for further clarification.

Experimental

Electrochemical experiments. A replication of the experimental flow system established and described by Petty [17] is shown in Figure 1 with each of the components lettered and described below. In this experiment, 150 mL of aqueous 0.2 M $KMnO_4$ (K) (Fisher Scientific, 99.8%) was the oxidized species present in the lower beaker (B). A saturated solution (70 g/L) of aqueous Na_2SO_4 (N) (Fisher Scientific, 99.2%) was flowed by gravity feed past an Mg electrode from a reservoir (R) located over 1 m above the lower beaker. The solution concentrations seem to be identical to those used in Petty's experiments, based on the available information. A 99.99% Mg anode (A) was employed. The cathode (C) was Pt foil. A glass delivery column (D) directed the flowing electrolyte into the lower beaker. The bottom of the delivery column was stuffed with glass wool (G) to filter any possible falling solid particles from the anode, as was described by Petty et al. [18]. The Pt foil (C) was contained in the cathode compartment, which was a glass cup filled with the Na_2SO_4 solution, with a porous frit (P) on the bottom.

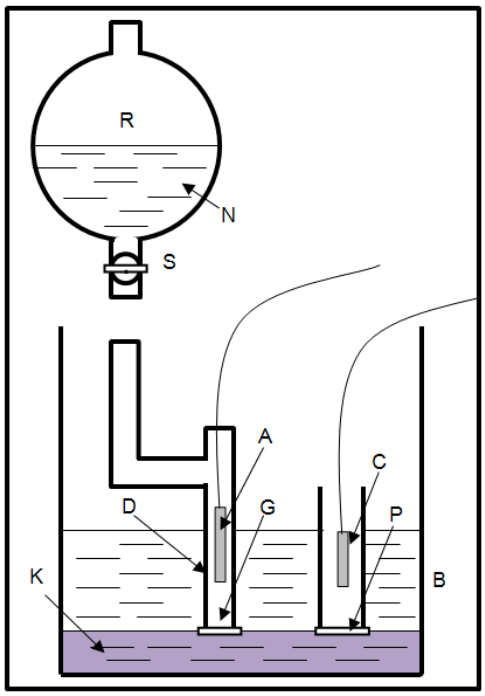

Figure 1. *Schematic of apparatus for study of electrolysis with flowing electrolyte. Explanations for the letter code are given in the text.*

The flowing action of the cell prevented the $KMnO_4$ in the lower beaker from making direct contact with the anode. Petty put forth that the porous frit in the cathode compartment prevented the $KMnO_4$ solution from making contact with the cathode or any products generated by the cathode [17, 18]. At the commencement of the experiment, the level of the $KMnO_4$ solution was slightly below the anodic chamber delivery column and the cathodic frit. This initial level is represented by (K) in Figure 1. The flow from the reservoir was started and electrolysis was initiated when the Mg anode made contact with the rising solution level. Although Petty indicated that the flow rate was established by the stopcock (S) [17], we found the rate to be controlled primarily by the quantity of glass wool placed at the bottom of the delivery column. Petty described the flow rate as "fairly rapid" [18]. A rate of ~0.75 ml/s was chosen, resulting in a total experimental time of ~2000 seconds. The exposed area of the Mg anode was ~4 cm^2 and the anodic applied current density was 3 mA/cm^2. Therefore, the total applied charge was 24 C. In keeping with Petty's parameters, immediately before initiation of the experiment, the $KMnO_4$ solution was filtered. After completion of the experiment, the beaker solution was again filtered accompanied by visual inspection as described by Petty. Petty did not indicate a filtering method. We used either gravity or vacuum filtration.

Additional experiments were performed with the same parameters, except the Mg anode was replaced by a Pt foil electrode. In these experiments, potentiostatic control was implemented (-1.6 V_{SCE}) rather than the galvanostatic control applied to the Mg anode. This potential was chosen because it was in the range of values expected at the Mg anode during the galvanostatic experiments after making allowances for the substantial ohmic potential drop (IR drop) present in the cell. Lastly, the experiment was performed with no electrode in the delivery column. This experiment was carried out with no electrochemical control and no counter electrode or reference electrode in place. In other words, the Na_2SO_4 solution simply flowed through the delivery column and into the beaker with no anode in place. All electrochemical experiments were performed with a Gamry Reference 600™ potentiostat controlled by the Gamry Framework™ software package. A saturated calomel electrode (SCE) was used as the reference electrode. All electrochemical experiments and potential values herein are in reference to an SCE.

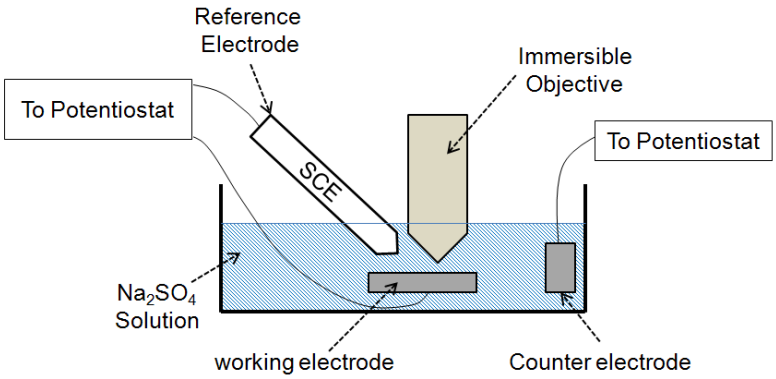

***Figure 2**. In situ cell employed for Raman analysis.*

Raman Analysis. Raman spectra were acquired on a Renishaw inVia Raman microprobe system. Spectra of dry precipitates produced in the flow cell experiments were acquired using a Leica 10X objective at a power of ~6 mW with 633 nm excitation and various integration times. Due to the various integration times, these spectra are presented as qualitative data and the intensities of the peaks cannot be directly quantitatively compared. Spectra acquired *in situ* during polarization experiments (described below) were acquired using a Leica 40X immersible objective with 514 nm excitation. All spectra acquired during *in situ* polarization experiments involving a Mg electrode were acquired with an integration time of 20 sec at a power of ~11 mW and peak intensities can be quantitatively compared. All spectra acquired during *in situ* polarization experiments involving a Pt electrode were acquired with an integration time

of 10 sec at a power of ~11 mW and peak intensities can be quantitatively compared. The *in situ* Raman measurements were performed on an upward facing working electrode: either an epoxy-mounted Mg electrode or a Pt foil electrode (Figure 2). The cell contained a Pt foil counter electrode, an SCE, and saturated Na_2SO_4 solution. The microprobe objective was immersed in the electrolyte immediately above the working electrode, providing enhanced focus and light collection. Raman spectra were collected during potentiodynamic polarization of the working electrode. Both cathodic and anodic polarization scans were performed on the Mg electrode; only cathodic scans were performed on the Pt electrode. All scans were performed at 1 mV/sec and originated at the OCP (-1.900 V_{SCE} and +0.155 V_{SCE} for Mg and Pt. respectively). The anodic Mg scan was terminated at -1.556 V_{SCE}. The cathodic scans were terminated at -2.585 V_{SCE} and -1.707 V_{SCE} for Mg and Pt, respectively. All spectra are shown with their original baselines (i.e., no baseline corrections were made).

Results

Reduction of $KMnO_4$

Although Petty performed the flowing electrolyte experiment with a variety of oxidizing agents, the most compelling evidence of reduction resulted from the experiments involving $KMnO_4$; therefore, that experiment was chosen for investigation. Petty indicated that filtration of the beaker's content after completion of the flow cell experiment provided a "Brown subst. which gave qual. tests for manganese dioxide" [17, 18]. Several experiments using Petty's flow cell were performed as noted above, specifically: (1) a cell with a Mg anode (identical to Petty's setup), (2) a cell with a Pt electrode, and (3) a "cell" with no electrode. Visual inspection presented no discernible visual difference in the amount of filtered precipitate(s) formed for the case of an Mg anode versus no electrode in the cell. (Figure 3). Moreover, experiments using a Mg anode were repeated applying a higher current density (~90 mA/cm^2 versus ~3 mA/cm^2). As can be seen in Figures 3a and 3c, no appreciable differences of the amount of the filtered precipitate were observed. If the presence of Mg^+ is assumed to account for the reduction of permanganate, the increased applied current density would presumably result in up to 30 times as much MnO_2 or at the very least a visually significant increase in the amount of precipitate. Finally, no appreciable difference was noted when Pt was used as the electrode in the column instead of Mg.

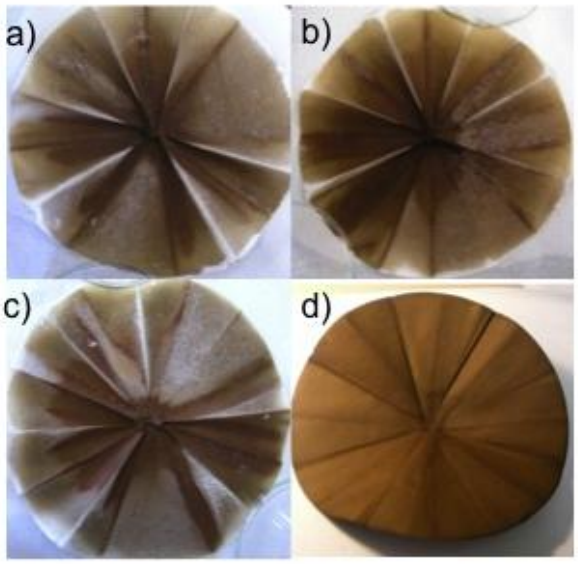

Figure 3. *Typical images of filter paper after experiments using $KMnO_4$ as oxidizing agent (gravity filtration). a) electrolysis using Mg anode, Na_2SO_4 as a switch electrolyte, applying 3mA/cm^2 of anodic current density, b) No electrode, c) electrolysis using Mg anode, Na_2SO_4 as a switch electrolyte, applying 90 mA/cm^2 of anodic current density, d) filtration of 150 ml of KMnO4 solution.*

To better qualify the identity of the resulting precipitates, Raman analysis was performed on the precipitates produced under each of the three conditions (Mg electrode, Pt electrode and no electrode). The resulting spectra (Figure 4) were remarkably similar. All three spectra displayed peaks at 380, 436, and 459 cm^{-1}, attributable to manganese oxides. The unresolved band between ~540 cm^{-1} and 725 cm^{-1} is also attributable to manganese oxide [27, 28]. Although this band was stronger in the spectrum of the precipitate obtained with the Mg anode, it is also present in the other two spectra. As noted above, the spectra of the precipitates were acquired with the same power but various integration times and, therefore, the intensity of peaks cannot be directly compared. Furthermore, all spectra displayed a strong, high baseline, likely due to fluorescence from permanganate ions.

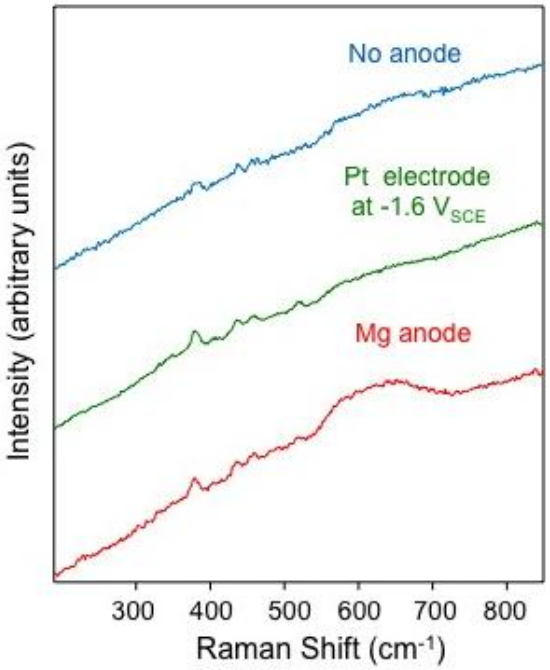

Figure 4. *Raman spectra of the filtered precipitates obtained in three different flow cells using $KMnO_4$ as oxidizing agent.*

In situ Raman Analysis.

To clarify the above results, *in situ* Raman analysis was performed to monitor molecular species present and generated at both an Mg and a Pt electrode immersed in saturated aqueous Na_2SO_4 under potential control. These results could then be used to establish possible species that were present in the flowing Na_2SO_4 during the flow cell experiments.

I) In situ Raman Analysis on Pt: Before the *in situ* experiments were undertaken, a Raman spectrum was acquired of the bulk Na_2SO_4 solution. As expected, this spectrum displayed one strong, sharp peak at 979 cm^{-1} attributable to the symmetric stretching mode of the sulfate ion [29]. Spectra were then acquired *in situ* at the surface of a Pt electrode in the Na_2SO_4 solution at approximately 30 s intervals during cathodic potentiodynamic polarization (Figure 5). The spectrum at OCP (+0.155 V_{SCE}) was identical to the bulk spectrum of the Na_2SO_4 solution and remained the same until the applied potential reached -1.34 V_{SCE}. At -1.34 V_{SCE}, a small peak appeared at 1120 cm^{-1}. As the scan continued, the 1120 cm^{-1} peak continued to increase in intensity and the sulfate peak at 979 cm^{-1} continued to decrease in intensity. The peak at 979 cm^{-1} disappeared when the potential reached -1.71 V_{SCE} and another peak at 580 cm^{-1} appeared, in addition to the one at 1120 cm^{-1}. One minute after completion of the scan,

when the potential control had been turned off, a spectrum acquired at the Pt surface showed only the strong 979 cm^{-1} sulfate peak, identical to the OCP spectrum shown at the top of Figure 5. Straightforward identification of the new peaks indicate that the 1120 cm^{-1} peak is attributable to SO_2, and the 580 cm^{-1} peak is attributable to $S_2O_4^{2-}$ [29].

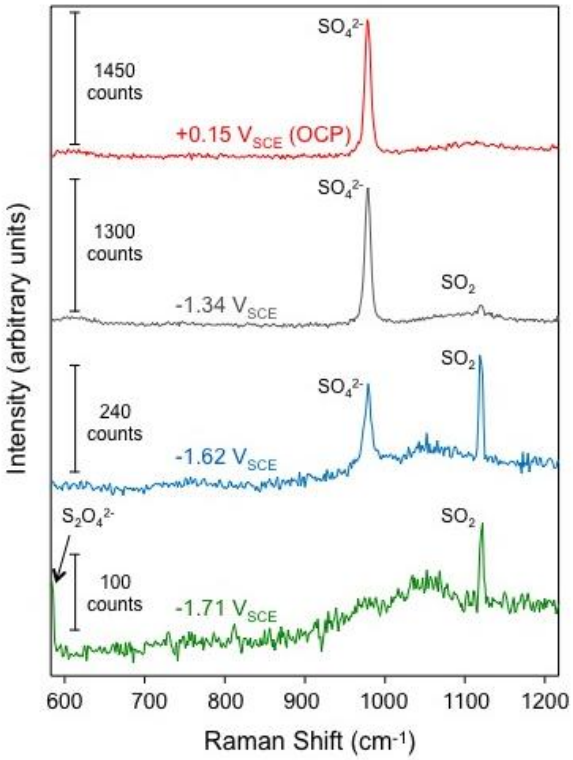

Figure 5. *In situ Raman spectra acquired during cathodic scan of Pt electrode in Na_2SO_4.*

II) In situ Raman Analysis on Mg: *In situ* Raman spectra were collected on an Mg electrode in the Na_2SO_4 solution during both anodic and cathodic polarization scans. Spectra acquired during the anodic scan (Figure 6) confirmed the presence of reduced sulfur species at the electrode. In fact, SO_2 was present at the Mg electrode at OCP (-1.90 V_{SCE}) before the scan even commenced.

It is interesting to note that during the initial steps of anodic polarization the ratio of the SO_4^{2-}/SO_2 peak areas increased as expected under anodic polarization. However, as the scan proceeded to more positive potentials, the spectra in Figure 6 indicate that more, not less, of the *reduced* product (SO_2) relative to the amount of SO_4^{2-} was present at the surface.

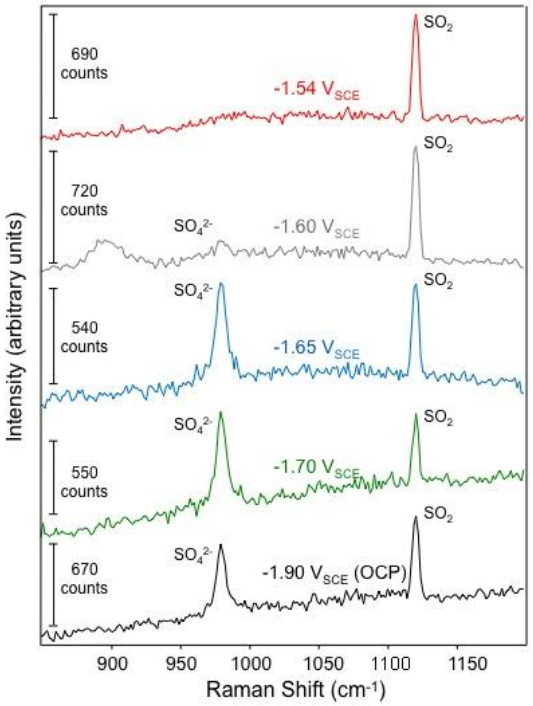

***Figure 6**. In situ Raman spectra acquired during anodic scan of Mg electrode in Na_2SO_4.*

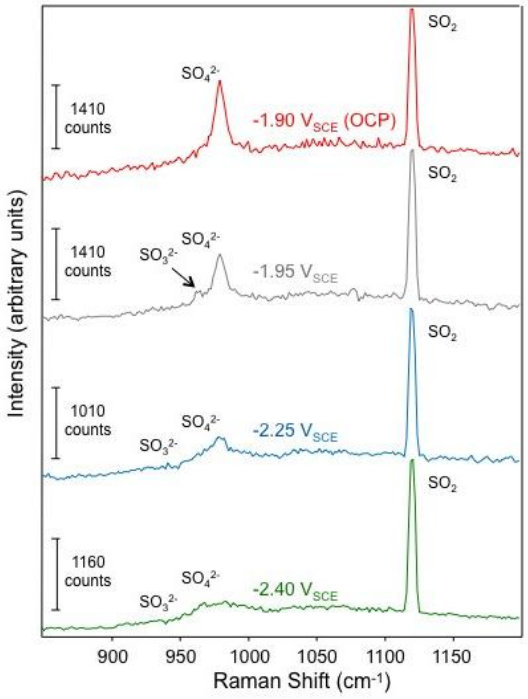

***Figure 7**. In situ Raman spectra acquired during cathodic scan of Mg electrode in Na_2SO_4.*

To further investigate species generated at an Mg electrode in a sulfate solution and perhaps obtain additional insight on the NDE, Raman spectra were also collected during a cathodic polarization scan on an Mg electrode in the sulfate solution. Some differences can be noted in the spectra taken during the cathodic scan (Figure 7) versus the anodic scan (Figure 6). As expected, the ratio of the peak area due to the reduced species (SO_2) to that of the sulfate ion continued to increase as the cathodic scan proceeded. Also of note was the presence of a peak at 963 cm^{-1}, attributable to SO_3^{2-} [29]. As the cathodic scan proceeded, this peak persisted, albeit as part of an unresolved band comprised of a combination of the 979 cm^{-1} sulfate peak and the 963 cm^{-1} sulfite peak.

Discussion

Reduction of $KMnO_4$. Petty made the somewhat reasonable assumptions that no reduction of $KMnO_4$ occurred as the result of transport across the cathode cell frit and that the flow action in the cell prevented the reduction of $KMnO_4$ arising from contact with the Mg anode. Therefore, some source of electrons must have been present in the flowing Na_2SO_4 solution, as this flow presented the only change to the contents of the beaker. Petty stated "no reduction products of sulfate ion have ever been detected in the anode compartment" [17]. However, even if this were true, the presence of other reducing species is possible, including contaminants, molecular hydrogen from the hydrogen evolution that certainly occurs on dissolving Mg by the NDE, pieces of Mg metal that survived filtration through the glass wool, or perhaps Mg^+. If the presence of a reductant other than Mg^+ can be established, then the existence of reduced manganese products is not evidence of the presence of Mg^+.

Petty reported "the amount of manganese dioxide isolated from the solution after electrolysis was definitely greater than the amount of manganese dioxide found when the original solution was filtered"[18]. In this respect, our results agree with Petty; visual observations of our filtered precipitate after electrolysis (Figure 3a) showed more precipitate than that of simply filtering the original $KMnO_4$ solution (Figure 3d). However, we did not observe more precipitate after electrolysis than in the "no electrode" cell (Figure 3b) and therefore it cannot be affirmed that the electrolysis on Mg leads to a significantly greater reduction of $KMnO_4$.

Using the Raman analysis performed on the precipitates produced under each of the three conditions (Mg electrode, Pt electrode and no electrode), it is possible to make a semi-quantitative comparison if the theoretical linear relationship between integration time and intensity is imposed. With that reasonable assumption, based on peak intensity, it is fair to say that the Pt and Mg electrodes produced the most manganese oxide products and the "no electrode" produced the least. Due to the exceptionally strong oxidizing power of the permanganate ion, these results are not surprising and merely confirm that the reduction of the permanganate ion is difficult to control in any laboratory experiment in which the permanganate ion is exposed and transferred through several steps.

In situ Raman Analysis. The spectra in Figure 5 confirm the reduction of sulfur from an oxidation state of 6+ to 4+ and 3+ in a potential range of -1.34 to -1.71 V_{SCE} at a Pt

electrode. It should be noted that IR drop in the solution was not corrected, so the real potentials at the Pt electrode were higher (less negative). Furthermore, the spectra in Figure 6 confirm the presence of reduced sulfur species at an Mg electrode in the potential range present in Petty's cell. These data strongly imply that reduced SO_4^{2-} species would have been generated in Petty's flow cell at the Mg electrode and that the source of these reduced species need not be attributed to the presence of Mg^+. These species would most certainly serve as reducing agents as they flowed into the permanganate solution and thereby dispel the conclusion that the only species that could have served as a reducing agent was Mg^+.

The following equations provide a redox sequence. At the Mg electrode, sulfate was reduced:

$$SO_4^{2-} + 2H_2O + 2e^- \rightarrow SO_2 + 4OH^- \qquad (1)$$

The standard potential for this reaction is -1.5 V_{SHE} or about -1.74 V_{SCE} [19]. Even though the conditions were not standard state, the reduction of sulfate is expected because the OCP of Mg is lower than this value. Sulfate reduction was observed at applied potentials as high as -1.54 V_{SCE}, which is above the standard potential. However, large ohmic potential drops were present and uncorrected for. Unfortunately, at higher potential values, the extent of hydrogen gas evolution was extreme and spectroscopic data could not be acquired, so the scan was halted.

SO_2 molecules that were generated at the Mg electrode and flowed with the solution could reduce permanganate in the bottom beaker:

$$2MnO_4^- + 3SO_2 + 4OH^- \rightarrow 2MnO_2 + 3SO_4^{2-} + 2H_2O \quad (2)$$

The standard potential for permanganate reduction is +0.59 V_{SHE} or about +0.35 V_{SCE} [19], which is significantly above the sulfate reduction potential so this reaction should go spontaneously to the right. During the Raman-monitored anodic polarization of Mg, copious hydrogen evolution was observed at the electrode. The large quantities of H_2 caused significant convection, which would be expected to result in a continual refreshment of the surface with the bulk sulfate solution. Even under these convective conditions, however, the reduced product, SO_2, dominated the spectra at more positive potentials (Figure 6). This increase in reduction of sulfate during anodic polarization of Mg is similar to that of enhanced hydrogen evolution observed under the same conditions. In other words, NDE involving sulfate reduction also occurs on Mg. This

phenomenon is specific to Mg, as the Pt electrode displayed the expected behavior of less reduced sulfate at higher applied potentials.

These results provide conclusive evidence of the presence of reduction products of SO_4^{2-} ions at the Mg electrode in the flow cell at a wide range of anodic potentials, including OCP. Although bubbles of SO_2 might be expected to rise in a static cell, individual SO_2 molecules (and probably SO_2 bubbles) would be swept into the flow of Petty's cell and would undoubtedly reduce permanganate ions in the beaker compartment of the flow cell. Furthermore, in all of the above experiments, hydrogen evolution proceeded with vigor at the Mg electrode. In Petty's flow cell, H_2 would also have been swept into the beaker and could have served as a reducing agent. Visual inspection of our flow cell experiments confirmed the flow of gaseous species into the beaker containing permanganate. Therefore, the claim that the flow of Mg^+ ions into the beaker compartment was the only possible explanation for the reduction of permanganate ions is invalid.

It should be noted that electron transfer reactions involving multiple electrons typically occur by a series of single electron steps [30]. In fact, gas phase studies have been undertaken on the transition from Mg^+ to Mg^{2+} [31, 32]. These studies were able to detect the exceptionally short-lived Mg^+ species *in the gas phase* with water at a pressure of 10^{-4} Torr. The stability involved solvation of an Mg^+ ion with a maximum of 5-6 water molecules. Attempts to maintain Mg^+ with greater amounts of solvation (higher water pressure) were unsuccessful and "consistent with theoretical calculations which show it is energetically favorable to form Mg^{2+} at higher degrees of solvation." [31]. These studies, therefore, provide strong evidence of the unlikelihood of the existence of Mg^+ in a bulk solution. Moreover, in recent studies using independent techniques such as atomic emission spectroscopy [33], the scanning vibrating electrode technique [34], and scanning electrochemical microscopy [35], researchers have not been able to detect the presence of Mg^+ and have reported that magnesium oxidizes via Mg^{2+} with no measureable lifetime for Mg^+. These sophisticated analytical observations suggest that Mg does indeed corrode via Mg^{2+} and are inconsistent with the transient existence of Mg^+.

The invalidity of the claim that Mg^+ was the only possible reducing agent to act on permanganate combined with the above-discussed literature investigations into the exceptionally short lifetime of Mg^+ species (generated under extreme conditions) casts serious doubt on any claims involving aqueous Mg^+ as a factor in the NDE.

Conclusions

In this work, an experiment that has been cited as evidence for the existence of Mg^+ [17] was repeated and investigated. The following conclusions can be made:

1. SO_4^{2-} was reduced to SO_2 on the surface of Mg at open circuit potential OCP (~-1.9 V_{SCE}) and under anodic and cathodic polarization mainly due to the low potential where Mg is dissolved. SO_2 will act as reducing agent in a solution containing MnO_4^{2-} ions. Hydrogen gas formed at the Mg surface might also reduce these ions. The existence of these species was not considered by Petty, who assumed that the only reducing agent that could have formed was Mg^+.

2. SO_4^{2-} was also reduced to SO_2 as well as to $S_2O_4^{2-}$ on Pt at low potentials (from ~-1.3 V_{SCE}), so the production of reducing species is not limited to Mg surfaces.

3. The rate of SO_4^{2-} reduction increased with increasing potential in a manner similar to the potential dependence of hydrogen evolution on Mg, which is known as the negative difference effect.

4. No appreciable differences in the amount of MnO_2 were detected after the electrolysis using a magnesium anode or just performing the experiment without a sample.

5. Because the existence of Mg^+ cannot be proven by this method, the Petty paper [17] should no longer be cited as clear evidence for the existence of Mg^+.

Acknowledgements

This work was partially supported by the Ministry of Economy and Competitiveness of Spain (MAT 2009-13530). Purchase of the Raman microprobe was supported by the National Science Foundation under Grant No. 0639163.

References

[1] W. Beetz, Philosophical Magazine, 1866, pp. 216 -269.
[2] P.F. King, Journal of the Electrochemical Society, 113 (1966) 536.
[3] W.J. James, M.E. Straumanis, B.K. Bhatia, J.W. Johnson, Journal of the Electrochemical Society, 110 (1963) 1117-1120.
[4] M.E. Straumanis, B.K. Bhatia, Journal of the Electrochemical Society, 110 (1963) 357-360.
[5] M.N. Hull, Journal of Electroanalytical Chemistry and Interfacial Electrochemistry, 38 (1972) A1-A4.
[6] H.H. Uhlig, R. Krutenat, Journal of the Electrochemical Society, 111 (1964) 1303-1306.
[7] G.G. Perrault, Journal of Electroanalytical Chemistry, 51 (1974) 107-119.
[8] G.G. Perrault, Journal of Electroanalytical Chemistry and Interfacial Electrochemistry, 27 (1970) 47-58.
[9] P.F. King, Journal of the Electrochemical Society, 110 (1963) 1113-1116.
[10] J.L. Robinson, P.F. King, Journal of the electrochemical society, 108 (1961) 36.
[11] S. Bender, J. Goellner, A. Heyn, S. Schmigalla, Materials and Corrosion- Werkstoffe Und Korrosion, 63 (2012) 707-712.
[12] G. Lee, J. Park, Geochimica Et Cosmochimica Acta, 102 (2013) 162-174.
[13] G.S. Frankel, A. Samaniego, N. Birbilis, Corrosion Science, 70 (2013) 104-111.
[14] N. Birbilis, A.D. King, S. Thomas, G.S. Frankel, J.R. Scully, Electrochimica Acta. (2014, "In press").
[15] M. Taheri, J.R. Kish, N. Birbilis, M. Danaie, E.A. McNally, J.R. McDermid, Electrochimica Acta, 116 (2014) 396-403.
[16] J.W. Turrentine, Journal of Physical Chemistry, 12 (1908) 448-467.
[17] R.L. Petty, A.W. Davidson, J. Kleinberg, Journal of the American Chemical Society, 76 (1954) 363-366.
[18] R. L. Petty. Thesis submitted in partial fulfillment of the requirements for the degree of Doctor of Philosophy, University of Kansas, (1953).
[19] M. Pourbaix, Atlas déquilibre electrochimiques, Gauthiers-Villars, Paris (1963).
[20] G.L. Song, A. Atrens, Advanced Engineering Materials, 1 (1999) 11-33.
[21] G. Baril, G. Galicia, C. Deslouis, N. Pebere, B. Tribollet, V. Vivier, Journal of the Electrochemical Society, 154 (2007) C108-C113.
[22] Web of science, http://apps.webofknowledge.com/CitationReport.do?product=UA&search_mode=CitationReport&SID=Q1QmCgjQ2iMcHwcHPWu&page=1&cr_pqid=10&viewType=summary.
[23] G. Song, A. Atrens, D. St John, X. Wu, J. Nairn, Corrosion Science, 39 (1997) 1981-2004.
[24] G. Baril, N. Pébère, Corrosion Science, 43 (2001) 471-484.
[25] M. Natta, Corrosion, 57 (2001) 712-720.
[26] G. Baril, C. Blanc, N. Pebere, Journal of the Electrochemical Society, 148 (2001) B489-B496.
[27] C. Julien, M. Massot, R. Baddour-Hadjean, S. Franger, S. Bach, J.P. Pereira- Ramos, Solid State Ionics, 159 (2003) 345-356.
[28] C.M. Julien, M. Massot, C. Poinsignon, Spectrochimica Acta Part a-Molecular and Biomolecular Spectroscopy, 60 (2004) 689-700.
[29] B. Meyer, M. Ospina, L.B. Peter, Analytica Chimica Acta, 117 (1980) 301-311.
[30] A.W. Bott, Current Separations, 16 (1997) 61-66.
[31] A.C. Harms, S.N. Khanna, A.B. Chen, A.W. Castleman, Journal of Chemical Physics, 100 (1994) 3540-3544.
[32] F. Misaizu, M. Sanekata, K. Tsukamoto, K. Fuke, S. Iwata, Journal of Physical Chemistry, 96 (1992) 8259-8264.
[33] J. Swiatowska, P. Volovitch, K. Ogle, Corrosion Science, 52 (2010) 2372-2378.
[34] G. Williams, H.N. McMurray, Journal of the Electrochemical Society, 155 (2008) C340-C349.
[35] R.M. Souto, A. Kiss, J. Izquierdo, L. Nagy, I. Bitter, G. Nagy, Electrochemistry Communications, 26 (2013) 25-28.

Evolution of Hydrogen at Dissolving Magnesium Surfaces

G.S. Frankel[1,2], A. Samaniego[2,3], and N. Birbilis[2]

[1]Fontana Corrosion Center, The Ohio State University, Columbus, OH USA
[2]Department of Materials Engineering Monash University, Clayton, VIC Australia
[3]Department of Materials Engineering, Corrosion and Durability, CENIM-CSIC, Madrid Spain

Corrosion Science 70 (2013) 104-111

Abstract

The origin of hydrogen evolved at dissolving magnesium surfaces, including those subjected to anodic polarisation, remains a topical issue. In this work, a critical appraisal of existing theories is presented, along with data from simultaneous polarisation and hydrogen collection tests. The observations invalidate mechanisms invoking the presence of univalent Mg^{+}. A combined experimental and thermodynamic analysis suggests that the ability of magnesium to support the cathodic reaction is enhanced during dissolution as the result of an increase in the exchange current density for the hydrogen evolution reaction, This mechanism can also explain high rates of hydrogen evolution in aluminium pits.

Keywords: A. Magnesium B. Galvanostatic C. Anodic dissolution

Introduction

Magnesium dissolution in aqueous solutions is accompanied by copious hydrogen evolution (HE). The potentials at which Mg dissolves are sufficiently low that HE dominates oxygen reduction at all values of pH. Mg and all its alloys generally exhibit open circuit potential values less than about -1.45 V_{SCE} in aqueous solutions [1-3]. HE continues at a significant rate even when an Mg sample is anodically polarised above its corrosion potential [4-7]. An interesting observation associated with this process is that the rate of HE often increases as the anodic polarisation of the Mg surface increases [4-7]. According to standard electrochemical kinetics, the rate of a cathodic reaction like HE from the reduction of hydronium ions or water should decrease exponentially, rather than increase, with increasing potential.

Assuming that Mg dissolves to form the divalent Mg^{2+} ion accompanied by HE from the reduction of water, the reactions involved are:

$$Mg \rightarrow Mg^{2+} + 2e^- \qquad (1)$$

$$2H_2O + 2e^- \rightarrow H_2 + 2OH^- \qquad (2)$$

The rates or current densities associated with Reactions 1 and 2 are defined as i_a and i_c, respectively. Under open circuit conditions, the anodic reaction of Mg dissolution is balanced by an equal rate of HE, such that $i_a = i_c$. Under anodic polarisation conditions, where a potentiostat is used to supply an external anodic current to an Mg electrode, Mg dissolution will occur at a higher rate than at OCP arising from the anodic polarisation. The average rate of dissolution during the polarisation time under anodic conditions can be assessed from the sample mass loss using Faraday's law [8]. Because of continued HE during anodic polarisation, the average net current supplied to the electrode by the potentiostat, i_{net}, will be less than the dissolution or anodic current density. In other words, some of the electrons generated by Mg dissolution are consumed by HE on the electrode surface rather than flowing through the potentiostat. So at an applied anodic potential or applied anodic current density, the net current density is the difference of the total anodic and cathodic current densities (assuming the area for both the anodic and cathodic reactions is the nominal exposed area):

$$i_{net} = i_a - i_c \qquad (3)$$

According to activation-controlled kinetics for the HE reaction, i_c should decrease as the applied potential increases. However, the rate of HE has been observed to increase as the applied anodic current and potential increase. In the context of Mg dissolution, this phenomenon whereby "cathodic hydrogen evolution" occurs on Mg well above open circuit potential and even when anodic potentials or currents are imposed, is often referred to as the "Negative Difference Effect" and has been discussed by numerous studies in recent years [4, 6, 7, 9, 10]. To explain why the rate of HE increases with increasing potential, Song and Atrens invoked the existence of an Mg^+ intermediate [6], which is a notion that had been put forward in 1954 by Petty et al. [11]. In this explanation, it is assumed that Mg metal dissolves to form univalent Mg^+ ions, not divalent Mg^{2+} ions:

$$Mg \rightarrow Mg^+ + e^- \qquad (3)$$

It is further presumed that some fraction of the Mg+ ions exists long enough to disengage from the surface and enter the solution at which point they are homogeneously oxidised by water in solution to hydrogen according to this chemical reaction:

$$Mg^+ + H_2O \rightarrow Mg^{2+} \tfrac{1}{2} H_2 + OH^- \qquad (4)$$

If the rate of univalent Mg ion production increases with increasing Mg dissolution rate, this mechanism would account for the observation of increasing rates of hydrogen evolution with increased applied current or potential under certain conditions. Although not explicitly stated in papers describing the mechanism involving univalent Mg ion [6], this assumption can be supported by the fact that single-step reactions rarely occur in electrochemistry, particularly for multi-electron reactions [12]. However, the existence of Mg^+ has never been verified.

Whether Mg oxidation occurs solely on the Mg electrode surface accompanied by HE as in Eqns 1 and 2 or forms Mg+ that is oxidised just away from the surface according to Eqns 3 and 4 is a fine distinction, but one that has significant implications for the proposed mechanism. Note that, while multi-electron reactions tend to occur by a combination of single electron steps, it is also known that electrochemical charge-transfer reactions occur much easier heterogeneously on catalytic surfaces than homogeneously in solution owing to the lower likelihood of collision of reactants in solution than with an electrode surface and the role of the potential drop at the interface

[12]. This would indicate that the unstable Mg^+ ion should oxidise readily on the electrode surface, although the rate of the reaction will depend on several factors including the catalytic properties of the surface, as will be described below.

The only published evidence for the sustained existence of Mg^+ in solution is in the paper by Petty et al. [11]. They flowed electrolyte past an Mg electrode polarised anodically and then into another vessel containing oxidised ionic species such as Ag^+ or MnO_4^-. The paper states that reduced forms of the species, metallic silver or MnO_2, respectively, were then qualitatively found in the bulk solution. No data, spectroscopy, or further details were provided, but the authors suggested that Mg^+ ions formed at the Mg electrode were transported into the second vessel and reduced the oxidised species. The work by Atrens and coworkers provides no direct evidence for the existence of Mg^+, only indirect evidence indicating that the observations are consistent with the formation of univalent Mg [4-7]. The real issue with the HE observed at dissolving Mg electrodes is not that it occurs (HE should occur on even on anodically polarised Mg because the potential is below the reversible potential for HE), but rather explaining why the rate of HE increases with increasing potential. The mechanism involving univalent Mg must consider that (significantly) more Mg^+ is produced as the total rate of Mg dissolution increases. Because there is no evidence for Mg^+ existence, there is no evidence for the increase in its production with potential.

In their early work on this topic, Song and Atrens discussed and then eventually discarded other mechanisms that might explain the increased rate of HE with potential [6, 7]. One mechanism involves the undermining and dislodging of second phase particles during dissolution, and then dissolution of these particles, which would result in HE. However, the phenomenon is also observed with very pure Mg so this undermining mechanism is unlikely, this unlikelihood recently validated by video imaging [13]. Another mechanism discussed by Atrens is the anodic formation of magnesium hydride, which then decomposes to form hydrogen gas [7]. However, this process also involves cathodic reactions, which should decrease in rate with increasing potential.

Atrens and colleagues presented a detailed model based on potential-varying surface coverage of an apparently protective oxide film in which they reported “can explain all the experimental measurements” [7]. The model considers the partial currents for the anodic and cathodic reactions assuming Tafel behavior, but that the reactions are blocked on the fraction of the surface covered by oxide film, θ. Assuming that θ

decreases with increasing potential, the rate of the cathodic HE reaction can increase with increasing potential even though the overpotential for the reaction decreases. The data in the paper shown to match the model were measured for dissolution of Mg in a neutral NaCl solution. In a closely following paper [6], Atrens et al. rejected the oxide surface coverage model because the increased HE phenomenon was also found in acidic HCl and H_2SO_4 solutions, where it was assumed that film formation on the Mg surface is not possible. As a result, over the past decade, the papers by Atrens and coworkers, along with several other researchers, have focused on the univalent Mg mechanism [4, 6, 7, 9, 14-17], despite the continued lack of evidence for the existence of Mg^+, supposedly because it has been the only model that can explain their experimental data. However, recent careful analyses have indicated that Mg dissolves with a stoichiometry of n = 2 [18, 19].

In this paper, we propose a simple explanation for the higher rate of HE based on increasing exchange current density for HE with increasing Mg dissolution rate. Additionally, experiments to measure the rate of HE at applied anodic current densities, similar to those that have been reported previously, are repeated and presented.

Experimental

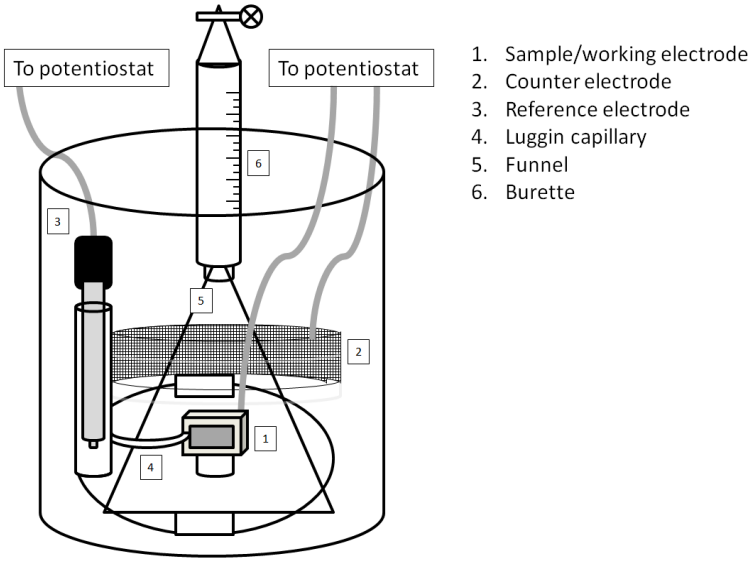

Figure 1. *Schematic of the setup for hydrogen gas collection during galvanostatic polarisation.*

Ultra high purity Mg (99.99%, Timminco, ON, Canada) with <10 ppm Fe was used. Prior to testing, samples were ground to 2000 grit and an insulated copper wire was attached to the rear of mounted specimens. The test assembly, shown schematically in Figure 1, allowed simultaneous application of a polarising signal along with real-time hydrogen collection. The exposed surface had a total area of about 3.5 cm^2. The experimental difficulties and limitations of such tests were recently documented [20].

A LIDA™ mixed metal oxide coated titanium mesh counter electrode (composed of pure Ti mesh with an applied coating of platinum group metal oxides) was used, along with a saturated calomel reference electrode. Approximately 1.6 l of 0.1 M NaCl was used as the electrolyte. Samples were polarised using a BioLogic® VMP 3 potentiostat under control of EC-Lab 10.17 software (BioLogic Inc., TN, USA).

Results

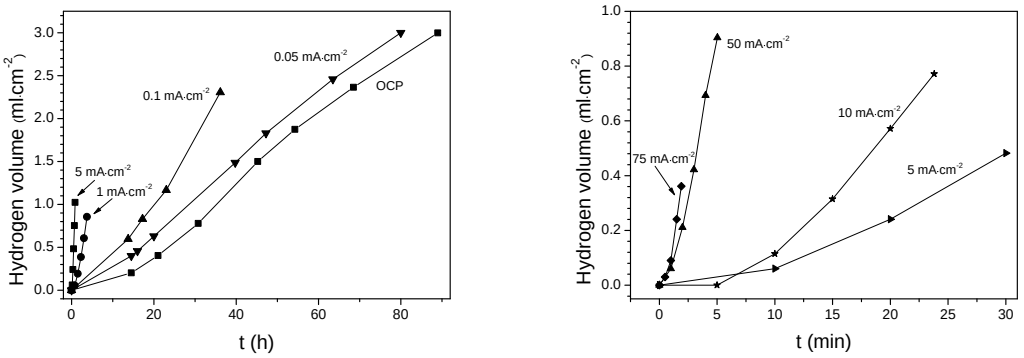

Figure 2. *Volume of hydrogen collected for different applied anodic current densities as a function of time. a) low current densities, b) high current densities. These data represent typical results from replicated experiments.*

Figure 2 shows the volume of hydrogen gas measured as a function of time for different applied anodic current densities. The slopes are relatively linear, and are shown in Figure 3 as the rate of hydrogen evolution as a function of the applied current density over the range of -10 to +75 mA/cm^2. In the cathodic region where negative currents are applied, the HE rate decreases as the applied cathodic current density decreases. The HE rate reaches a minimum at the open circuit potential when the applied current is zero, and then increases as the applied anodic current density increases. These observations are similar to those presented previously [16]. The amount of hydrogen is greater for a given cathodic current density than for an anodic current density of the same magnitude. However, the rate of HE in the anodic region is very large considering

that the polarity of the applied potential is opposite of that for the HE reduction reaction.

The potential was measured during the galvanostatic experiments, and the rate of hydrogen evolution is plotted in Figure 4 on a log scale as a function of the measured potential. These values of potential are not corrected for ohmic potential drop. The effects of ohmic potential drop on these plots are discussed below.

Figure 5 shows the galvanostatic polarisation curve plotted using the applied current densities and the measured potentials, as collected from individual galvanostatic measurements (not corrected for ohmic potential drops). Note that the potentials were measured for different applied currents, but the plot is presented in the reverse fashion to be consistent with the previous plot.

Discussion

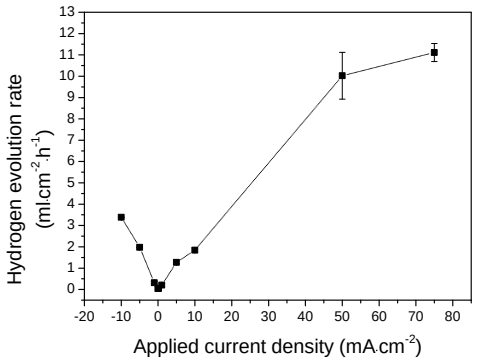

Figure 3. *Rate of hydrogen production as a function of applied current density.*

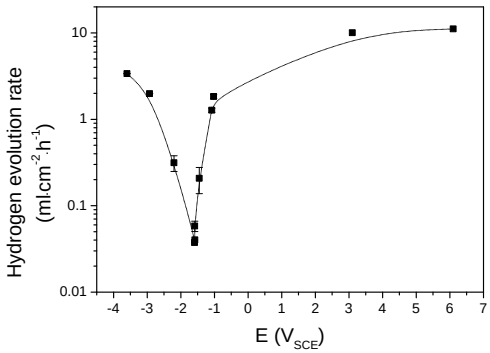

Figure 4*. Rate of hydrogen production as a function of measured potential, uncorrected for ohmic potential drop. The curve was added as an aide-to-the-eye.*

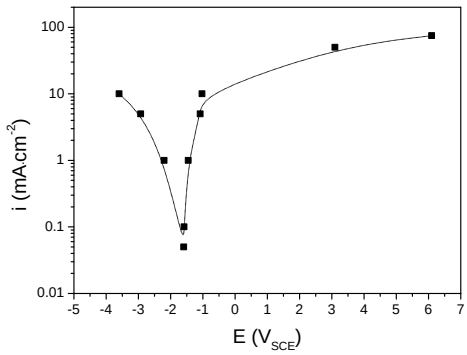

Figure 5. *Polarization curve determined from steady state galvanostatic current measurements. Note that the potential is not corrected for ohmic potential drop. The curve was added as an aide-to-the-eye.*

The results in Figure 3 show that the rate of hydrogen evolution increases with increasing potential, but only at potentials above the OCP where the rate of Mg dissolution is high. In the cathodic region, the expected Tafel behaviour is observed, as shown in Figure 4.

The extent of increase in the HE rate actually should be evaluated by comparison with the expected rate at a given potential based on extrapolation of the cathodic Tafel behaviour. However, to make this comparison, the ohmic potential drop must first be assessed. Based on current interrupt measurements made in separate experiments, it is expected that the ohmic resistance varied from about 10 to 25 ohms over the range of current applied. Larger resistances were found at the large applied currents because of the copious hydrogen bubble production at the surface. For an applied current density of 10 mA/cm^2, the current was about 35 mA, and the ohmic potential drop was about 350 mV. This would bring the point at -10 mA/cm^2 almost in line with the other cathodic points in the semilog plot, which is reasonable because the hydrogen evolution rate is equivalent to a current density and Tafel kinetics are expected on the cathodic side. For the applied current densities of 50 and 75 mA/cm^2, or currents of 170 and 250 mA, respectively, the ohmic potential drop was over about 4 and 6 V, respectively. Considering these large ohmic potential drops, the data points for 50 and 75 mA/cm^2 would be positioned in the region of -1 to 0 V SCE, which is along the extrapolated anodic Tafel region.

Extrapolating the cathodic Tafel region to the ohmically-corrected potentials measured during application of anodic currents, the expected rate of HE would be expected to be less than 0.01 ml/cm^{2}h or on the order of 0.025 mA/cm^2. These values are about 3 orders of magnitude lower than the measured values of HE at those ohmically-corrected potentials. As mentioned above, the challenge is to explain why the rate of HE is so high in this region. A new proposed mechanism is given below.

Figure 6 shows that, even though the rate of HE increased with increasing applied current density and potential, the total amount of hydrogen generated decreased for these experiments in which 50 C of charge was passed. The hydrogen volume can be converted to a charge, and the axis on the right side of Figure 6 shows the normalised hydrogen charge. The hydrogen charge for the lowest anodic current is greater than the anodic charge passed because the net anodic current was small compared to the open circuit corrosion current, so the amount of dissolution was much greater than the anodic charge applied.

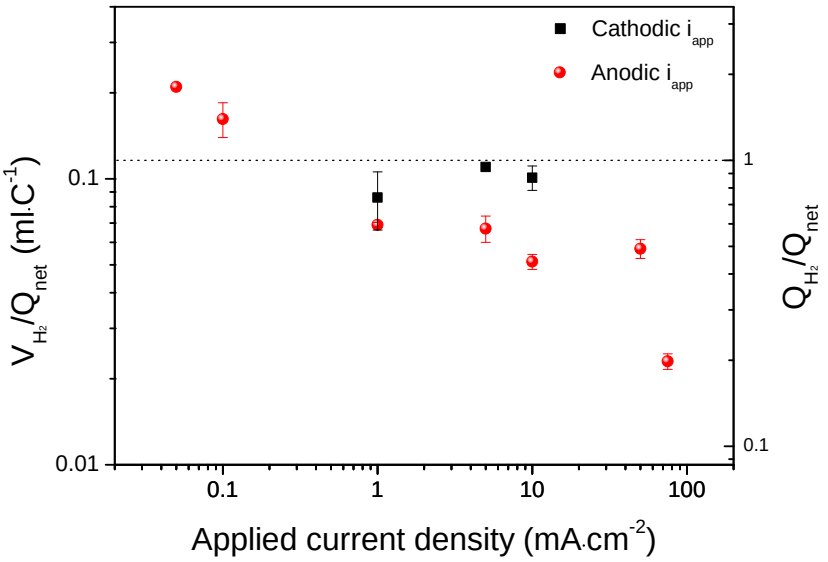

Figure 6. *Volume of hydrogen produced normalised to the net charge. Right hand axis shows the charge associated with the hydrogen production normalised to the net charge. The net charge for all experiments was 50 C. The dashed line is given to facilitate comparison with a charge ratio of 1.*

The amount of hydrogen generated for applied cathodic currents was approximately equal to the applied or net charge passed (the normalised charge was close to unity). This indicates that the hydrogen collection efficiency was quite good. However, during the course of the experiment, hydrogen bubbles collected on the funnel and burette surfaces, so the collection efficiency was certainly less than 100%. Furthermore, it is expected that some hydrogen was absorbed into the Mg metal, however analysis of this was neglected.

The normalised amount of hydrogen evolution decreased to about 20% of the net applied anodic charge at the highest applied current density of 75 mA/cm^2 even though the HE rate continued to increase. The trend of decreasing hydrogen volume for a given net anodic charge suggests that the HE rate might start to decrease at sufficiently-high applied anodic current densities and potentials. It is expected that HE should cease when the IR-corrected potential exceeded the reversible potential for the HE reaction (HER), $E_{rev,HER.}$ However, that point was not observed in this work, and, as described below, it might not be possible to apply a sufficiently high Mg dissolution rate to polarise to that potential.

It should be noted that a limitation on the amount of hydrogen evolved is not a criterion or possibility for the theories purporting the existence of Mg^{+}. In such theories, as the hydrogen is evolved from a chemical reaction, the amount of hydrogen evolved ideally should scale with the amount of Mg^{+} produced. This would suggest that for a fixed anodic charge (of any current density), the total amount of hydrogen should be identical. The experimental evidence therefore suggests this is a major weakness or flaw in any theory purporting existence of Mg^{+}.

Effect of Hydrogen Evolution Kinetics

As described above, the data for increasing rates of HE with increasing potential could be consistent with the notion of univalent Mg formation, even though this species has never been found. However, the decreasing amount of hydrogen evolved with increasing applied currents for a given anodic charge indicates that the mechanism for HE does not involve univalent Mg. An alternative explanation for this observation is that the kinetics of the HER at a dissolving Mg surface increase owing to changes in thermodynamic or kinetic factors. Assuming activation-controlled kinetics, the Tafel equation can be used to describe the HER rate at an Mg surface because the potential, E, is far from the reversible potential for HER, $E_{rev,HER}$:

$$i_{HER} = i_{0,HERonMg} 10^{\left(\frac{-(E-E_{rev,HER})}{b}\right)} \quad (5)$$

where i_{HER} is the current density associated with the HER at any potential, $i_{0,HERonMg}$ is the exchange current density for HER on the Mg surface, and b is the Tafel slope. For fixed values of E_{rev}, i_0, and b, the rate of HER should decrease exponentially as E increases. The fact that the HER rate in fact increases as E increases is the definition of the phenomenon of interest here.

The increased rate of HER at higher potentials might be caused by changes in values of the parameters in Eqn. 5, i.e. E_{rev}, i_0, and b, which are typically considered to be independent of potential. In other words, it is possible that, as the Mg dissolution rate increases, one or more of these values change in a way that results in an increase in HER rate at higher potential.

A recent paper by Bender et al. suggests that the HER rate increases with increasing Mg corrosion because of hydrolysis of the Mg ions, which increases the local acidity and

forces the HER toward more hydrogen evolution (the forward direction in Eqn 4) owing to LeChatelier's principle [10]. This notion merits further analysis. The suggestion made by Bender et al. [10] can be advanced by considering the hydrolysis of the Mg^{2+} ion, which can occur by the following reactions:

$$Mg^{2+} + H_2O = Mg(OH)^{+} + H^{+} \qquad (6)$$
$$Mg^{2+} + 2OH^{-} = Mg(OH)_2\,(s) \qquad (7)$$

According to Baes and Mesmer, hydrolysis in solutions with high concentrations of Mg^{2+} ion occurs according to the following reaction [21]:

$$4Mg^{2+} + 4H_2O = Mg_4(OH)_4{}^{4+} + 4H \qquad (8)$$

The equilibrium constants for reactions 6, 7, and 8 are $10^{-11.44}$, $10^{11.15}$, and $10^{-39.75}$, respectively [21]. The magnitude of these constants explains the alkaline nature of the Mg ion, and suggests that the extent of hydrolysis and the subsequent effect on the HER are low. Determination of the H^{+} concentration requires knowledge of the thermodynamic properties of all the species.

A speciation calculation was performed with the Stream Analyzer software package from OLI Systems, and the results are shown in Table 1. The natural pH was determined for solutions with varying $MgCl_2$ concentrations and then the Mg ion speciation was determined at those natural pH values. O_2 and CO_2 were assumed not to be present because it is likely that the solution near a Mg sample is deaerated by the copious hydrogen evolution. The convection associated with this bubble formation, which was quite vigorous at the highest rates, would also prevent the surface Mg^{2+} ion concentration from increasing to very high values. The results show that the acidity increases with increasing Mg^{2+} ion concentration, as suggested by Bender et al. [10]. However, the increase is small owing to buffering by the Mg ions. The pH changes by only about 2 units as the concentration of $MgCl_2$ increases to saturation at 5.7 M. It should be noted that the software database did not include the $Mg_4(OH)_4{}^{4+}$ ion and so does not appear in Table 1. $Mg(OH)_2$ is in the database, but was only found to occur at pH > 8.5. The vigorous hydrogen evolution at the Mg electrodes with high applied anodic current likely created convection that would prevent the surface concentration from increasing to very high values.

Table 1. *Concentration of species (M) in $MgCl_2$ solutions of different concentrations at their natural pH values.*

$[MgCl_2]$ (M)	Natural pH	$[H^+]$ (M)	$[Mg^{2+}]$ (M)	$[MgOH^+]$ (M)	$[MgCl_2.6H_2O]$ (M)
0.1	6.62	3.28×10^{-7}	0.1	2.70×10^{-7}	0
0.2	6.51	4.35×10^{-7}	0.2	3.84×10^{-7}	0
0.3	6.43	5.15×10^{-7}	0.3	4.74×10^{-7}	0
0.4	6.37	5.84×10^{-7}	0.4	5.49×10^{-7}	0
0.5	6.31	6.40×10^{-7}	0.5	6.19×10^{-7}	0
0.6	6.26	6.98×10^{-7}	0.6	6.78×10^{-7}	0
0.7	6.21	7.48×10^{-7}	0.7	7.38×10^{-7}	0
0.8	6.16	7.99×10^{-7}	0.8	7.92×10^{-7}	0
0.9	6.11	8.52×10^{-7}	0.9	8.42×10^{-7}	0
1.0	6.06	8.95×10^{-7}	1	8.98×10^{-7}	0
1.1	6.02	9.29×10^{-7}	1.1	9.64×10^{-7}	0
1.2	5.98	9.73×10^{-7}	1.2	1.02×10^{-6}	0
1.3	5.94	1.01×10^{-6}	1.3	1.08×10^{-6}	0
1.4	5.89	1.05×10^{-6}	1.4	1.13×10^{-6}	0
1.5	5.85	1.09×10^{-6}	1.5	1.20×10^{-6}	0
1.6	5.81	1.24×10^{-6}	1.6	1.14×10^{-6}	0
1.7	5.77	1.17×10^{-6}	1.7	1.31×10^{-6}	0
1.8	5.73	1.20×10^{-6}	1.8	1.38×10^{-6}	0
1.9	5.69	1.24×10^{-6}	1.9	1.44×10^{-6}	0
2.0	5.65	1.27×10^{-6}	2.0	1.50×10^{-6}	0
2.5	5.50	1.29×10^{-6}	2.5	2.07×10^{-6}	0
3.0	5.27	1.57×10^{-6}	3.0	2.26×10^{-6}	0
3.5	5.10	1.67×10^{-6}	3.5	2.75×10^{-6}	0
4.0	4.94	1.74×10^{-6}	4	3.32×10^{-6}	0
4.5	4.79	1.78×10^{-6}	4.5	3.99×10^{-6}	0
5.0	4.65	1.79×10^{-6}	5	4.77×10^{-6}	0
5.1	4.62	1.91×10^{-6}	5	4.46×10^{-6}	0.1
5.2	4.59	2.05×10^{-6}	5	4.17×10^{-6}	0.2
5.3	4.56	2.20×10^{-6}	5	3.89×10^{-6}	0.3
5.4	4.54	2.30×10^{-6}	5	3.71×10^{-6}	0.4
5.5	4.51	2.46×10^{-6}	5	3.47×10^{-6}	0.5
5.6	4.48	2.64×10^{-6}	5	3.23×10^{-6}	0.6
5.7	4.46	2.76×10^{-6}	5	3.09×10^{-6}	0.7

According to the Nernst Equation for the HER, E_{rev} will increase by 0.059 V for each unit decrease in pH. Furthermore, according to the Tafel kinetics shown in Eqn. 4, the rate of HER at a given potential will increase for each pH unit decrease by $10^{(0.059/b)}$. Potentiodynamic polarisation curves measured on this pure Mg (not shown here) indicated Tafel slopes of about -0.26 V/dec. Values of cathodic Tafel slopes taken from recently published polarisation curves on Mg [2, 22, 23] indicate an average value of about -0.3 V/dec. It should be noted that reasons for the high values of Tafel slope for HE on Mg have not been provided in the literature. Assuming a Tafel slope of -0.3 V/dec, the maximum increase in the rate of HER caused by the increase in E_{rev} (at saturation) would be a factor of 1.5. As described above, this is much less than the increase in the rate of HER compared to the expected value from the extrapolated cathodic Tafel region. Therefore, the effect of hydrolysis on the HER rate through changes in E_{rev} can only account for a small part of the very high HER rates observed.

The true area of the electrode will increase because of Mg dissolution. This increase in true area will result in an increase in nominal current density determined with the nominal exposed area. However, it is not possible for any increase in area to account for the large increase in the rate of the HER observed during anodic dissolution of Mg.

A Model for Increasing Anodic HE Based on Increasing Exchange Current Density

As mentioned above, it is possible that changes in E_{rev}, i_0, or b might cause the rate of HE to increase with increasing potential. Increases in E_{rev} were shown to have only a small effect. It is possible that the Tafel slope b for the HER changes as the rate of Mg dissolution increases. However, there is no basis to expect such behaviour. On the other hand, the rate of HER could also increase if the exchange current density increased with increasing potential, and a rationale for such behaviour can be provided, as discussed below.

Consider now that the catalytic activity of the dissolving Mg surface for the HE reaction, as embodied by the exchange current density, $i_{0,HERonMg}$, increases as the rate of Mg dissolution increases. The catalytic activity of a surface is known to have a huge impact on the rate of HE, with $i_{0,HER}$ varying for different pure metals from the range of 10^{-3} A/cm^2 for the Pt-group metals, the best-known catalysts, to the range of 10^{-12} A/cm^2 for noncatalytic metals like Hg and Pb [12].

The primary assumption here is that the catalytic nature of the dissolving Mg surface, and thus $i_{0,HER}$, increase with increasing Mg dissolution rate, without considering partial coverage of the surface by an oxide film. This assumption could result in an increasing rate of HE with increasing potential if the variation of $i_{0,HER}$ were larger than the effect of the exponential term in Equation 5.

A fundamental assumption underlying the mixed potential theory of corrosion is the independence of the anodic and cathodic half reactions [24]. However, there are instances where the half reactions can affect each other. For example, the anodic region of a potentiodynamic polarisation curve for Al and its alloys will be altered if the scan is initiated in the cathodic region owing to cathodic corrosion from cathodically produced OH^- ions. A related phenomenon occurs in Mg alloys in which the surface passivity is enhanced by the alkalisation of the local electrolyte during the cathodic polarisation. We are proposing here that the kinetics of HE are affected by the rate of Mg anodic dissolution. The phenomenon is shown schematically in Figure 7. A series of cathodic polarisation lines representing HE kinetics is overlaid onto a line representing Mg dissolution. The reversible potential for HE was shown above to increase as a result of Mg ion hydrolysis, but is assumed here to be invariant for simplicity. When the Mg dissolution rate is low, including the cathodic region of the polarisation curve, $i_{0,HER}$ is assumed to be relatively unchanged. However, it is posited that $i_{0,HER}$ increases from $i_{0,HER,1}$ to $i_{0,HER,4}$ as the rate of Mg dissolution increases from i_1 to i_4. As a result of this increase, the rate of HE at any given potential is higher than what it would have been if the catalytic nature of the surface were unchanged. The effective HE polarisation curve, given as a bold line in the figure, reaches a minimum and then increases as the rate of Mg dissolution increases with potential.

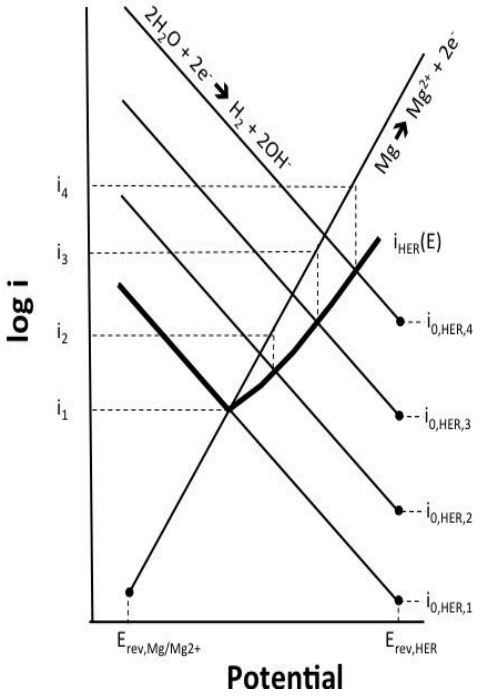

Figure 7. *Schematic Evans diagram explaining the increase of HER with increasing potential by the effects of exchange current density for HER changing as the Mg dissolution rate changes. The bold line represents the HE current density as a function of potential.*

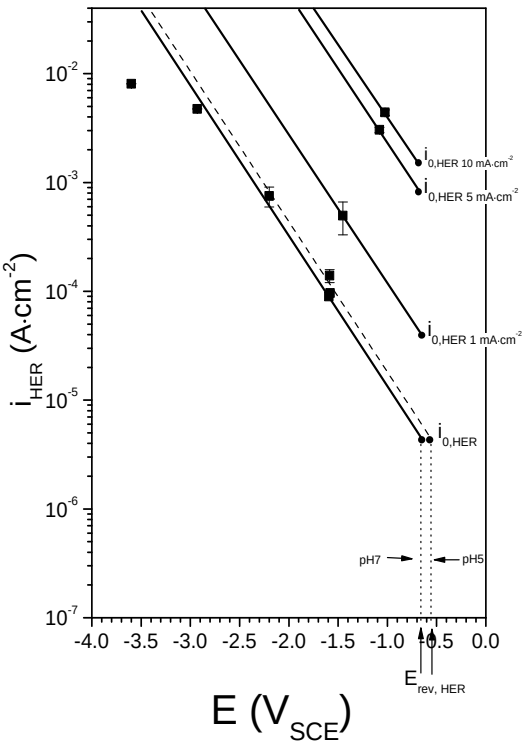

Figure 8. *Overlay of Tafel slopes onto data taken from Figure 4 and converted to hydrogen evolution current density as a function of the potential. The effects of changing $E_{rev,HER}$ associated with a decrease change in pH from hydrolysis and changing $i_{o,HERonMg}$ associated with a change in the catalytic nature of the surface are indicated.*

Mg is an extremely reactive metal, and will oxidise readily upon exposure to a small amount of oxygen gas. It is reasonable that such a reactive surface could also be catalytic toward other reactions, such as HE, and that the catalytic nature of a metallic surface could change with the rate of metal dissolution. The exact nature of the catalytic surface is unknown at this time, and other evidence for the catalytic nature of the surface is not available. However, standard methods exist to assess the catalytic properties of surfaces [25].

The magnitude of the increase in $i_{0,HER}$ can be assessed by applying the analysis shown in Figure 7 to the data shown in Figure 4. The data points in Figure 8 are those from Figure 4 in a potential range close to the OCP where ohmic effects are minimised, with the hydrogen generation rate converted to current density. A line fitted to the cathodic part of the curve (where cathodic net currents were applied) results in a Tafel slope of -0.75 V/dec. The reason for this high value of *b* is not known. Extrapolation of this Tafel line to $E_{rev,HER}$, which is -0.413 V_{SHE} = -0.653 V_{SCE} assuming that the solution at the

electrode is deaerated and pH = 7, provides $i_{o,HERonMg}$ in the cathodic part of the curve, about 4 x 10^{-6} A/cm^2. This is actually a rather high value of exchange current density.

The effect of a decrease in pH of 2 units to pH 5 associated with hydrolysis at saturation, which is a maximum possible change, is shown by a shift in the line to the somewhat higher value of $E_{rev,HER}$. As mentioned, convection will likely prevent such a large increase in Mg ion concentration. Furthermore, the continued HER at the Mg surface will balance out this pH change to an extent. Nonetheless, this maximum change is seen to be small.

Ignoring the effect of any pH change and assuming *b* is constant, the Tafel line can be shifted upward reflecting the increases in $i_{o,HERonMg}$ that would provide the values of hydrogen generation or i_{HER} measured during anodic polarisation. The $i_{o,HERonMg}$ values are seen to be 4 x 10^{-5}, 8 x 10^{-4}, and 1.5 x 10^{-3} A/cm^2 for applied current densities of 1, 5, and 10 mA/cm^2, respectively.

This mechanism might be applicable to other metals. A similar situation exists for Al and Al alloys, which also evolve hydrogen during active dissolution such as at the bottom of a pit. Al surfaces, like Mg, are thought to have low $i_{0,HER}$, but active Al pits continually evolve hydrogen gas and only stop when the pit repassivates. Hydrogen gas generation is not observed on the nearby passive surface, which is at a potential only slightly higher than the pit bottom and certainly still below $E_{rev,HER}$. The reason for the higher rate of HE is probably the catalytic nature of the actively dissolving Al pit surface relative to the passive surface, despite differences in the local solution composition. The rate of HE can be easily determined from analysis of the dissolution rate of thin film Al electrodes, and was found to be about 15-20% of the anodic dissolution rates even at high applied anodic potentials [26]. This situation is identical to that observed during Mg dissolution; the potential at an actively dissolving Al pit surface is well below $E_{rev,HER}$, and the actively dissolving surface is very catalytic. It is possible that a lower-valent Al ion such as Al^+ or Al^{2+} could form and account for the high rate of HE at anodic potentials, but there is no evidence for stable formation of these ions either. For Al thin films, the dissolution current density is typically extremely high, on the order of tens of A/cm^2, which means that the rate of HE is also extremely high, on the order of A/cm^2. This value is much greater than the current densities applied to the much larger electrode in this study, but indicates the unlikelihood of polarising the Mg to a potential where HE would stop, above $E_{rev,HER}$.

The increased exchange current density mechanism could be more broadly applicable to other active metals such as Fe, which also dissolves at potentials below the HE reversible potential. However, Mg and Al are so active that the potentials at which they dissolve are far below $E_{rev,HER}$ and the effect is magnified compared to other less active metals.

Conclusions

1. Hydrogen gas was collected from Mg surfaces polarised galvanostatically in 0.1 M NaCl solution over a range of anodic and cathodic current densities. The rate of hydrogen evolution was minimum at the open circuit potential, and increased with increasing applied anodic or cathodic current.

2. The total amount of hydrogen collected for a fixed applied charge was not the same with increasing current density. The total amount of hydrogen collected was observed to decrease with increasing current density, which would invalidate any assertions of the existence of Mg^{+} on the basis that the amount of hydrogen evolved should be identical for the same amount of Mg^{+} formed.

3. A mechanism explaining the increased rate of hydrogen evolution with increasing anodic potential was proposed in which the exchange current density for the hydrogen evolution reaction was assumed to increase as the rate of Mg dissolution increases. An analysis suggests that this value might increase by many orders of magnitude as the applied anodic current density increases.

4. This mechanism, describing an increase in the catalytic nature of the metal surface during dissolution, might also explain the high rate of hydrogen evolution in actively dissolving Al pits.

Acknowledgements

Financial support of the Australian Research Council is gratefully acknowledged. AS also thanks the Ministry of Economy and Competitiveness of Spain (MAT 2009-13530). The authors thank Omar Lopez-Garrity for performing the speciation calculations.

References

[1] N. Birbilis, M.K. Cavanaugh, A.D. Sudholz, S.M. Zhu, M.A. Easton, M.A. Gibson, A combined neural network and mechanistic approach for the prediction of corrosion rate and yield strength of magnesium-rare earth alloys, Corrosion Science, 53 (2011) 168-176.
[2] Z.X. Qiao, Z.M. Shi, N. Hort, N.I.Z. Abidin, A. Atrens, Corrosion behaviour of a nominally high purity Mg ingot produced by permanent mould direct chill casting, Corrosion Science, 61 (2012) 185-207.
[3] A.D. Sudholz, N. Birbilis, C.J. Bettles, M.A. Gibson, Corrosion behaviour of Mg-alloy AZ91E with atypical alloying additions, Journal of Alloys and Compounds, 471 (2009) 109-115.
[4] A. Atrens, W. Dietzel, The negative difference effect and unipositive Mg+, Adv. Eng. Mat., 9 (2007) 292-297.
[5] Z.M. Shi, J.X. Jia, A. Atrens, Galvanostatic anodic polarisation curves and galvanic corrosion of high purity Mg in 3.5% NaCl saturated with Mg(OH)(2), Corrosion Science, 60 (2012) 296-308.
[6] G. Song, A. Atrens, D. St John, X. Wu, J. Nairn, The anodic dissolution of magnesium in chloride and sulphate solutions, Corros. Sci., 39 (1997) 1981-2004.
[7] G. Song, A. Atrens, D. Stjohn, J. Nairn, Y. Li, The electrochemical corrosion of pure magnesium in 1 N NaCl, Corros. Sci., 39 (1997) 855-875.
[8] G.S. Frankel, Techniques for Corrosion Quantification, 2nd Ed., in: E.N. Kaufmann (Ed.) Characterization of Materials, Wiley VCH, NY, 2012.
[9] S. Bender, J. Goellner, A. Atrens, Corrosion of AZ91 in 1N NaCl and the mechanism of magnesium corrosion, Adv. Eng. Mat., 10 (2008) 583-587.
[10] S. Bender, J. Goellner, A. Heyn, S. Schmigalla, A new theory for the negative difference effect in magnesium corrosion, Materials and Corrosion-Werkstoffe Und Korrosion, 63 (2012) 707-712.
[11] R.L. Petty, A.W. Davidson, J. Kleinberg, The anodic oxidation of magnesium metal – Evidences for the existence of unipositive magnesium. J. Amer. Chem. Soc., 76 (1954) 363-366.
[12] J.O.M. Bockris, A.K.N. Reddy, Modern Electrochemistry, 2nd ed., Kluwer Academic / Plenum Publishing, New York, 2000.
[13] N.T. Kirkland, G. Williams, N. Birbilis, Observations of the galvanostatic dissolution of pure magnesium, Corros. Sci., 65 (2012) 5-9.
[14] F.E.T. Heakal, A.M. Fekry, M.Z. Fatayerji, Influence of halides on the dissolution and passivation behavior of AZ91D magnesium alloy in aqueous solutions, Electrochim. Acta, 54 (2009) 1545-1557.
[15] L.J. Liu, M. Schlesinger, Corrosion of magnesium and its alloys, Corros. Sci., 51 (2009) 1733-1737.
[16] Z.M. Shi, J.X. Jia, A. Atrens, Galvanostatic anodic polarisation curves and galvanic corrosion of high purity Mg in 3.5% NaCl saturated with Mg(OH)(2), Corros. Sci., 60 (2012) 296-308.
[17] T.R. Thomaz, C.R. Weber, T. Pelegrini, L.F.P. Dick, G. Knornschild, The negative difference effect of magnesium and of the AZ91 alloy in chloride and stannate-containing solutions, Corros. Sci., 52 (2010) 2235-2243.
[18] J. Swiatowska, P. Volovitch, K. Ogle, The anodic dissolution of Mg in NaCl and Na2SO4 electrolytes by atomic emission spectroelectrochemistry, Corros. Sci., 52 (2010) 2372-2378.
[19] G. Williams, H.N. McMurray, Localized corrosion of magnesium in chloride-containing electrolyte studied by a scanning vibrating electrode technique, J. Electrochem. Soc., 155 (2008) C340-C349.
[20] N.T. Kirkland, N. Birbilis, M.P. Staiger, Assessing the corrosion of biodegradable magnesium implants: A critical review of current methodologies and their limitations, Acta Biomaterialia, 8 (2012) 925-936.
[21] C.F. Baes, R.E. Mesmer, The Hydrolysis of Cations, John Wiley & Sons, Inc., New York, 1976.
[22] Y. Feng, R.C. Wang, C.Q. Peng, K. Qiu, N.G. Wang, C. Zhang, J.P. Zhang, Aging behaviour and electrochemical properties in Mg-4.8Hg-8Ga (wt.%) alloy, Corrosion Science, 52 (2010) 3474-3480.
[23] M.C. Turhan, Q.Q. Li, H. Jha, R.F. Singer, S. Virtanen, Corrosion behaviour of multiwall carbon nanotube/magnesium composites in 3.5% NaCl, Electrochimica Acta, 56 (2011) 7141-7148.
[24] C. Wagner, W.E. Traud, The analysis of corrosion procedures through the interaction of electrochemical partial procedures and on the potential difference of mixed electrodes, Zeitschrift Fur Elektrochemie Und Angewandte Physikalische Chemie, 44 (1938) 391-402.
[25] A.J. Bard, L.R. Faulkner, Electrochemical Methods: Fundamentals and Applications, Wiley, New York, 2000.
[26] G.S. Frankel, Growth of 2-D pits in thin film aluminum, Corros. Sci., 30 (1990) 1203-1218.

Hydrogen Evolution During Anodic Polarization of Mg Alloyed with Li, Ca, or Fe

A. Samaniego[a,b,c], N. Birbilis[b], X. Xia[b] and G.S. Frankel[a]

[a]Fontana Corrosion Center, The Ohio State University, Columbus, OH, USA

[b]Department of Materials Engineering, Monash University, Clayton, VIC 3800. Australia

[c]National Centre for Metallurgical Research (CENIM-CSIC). Department of Materials Engineering, Corrosion and Durability, Madrid, 28040, Spain.

Abstract

The origin of high rates of hydrogen evolution (HE) on dissolving Mg, the so-called negative difference effect, remains of practical interest. Recent studies have suggested that the ability of Mg to support the cathodic reaction is enhanced during dissolution and that enrichment of noble impurity elements at the dissolving Mg surface may also play a role in enhanced rates of HE. To begin to uniquely address the role played by other elements, Mg was intentionally alloyed with Li, Ca or Fe. Hydrogen collection was performed during anodic galvanostatic polarization tests. An Mg-Li alloy containing 33 at% Li exhibited similar rates of anodic HE as pure Mg. Because Li dissolves with a valence of +1, any mechanism of anodic HE involving a lower valence state such as Mg^{+}, is therefore ruled out. Mg-Ca and Mg-Fe alloys exhibited higher rates of anodic HE than pure Mg. They also exhibited a minimum of the HE rate under cathodic polarization instead of at the open circuit potential, the latter being the case for pure Mg and Mg-Li. The role of alloying elements in the HE on Mg and the implications for the mechanism of anodic HE are discussed.

Keywords: Magnesium, Alloying, hydrogen evolution, negative difference effect, corrosion.

Introduction

For more than a century, different mechanisms have been proposed to explain the so-called "negative difference effect" (NDE) observed on magnesium, which can be described as an increase in the amount of hydrogen evolved with increasing applied anodic potential. The NDE phenomenon should be totally understood in order to wholly assess the utility of Mg as an electrode or structural material, the latter situation related to corrosion. Several mechanisms for the source of superfluous hydrogen evolution (HE) have been discussed, including the chemical reaction of univalent magnesium (Mg^{+}) in solution away from the metal surface [1, 2] producing hydrogen via water reduction; metal loss by disintegration (termed the "chunk effect") [3, 4] in which dislodged Mg metal dissolves independently of the substrate; partially protective film disruption [5-7] in which Mg directly reacts with water; decreasing pH attributed to the hydrolysis of Mg [8], the hydrated electron (attached to water molecules) acting as strong reductant [9]; hydride formation [10, 11]; and the formation of aqueous H atoms [12]. The above mechanisms will not be reviewed here, as the relevant references have been provided. However, aided by modern analytic equipment, the recent literature has evolved towards a contemporary understanding that does not support the above-proposed mechanisms.

We recently proposed that the catalytic nature of Mg surfaces could be increased during anodic polarization, thereby increasing the rate of the cathodic reaction and hence HE [13]. This was a concept and not a mechanistic explanation for why the catalytic nature may be enhanced. Even more recently, Williams et al. reported that cathodic currents were sustained at spatially separated locations on the dissolving Mg surface during anodic polarization [14], which is among the most definitive experiments to date indicating that cathodic activity (as in reduction reactions) can occur on the anode surface at appreciable rates. Subsequently, simple electrochemical tests confirmed that the enhanced catalytic behavior of Mg is the consequence of anodic dissolution [15]. However, the precise physical processes causing the enhancement of catalytic activity are still unclear. The realization of such physical processes is likely to be an area of active research given the growing interest in Mg products. In this respect, a study by Taheri et al. [16] used analytical transmission electron microscopy (TEM) to study cross-sections of the Mg surface that had been anodically polarized. The results indicated that sites of enhanced cathodic activity were covered with a bilayer film consisting of MgO inner layer and an outer layer of precipitated $MgOH_2$. It was also noted that small Fe-rich particles existed within the surface film. These particles,

resulting perhaps from preferential enrichment on the surface, could be one source that serves to catalyze the HE reaction. Metallic iron particles on the surface at the low polarization potentials should be sites where HE would occur at high rates.

To clarify the role of alloying additions to Mg on the rate of anodic HE, alloys containing relatively high amounts of Li, Ca or Fe were studied in this work. These elements were specifically selected because of their expected behavior as alloying elements during dissolution of Mg. Li is a more reactive metal than Mg and so should dissolve preferentially when present in Mg as a solute element. It also exists in the oxidized form with a single oxidation state, Li^+. Therefore, if a strong NDE is observed during dissolution of Mg-Li, the mechanism could not be related to the formation of lower valence intermediates, which has been previously proposed for Mg [1, 2, 17-19]. Ca is also more reactive than Mg and so should preferentially dissolve, but it forms a divalent ion (Ca^{2+}). In contrast, Fe is more noble than Mg and so should enrich on the surface during dissolution owing to preferential dissolution of Mg. It is expected that the enriched Fe could enhance support of the cathodic reaction and promote the NDE.

Experimental

The alloys studied (Mg-Ca, Mg-Li and Mg-Fe) were all produced by induction melting under an inert gas (argon) atmosphere. The melt was maintained at a temperature of ~730 ºC within a mild steel crucible coated with graphite. The compositions of alloys tested are given in Table 1, along with commercially obtained pure Mg. The precise composition was confirmed via inductively coupled plasma atomic emission spectrometry (ICP-AES); the same Mg-Ca alloy was previously described by Kirkland et al. [20], and the Mg-Fe alloy by Gandel et al. [21].

***Table 1**. Composition, in wt. %, of alloys tested herein as measured by ICP-AES.*

Alloy	Mg	Fe	Ca	Li	Al	Mn	Y	Cu, Ni
Pure Mg	Bal.	0.004	-	-	0.01	0.01	-	<0.005
Mg-Fe	Bal.	1.32[a]	-	-	0.005	0.022	-	<0.005
Mg-Ca	Bal.	0.004	28.0[b]	-	0.01	0.01	-	<0.005
Mg-Li	Bal.	0.003	-	10.94[c]	3.29	0.01	0.59	<0.005

[a] *equivalent to ~0.5 at. %.*

[b] *equivalent to ~19 at. %.*

[c] *equivalent to ~33 at. %.*

Scanning Electron Microscopy (SEM) was carried out in backscattered electron mode using an FEI Quanta 3D-FEG. Specimens for SEM were metallographically prepared to a 0.05 micron alumina suspension finish.

Prior to electrochemical testing, an insulated copper wire was attached to the rear of samples that were then mounted in epoxy and ground. The test assembly allowed simultaneous application of a polarizing signal along with real-time hydrogen collection as was described previously [13]. The experimental difficulties and limitations of such tests were documented previously by Kirkland et al. [22]. Due to the different specimen geometries, the Mg-Li samples had an exposed area of ~1.5 cm^2, whereas the area for Mg-Fe and Mg-Ca specimens was ~4.8 cm^2. The difference in area is not expected to have an appreciable influence on the HE results, which were all area corrected. However, the different areas resulted in different ohmic potential drops during potential measurements due to the larger current needed to achieve a given current density on larger surface areas. A saturated calomel electrode (SCE) was used as the reference electrode along with a mixed metal oxide coated titanium mesh counter electrode (Ti mesh with an applied coating of platinum group metal oxides). Approximately 1600 mL of 0.1 M NaCl was used as the electrolyte. A total net charge of 50 C was passed at different applied anodic (0.1, 1, 5, 10, 50 and 75 mA/cm^2) and cathodic (-1, -5, -10 mA/cm^2) current densities. All tests were carried out at least 2 times. All the experimental conditions except for the alloy composition and exposed area were similar to those reported previously for experiments on pure Mg [13], allowing for direct comparison.

Results

Figure 1 shows the equilibrium phase diagrams of the binary alloys Mg-Li, Mg-Ca and Mg-Fe. The phase diagrams indicate that the Mg-Li alloy, which contained ~33 at.% Li, possessed a BCC structure as opposed to the conventional HCP Mg structure. The Mg-Ca alloy with ~19 at.% Ca, should have an α-Mg matrix with the Mg_2Ca secondary phase. The Mg-Fe alloy with ~ 0.5 at.% Fe should exhibit an α-Mg matrix with a pure Fe phase (insoluble pure BCC-Fe particles).

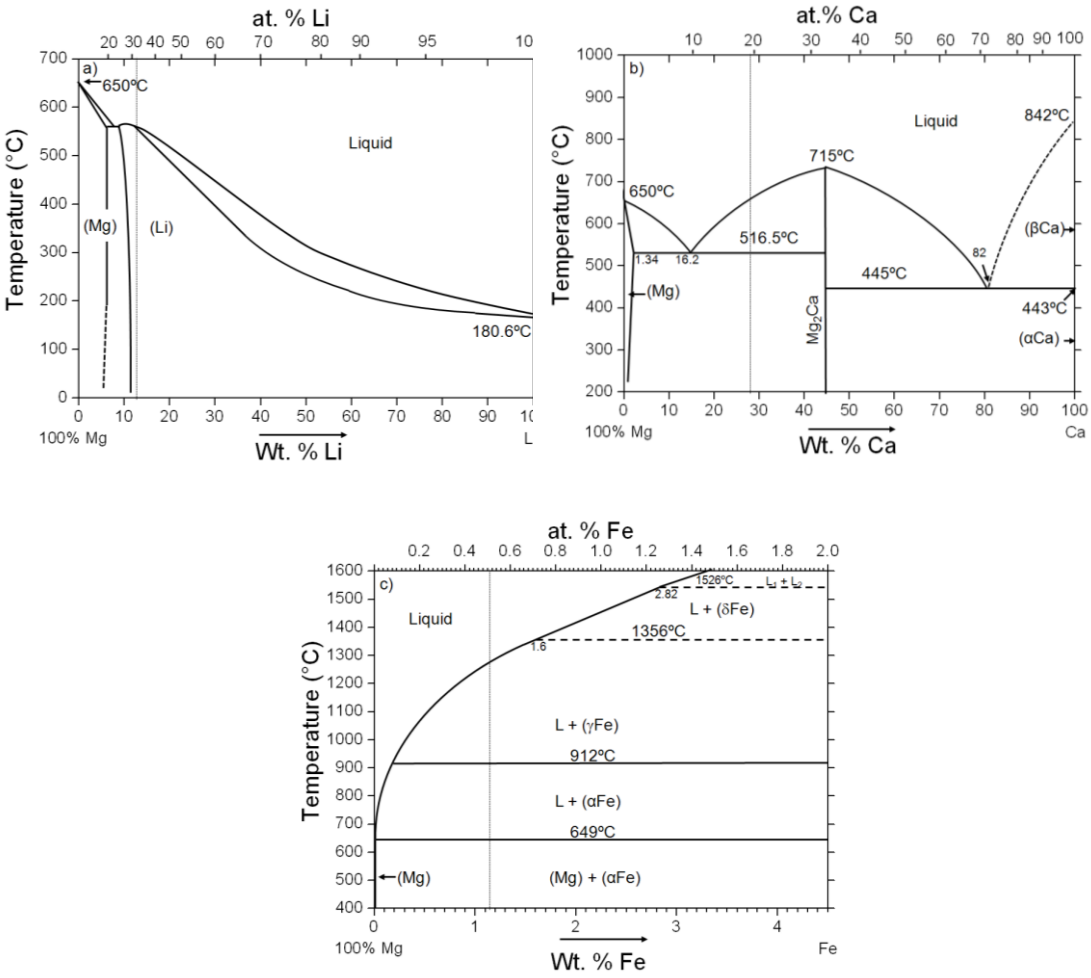

Figure 1. *Equilibrium phase diagrams for: a) Mg-Li, b) Mg-Ca c) Mg-Fe. These phase diagrams are based on those published by Nayeb-Hashemi and Clark [23].*

The microstructure of the alloys tested herein were analyzed via SEM, and are shown in Figure 2. The microstructures were found to be those indicated from the phase diagrams. Figure 2a indicates that micron sized pure Fe particles were present in the α-Mg matrix in the case of the Mg-Fe alloy. The microstructure of the Mg-Ca alloy contained a large volume fraction of Mg_2Ca, present as both as constituent-type particles and a finer eutectic structure, Figure 2b. As the composition of the alloy is close to the Mg_2Ca phase field, the volume fraction of Mg_2Ca (seen as the 'light' phase) was concomitantly large. The Mg-Li alloy exhibited a relatively uniform BCC Mg-Li matrix with some micron-sized Al_2Y particles, Figure 2c. The low levels of Al and Y were included in this alloy for purposes not relevant to this study. The affinity for Al and Y to co-segregate and form a compound excluding both Mg and Li was anticipated, and indeed occurred. All three alloys tested were not single phase due to the low solubility of alloying elements in Mg [24]. Furthermore, they each likely suffered incongruous dissolution of the less noble elements they contained. As a result, the

dissolution mechanisms were likely quite complex. However, analysis of the dissolution mechanism was not performed because it was not the focus of this work. It is supposed that the alloy surfaces reached a steady-state condition after an initial transition period as shown in Figure 3. The complications of the dissolution process were not considered to be an impediment for this study of the HE kinetics on Mg alloys. Most applications of Mg involve alloys and understanding the influence of alloying should provide insight into the NDE. The alloy containing Fe necessarily had a lower proportion of alloying element than the others. Mg-Fe alloys are difficult to produce owing to the full insolubility of Fe in Mg, along with a significant density difference. Furthermore, the Mg-Fe alloy studied herein represents the highest Fe loading in any Mg alloy previously reported in the literature.

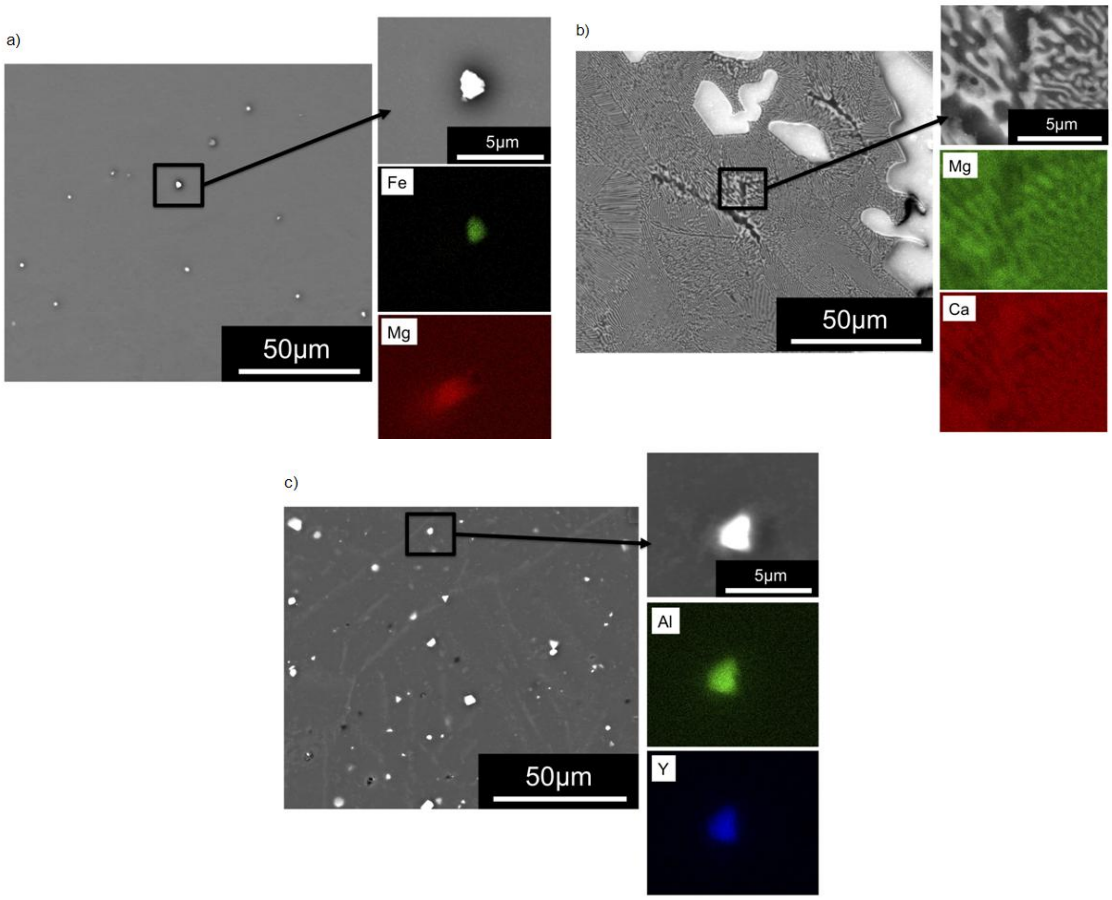

Figure 2. *Backscattered electron micrographs and accompanying EDXS mapping for (a) Mg-Fe, (b) Mg-Ca, and (c) Mg-Li alloys tested herein*

Figure 4 shows the steady state rate of HE as a function of the applied current density over the range of -10 to +75 mA/cm^2, both on linear and log axes, for the three alloys and pure Mg, the latter being taken from a previously reported study [13]. All

three of the Mg-alloys exhibited the NDE, with high rates of HE at high applied anodic current densities. Mg-Fe and Mg-Ca exhibited values of hydrogen evolution rates at their open circuit potentials (OCPs) of 3.3 and 2.9 ml/cm^{2}h (8 and 7 mA/cm^2), which are much higher than those observed on Mg and Mg-Li (0.04 and 0.02 ml/cm^{2}h, or 0.09 and 0.05 mA/cm^{2,} respectively). Mg-Li exhibited very similar behavior as pure Mg, in that the HE rates were similar at any given applied current density and the minimum HE rate was determined to be at the OCPs. However, some notable differences are observed from the behavior of Mg-Ca and Mg-Fe. These two alloys exhibited higher rates of HE during anodic polarization. Furthermore, the minimum HE rates for both were at the lowest applied cathodic current density (-1 mA/cm^2) and not at OCP, as seen in the inset of Figure 4a. Both also exhibited a lower rate of HE at the lowest applied anodic current density (+1 mA/cm^2) than what was measured at OCP. Under high applied anodic current densities, however, the HE rate of both increased, reaching very high values, which were higher than those initially observed at OCP.

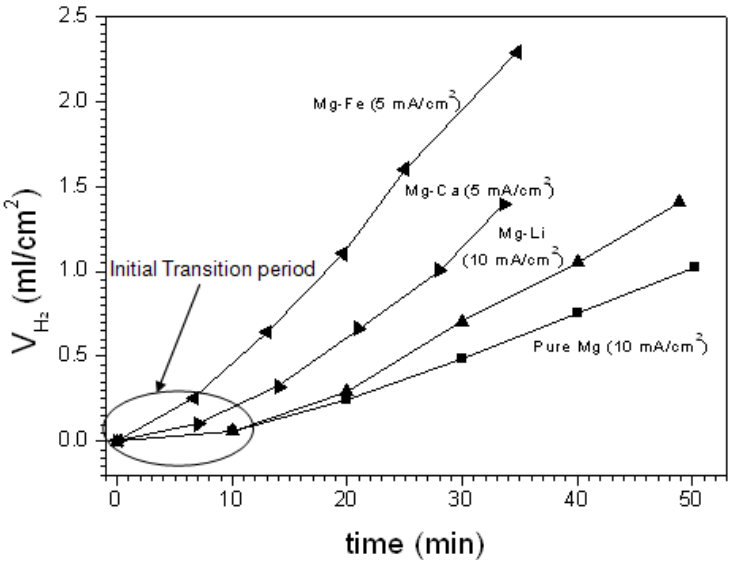

Figure 3. *Volume of hydrogen collected as a function of time showing an initial transition period on pure Mg, Mg-Li, Mg-Ca and Mg-Fe. These data represent typical results from replicated experiments. The solution was 0.1 M NaCl and 50 C of net charge was passed at each current density.*

As previously reported for pure Mg [13, 25], the extent of the HER during anodic polarization was large (readily achieving many mA/cm^2), in spite of the polarity of the applied current being opposite to that of the HE reaction (HER). Furthermore, the increasing rate of HE with increasing potential is in contrast to what is expected from the Butler-Volmer or Tafel relations [26, 27]. Open circuit potential measured from Mg-Li, Mg-Ca and Mg-Fe were -1.68, -1.82 and -1.59 V_{SCE} respectively. In addition, the

potential measured during the galvanostatic experiments indicates that a large ohmic potential drop occurred. However, as discussed previously, the corrected potential would be positioned in the region of -1 to 0 V_{SCE}, which is along the extrapolated anodic Tafel region and not shown herein.

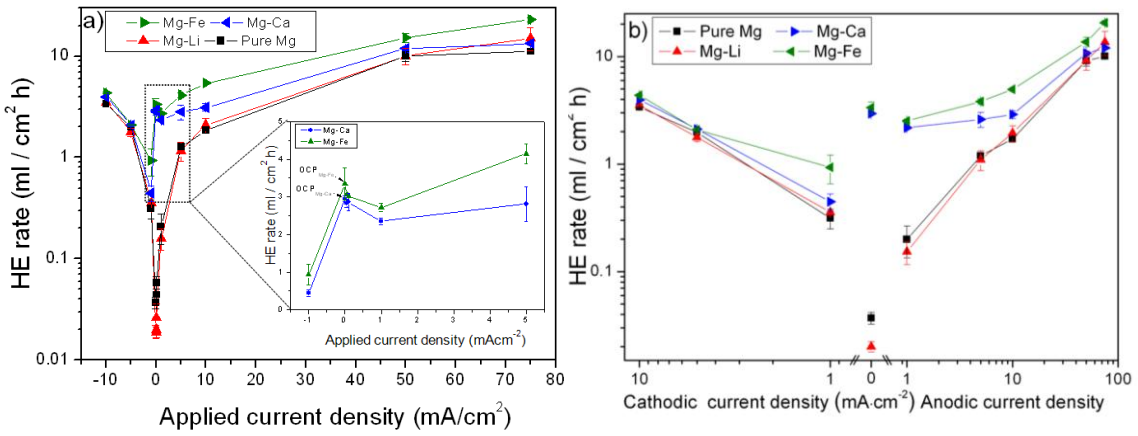

Figure 4. *Rate of hydrogen production as a function of applied current density (i_{app}) of the four alloys (Pure Mg [13], Mg-Li, Mg-Ca and Mg-Fe). The solution was 0.1 M NaCl. The error bars are standard deviation. The deviation is smaller than the symbols for points that have no error bars. a) HER in log scale and i_{app} in linear scale. b) HER and i_{app} in log scale. i_{app}= 0.05 and 0.1 mA/cm^2 are not represented in this plot*

The total volume of H_2 produced during polarization and the associated charge were determined for each alloy and are represented in Figure 5 normalized to the net charge passed, which was 50 C for both anodic and cathodic experiments. Figure 5 indicates that the normalized hydrogen charge measured during applied cathodic current density (cathodic i_{app}), exhibited values very close to 1 for the three binary alloys and pure Mg, with the exception of Mg-Fe at i_{app} = -1mA/cm^2, where the normalized hydrogen charge was higher than two. Figure 5a shows that the total volume of hydrogen generated for a constant applied charge on Mg-Li decreased from that collected at OCP to that evolved at +0.1 mA/cm^2, while the hydrogen generated was not significantly changed for further increases in applied anodic current density. Mg-Ca and Mg-Fe exhibited a clear decrease of hydrogen volume from OCP to +75 mA/cm^2 (figures 5b,c). Even though the rate of HE increased with increasing applied current density, the total amount of hydrogen generated for the constant applied charge decreased.

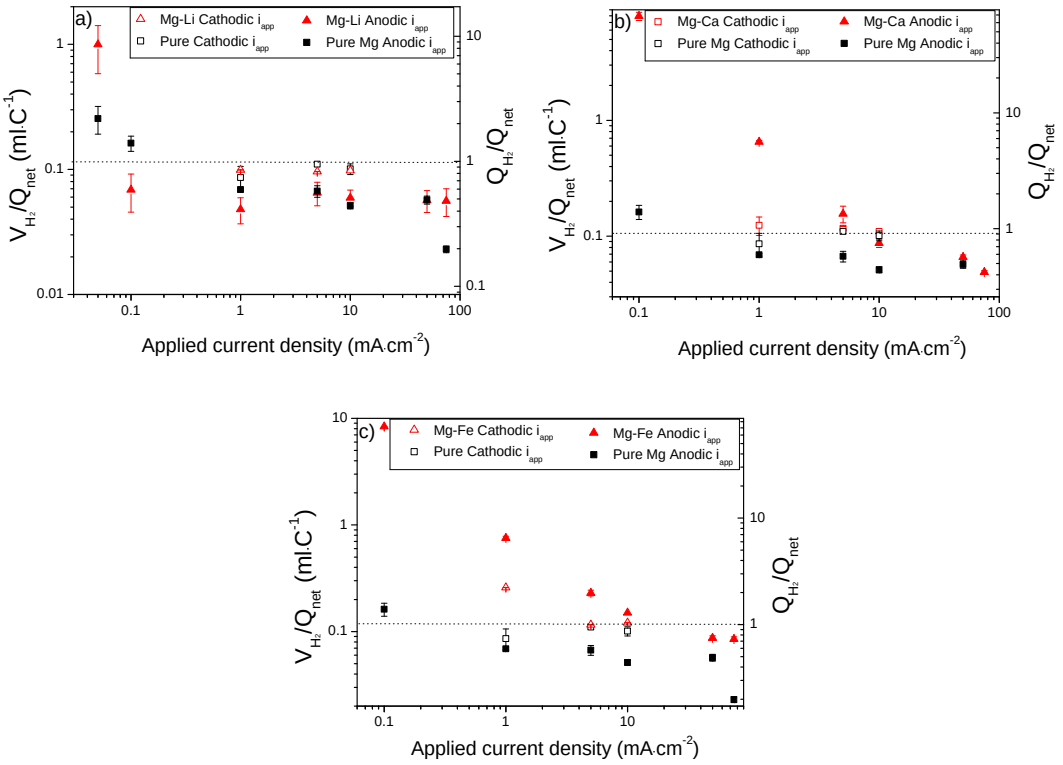

Figure 5. *Volume of hydrogen produced normalized to the net charge for a) Mg-Li, b) Mg-Ca and c) Mg-Fe compared to Pure Mg [13]. Right hand axis shows the charge associated with the hydrogen production normalized to the net charge. The net charge for all experiments was 50 C. The dashed line is given to facilitate comparison with a charge ratio of 1. The error bars are standard deviation. The deviation is smaller than the symbols for points that have no error bars.*

Discussion

Figure 4a shows that Mg - 33 at. % Li exhibited similar hydrogen evolution rates as those evolved on pure Mg under the same applied current densities. One third of the atoms in this alloy were Li, which is nominally more reactive than Mg, so preferential dissolution of Li may be expected in the alloy. Because Li dissolves via the Li^+ ion and has no stable higher valence states, the observation of strong NDE on Mg-Li, with anodic HE rates similar to those observed on pure Mg, indicates that the NDE mechanism does not involve the oxidation of lower valence cations in solution, as has been proposed for Mg [17-19]. If the NDE were caused by oxidation of univalent Mg in solution, then the smaller number of Mg atoms dissolved for a given net charge should have resulted in less HE for the Mg-Li alloy. Figure 5 shows that, even though the rate of HE increased with increasing applied current density, the total amount of hydrogen generated for the constant applied charge decreased all three alloys. These observations

suggest that Mg^{+} is both not present and not responsible for NDE, in line with other recent reports [4, 13, 28-31].

Figure 4 shows that the HE rate for Mg and Mg-Li was lowest at the OCP, with the rate increasing steadily with increasing applied cathodic or anodic current density. The behavior in the cathodic region was consistent with that expected from the Tafel equation:

$$i_{HE} = i_{0,H,Mg}\ 10^{\left(\frac{-(E-E_{rev,H})}{b}\right)} \quad (1)$$

Where i_{HE} is the current density of the HER, E is the potential, $E_{rev,H}$ is the reversible potential for the HER, $i_{0,H,Mg}$ is the exchange current density for HER on the Mg surface, and b is the associated Tafel slope. The behavior in the anodic region, which is evidence of the NDE, is not consistent with Eqn 1. It was previously suggested that the increasing rate of HE during anodic polarization could be explained by an increase in the exchange current density for HER during Mg dissolution [13]. In that paper, this concept was notional with no detailed explanation given. As described in the introduction, recent papers have given evidence that enrichment of noble element impurities such as Fe could generate on the surface of dissolving Mg and that these elements could be the sites of enhanced cathodic activity. Alternatively, the dissolving Mg surface might change in other ways that make it more reactive and catalytic, for instance by changes in the nature of films present on the dissolving surface.

Mg-Fe and Mg-Ca both behaved differently than Mg and Mg-Li in that the rate of HE exhibited a local maximum at the OCP, with lower rates of HE at small anodic and cathodic current densities than at OCP (Figure 4). It is possible to explain the behavior of these alloys using the notion of variable exchange current density. First, consider the cathodic region of the polarization curves shown in Fig. 4b. The HE rate of all alloys decreased as the applied cathodic current density decreased. The potential scales with the applied current density, so this is a kind of polarization curve, and it would be expected that the rate of HE should be lower at OCP than in the cathodic region. It is notable that both Mg-Ca and Mg-Fe exhibited corrosion rates that were approximately two orders of magnitude higher than those for pure Mg and Mg-Li (7, 8 mA/cm^2 and 0.09, 0.05 mA/cm^2, respectively, after converting HE rate to current density). The much higher HE rate at OCP than at -1 mA/cm^2 for Mg-Ca and Mg-Fe suggests that the high rate of corrosion at OCP changed the nature of the surface and

thus increased the value of $i_{0,H,Mg}$ even at OCP relative to the cathodic polarized condition. For Mg-Fe, a deviation in the relationship between HE rate and applied current density happened even in the cathodic region as a relatively high rate of HE was observed at -1 mA/cm^2. This is different than the Mg-Ca case, which continued in the same relationship observed at higher cathodic currents, even at -1 mA/cm^2, and is an indication of a change in the surface even for an applied cathodic current as a result of the high rate of corrosion of Mg-Fe in the cathodic region. The Mg and Mg-Li samples exhibited much lower rates of corrosion so the surfaces were not greatly changed at OCP and the $i_{0,H,Mg}$ did not increase until anodic currents were applied.

In the anodic region of polarization, the rate of HE increased monotonically with applied current density for Mg and Mg-Li, which is consistent with the notion of the increasing rate of dissolution increasing $i_{0,H,Mg}$ and causing the HE rate to increase despite the increase in potential. Even an applied anodic current density as low as 0.05 mA/cm^2, which is equivalent to the corrosion rate at OCP for Mg-Li, impacted the surface and caused an increase in $i_{0,H,Mg}$ and in the rate of HE for Mg and Mg-Li. In contrast, applied anodic current densities as large as 1 mA/cm^2 were still small relative to the OCP corrosion rate for Mg-Ca and Mg-Fe, so they caused little change to the surface condition and thus had little influence on $i_{0,H,Mg}$. As a result, the HE rate decreased for applied anodic current densities that were small relative to the OCP rate. The decrease in HE rate for this small increase in anodic current is what would be expected from Eqn. 1. The same might have been observed for Mg and Mg-Li had applied current densities in the range of 0.01 mA/cm^2 been probed.

According to the original definition of the NDE, the strength of the effect is given by the difference between the rate of HE at OCP and the rate at an applied anodic potential [1, 17]. It might therefore be considered that the NDE for Mg and Mg-Li was greater than for Mg-Ca and Mg-Fe. However, the rates of HE at the highest applied anodic current densities were similar and the y axes in Fig 4 are on a log scale. Therefore, the increase in HE rate was not vastly different for all four samples. Considering that the HE at the potentials achieved during anodic polarization should be values extrapolated from the rates in the cathodic region of the HE polarization curve [13], the rates of HE during anodic polarization are high for all of the alloys studied.

It is interesting that the dependency of hydrogen evolution rate on applied current densities was similar for the Mg-0.5 at.%Fe and Mg-19 at.%Ca alloys. The behaviors of Fe and Ca in an Mg matrix were expected to be very different. Fe is more

noble than Mg and it can efficiently support the cathodic reaction. According to Figure 2a, micro-particles of pure Fe were present in the alloy. Conversely, Ca is much more reactive than Mg and it should increase the corrosion rate of the alloy due to the preferential dissolution of Ca. Hence, Fe is expected to support the cathodic reaction while Ca is expected to increase the anodic reaction, which has been shown by conventional potentiodynamic polarization tests [20, 32]. Despite their differing mechanistic influence on corrosion, the influences of Fe and Ca on the NDE were quite similar (bearing in mind that there was ~20 times greater Ca in the Mg-Ca alloy than there was Fe in the Mg-Fe alloy), as the minimum HER in both alloys was revealed under cathodic polarization (-1mA/cm^2), both had high hydrogen evolution rates at OCP and, in both cases, hydrogen evolution rates decreased under small applied anodic current densities (up to 1 mA/cm^2). Li influenced the NDE of Mg to a lesser extent than Ca or Fe.

Focusing on the role of Fe, Fe particles were observed in the Mg surface film after anodic dissolution of Mg with 40 ppm Fe [16]. The commercially pure Mg used in that work was from the same material batch that was tested in our previous work and is shown as pure Mg in this work. The binary Mg-Fe alloy tested in this study had much higher Fe content (13,000 ppm Fe) and so should have accumulated Fe in the surface film faster. This might explain the higher rates of HE on the Mg-Fe alloy. The pure Mg, Mg-Li and Mg-Ca alloys all had similar Fe contents and it is likely that Fe accumulated on the surface of all three at similar rates during dissolution. This might explain the similar HE behavior of pure Mg and Mg-Li. However, the Mg-Ca alloy had 300 times less Fe than the Mg-Fe, but exhibited similar HE behavior.

The results of this study indicate that enrichment of noble elements like Fe on the surface of dissolving Mg plays a dominant role in the mechanism of anodic HE, but that another mechanism must also be important. The similarity of the HE behavior of Mg-Ca and Mg-Fe is probably coincidental as their respective behaviors must be the result of different mechanisms. It is possible that the anodic enhancement associated with Ca simply increases the catalytic activity through an increase in the exchange current density. Even though enhanced HE behavior during anodic polarization has mainly studied in Mg, it might in fact be universal for reactive metals. Based on the results of this work, it seems likely to occur on Ca, perhaps even at enhanced rates. Assessing the contribution of surface films and elemental enrichment to the NDE will be the focus of future work.

Conclusions:

The rate of hydrogen evolution on Mg alloys containing relatively high concentrations of Li, Ca or Fe was measured at different values of applied current density to investigate the influence of noble element enrichment on the so-called negative difference effect (NDE). The following conclusions can be made:

1. The NDE was observed on all of the materials studied: pure Mg, Mg-Li, Mg-Ca and Mg-Fe.
2. The alloy with ~33 at.% Li exhibited similar hydrogen evolution behavior as pure Mg. This indicates that the mechanism does not involve the formation of lower valent ions because Li dissolves only as Li^+.
3. Alloys with ~19 at. % Ca or ~0.5 at. % Fe exhibited much higher free corrosion rate than pure Mg. These alloys also exhibited lower rates of hydrogen evolution at small anodic or cathodic applied current densities than at OCP, which is different than for pure Mg and Mg-Li. The large OCP corrosion rates might explain this behavior.
4. The behavior of Mg-Ca indicates that a mechanism other than noble element enrichment on the surface of dissolving Mg might play a role in the NDE mechanism, and that enhanced dissolution is accompanied by enhanced NDE.

Acknowledgements

This work was partially supported by the Ministry of Economy and Competitiveness of Spain (MAT 2009-13530). The Monash Centre for Electron Microscopy is gratefully acknowledged. NB gratefully acknowledges the Australian Research Council.

References

[1] J.W. Turrentine, Journal of Physical Chemistry, 12 (1908) 448-467.
[2] R.L. Petty, A.W. Davidson, J. Kleinberg, Journal of the American Chemical Society, 76 (1954) 363-366.
[3] M.E. Straumanis, B.K. Bhatia, Journal of the Electrochemical Society, 110 (1963) 357-360.
[4] M.N. Hull, Journal of Electroanalytical Chemistry and Interfacial Electrochemistry, 38 (1972) A1-A4.
[5] P.F. King, Journal of the Electrochemical Society, 110 (1963) C178-C178.
[6] R. Tunold, H. Holtan, M.B. Haggberge, A. Lasson, R. Steenhansen, Corrosion Science, 17 (1977) 353-365.
[7] J.L. Robinson, P.F. King, Journal of the electrochemical society, 108 (1961) 36.
[8] S. Bender, J. Goellner, A. Heyn, S. Schmigalla, Materials and Corrosion-Werkstoffe Und Korrosion, 63 (2012) 707-712.
[9] G. Lee, J. Park, Geochimica Et Cosmochimica Acta, 102 (2013) 162-174.
[10] F. Cao, Z. Shi, J. Hofstetter, P.J. Uggowitzer, G. Song, M. Liu, A. Atrens, Corrosion Science, 75 (2013) 78-99.
[11] G.G. Perrault, Journal of Electroanalytical Chemistry, 51 (1974) 107-119.
[12] H.H. Uhlig, R. Krutenat, Journal of the Electrochemical Society, 111 (1964) 1303-1306.
[13] G.S. Frankel, A. Samaniego, N. Birbilis, Corrosion Science, 70 (2013) 104-111.
[14] G. Williams, N. Birbilis, H.N. McMurray, Electrochemistry Communications, 36 (2013) 1-5.
[15] N. Birbilis, A.D. King, S. Thomas, G.S. Frankel, J.R. Scully, Electrochimica Acta, 132 (2014) 277-283.
[16] M. Taheri, J.R. Kish, N. Birbilis, M. Danaie, E.A. McNally, J.R. McDermid, Electrochimica Acta, 116 (2014) 396-403.
[17] G. Song, A. Atrens, D. St John, X. Wu, J. Nairn, Corrosion Science, 39 (1997) 1981-2004.
[18] A. Atrens, W. Dietzel, Advanced Engineering Materials, 9 (2007) 292-297.
[19] Z. Shi, J.X. Jia, A. Atrens, Advanced Engineering Materials, 14 (2012) 324-334.
[20] N.T. Kirkland, N. Birbilis, J. Walker, T. Woodfield, G.J. Dies, M.P. Steiger, Journal of Biomedical Materials Research Part B-Applied Biomaterials, 95B (2010) 91-100.
[21] D.S. Gandel, M.A. Easton, M.A. Gibson, N. Birbilis, Materials Chemistry and Physics, 143 (2014) 1082-1091.
[22] N.T. Kirkland, N. Birbilis, M.P. Staiger, Acta Biomaterialia, 8 (2012) 925-936.
[23] I. Polmear, Light Alloys, Fourth ed., Butterworth-Heinemann, United kingdom, 2005.
[24] Z.M. Shi, J.X. Jia, A. Atrens, Corros. Sci., 60 (2012) 296-308.
[25] J.A.V. Butler, Transactions of the Faraday Society, 19 (1924) 0729-0733.
[26] T. Erdey-Gruz, M. Volmer, Zeitschrift Fur Physikalische Chemie-Abteilung a-Chemische Thermodynamik Kinetik Elektrochemie Eigenschaftslehre, 150 (1930) 203-213.
[27] R.M. Souto, A. Kiss, J. Izquierdo, L. Nagy, I. Bitter, G. Nagy, Electrochemistry Communications, 26 (2013) 25-28.
[28] G. Williams, H.N. McMurray, Journal of the Electrochemical Society, 155 (2008) C340-C349.
[29] J. Swiatowska, P. Volovitch, K. Ogle, Corrosion Science, 52 (2010) 2372-2378.
[30] A. Samaniego, B.L. Hurley, G.S. Frankel, Journal of Electroanalytical Chemistry.
[31] D.S. Gandel. Thesis submitted in partial fulfillment of the requirements for the degree of Doctor of Philosophy, Monash University, Melbourne, Australia (2014).
[32] A.A. Nayeb-Hashemi, C.J. B.,Phase diagrams of binary magnesium alloys., ASM Interntional, Ohio, 1988.

Discusión Capítulo I

Profundización en los Mecanismos de Corrosión del Magnesio y el Efecto Diferencial Negativo (NDE).

Tras realizar una extensa revisión bibliográfica de los mecanismos propuestos en los últimos 150 años para explicar el efecto diferencial negativo (NDE), se observó una fuerte controversia relativa a la explicación de este fenómeno. La teoría más extendida en la actualidad es aquella que implica la existencia de intermedios de menor estado de oxidación del teórico (Mg^{+}), como responsables de las elevadas velocidades de liberación de hidrógeno y pérdidas de peso observadas al aplicar una polarización anódica. Sin embargo, en los últimos años, la presencia de magnesio monovalente (Mg^{+}) no ha podido ser confirmada mediante técnicas analíticas modernas y estudios recientes han concluido que el magnesio se disuelve vía Mg^{2+}, sin involucrar ninguna especie intermedia como Mg^{+} [103-105]. Esto creó una fuerte controversia ya que, implican la existencia de evidencias sobre la existencia de Mg^{+} [88], como de la no existencia de este intermedio de reacción [103-105]. Con el objetivo de aclarar esta discusión, los estudios realizados en 1953 sobre las evidencias de Mg^{+}, fueron reproducidos y analizados en profundidad utilizando técnicas complementarias.

- **Estudios sobre las evidencias del magnesio monovalente (Mg^{+}):** mediante espectroscopia RAMAN "in situ" sobre una muestra de magnesio en solución de $NaSO_4$, pudo observarse que el anión sulfato se reduce de manera espontanea, formando SO_2, sin necesidad de aplicar ningún tipo de polarización. Al realizar un barrido de potencial catódico en este medio, se observó que la especie reducida (SO_2) comenzó a dominar el espectro, tal como cabe esperar al situarse en potenciales más reductores. Sin embargo, al aplicar un barrido de potencial anódico, aunque inicialmente se observó un aumento de la señal correspondiente a la especie oxidada (SO_4^{2-}), respecto a la señal de la especie reducida (SO_2), al alcanzar polarizaciones mayores, se observó una tendencia inversa y la especie reducida comenzó a dominar el espectro, hasta que finalmente la especie SO_4^{2-} desapareció completamente. Este comportamiento, recuerda al efecto diferencial negativo (NDE), ya que, en ambos casos, se observó un aumento de una reacción catódica al aplicar un potencial anódico.

Para eliminar la posible relación de estas observaciones con la presencia de Mg^{+}, se realizó un barrido de potencial catódico sobre un electrodo de platino inmerso en la misma solución de sulfato sódico (Na_2SO_4). Desde el potencial en circuito abierto hasta -1.34 V_{SCE}, únicamente se observó una señal correspondiente al anión SO_4^{2-}. Sin embargo al alcanzar potenciales suficientemente bajos (<-1.34 V_{SCE}), se observó la presencia de SO_2 y a potenciales aún más bajos, se observó la presencia de $S_2O_3^{2-}$. Cabe destacar que los potenciales, donde se detectó la presencia de estas especies reducidas, son ligeramente superiores al potencial en circuito abierto del magnesio en solución de sulfato (-1.9 V_{SCE}), por lo que se encuentran en un rango de potencial similar al esperable al aplicar una polarización anódica sobre magnesio. De esta manera, se demostró que la presencia de especies reducidas de sulfato no está limitada a la presencia de magnesio, ya que también fueron observadas sobre un electrodo de platino en el mismo rango de potencial.

Por lo tanto, en este estudio, se estableció la presencia de especies reductoras, no consideradas por Petty durante sus experiencias en 1953 [88, 106] y que pudieron actuar como agentes reductores. Es decir, en contraposición con las suposiciones realizadas por Petty, cuando el magnesio metálico entra en contacto con soluciones de Na_2SO_4, existen especies reductoras adicionales que pudieron causar las observaciones experimentales descritas por Petty en sus estudios, sin necesidad de involucrar especies intermedias como el magnesio monovalente (Mg^{+}).

Por otro lado, en contraposición a lo reportado por Petty, no se encontraron diferencias apreciables en la cantidad de agente oxidante reducido al realizar la electrolisis utilizando un ánodo de magnesio o al reproducir sus experimentos sin ninguna muestra (únicamente mezclando las soluciones utilizando el mismo set-up). De estos estudios, se puede concluir que la existencia de Mg^{+} no pudo ser demostrada por Petty en 1953 y por lo tanto, en la actualidad no existe ninguna evidencia científica sobre la existencia de este intermedio de reacción.

Debido a estudios recientes que concluyeron que el magnesio se disuelve vía Mg^{2+}, parece razonable pensar que la existencia de Mg^{+}, como responsable del efecto diferencial negativo (NDE), es muy improbable. Por lo tanto, y tras realizar un análisis en profundidad de los datos experimentales, se propuso un mecanismo alternativo capaz de explicar el NDE.

- **Mecanismo propuesto para explicar el efecto diferencial negativo:** una explicación alternativa para el incremento de la velocidad de desprendimiento de hidrógeno al aplicar potenciales anódicos, es que la cinética de esta reacción, sobre la superficie de magnesio en disolución, aumente debido a cambios termodinámicos o a factores cinéticos. Asumiendo control por activación, la ecuación de Tafel puede ser utilizada para describir la velocidad de desprendimiento de hidrógeno, ya que, sobre la superficie de magnesio, el potencial (E), está lejos del potencial reversible (E_{revH}):

$$i_{HER} = i_{0,H,M} 10^{\left(\frac{-(E-E_{rev,H})}{b}\right)} \quad (1)$$

Donde i_{HER} es la densidad de corriente asociada a la velocidad de desprendimiento de hidrógeno a un potencial dado, $i_{O,H,M}$ es la corriente de intercambio para el desprendimiento de hidrógeno sobre una superficie de magnesio, y b es la constante de Tafel para esta reacción. Habitualmente se considera que $i_{O,H,M}$, E_{rev} y b son constantes, por lo que, al incrementar el potencial, i_{HER} se reduce exponencialmente. Sin embargo, en el magnesio se observa un aumento de i_{HER} al aplicar potenciales anódicos y es posible que este efecto se deba a cambios en E_{rev}, i_0, or b. Cambios en E_{rev} producirían un efecto pequeño que no podría explicar los datos experimentales y no existen bases científicas para esperar posibles cambios en la pendiente de Tafel. Por lo tanto, se propuso un mecanismo en el cual la corriente de intercambio, $i_{O,H,M}$, no es constante y que varía conforme se aplica un potencial anódico.

Consideremos ahora que la actividad catalítica de la superficie para la reacción de desprendimiento de hidrógeno, representada por la corriente de intercambio, $i_{O,H,M}$, aumenta a medida que aumenta la velocidad de disolución de Mg. La actividad catalítica de una superficie tiene un gran impacto en la velocidad de generación de hidrógeno ya que $i_{O,H,M}$, varia de 10^{-3} A/cm^2 para los metales del grupo del Pt, los catalizadores más conocidos , a 10^{-12} A/cm^2 para metales no catalíticos como Hg y Pb [55].

La suposición principal de este mecanismo, es que la naturaleza catalítica de la superficie de Mg en disolución, y por lo tanto $i_{O,H,M}$, aumentan con el aumento de la velocidad de disolución de Mg, sin tener en cuenta la cobertura parcial de la superficie por una película de óxido. Esta hipótesis podría dar lugar a un aumento en la velocidad de generación de hidrógeno con el aumento del potencial si la variación de $i_{O,H,M}$ es

superior al efecto del término exponencial en la ecuación 1. Este fenómeno se muestra esquemáticamente en la Figura 4.1.

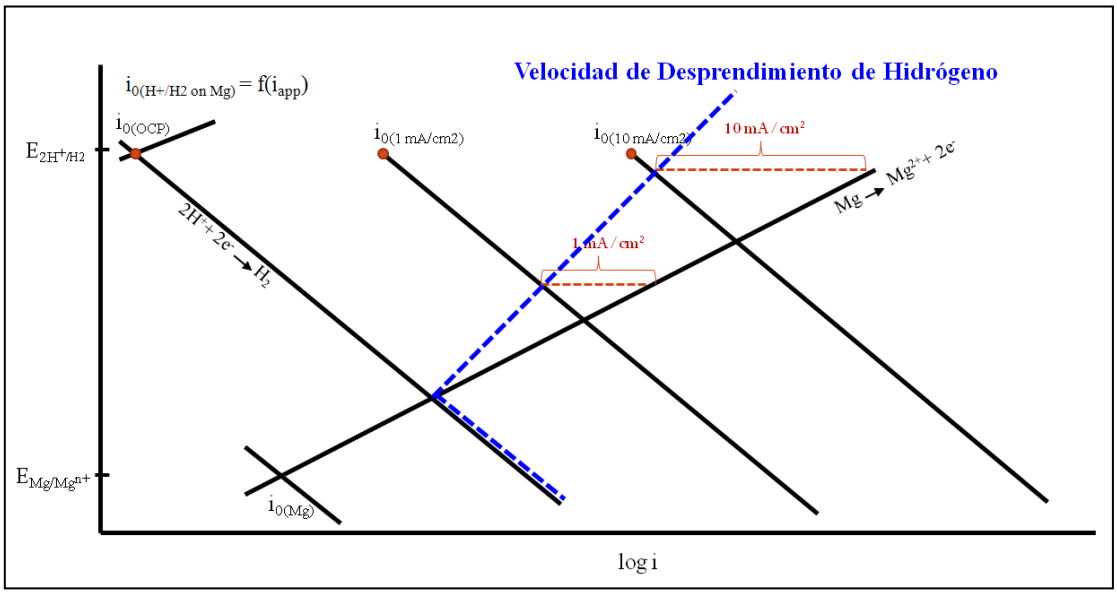

Figura 4.1. *Diagrama de Evans donde se explica el incremento de la reacción de desprendimiento de hidrógeno por el efecto del incremento de* i_0 *al aumentar la corriente anódica aplicada.*

El Mg es un metal extremadamente reactivo, y se oxida fácilmente tras la exposición a una pequeña cantidad de oxígeno gaseoso. Por lo tanto, es razonable pensar que una superficie tan reactiva, también podría ser catalítica hacia otras reacciones, tales como la de desprendimiento de hidrógeno, y que la naturaleza catalítica de una superficie metálica podría cambiar con la velocidad de disolución de metal.

Por otro lado, este mecanismo podría ser aplicable a otros metales tales como el aluminio, donde existe una situación experimental similar, ya que se observa una evolución de hidrógeno anormalmente alta en el interior de las picaduras de este metal. Como en el magnesio, las superficies de aluminio presentan bajos valores de $i_{O,H,M}$. Sin embargo, de las picaduras activas se desprende de forma continua hidrógeno gaseoso que solo desaparece cuando se produce la repasivación. La generación de hidrógeno no es observada en las zonas pasivadas donde el potencial es ligeramente superior que en el interior de la picadura y, en cualquier caso, por debajo de $E_{rev,\ HER}$. La causa de este mayor desprendimiento de hidrógeno observado en las picaduras de aluminio,

probablemente sea la diferencia en la capacidad catalítica de la superficie en el interior de la picadura comparada con la del material pasivado.

Este mecanismo ha tenido una buena aceptación en la comunidad científica y ha suscitado interés. Muy recientemente, otros autores han realizado varios estudios confirmando un aumento de la capacidad catalítica de la superficie de magnesio al disolverse [4, 102]. Más aún, Taheri y colaboradores [101], describieron que este aumento de la actividad catalítica, observado al aplicar potenciales anódicos, se debe a un incremento en la concentración de impurezas catódicas en las capas superficiales formadas sobre las superficies parcialmente disueltas. Se propuso que estás impurezas, con unas densidades de corriente de intercambio para la generación de hidrógeno mucho mayores que las del magnesio, podrían catalizar la reacción y producir el aumento en la generación de hidrógeno observado experimentalmente.

- **Influencia de Li, Fe y Ca sobre el efecto diferencial negativo:** Con el fin de clarificar en mayor medida el efecto de las impurezas en el mecanismo de corrosión del magnesio, se realizó un último estudio sobre este tema, en el cual se añadió una cantidad significativas de impurezas sobre magnesio puro y se midió la velocidad de generación de hidrógeno producido al aplicar diferentes densidades de corriente, tanto anódicas como catódicas. Las impurezas seleccionadas fueron Fe, Ca y Li y se adicionó un 0.5, 19 y 33 % atómico respectivamente.

Se observó que la presencia de elevadas cantidades de litio (uno de cada tres átomos de la aleación era litio), tuvo una influencia pequeña sobre el efecto diferencial negativo (NDE), ya que las velocidades de desprendimiento de hidrógeno observadas para cada densidad de corriente aplicada, fueron muy similares a las obtenidas sobre magnesio puro. Teniendo en cuenta que el litio es un metal alcalino, más activo que el magnesio, la presencia de NDE, similar a la observada en magnesio puro, corrobora la baja probabilidad de que el Mg^+ sea el responsable del NDE, ya que el Li se disuelve vía Li^+ por lo que la posibilidad de producir intermedios de reacción de menor estado de oxidación se reduce drásticamente.

Pese a que el comportamiento teórico del Fe y del Ca en una matriz de magnesio es completamente diferente (el Fe presenta un comportamiento catódico respecto al Mg, mientras que el Ca se comporta anódicamente), su influencia en el NDE es muy similar y en los dos casos se observaron diferencias significativas respecto al comportamiento del magnesio puro. Ambas aleaciones presentaron una velocidad de corrosión en

circuito abierto muy superior a la del magnesio puro y la mínima velocidad de generación de hidrógeno se encontró bajo polarización catódica. Esto implica que la capacidad catalítica de estas aleaciones no solo aumenta al aumentar la velocidad de disolución del metal, sino que también se ve afectada al disminuir la velocidad de disolución durante la polarización catódica.

De este estudio, se concluyó que cuando la velocidad de disolución de metal en circuito abierto es suficientemente grande, polarizar anódicamente también afecta la velocidad de disolución, disminuyendo la densidad de corriente de intercambio para la reacción catódica o lo que es lo mismo, disminuye la capacidad catalítica de la superficie. En el magnesio puro y en la aleación de Mg-Li, este efecto no fue observado ya que la velocidad de disolución en circuito abierto era muy pequeña y los posibles cambios derivados de la polarización catódica sobre la corriente de intercambio no fueron significativos. Se sugirió la presencia de un mínimo en la velocidad de disolución del metal por debajo del cual no se producen cambios significativos en la corriente de intercambio, $i_{O,H,M}$ y por tanto, la variación de la corriente de intercambio con la velocidad de disolución del metal podría variar como se muestra en la siguiente figura:

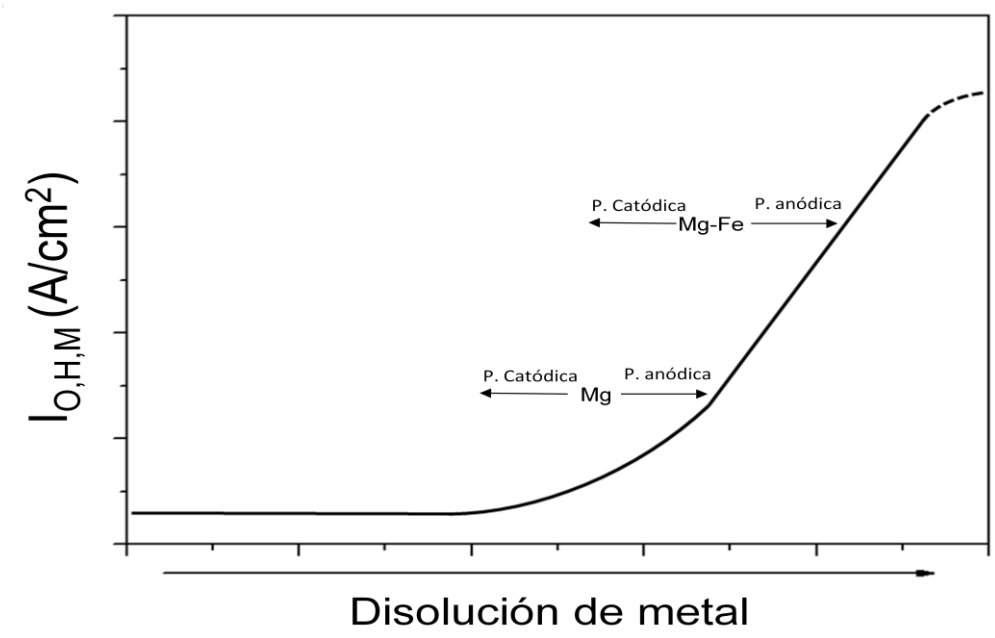

Figura 4.2. *Variación propuesta de la corriente de intercambio ($i_{O,H,M)}$ con la disolución del metal.*

Capítulo II

Caracterización de las películas de óxidos superficiales y de las capas de productos de corrosión de las aleaciones AZ31 y AZ61.

Introducción

El efecto del aluminio, como elemento de aleación para mejorar la resistencia a la corrosión en las aleaciones de magnesio, ha sido estudiado en un importante rango de condiciones experimentales. En las aleaciones del sistema Mg-Al, la mayor afinidad del aluminio por el oxígeno tiende a producir una capa pasiva de óxido de aluminio o una mezcla de óxidos de aluminio y magnesio que pueden dar una estabilidad adicional a la superficie estudiada. Muchos estudios se han llevado a cabo para evaluar la relación de la micro estructura (cantidad y distribución de la fase β en la aleación) o la cantidad de aluminio en la aleación y su influencia en la corrosión. Sin embargo, pocos estudios se han centrado en las características de las películas espontáneamente formadas en contacto con la atmósfera cuyo efecto en la corrosión puede ser importante. La composición de estas películas de óxido puede variar con el tiempo de almacenamiento, y capas adicionales de hidróxidos y carbonato pueden adherirse sobre las películas de óxido inicialmente formadas, modificando su influencia sobre la corrosión. Con el fin de evaluar este efecto, se caracterizó y comparó la influencia de los óxidos superficiales formados tras pulir las muestras mecánicamente y tras almacenar las probetas durante 6 meses en el laboratorio. Así mismo se comparó la influencia del contenido de aluminio sobre la corrosión en dos aleaciones con diferente contenido de este metal. Las aleaciones escogidas fueron la AZ31 y AZ61, con contenidos de aluminio de un 3 y 6% respectivamente. Se eligieron estás aleaciones por las diferentes cantidades de fase β esperadas sobre las aleaciones y para analizar en profundidad estudios previos que sugirieron que un 4% de Al en las aleaciones de Mg aumentan significativamente la resistencia a la corrosión debido a la influencia de Al en la película pasiva MgO.

Para concluir estos estudios, se realizó un estudio sobre la influencia de los productos de corrosión de estas aleaciones durante su ataque en soluciones de cloruro sódico.

Resultados Capítulo II

Los resultados obtenidos durante la elaboración de esta tesis doctoral, relacionados con este tema, se muestran en esta sección en forma de publicaciones. Los artículos publicados fueron los siguientes:

Effect of naturally formed oxide films and other variables in the early stages of Mg-alloy corrosion in NaCl solutions. S. Feliu Jr., C. Maffiotte, A. Samaniego, J. C. Galván, V. Barranco. Electrochimica Acta, 56, 12 (2011) 4554-4565.
doi:10.1016/j.electacta.2011.02.077

Effect of the chemistry and structure of the native oxide surface film on the corrosion properties of commercial AZ31 and AZ61 alloys. S. Feliu Jr., C.Maffiotte, A.Samaniego, J.C. Galván, V. Barranco. Applied Surface Science, 257, 20, (2011) 8558-8568.
doi:10.1016/j.apsusc.2011.05.014

Combined effect of composition and surface condition on corrosion behaviour of magnesium alloys AZ31 and AZ61. Corrosion Science 68, (2013) 66-71. A.Samaniego, I. Llorente, S. Feliu Jr.
http://dx.doi.org/10.1016/j.corsci.2012.10.034

En revisión en la revista Corrosion Science:

Corrosion product layers on magnesium alloys AZ31 and AZ61: Characterisation and protective ability. A. Samaniego, I llorente, S Feliu Jr.

Effect of Naturally Formed Oxide Films and Other Variables in the Early Stages of Mg-alloys Corrosion in NaCl Solution

Sebastián Feliu (Jr)[a] , C. Maffiotte[b], Alejandro Samaniego[a] ,Juan Carlos Galván[a], Violeta Barranco[a,c].

[a]Centro Nacional de Investigaciones Metalúrgicas CSIC, Avda. Gregorio del Amo 8, 28040 Madrid, Spain,

[b]CIEMAT. FNL (edificio 2), Avda. Complutense, 22, 28040 Madrid, Spain

[c]Instituto de Ciencias de Materiales de Madrid, ICMM, Consejo Superior de Investigaciones Científicas, CSIC, Sor Juana Inés de la Cruz, 3, Cantoblanco, 28049, Madrid, Spain

Electrochimica Acta 56 (2011) 4554–4565

Abstract

The influence of initial surface conditions on the subsequent corrosion behaviour of AZ31 and AZ61 magnesium alloys in 0.6 M NaCl solution has been studied using electrochemical impedance spectroscopy. For obtaining the different surface conditions, some of the specimens were immersion tested with the surface in the as-received condition, while others were tested immediately after mechanical polishing, and part of the polished specimens after six months of exposure to the laboratory atmosphere. Considering the evolution of the high-frequency capacitive arc of the Nyquist diagram, whose diameter is related to the corrosion process, a clear effect of the initial surface conditions is observed only in the early stages of testing. This effect is especially significant for the freshly polished specimens.

Keywords: Magnesium alloys; Aluminium; Chloride; Electrochemical impedance spectroscopy; X-ray photoelectron spectroscopy.

1. Introduction

Magnesium and its alloys, especially Mg-Al alloys, have aroused great scientific and technological interest over the last two decades. From a practical point of view, magnesium is the lowest density structural metal, making it attractive for use in the automotive, aerospace, IT and electronics industries, and in the development of new biomaterials for orthopaedic and cardiovascular applications, where weight plays a decisive role. However, being one of the most chemically active metals, the use of magnesium is sometimes limited by its inadequate resistance to atmospheric and aqueous corrosion. There is a need for more complete information on the factors that influence the corrosion of these materials, and the present work aims to contribute to this knowledge.

The effect of aluminium as an alloying element to improve the corrosion resistance of magnesium has been studied in a wide range of experimental conditions, such as exposure to dry oxygen [1,2], ambient atmospheres [3-5], atmospheres with a high degree of humidity [6-10], in immersion in distilled water [11], in saline solutions or atmospheres [12-24], etc. In Mg-Al alloys the greater oxygen affinity of aluminium tends to produce passivating aluminium oxide films or mixtures of Mg and Al oxides, which can give special stability to the exposed surface [14,25,26].

Many researchers have carried out studies to find relationships between the alloy microstructure (amount and distribution of β-phase precipitates) or the Al content in the bulk alloy and its corrosion resistance [13,14,16,18,20,27,28]. A much smaller number of researchers have studied the characteristics of the thin passivating layers on the surface of the metal, which are formed in contact with the atmosphere or in solutions of low aggressivity [1,3,4,29,30].

Metals normally oxidise rapidly when exposed to oxygen. However, after just a short time (i.e. a few minutes), when a very thin oxide layer has formed, the reaction virtually ceases. Some time ago Cabrera and Mott [31] attributed the formation of this film to the effect of a strong electric field in the oxide associated with the presence of oxygen ions adsorbed on the outer surface of the metal. In a very thin film the electric field is enormous, but as the film thickens the effect of the electric field is reduced and the growth rate soon falls to a very low value.

The thickness of the film formed in air on magnesium-based materials is initially around 2-3 nm, and can slowly increase up to some 4-7 nm after months of exposure at room

temperature [1,3,4,32]. The surface composition of this oxide film can change significantly during ambient storage. Extra layers of hydrated and carbonated products of the magnesium oxide can be added to the original oxide film [1,3,33]. An increase in water molecules in the film has been reported for long ambient exposure times [29]. Hydrophobic organic-matter can also be picked up from the atmosphere [3]. Changes have been observed in the film growth rate depending on the nature of the compounds that form the film, e.g. the presence of a crystalline $Mg(OH)_2$ after long exposure times [3]. Besides the influence of exposure time, composition and environmental conditions, film properties also depend on the tested alloy, in particular its microstructure and the presence of precipitates and inclusions [30]. In fact, the precise nature and properties of passivating films on the surface of Mg alloys formed in air or in aqueous solution is still open to debate.

Oxide film formation and properties, such as protectiveness, may be sensitive to the conditions in which they form. Laboratory tests normally refer to the behaviour of surfaces that are mechanically polished prior to testing, for metallographic observation and to remove impurities and corrosion product layers formed during storage. It is of theoretic and practical interest to know to what extent these experimental results are dependent on the characteristics of the spontaneously formed oxide film. With these ideas, the present research compares corrosion resistance results obtained for freshly polished surfaces, on which immediately tends to form the oxide film, to polished surfaces that have been aged for six months, and surfaces just in the as-received condition. The tests have focused on the aluminium-containing magnesium alloys AZ31 and AZ61, with approximately 3 and 6% Al, respectively. As is known, the aluminium content and microstructure are important factors in the corrosion behaviour of Mg-Al alloys [23,24,27]; the microstructure of the AZ31 alloy is formed practically by an α-matrix with Al in solid solution (Fig. 1a), while a large part of the Al in the microstructure of the AZ61 alloy is precipitated in the form of β-phase (Fig. 1b). The corrosion medium was a 0.6 M solution of sodium chloride at ambient temperature. It has been especially interesting to observe the differences in behaviour during the first days of testing, when the effect of the oxide film is most clearly distinguished.

2. Experimental

The chemical compositions of the tested magnesium alloys, AZ31 and AZ61, are listed in Table 1. They were fabricated in wrought condition and supplied in plates of 3 mm thickness by Magnesium Elecktron Ltd.

Table 1. *Bulk composition of the AZ31 and AZ61 alloys.*

Material	Al	Zn	Mn	Si	Cu	Fe	Ni	Ca	Zr	Others
AZ31	3.1	0.73	0.25	0.02	<0.001	0.005	<0.001	0.0014	<0.001	<0.30
AZ61	6.2	0.74	0.23	0.04	<0.001	0.004	<0.001	0.0013	<0.001	<0.30

Essential points of the metallurgical preparation of the sheet magnesium alloys that may influence surface properties in the as-received condition include heat treatment and hot rolling operations. Unfortunately, it has not been possible to obtain supplier's information on the various stages of manufacturing of the purchased AZ31 and AZ61 sheets used in the research. In the work we have tried to characterize the as-received conditions by analysis of XPS and AFM results, which are compared with those for the corresponding polished surfaces. To produce the polished surface condition, the specimens with the surface in the as-received condition were dry ground through successive grades of silicon carbide abrasive papers, followed by finishing with 3 and 1 μm diamond paste, cleaned in water and dried in hot air.

For XPS analyses, photoelectron spectra were acquired with a Fisons MT500 spectrometer_equipped with a hemispherical electron analyser (CLAM 2) and a non-monochromatic magnesium Kα X-ray source operated at 300 W. The specimens were mechanically fixed on small flat discs supported on an XPZ manipulator placed in the analysis chamber. The residual pressure in this ion-pumped analysis chamber was maintained below 10^{-8} Torr during data acquisition. Spectra were collected for 20-90 min., depending on the peak intensities, at a pass energy of 20 eV, which is typical of high-resolution conditions. The intensities were estimated by calculating the area under each peak after smoothing and subtraction of the S-shaped background and fitting the experimental curve to a mix of Lorentzian and Gaussian lines of variable proportion. Although specimen charging was observed, it was possible to determine accurate binding energies (BE) by referencing to the adventitious C1s peak at 285.0 eV. Atomic ratios were computed from peak intensity ratios and reported atomic sensitivity factors [34]. The sampled areas were 1×1 mm^2. The energy resolution is about 0.8 eV.

Bombardment was performed using an EXO5 ion gun incorporated in the equipment, provided with a scanning unit to track the beam and operating at a voltage of 5 kV, an intensity of 10 mA and a pressure of 1×10^{-7} Torr. The sample current was 1 μA during bombardment.

The thickness of the native oxide film on the surface of the magnesium specimens was calculated using the expression given by Strohmeier [35]

$$d_o\ (nm) = \lambda_{oxide} \sin\theta \ln [I_{oxide} \times \lambda_{metal} \times N_{metal})/(I_{metal} \times \lambda_{oxide} \times N_{oxide}) + 1]$$

where d_o is the thickness of the magnesium oxide layer (in nm); θ is the photoelectron output angle; I_{metal} and I_{oxide} are the intensities of the magnesium components in the metallic state and as oxide from the Mg 2p peak; λ_{metal} and λ_{oxide} are the mean free paths of photoelectrons in the substrate and the oxide layer; and N_m and N_o are the volume densities of magnesium atoms in metal and oxide. The values of λ_{metal} and λ_{oxide} are 3.0 nm [36] and 2.6 nm [37,38], respectively, and an N_{metal}/N_{oxide} ratio of 1.24 was used [39].

For metallographic characterisation, the specimens were dry ground through successive grades of silicon carbide abrasive papers from P120 to P2000 followed by finishing with 0.1 µm diamond paste. The surface of the specimens was examined by scanning electron microscopy (SEM) using a JEOL JSM-6400 microscope equipped with Oxford Link energy-dispersive X-ray (EDX) microanalysis hardware.

Images of the specimen surfaces were also obtained in original and polished condition using an atomic-force microscope (AFM). All images (20 x 20 µm) were taken in the 5100 AFM/SPM from Agilent Technologies working in tapping mode using Si type AFM cantilevers with a normal spring constant of 40 N/m and a typical radius of 10 nm from Applied Nanostructures. Images were acquired at a resolution of 512 x 512 points and subjected to first-order flattening. After flattening, the RMS roughness (root-mean-squared roughness) was calculated.

Electrochemical impedance measurements were conducted in 0.6 M NaCl for different times up to 28 days at room temperature (~25ºC) and pH 5.6, although the pH evolved freely during the experiment. An AUTOLAB potentiostat, model PGSTAT30, with frequency response analyser software was used. The frequency ranged from 100 kHz to 1 mHz with 5 points/decade, whereas the amplitude of the sinusoidal potential signal was 10 mV with respect to the open circuit potential. A typical three-electrode set-up was employed: Ag/AgCl and graphite were used as reference and counter electrodes, respectively, and the material under study was the working electrode.

3. Results

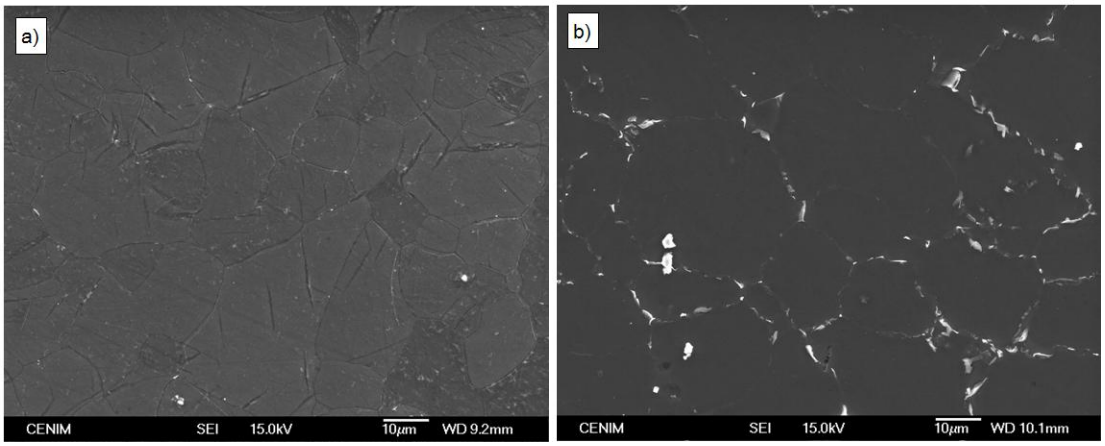

Figure 1. *SEM micrographs: (a) AZ61 alloy, (b) AZ31 alloy.*

3.1. Characterisation of the pre-existing oxide film

High-resolution O1s spectra of the oxide films formed spontaneously on AZ31 and AZ61 alloys are presented in Fig. 2. The spectra obtained on the non-sputtered surface (Figs. 2a, 2d, 2g, 2j) are fairly similar, containing one single component at a binding energy of 532.2 eV associated with the presence of oxygen in hydroxide form [1,3]. Figs. 2b, 2e, 2h, 2k, 2c, 2f, 2i, 2l show the spectra obtained after 5 and 10 minutes of sputtering. The most intense component, at a binding energy of 531.2 eV, is associated with the presence of oxygen in the form of magnesium oxide, MgO [2], and the less intense component, at a binding energy of 533.2 eV, could be attributed to the presence of oxygen in the form of Al_2O_3 for the case of polished surfaces, or in the form of $MgAl_2O_4$ for surfaces in the as-received condition [40]. The spectra obtained after 10 minutes of sputtering were similar to those acquired after 5 minutes.

The Mg2p high resolution XPS spectra obtained on the native oxide film formed spontaneously on AZ31 and AZ61 alloys are shown in Fig.3. For the non-sputtered surfaces (Figs. 3a, 3d, 3g, 3j) the spectra are fairly similar, containing one single component at a binding energy of 50.8 eV associated with the presence of magnesium in the form of magnesium hydroxide in the case of polished surfaces, or perhaps in the form also of $MgAl_2O_4$ for surfaces in the as-received condition [40,41]. Figs. 3b, 3e, 3h, 3k show the spectra obtained after 5 minutes of AIB. The spectrum observed on the polished surface of AZ31 alloy (Fig. 3e) shows two components of similar intensity, one at a binding energy of 48.6 eV associated with the presence of magnesium in

metallic state and another at a binding energy of 50.8 eV which may be associated with the presence of magnesium in the form of magnesium oxide (demonstrated by the O1s peak, Fig. 2e)). On the polished AZ61 alloy (Fig. 3k), it should be noted the lower intensity of the metallic magnesium signal when compared with that of the Mg^{2+}. This result is interpreted as being due to the greater thickness of the native oxide film in this last case. The spectra obtained after 10 minutes of sputtering on the AZ31 and AZ61 polished surfaces were fairly similar (Figs 3f and 3l).

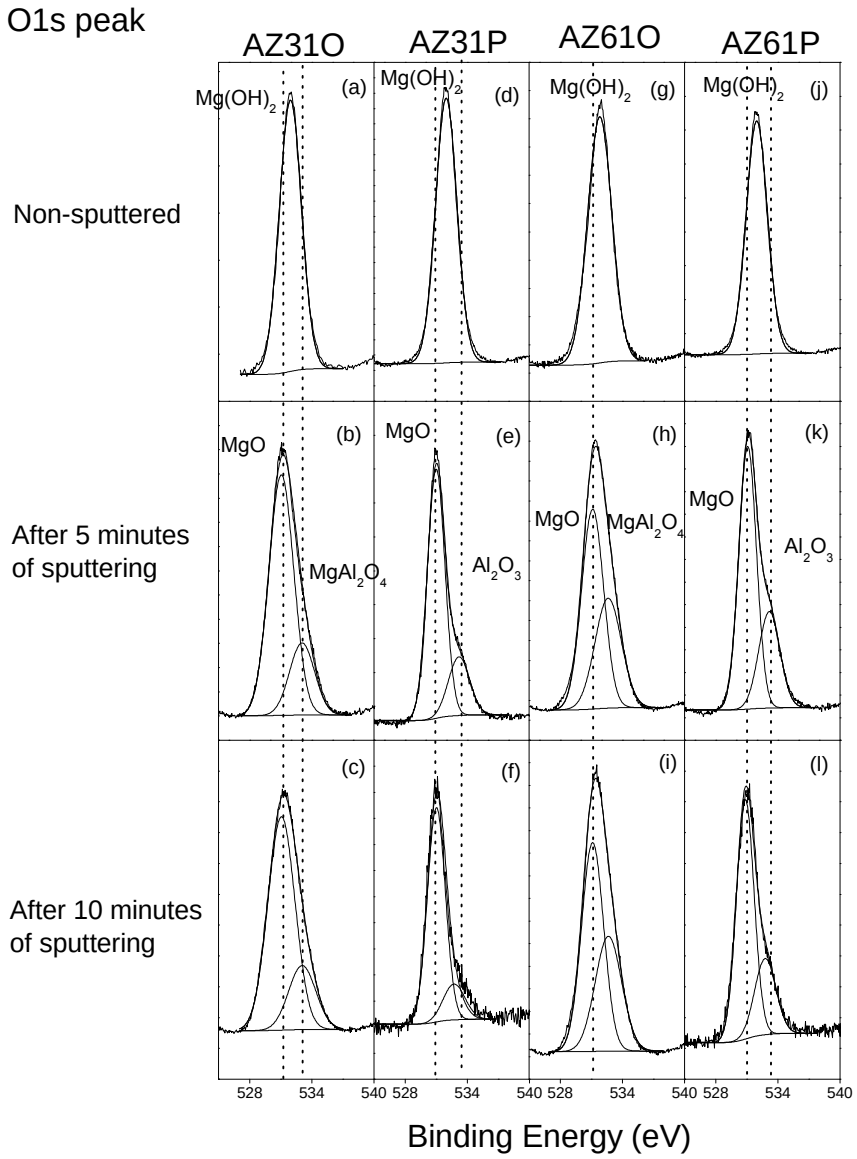

Figure 2. *XPS MgO1s spectra of the AZ31 and AZ61 alloys in the original (O) and polished (P) surface conditions.*

Table 2 gives the element composition obtained by XPS on the as-received and polished surfaces of the AZ31 and AZ61 alloys and its variation with sputtering time. Among the

various differences between these two surface states, attention is drawn to the presence of a significant amount of calcium on the original (as-received) surfaces of both alloys which disappears after surface polishing. In general, 5 min. of sputtering (shortest sputtering time tested) is seen to be sufficient to remove the calcium content detected on the original alloy surfaces. This calcium probably forms part of the composition of mixed oxides and carbonates in the outermost stratum of the oxide film. It might come from the calcium present as an impurity in the bulk alloy (Table 1) [40,41] or be an impurity from the processing of the magnesium alloy sheets.

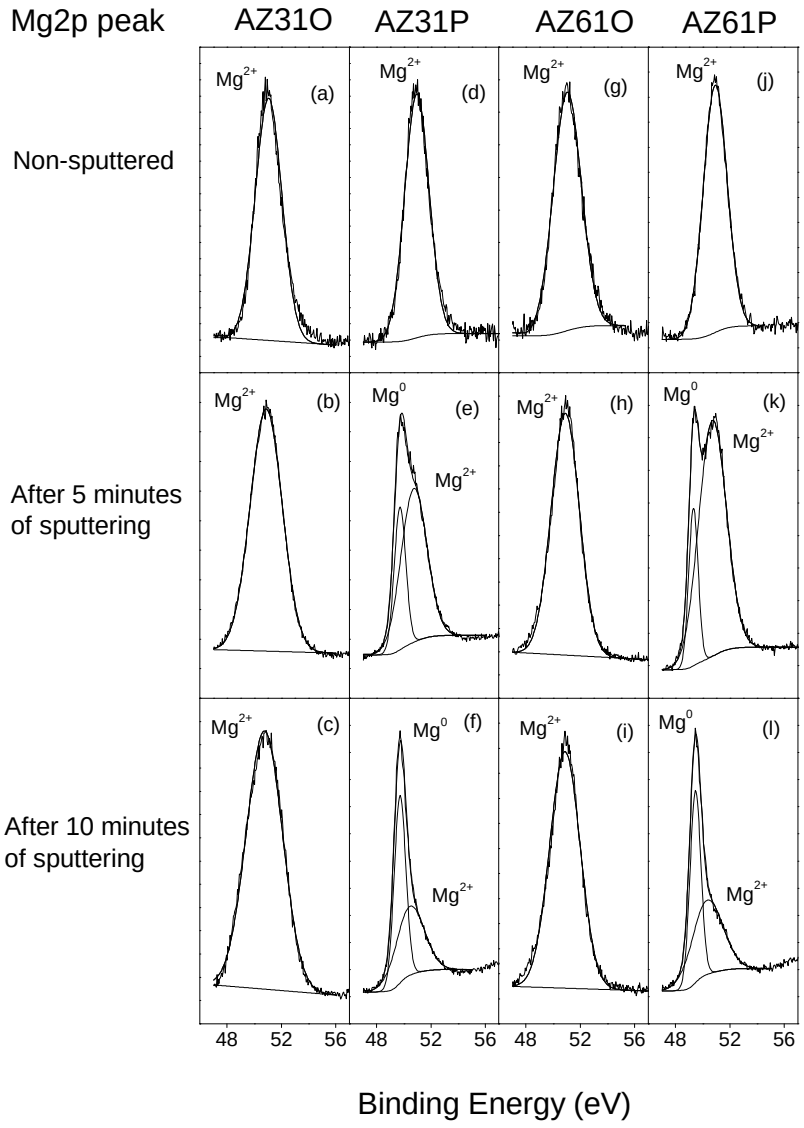

Figure 3. *XPS Mg2p spectra of the AZ31 and AZ61 alloys in the original (O) and polished (P) surface conditions.*

The O/(Mg+Al) atomic ratios obtained on the non-sputtered surface of the original AZ31 and AZ61 alloys reach values close to 1.6 (Table 2), which tends to suggest the possibility that the outer film is mainly formed by $Mg(OH)_2$. On the non-sputtered surface of the polished alloys this ratio reaches values of close to 3. The spontaneous formation of magnesium carbonate on the freshly polished surfaces presumably accounts for this increase. After 5 min. of sputtering, significant amounts of aluminium appear in the oxide film, especially with the AZ61 alloy.

Table 2. *Atomic composition of the surface of the AZ31 and AZ61 alloys in original (as-received) and polished conditions.*

	Time of sputtering (min)	% C	% O	% Mg	% Al	% Ca	O/(Mg+Al)	Al/(Mg+Al) X100
Original Surface								
AZ31	0	51	30	16	2	1	1,6	11
	5	5	53	38	4	0	1.25	10
	10	4	52	38	6	0	1.2	14
AZ61	0	65	21	10	3	1	1.6	23
	5	11	55	26	8	0	1.6	24
	10	5	56	28	11	0	1.4	28
Polished Surface								
AZ31	0	51	35	12	2	0	2.5	14
	5	0	41	54	5	0	0.7	8
	10	0	18	75	6	0	0.2	7
AZ61	0	37	47	13	3	0	3	19
	5	0	46	46	8	0	0.9	15
	10	0	21	68	11	0	0,3	14

On the sputtered surface of the polished AZ31 and AZ61 alloys, a considerable increase in the magnesium content is seen to coincide with a decrease in the oxygen content (Table 2). Five minutes of sputtering is sufficient to remove the significant carbon content detected on the surface of the alloys. The thin outer film of magnesium oxides formed as a result of the polishing process is probably uniform, homogeneous and continuous. In contrast, no great variation in the magnesium or oxygen contents is detected on the original surface of the AZ31 and AZ61 alloys when the sputtering time is raised from 5 to 10 minutes, and the presence of carbon is noted after 10 minutes of sputtering. These results tend to suggest that the external oxide film resulting from the

fabrication of the wrought alloys has a non-uniform distribution (e.g., in the form of islands) over the alloy surface and is discontinuous and porous. AFM images (Fig. 4) tend to support this interpretation.

From XPS determinations of oxide film thickness the superficial film formed on the polished AZ61 alloy is some 2 nm thicker than on the AZ31 alloy (Table 3). On the other hand, the presence of a coarse discontinuous outer layer of magnesium and aluminium oxides on the original surface of the AZ31 and AZ61 alloys has prevented in this case to make similar estimates of native oxide film thickness.

Table 3. *Thickness of air-formed oxide film on polished specimens.*

Material	Film thickness (nm)
AZ31	3.2
AZ61	5.1

As Table 4 shows, the roughness values of the specimens in the original conditions are about seven times greater than in the polished condition. Nanometric scale details of the typical surface roughness exhibited by the tested specimens are given in Fig. 4.

Table 4*. Roughness values obtained with atomic force microscopy. The values are the averages of four determinations.*

Specimens	RMS (nm)
Original surface	
AZ31	197.9
AZ61	116.2
After polishing	
AZ31	29.1
AZ61	17.1

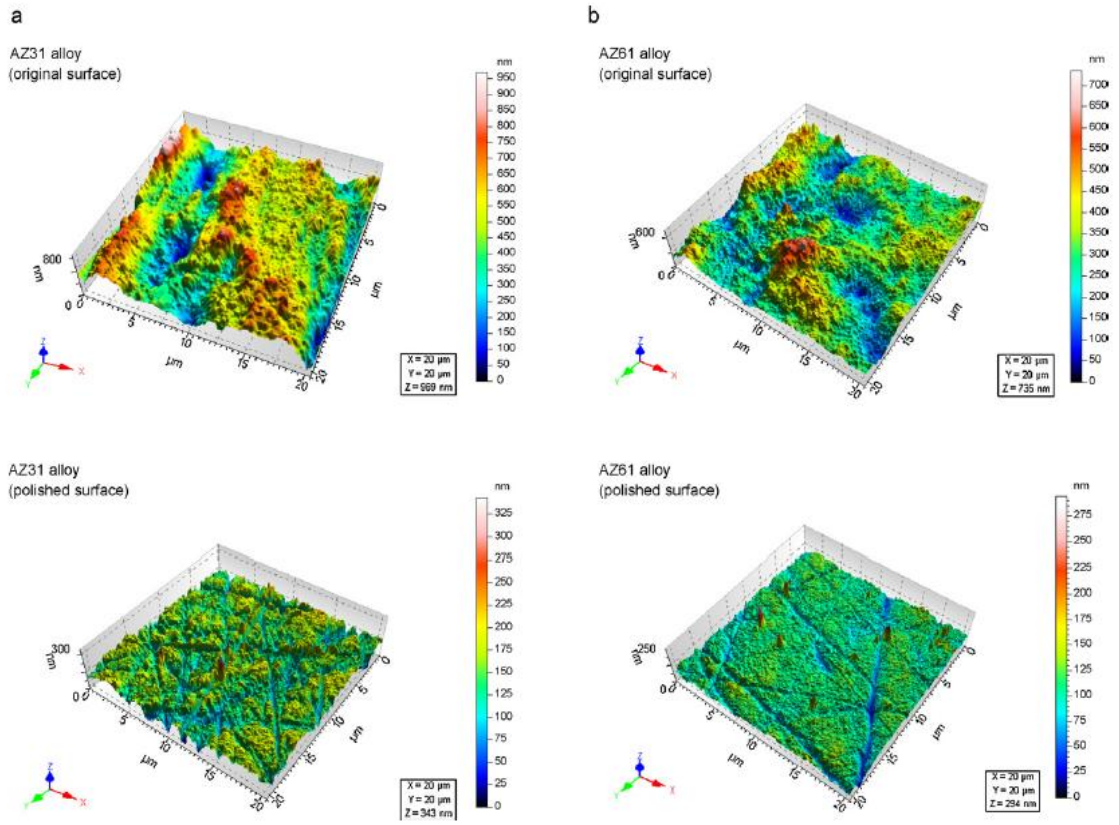

Figure 4. *AFM images of the surfaces in the original (O) and polished (P) surface conditions for: (a) AZ31 alloy and (b) AZ61 alloy.*

3.2. Electrochemical impedance measurements

The evolution of the corrosion process has been monitored by means of impedance measurements (Fig. 5) with the specimens immersed in 0.6 M NaCl solution. Bode plots of the phase angle δ show the existence of two time constants, which in the Nyquist diagrams mean the presence of a capacitive loop at high frequencies (HF) and an inductive loop at low frequencies (LF), Fig. 5.

Since there is some impedance frequency dispersion behaviour in the measurements, a constant phase element (CPE) was used to fit the experimental spectra. The equivalent circuit depicted in Fig. 6 served to obtain the parameters of the R_{HF}–CPE capacitive arc. The non-ideal capacitive behaviour is represented by the CPE, which depends on the frequency independent parameters Q and n, in accordance with the impedance function $CPE=Q^{-1}(j\omega)^{-n}$.

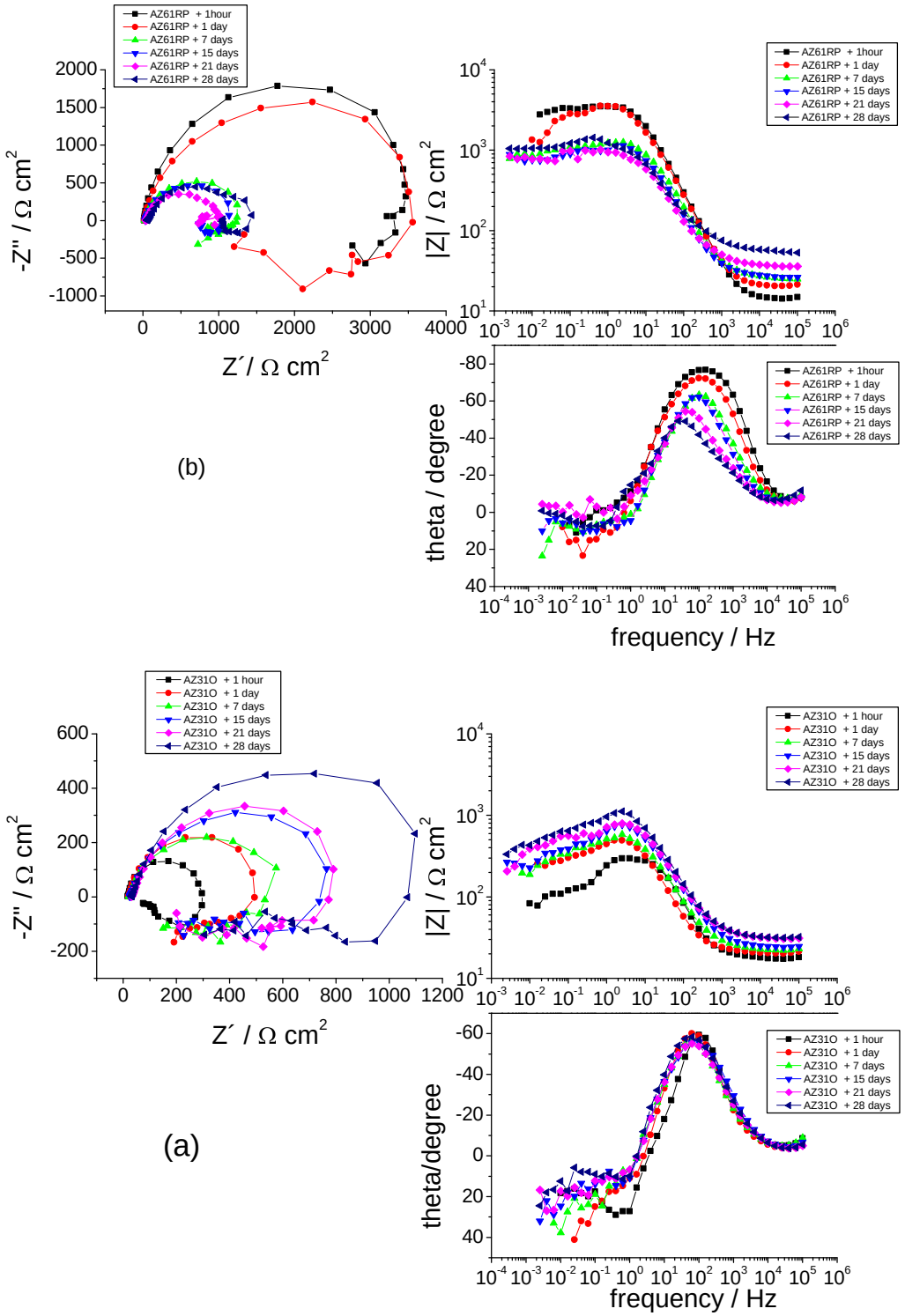

Figure 5. *Example of impedance diagrams for the tested alloys. Nyquist and Bode plots, (a) for alloy AZ31, surface in the original (as-received) condition, and (b) for alloy AZ61, surface in the freshly polished condition.*

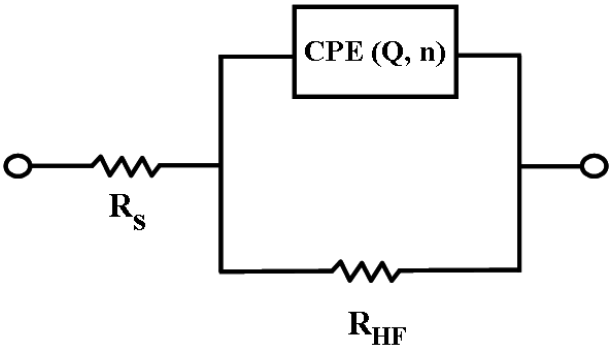

Figure 6. *Equivalent circuit used to analyse the electrochemical impedance behaviour of the tested alloys.*

In Fig. 6, R_{HF} denotes the high frequency resistance and R_S is the solution resistance. The fitting covered frequencies between ~ 5 and 10^4 Hz. Table 5 is a representative example of the values of Q and n (pertaining to the CPE) which resulted from the fitting procedure applied to the different tested specimens, in this case referred to the alloy AZ31 in the original condition.

Q and n data were converted into capacitance (C) data using the relationship [42]:

$$C = Q\ (\omega_{max})^{n-1}$$

In which ω_{max} is the frequency at which the imaginary part of the impedance has a maximum.

Table 5. *Values of the Q and n components of the CPE, for alloy AZ31 alloy tested in the freshly polished condition, after different immersion times.*

Immersion time (hours)	Q (s^n/Ω)	n
1	2.60×10^{-5}	0.952
24	4.04×10^{-5}	0.960
168	4.02×10^{-5}	0.840
360	3.88×10^{-5}	0.824
504	3.38×10^{-5}	0.845
672	2.94×10^{-5}	0.856

4. Discussion

4.1. Changes in surface films during immersion time

In the literature concerning the corrosion behaviour of magnesium alloys in aqueous solutions the capacitive loop in the HF region has always been attributed to the charge transfer reaction of the corrosion process [22,24,27,43,44], and the diameter, R_{HF}, of the loop has been inversely related to the corrosion rate by means of the Stern-Geary equation [45].

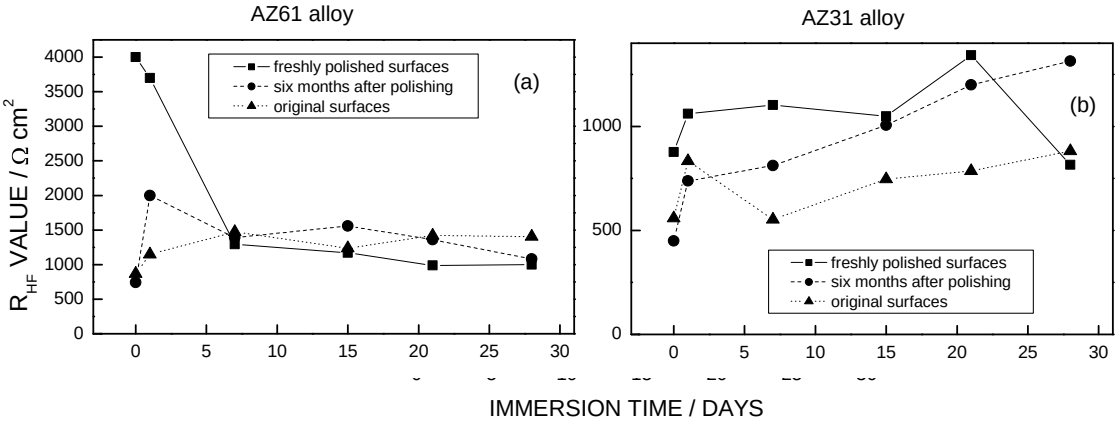

Figure 7. *Variation in R_{HF} values as a function of surface conditions and alloy type over 28 days immersion.*

Fig. 7 displays these R_{HF} values for the AZ31 and AZ61 alloy specimens as a function of surface conditions and immersion time. The evolution of R_{HF} reveals that the surface conditions exert a certain effect during the initial stages of testing. During the first day of immersion the specimens present traits that are not seen in exposure for longer times; the predominant trend is for the R_{HF} to increase with immersion time. An exception can be seen in the case of specimens dipped into solution immediately after polishing, which show relatively little variation of the R_{HF} values throughout the first day. For times of more than 1 day up to approximately 10 days, the tendency for many specimens is the reverse, with a reduction in R_{HF} with immersion time. Attention is drawn to the high R_{HF} values for the AZ61 alloy specimen tested immediately after polishing (RP condition). Mechanical polishing probably leaves the metallic surface in an especially reactive estate that promotes the immediate growth of a protective film more perfect than that resulting in 6 months of laboratory atmosphere exposure (PE condition) or that covering the as-received surface (original, O condition).

As an illustration of the magnitude of the effect of surface preparation on the corrosion rate we will consider the data for the first hour of immersion, when this effect is more pronounced (data shown graphically in Fig. 7). From the Stern-Geary equation we can assume the existence of an inverse proportionality between corrosion current (directly related to corrosion rate) and the value of R_{HF} (this coincident with the charge transfer resistance of the corrosion reaction). In the case of the results obtained with specimens of the same alloy and exposed to identical aggressive medium, the constant of proportionality between corrosion rate and $1/R_{HF}$ must be essentially the same. This fact facilitates comparisons. So, it is possible to deduce from the data obtained in the investigation that the corrosion rate of AZ31 alloy in the freshly polished condition was almost half that in the original condition, and the decrease in the case of the AZ61 alloy was by almost a factor of five.

The differences in the evolution of R_{HF} with immersion time may be due to the offsetting of two opposing effects: blocking of possible pores in the pre-existing film with incipient corrosion products and, on the other hand, dissolution of this film by the saline solution. The relative weight of each effect cannot be estimated, so it is not possible to predict the results, although it may be supposed that the first effect will predominate at the start of testing and the latter will take precedence after about 24 h of immersion. By prolonging immersion time, the complete dissolution, transformation or replacement of the pre-existing film with a new film formed by reaction of the metal surface with the aqueous medium, as well the simultaneous growth of an outer thick layer of corrosion product on the surface should influence the later evolution of R_{HF} values. Attempts which have been made in the literature [12,27,28,43,44,46] to interpret the impedance data of magnesium and its alloys in aqueous media suggest a corrosion process controlled mainly by the thin oxide film formed on the metal surface, the metal dissolution occurring at the bare parts of the film.

Studies conducted by different researchers mention the formation of the additional layer of corrosion product precipitated on the surface of the magnesium and its alloys immersed in aqueous solutions [12,24,30,43]. This layer can reach a thickness of 15-200 µm after 10 days of immersion in 0.6 M NaCl solution [24], and presents a rather high porosity; its growth appears to exert a relatively small influence on the kinetics of the corrosion process.

Many studies have confirmed that the outer layer of corrosion product consists mainly of brucite ($Mg(OH)_2$), which formation is predictable because magnesium dissolution

favours the production of OH^- ions from the cathodic reaction, increasing the pH and allowing the formation of magnesium hydroxide layer by means of a precipitation reaction [15,46].

The overall reactions for the corrosion of magnesium can be written as

$$Mg = Mg^{2+} + 2e$$
$$2\,H_2O + 2e = H_2 + 2OH^-$$

The magnesium dissolution occurs in the film free areas and the Mg^{2+} ions diffuse to react with the hydroxyl ions OH^- to form the porous layer of $Mg(OH)_2$ on top of the inner barrier film.

It would be important to have a better understanding of all details about the nature and characteristics of the protective films on the metal surface, that have an influence on the corrosion process. XRD data of the surface of specimens corroded under experimental conditions similar to those in this work have shown the expected formation of brucite ($Mg(OH)_2$) as the main corrosion product [24]. In other XPS and XRD analyses conducted by several groups of investigators [13,18,30], the same conclusion was reached regarding the composition of the external layer formed during the corrosion of magnesium and its alloys in aqueous solution. A problem in these type of investigations is that this thick layer of corrosion product makes difficult to extend the analysis to the very thin film at the metal surface, which is precisely the one that seems to exert the greatest influence on the corrosion process.

One point emerging in the set of R_{HF} values (Fig. 7) is the clear tendency for alloy AZ61 to present in the first 20-25 days higher values than the alloy AZ31 for the same immersion times. This greater resistance is in agreement with results reported in the literature which suggests a possible beneficial effect of Al content on the corrosion resistance of Mg-Al alloys, perhaps due to some improvement of the protective properties of the surface film [20,25]. Comparison of the R_{TH} values for these two alloys shows another difference. After the first day of immersion, the R_{HF} values of the AZ61 alloy specimens show a rather moderate tendency to decrease with time, an effect that continues up to the 28 days of testing (Fig. 7). Curiously, with alloy AZ31 the reverse tendency seems to predominate. It is considered a relevant fact that the R_{HF} values obtained with the two alloys converge in time towards relatively similar values. Since stationary values take a significant time to become established, it should be

noticed that short-term measurements may give rise to misleading comparisons of corrodibility without specifying the time during which alloys AZ31 and AZ61 have been immersed in the aggressive solution.

The above results are logically linked to changes experienced by the specimen surfaces during exposure to the 0.6 M NaCl solution. In this respect, the following features are highlighted: (i) the marked tendency of the AZ61 alloy for the capacitive arc size to decrease with immersion time from the first day (Fig. 5b); (ii) the moderate tendency of the AZ31 alloy for the capacitive arc size to grow from the start of the test (Fig. 5a); and (iii) for longer immersion times, the evolution of the capacitive arc to a practically steady state size with both alloys. In case (i), the decrease in the capacitive arc size with time suggests a weakening of the protective action of the film covering the metallic surface, probably due to progressive dissolution or deterioration of the air-formed film in contact with the aggressive 0.6 M NaCl solution.

Since the films formed in an aqueous environment are not equal to the films formed in air, once a specimen is placed in solution the pre-existing film on its surface may be transformed, reconstructed, or replaced by a new and also very thin film on the metallic surface, whose occurrence is probably related to the Cabrera-Mott mechanism of film growth. Various studies [5,12,15,30,47-49] on the behaviour of Mg and its alloys in immersion mention the presence of a very thin MgO film (just a few nanometres thick) on the metallic surface. In the above case (i) the effect of all these possible processes obviously cannot compensate the weakening of the protective action of the film. In case (ii), the increased capacitive arc size with immersion time suggests a reinforcement of the protective action of the films coating the metallic surface. On alloy AZ31 the initial film may be less protective and its effect on the specimen's behaviour will tend to disappear relatively quickly; a leading role may soon be taken by the new films formed as a result of the reaction with the aqueous medium, whose consolidation and growth must be attributed responsibility for the moderate tendency for the capacitive arc size to increase. In case (iii) the practical equalling of the arcs corresponding to the different initial surface conditions with immersion time suggests the evolution of the specimens towards states of similar surface constitution and activity. When the immersion time increases from approximately 10 days to 28 days (maximum immersion time), the R_{HF} value tends to a steady state value, which reflects the attainment of a dynamic balance between the corrosion and continuous film reconstruction processes; the drop in R_{HF} values for alloy AZ61 and the increase for alloy AZ31 with immersion time resulting in o a notable reconciliation of the points corresponding to both alloys after about 20 days.

4.2. Capacitance values

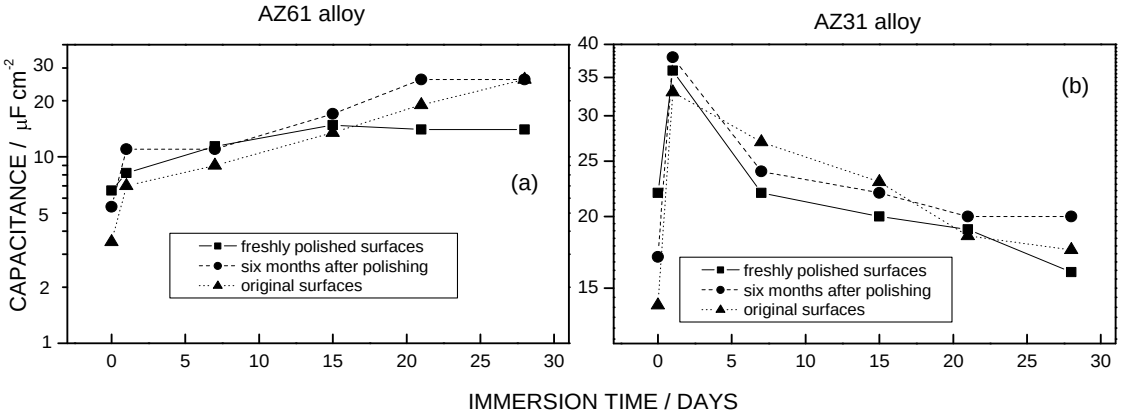

Figure 8. *Variation in capacitance values as a function of surface conditions, alloy type and immersion time.*

Fig. 8 displays the capacitance values associated with the capacitive loop of the impedance diagrams. Comparing the graphs for alloys AZ31 and AZ61, it can be seen that these capacitance values in the first 24 h of immersion are clearly higher in the case of the AZ31 alloy specimens than for AZ61. Subsequently, over the next 15 days, the capacitance values continue to be greater for AZ31, though tending to decrease, while the values for AZ61 tend to increase gradually, so that the values for both alloys converge on practically similar capacitance values. After 15-20 days, the capacitance values for all the tested specimens are grouped around 15-20 $\mu F/cm^2$.

The higher initial values of capacitance for alloy AZ31 compared with those for alloy AZ61 (Fig. 8) suggest either the presence of thinner films, according to the inverse relationship between capacitance and film thickness of the flat capacitor formula [46], or more defective films which leaves a greater fraction of metallic surface area in contact with the electrolyte [50]. Curiously, despite the considerably different values of surface roughness (Fig. 3 and Table 4), no significant differences in capacitance have been observed when comparing the capacitance values for the as-received and polished surfaces (Fig. 8). The complex relationship that can exist between roughness and true surface area could perhaps explain this fact [51-53].

4.3. Inductive loop

As already commented, the impedance diagrams in this study are characterised by a capacitive loop at HF followed by a well-marked inductive loop at LF. Elucidating the precise nature of the inductive loop seems rather complicated and is of no practical

relevance with regard to information on the corrosion rate. Nevertheless, the repeated presence of an inductive loop in the impedance diagrams obtained in this work merits some attention.

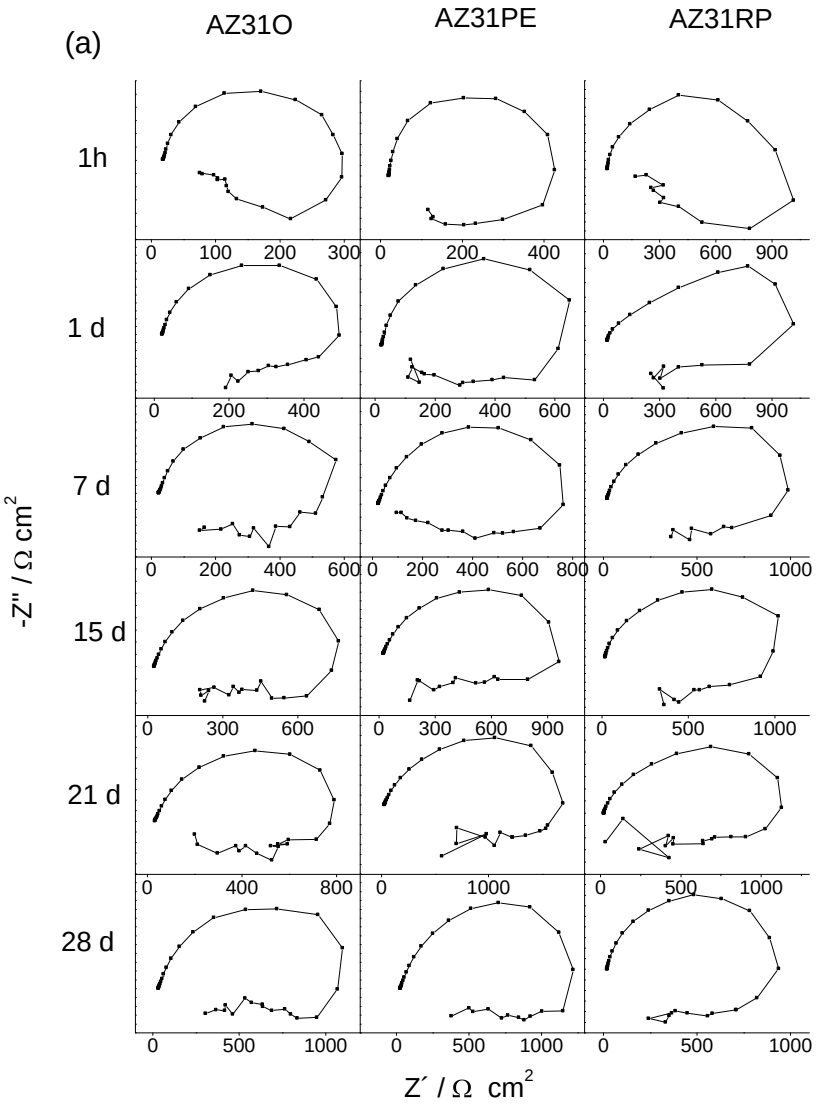

Figure 9. *Variation in Nyquist plots for (a) AZ31 and (b) AZ61 specimens with immersion time (hours or days on the Y-axis) and surface conditions (O, original surface; PE, six months after polishing; RP, freshly polished, on the X-axis).*

Numerous examples of such inductive loops can be found in the literature. An inductive effect may be explained by different reasons. It is normally related with the adsorption of active species on the metallic surface, whose coverage depends on the electrode potential variations during the measurements [54-56]. In the corrosion of magnesium and its alloys, where Mg^{2+} ion production seems to occur in two steps, the intermediate Mg^{+} should be the adsorbed specie [43-46].

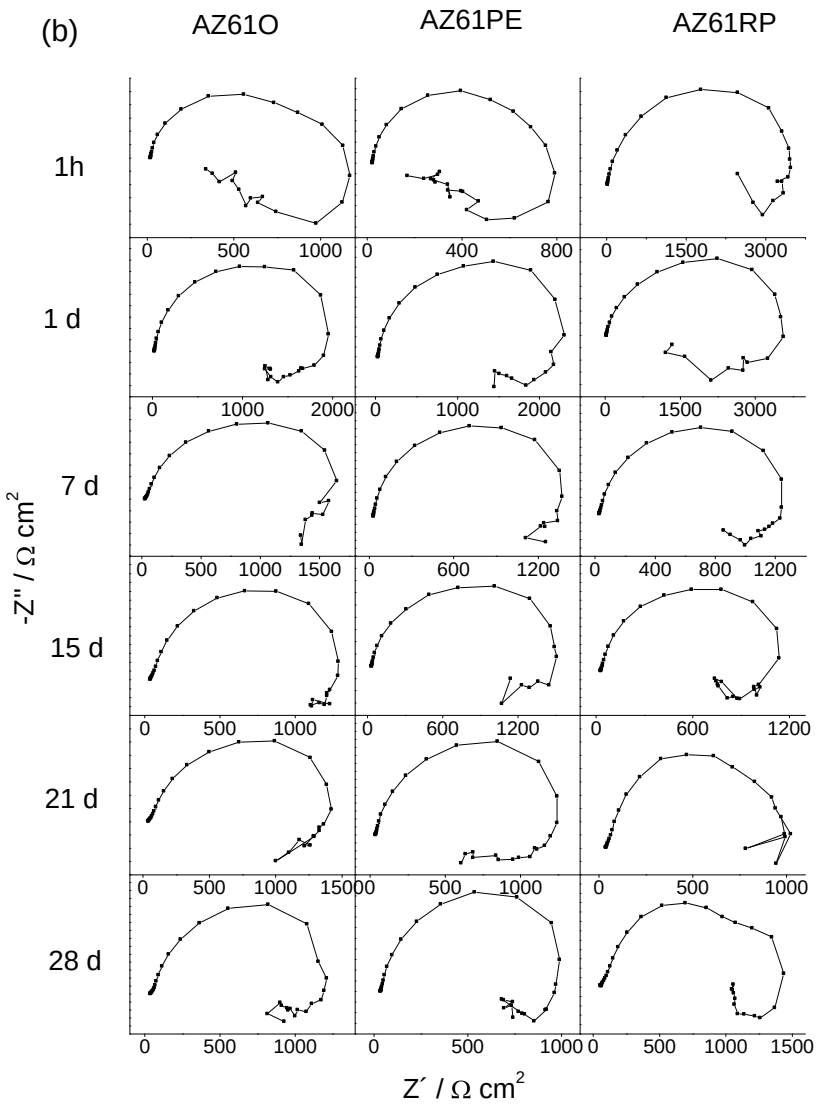

Figure 9. *Variation in Nyquist plots for (a) AZ31 and (b) AZ61 specimens with immersion time (hours or days on the Y-axis) and surface conditions (O, original surface; PE, six months after polishing; RP, freshly polished, on the X-axis).*

The notable size of the inductive loops in this work may be seen in Fig. 9. Their size seems to be related somehow with the R_{HF} value and, therefore, with the surface activity of the specimens in the corrosive medium.

Immersion time has also been seen to have an effect on the relative size of the inductive loop. If the loop size is expressed as the diameter of the semicircle that fits it, and δ is the ratio between the diameters of the inductive and capacitive loops, after two hours of immersion δ values of the order of 0.7-0.8 have been obtained with practically all the tested alloys and surface conditions. At longer immersion times, between 1 and 28 days,

the δ ratio continues to be of the order of 0.7-0.8 for alloy AZ31 but decreases significantly with alloy AZ61 to approximately 0.3-0.4.

5. Conclusions

(1) The corrosion behaviour of magnesium alloys AZ31 and AZ61 in several initial surface conditions has been studied by the EIS technique, specially trying to relate the experimental circumstances of the oxide film formation in the air with the subsequent behaviour of the alloys immersed in 0.6 M NaCl solution. A certain effect of initial surface conditions is observed only in the early stages of the test. Attention is drawn to the high capacitive loop diameter values (R_{HF}) of the Nyquist diagrams in the case of the specimens tested immediately after mechanical polishing, compared to those tested after 6 months of exposure laboratory ambient, or in the as-received condition. After an initial period which does not last for more than about 7 days, no effect attributable to the initial surface condition of the specimens is generally seen.

(2) With regard to the effect of the alloy type, in the first days of immersion a tendency of alloy AZ61 to show the highest R_{HF} values (lower corrosion rates) is observed. After 15 days of testing the differences between the impedance diagrams of alloys AZ61 and AZ31 are notably smaller, although the AZ61 alloy continues to show the largest R_{HF} values.

(3). A clear effect of the alloy type but not of the surface condition on the capacitance values has been shown. Attention is also drawn to the different behaviour of the AZ31 and AZ61 alloys with regard to the inductive loop.

Acknowledgment

We wish to express our gratitude to Prof. S. Feliu for several clarifying and stimulating discussions during the course of this work. Also, the authors gratefully acknowledge the financial support for this work from the Ministry of Science and Innovation of Spain (MAT 2009-13530)

References

[1]. V. Fournier, P. Marcus, I. Olefjord, Sur. Interface Anal., 34 (2002) 494.
[2]. J. Kim, K.C. Wong, P.C. Wong, S.A. Kulinich, J.B. Metson, K.A.R. Mitchell, Appl. Sur. Sci., 253 (2007) 4197.
[3]. C. Fotea, J. Callaway, M.R. Alexander, Sur. Interface Anal., 38 (2006) 1363.
[4]. N.S. McIntyre, C. Chen, Corros. Sci., 40 (1998) 1697.
[5]. J.H. Nordlien, S. Ono, N. Masuko, K. Nisancioglu, Corros. Sci., 39 (1997) 1397.
[6]. S.J. Splinter, N.S. McIntyre, Surf. Sci., 314 (1994) 157.
[7]. R. Lindström, J.-E. Svensson, L-G. Johansson, J. Electrochem. Soc., 149 (2002) B103.
[8]. R. Lindström, L.-G. Johansson, G.-E. Thompson, P. Skeldon, J.E. Svensson, Corros. Sci.,46 (2004) 1141.
[9]. M. Jönsson, D. Persson, R. Gubner, J. Electrochem. Soc., 154 (2007) C684.
[10]. M. Jönsson, D. Persson, D. Thierry, Corros. Sci., 49 (2007), 1540.
[11]. J.H. Nordlien, S. Ono, N. Masuko, K. Nisancioglu, J. Electrochem. Soc., 142 (1995), 3320.
[12]. G. Baril, N. Pebere, Corros. Sci., 43 (2001) 471.
[13]. G. Ballerini, U. Bardi, R. Bignucolo, G. Ceraolo, Corros. Sci., 47 (2005) 2173.
[14]. G. Song, A. Atrens, X. L. Wu, B. Zhang, Corros. Sci., 40 (1998) 1769.
[15]. G. Song, A. Atrens, D. Stjohn, J. Naim, Y. Li, Corros. Sci.,39 (1997) 855.
[16]. G. Song, A. Atrens, M. Dargusch, Corros. Sci., 41 (1999) 249.
[17]. R. Lindström, L.-G. Johansson, J.-E. Svensson, Mat. and Corros., 54 (2003) 587.
[18]. R. Ambat, N.N. Aung, W. Zhou, Corros. Sci., 42 (2000) 1433.
[19]. S. Mathieu, C. Rapin, J. Steinmetz, P. Steinmetz, Corros. Sci., 45 (2003) 2741.
[20]. G. Song, A. Atrens, Adv. Eng. Mat., 1 (1999) 11.
[21]. G. Song, A. Atrens, Adv. Eng. Mat., 9 (2007) 177.
[22]. G.L. Makar, J. Kruger, J. Electrochem. Soc., 137 (1990) 414.
[23]. A. Pardo, M.C. Merino, A.E. Coy, R. Arrabal, F. Viejo, E. Matykina, Corros. Sci., 50 (2008) 823.
[24]. 24. A. Pardo, M.C. Merino, A.E. Coy, F. Viejo, R. Arrabal, S. Feliu Jr., Electrochim. Acta, 53 (2008) 7890.
[25]. J.H. Nordlien, K. Nisancioglu, S. Ono, N. Masuko, J. Electrochem. Soc., 143 (1996) 2564.
[26]. J.H. Nordlien, K. Nisancioglu, S. Ono, N. Masuko, J. Electrochem. Soc., 144 (1997) 461.
[27]. S. Mathieu, C. Rapin, J. Hazan, P. Steinmetz, Corros. Sci., 44 (2002) 2737
[28]. G. Galicia, N. Pebere, B. Tribollet, V. Vivier, Corros. Sci., 51 (2009) 1789.
[29]. C. Chen, S.J. Splinter, T. Do, N.S. McIntyre, Surf. Sci., 382 (1997) L652.
[30]. M. Santamaria, F.Di Quarto, S. Zanna, P. Marcus, Electrochim. Acta, 53 (2007) 1314.
[31]. N. Cabrera, N.F. Mott, Rep. Progr. Phys., 12 (1948) 163.
[32]. S. Feliu Jr., M.C. Merino, R. Arrabal, A.E. Coy, E. Matykina, Sur. Interface Anal., 41 (2009)143.
[33]. M. Jönsson, D. Persson, C. Leygraf, Corros. Sci., 50 (2008) 1406.
[34]. C.D. Wagner, L.E. Davis, M.V. Zeller, J.A. Taylor, R.H. Raymond, L.H. Gale, Surf. Interface Anal., 3 (1981) 211.
[35]. B.R. Strohmeier, Surf. Interface Anal., 15 (1990) 51.
[36]. S. Tanuma, C.J. Powell, D.R. Penn, Surf. Interface Anal., 17 (1991) 911.
[37]. A. Akkerman, T. Boutboul, A. Breskin, R. Chechik, A.Gibrekhterman, Y. Lifshitz, Phys. Stat. Sol (b), 198 (1996) 769.
[38]. C.J. Powell, A. Jablonski, NIST Electron Inelastic-Mean-Free-Path Database, SRD 71, US Departament of Commerce, National Institute of Standards and Technology, Gaithersburg, MD (2000).
[39]. M. Liu, S. Zanna, H. Ardelean, I. Frateur, P. Schmutz, G. Song, A. Atrens, P. Marcus, Corros. Sci., 51 (2009) 1115.
[40]. S. Feliu Jr., C. Maffiotte, J.C. Galván, A. Pardo, M. C. Merino, R. Arrabal, The Open Surface Science Journal, 3 (2011), 1-14.
[41]. S. Feliu Jr., J.C. Galván, A. Pardo, M.C. Merino, R. Arrabal, The Open Corrosion Journal, 3 (2010) 80-91.
[42]. C.H. Hsu, F. Mansfeld, Corrosion, 57 (2001) 747.
[43]. N. Pebere, C. Riera, F. Dabosi, Electrochim. Acta, 35 (1990) 555.
[44]. G. Song, A. Atrens, D. St. John, X. Wu, J. Nairn, Corros. Sci., 39 (1997) 1981.

[45]. M. Stern, A.L. Geary, J. Electrochem. Soc., 104 (1957) 56.
[46]. G. Baril, G. Galicia, C. Deslouis, N. Pebere, B. Tribollet, V. Vivier, J. Electrochem. Soc., 154 (2007) C108.
[47]. G. Galicia, N. Pebere, B. Tribollet, V. Vivier, Corros., Sci., 51 (2009) 1789.
[48]. N. Hara, Y. Kobayashi, D. Kagaya, N. Akao, Corros. Sci., 49 (2007) 166.
[49]. M. Liu, P. Schmutz, S. Zanna, A. Seyeux, H, Ardelean, G. Song, A. Atrens, P. Marcus, Corros. Sci., 52 (2010) 562.
[50]. V. Barranco, S. Feliu Jr., S. Feliu, Corros. Sci., 46 (2004), 2221.
[51]. M.G. Donoso, A. Méndez-Vilas, J.M. Bruque, M.L. González-Martín, Int. Biodet. & Biodegradation, 59 (2007) 245.
[52]. R.D. Armstrong, R.A. Burnham, J. Electroanal. Chem., 72 (1976), 257.
[53]. U. Rammelt, G. Reinhard, Corros. Sci., 27 (1987) 373.
[54]. I. Epelboin, C. Gabrielli, M. Keddam, H. Takenouti, Electrochim. Acta, 20 (1975) 913.
[55]. W.J. Lorenz, F. Mansfeld, Corros. Sci., 21 (1981) 647-672.
[56]. M. Metikos-Hukovic, R. Babic, Z. Grubac, J. Appl. Electrochem., 32 (2002) 35.

Effect of the Chemistry and Structure of the Native Oxide Surface Film on the Corrosion Properties of Commercial AZ31 and AZ61 Alloys

Sebastián Feliu (Jr)[a] , C. Maffiotte[b], A. Samaniego[a], Juan Carlos Galván[a], Violeta Barranco[a,c].

[a]Centro Nacional de Investigaciones Metalúrgicas CSIC, Avda. Gregorio del Amo 8, 28040 Madrid, Spain,
[b]CIEMAT-DT (edificio 30), Avda. Complutense, 22, 28040 Madrid, Spain
[c]Instituto de Ciencias de Materiales de Madrid, ICMM, Consejo Superior de Investigaciones Científicas, CSIC, Sor Juana Inés de la Cruz, 3, Cantoblanco, 28049, Madrid, Spain

Applied Surface Science 257 (2011) 8558–8568

Abstract:

The purpose of this study has been to advance in knowledge of the chemical composition, structure and thickness of the thin native oxide film formed spontaneously in contact with the laboratory atmosphere on the surface of freshly polished commercial AZ31 and AZ61 alloys with a view to furthering the understanding of protection mechanisms. For comparative purposes, and to more fully describe the behaviour of the native oxide film, the external oxide films formed as a result of the manufacturing process (as-received condition) have been characterised. The technique applied in this research to study the thin oxide films (thickness of just a few nanometres) present on the surface of the alloys has basically been XPS (X-ray photoelectron spectroscopy) in combination with ion sputtering. Corrosion properties of the alloys were studied in 0.6M NaCl by measuring charge transfer resistance values, which are deduced from EIS (electrochemical impedance spectroscopy) measurements after 1 hour of exposure. Alloy AZ61 generally showed better corrosion resistance than AZ31, and the freshly polished alloys showed better corrosion resistance than the alloys in as-received condition. This is attributed to a combination of (1) higher thickness of the native oxide film on the AZ61 alloy and (2) greater uniformity of the oxide film in the polished condition. The formation of an additional oxide layer composed by a mixture of spinel ($MgAl_2O_4$) and MgO seems to diminish the protective properties of the passive layer on the surface of the alloys in as-received condition.

Keywords: Magnesium alloys, native oxide film; chemistry and structure; corrosion properties; XPS

1. Introduction

The chosen study materials are Mg-Al alloys, which have aroused great scientific and technological interest over the last two decades. From a practical point of view magnesium is the structural metal of lowest density, which makes it highly attractive for use in the automotive, aerospace, IT and electronics industries, as well as in the development of new biomaterials for orthopaedic and cardiovascular applications where weight plays a decisive role. However, as magnesium is one of the chemically most active metals, insufficient resistance to atmospheric and aqueous corrosion sometimes limits its applications. Thus it is desirable to have as complete as possible information on the factors that influence the corrosion of these materials.

In the literature a great deal of attention has been paid to the role of the β-phase on the corrosion mechanism of magnesium/aluminium alloys. A generally accepted idea is that this phase acts as an effective cathode and/or barrier against corrosion, depending on its size and distribution [1]. Therefore, the alloy microstructure plays a key role in determining the corrosion susceptibility of magnesium-aluminium alloys, especially for high aluminium alloys such as the well-known AZ91 alloy (~ 9 wt.% Al). The present study concerns the corrosion behaviour of the AZ31 and AZ61 alloys. Since AZ31 is essentially a single-phase alloy with 3 wt%. aluminium in solid solution and that more than 90% fraction of the alloy AZ61 may also correspond to this phase, it can be concluded that, in the case of both alloys, the measured values should be very closed to those of the matrix phase. In this case, Song and Xu [2] commented that the crystalline variables, such as the grain size (grain boundary) and crystal defects (dislocation and twin), the surface state (e.g. roughness and purity), will become dominating factors affecting the corrosion behavior. In our previous studies [3-6], we observed that the properties of the oxide/hydroxide film formed on the surface often affect the corrosion behaviour of the magnesium alloy in the atmosphere [3-4] or in NaCl solution [5-6].

In immersion tests in saline solution, during the early stages of exposure (before the formation of visible black spots on the surface), the protective properties of the alloy seem to depend mainly on the chemistry and structure of thin native oxide films spontaneously formed in contact with the atmosphere. As Nordlien et al. [7, 8] and Lunder et al [9] suggested, the original air-formed film is a highly stable form of oxide and preserves its properties when the specimen is exposed to the aqueous environment. Santamaria et al. [10] report that, in aqueous solution, a Mg hydroxide layer can grow while an ultra-thin MgO layer is maintained at the metal interface.

One of the main obstacles to obtaining information on the native oxide film is that of its small thickness (just a few nm), which is often too small to produce a sufficient signal for conventional materials characterisation techniques (SEM/EDX, XRD or TEM) [11]. In contrast, XPS surface analysis technique, allows the analysed thickness to be reduced to only 3 nm and supplies information on the oxidation state of the detected element. Another drawback is that, as a result of the high affinity of magnesium to O2, H2O, CO and CO2, magnesium alloys react with the ambient atmosphere contaminating the surface. The outer layer of the native oxide film is spontaneously covered by a layer of hydroxyl and carbonate groups and destructive depth profile techniques such as ion sputtering have to be used. This technique may cause some artefacts as enrichment of elements in multi-component materials (preferential sputtering) [12], bond breaking and decomposition of oxides, phase formation, segregation, roughness formation [13].
Oxide film formation and properties such as its protectiveness may be sensitive to the conditions under which it grows. Laboratory tests normally refer to the behaviour of surfaces that have been mechanically polished prior to testing, in order for metallographic observation and the removal of impurities and oxidation/corrosion product layers formed during the manufacturing process and subsequent storage of the alloy. However, it is of practical interest to obtain information on the chemical composition of the surface of the alloys in as-received condition (untreated surface). In many applications magnesium alloys are used without further treatments [14], while on the other hand surface modification treatments such as conversion coating treatment are generally applied directly on the as-received surface, which may influence the formation and properties of these coatings [15]. From a scientific point of view, the literature contains controversial views relating to the effect of skin characteristics on the corrosion performance of magnesium alloys [16]. Song et al. [17] reported that the skin of die cast AZ91D showed better corrosion resistance than the interior. The opposite conclusion was obtained by Yu and Uan [18] and Zhang et al [14]. Recently, Song and Xu [2] have observed an improvement in the corrosion performance of AZ31B Mg alloy sheet by surface polishing. In general, these studies correlate corrosion properties with the microstructure of the skin layer and the impurity concentration.

The objectives of this research are as follows:

1. To study the chemical composition of the native oxide film that forms spontaneously on the surface of AZ31 and AZ61 alloys after polishing with the aim of finding possible relationships between the alloying element contents in

the bulk material, thickness of the oxide film formed, and amount of Al segregated to the outer surface.

2. To analyse the influence of surface condition in the chemistry of the nano layers formed on the outer surfaces of the Mg-Al alloys
3. To contribute to better understanding of the influence of surface conditions, particularly the chemistry of the nano layer, on the corrosion resistance of the Mg-Al alloys in 0.6 M NaCl solution.

2. Experimental

2.1. Materials

The chemical compositions of the tested magnesium alloys, AZ31 and AZ61, are listed in Table 1. They were fabricated in wrought condition and supplied in plates of 3 mm thickness by Magnesium Elecktron Ltd.

Table 1. *Chemical composition of Mg-Al alloys (wt%)*

Material	Al	Zn	Mn	Si	Cu	Fe	Ni	Ca	Zr	Others
AZ31	3.1	0.73	0.25	0.02	<0.001	0.005	<0.001	0.0014	<0.001	<0.30
AZ61	6.2	0.74	0.23	0.04	<0.001	0.004	<0.001	0.0013	<0.001	<0.30

Essential points of the metallurgical preparation of the sheet magnesium alloys, that may influence surface properties in the as-received condition, include heat treatment and hot rolling operations. Unfortunately, it has not been possible to obtain supplier's information on the various stages of manufacturing of the purchased AZ31 and AZ61 sheets used in the research. In the work we have tried to characterize the as-received conditions by analysis of XPS results, which are compared with those for the corresponding polished surfaces.

2.2. Surface conditions

The research compares the behaviour of specimens of the above alloys in the following surface conditions:

- Specimens in as-received condition, which means that the surface of the samples was untreated, only cleaned with distilled water and dried with hot air. As these were commercial specimens, we do not know the exact time of exposure to the atmosphere between manufacturing and characterisation.

- Freshly polished specimens. They were dry ground through successive grades of silicon carbide abrasive papers from P600 to P2000 followed by finishing with 3 and 1 μm diamond paste, cleaned in water and dried with hot air. Due to the high affinity of magnesium to the ambient atmosphere, it was attempted to keep the exposure time to the atmosphere before characterisation of the specimens to a minimum, around 1 hour.

2.3. Metallographic characterisation

Two etching reagents were used: (a) nital 2%, 2 ml HNO3 + 98 ml H2O, to reveal the constituents and general microstructure of alloy AZ61, and (b) 4.6 g picric acid + 10 ml acetic acid + 70 ml ethanol + 10 ml H2O to reveal the grain boundaries of alloy AZ31.
The tested specimens were examined by scanning electron microscopy (SEM) using a JEOL JXA 840A unit operating with Rontec EDR288 software for EDX spectra acquisition and image digitalisation.

2.4. XPS analysis

XPS analysis was performed with a Perkin-Elmer PHI 5400 spectrometer equipped with a Mg Kα excitation source (hν = 1253.6 eV) and a beam size of 1 mm diameter. The spectrometer was calibrated using copper, gold and silver standards. Typical operation conditions were: X-ray gun, 15 kV, 20 mA; pressure in the sample chamber ~ 10^{-9} Torr; pass energy, 89.50 eV for general spectra (0-1100 eV) and 35.75 eV for high resolution spectra. In order to take into account the charging effects on the measured binding energies, these energies have been determined by referencing to the adventitious C 1s peak at 284.8 eV. The intensities were estimated by calculating the area under each peak after smoothing and removing the background using the modified method of Shirley and adjusting the experimental curve to a Gaussian-Lorentzian ratio variable curve using an iterative algorithm. The measurements were performed at take-off angles of 45° with respect to the sample surface. The analysis area was 1 mm x 1 mm, therefore, Gray Munro et al. [19] indicate that with this analysis area XPS results give an average surface chemistry over all phases of the material.

Composition-depth profiling was performed by sequential XPS surface analysis and ion sputter etching using a 4.0 keV argon ion flux. Calibration of the ion sputter etching rate (5 $nm.min^{-1}$) was achieved by depth profiling a SiO2 thin film of known thickness. The actual sputtering rate was determined from the change in oxide film thickness. Pressure in the sample chamber during this process was ~10^{-7} Torr. (bombardment). C1s, O1s, Mg2p, Al2s and Ca2p high resolution XPS spectra were obtained on the surface of the samples in as-received condition after 0.5, 1.25, 2, 3, 4.25, 5, 6.5, 10, 15, 17, 20, 25, 30 and 40 minutes of ion sputtering.

2.5. EIS measurements

Electrochemical impedance measurements were conducted in 0.6 M NaCl at room temperature (~25ºC), after 1 hour immersion. An AUTOLAB potentiostat, model PGSTAT30, with frequency response analyser (FRA) software was used. The frequency ranged from 100 kHz to 1 mHz with 5 points/decade, whereas the amplitude of the sinusoidal potential signal was 10 mV with respect to the open circuit potential. A typical three-electrode set-up was employed: Ag/AgCl and graphite were used as reference and counter electrodes, respectively, and the material under study was the working electrode.

2.6. Low Angle X-Ray diffraction measurements

X-ray diffraction (XRD) measurements were carried out with a Bruker AXS D8 diffractometer in grazing incidence condition. In the setup used, a X-ray Co tube is equipped with a Goebel mirror optics to obtain a parallel and monochromatic X-ray beam. A current of 30 mA and a voltage of 40 KV were employed as tube setting. XRD data were collected with a beam incidence angle of 1º and 2θ scan between 20 and 110º with a step size of 0.03ºand a counting time of 4 s/step

3. Results

3.1. Microstructure of the tested materials

As can be seen in Figure 1, the microstructure of alloy AZ31 is formed almost entirely of the α-matrix (Fig. 1b), whereas in the microstructure of alloy AZ61 a considerable

part of the aluminium has precipitated in the form of β-phase at the grain boundaries (Fig. 1a).

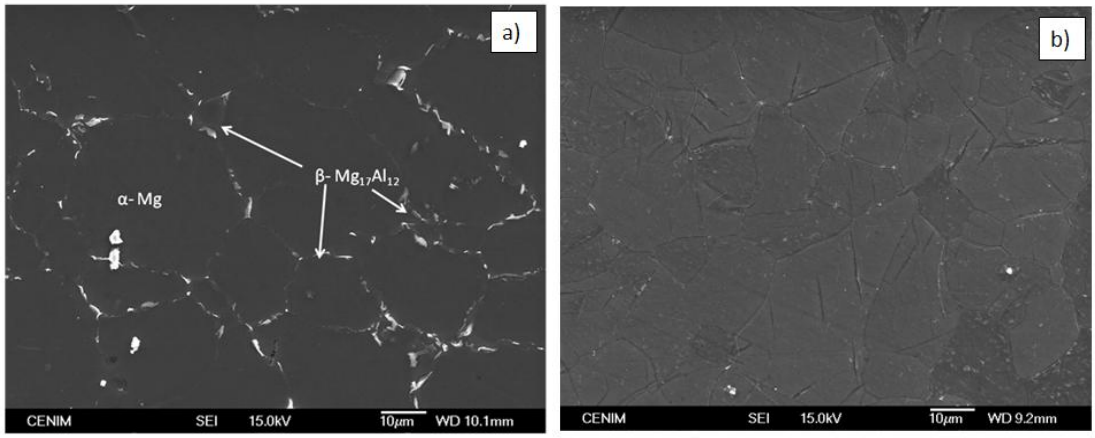

Figure 1. *SEM micrographs: (a) AZ61 alloy, (b) AZ31 alloy.*

3.2. Mg 2p XPS spectra

The evolution with sputtering time of the Mg2p high resolution XPS spectrum obtained on the native oxide film formed spontaneously on the surface of alloys AZ31 and AZ61 in polished condition is shown in Figures 2a-2h. The spectra obtained for other sputtering times are fairly similar and are not shown. Throughout the work, in order to avoid repeating similar spectra, only those necessary to support the corresponding facts are displayed. The spectra obtained on the non-sputtered surface (Figs 2a-2b) are fairly similar, containing one single component at a binding energy of 50.8 eV associated with the presence of magnesium in the form of magnesium hydroxide/carbonate [20]. Figures 2c-2d show the spectra obtained after 3 minutes of sputtering. This was the shortest sputtering time necessary for the appearance of a small shoulder, at a binding energy of 49.7 eV, associated with the presence of magnesium in metallic state in alloy AZ31 (Fig 2c). In contrast, no such shoulder is seen on alloy AZ61 (Fig. 2d). After 5 minutes of sputtering, the intensity of the metallic magnesium component is similar to that of Mg2+ in the case of alloy AZ31 (Fig. 2e) or lower in the case of alloy AZ61 (Fig. 2f). The metallic magnesium component observed in the AZ61 alloy is likely due to the thinner film on the second phase. During these first 5 minutes of sputtering, the absence of significant changes in the binding energy of the Mg2+ signal tends to support the claim that sputtering does not alter the oxidation states of surface species. After ten minutes of sputtering (Figs. 2g-2h) a shift of approximately 0.6 eV towards lower binding energies of the second component which may be associated with a charging effect.

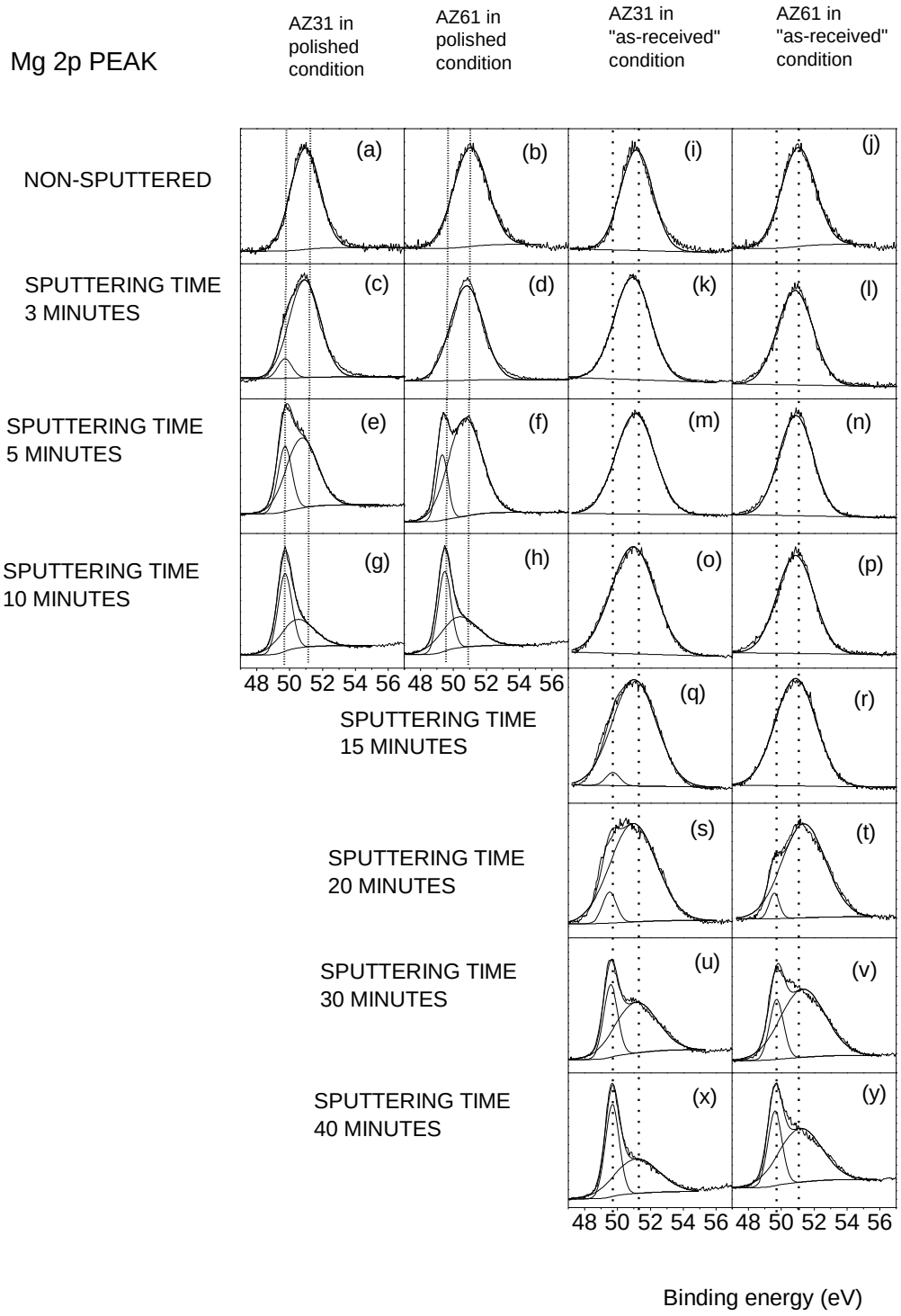

Figure 2. *XPS Mg 2p spectra of the AZ31 and AZ61 alloy in polished and as-received condition.*

3.3. Al2s XPS spectra

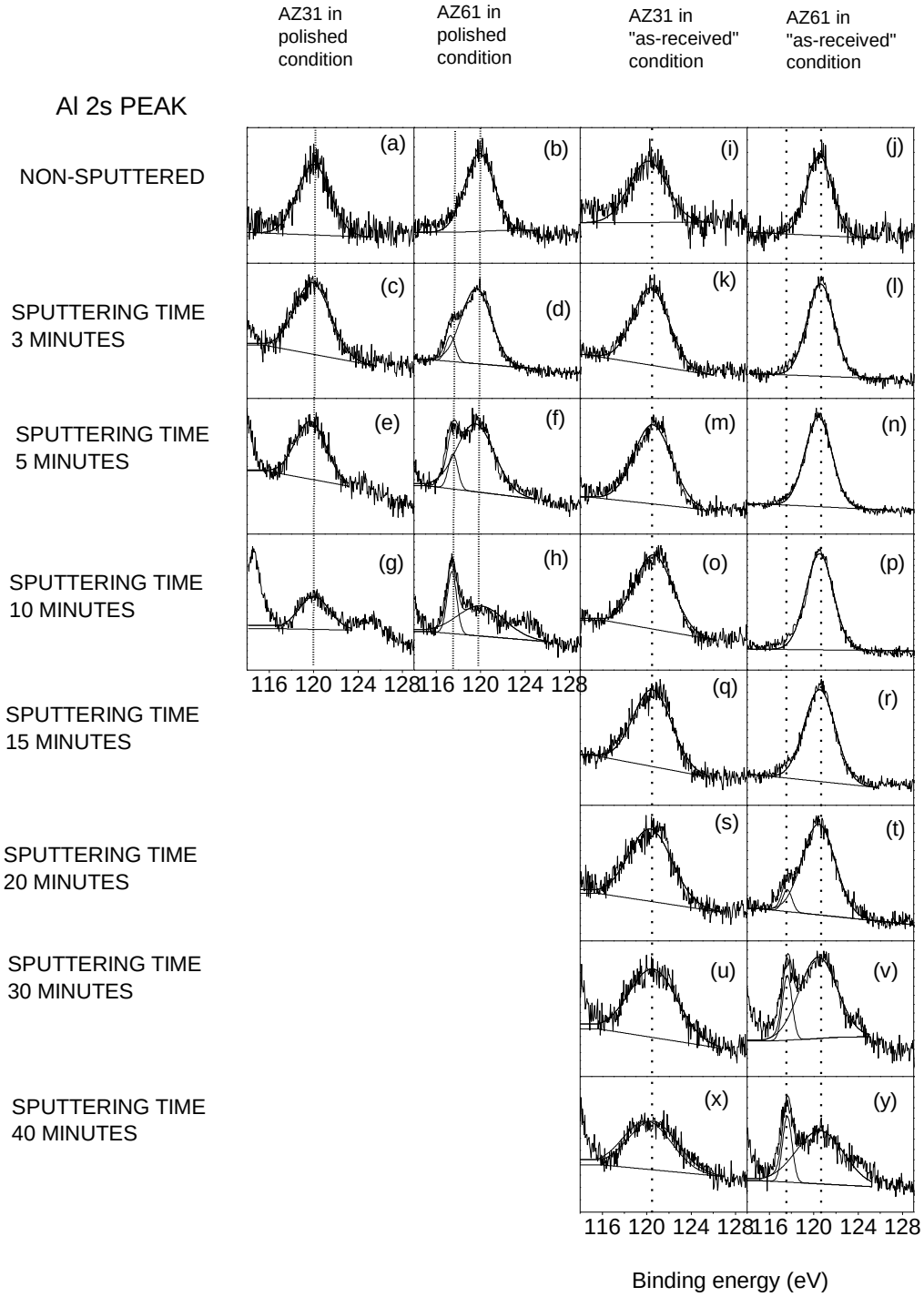

***Figure 3**. XPS Al 2s spectra of the AZ31 and AZ61 alloy in polished and as-received condition*

Due to strong overlap between the second bulk plasmon of the metallic Mg2p peak and the Al2p peak observed in our measurements, we have measured the Al2s peak instead of the Al2p peak [21]. The evolution with sputtering time of the Al2s high resolution

XPS spectrum obtained on the oxide film formed spontaneously on the surface of alloys AZ31 and AZ61 in freshly polished condition is compared in Figures 3a-3h. The spectra obtained on the non-sputtered surface (Figs. 3a-3b) contain one single component at a binding energy between 119.3-119.7 eV associated with the presence of aluminium in the form of Al3+. In contrast to alloy AZ31 (Fig. 3c), attention is drawn to the presence of a significant metallic Al signal, which appears at approximately 117.3 eV, in the spectrum obtained on alloy AZ61 after 3 minutes of sputtering (Fig. 3d), whose intensity tends to rise with sputtering time (Figs. 3f and 3h). On alloy AZ31, no appreciable changes have been observed in the shape or position of the spectra after longer sputtering times (Figs. 3e and 3g). The evolution of the oxidation state of aluminium, observed by XPS, in the Mg-Al alloys with depth profiling has been assessed in very few studies. We have not found data about alloy AZ61, only metallic Al peaks have been detected on AZ91 alloys by Liu et al. [22] and Wang et al. [23], and significant quantities of Al2O3 have been detected on AZ31 alloys after prolonged sputtering by Wang et al [24-27] and, Wang [28].

3.4. C1s XPS spectra

Table 2. *Areas of CO_3^{2-} from fitting of C1s peak (in CPS eV)*

Sputtering time (minutes)	Polished condition	
	AZ31 alloy	AZ61 alloy
0	173	177
0.5	179	204
1.25	116	164
2	63	91

Figure 4 shows a comparison of the high-resolution C1s XPS spectra for alloys AZ31 and AZ61. The spectra can be fitted using two components at different binding energies: at 285.0 eV, which may be associated with the presence of C–C/C–H groups; and a less intense component about 4.5–5.0 eV higher which is associated with the presence of magnesium carbonate [20]. The first component, C–C/C–H groups, appears on the outer surface (<3 nm in thickness) of almost any metal in contact with the atmosphere at room temperature, irrespective of its composition. Magnesium carbonate formation can be explained by the diffusion of CO2 from the environment and its reaction with the oxide film on the freshly polished surface [29]. Table 2 shows the area of the magnesium carbonate component calculated from the fitting of C1s spectra (Fig. 4). Due to the small differences in the atomic percentage of carbonate

obtained from the C1s spectra on the surface of the AZ31 and AZ61 alloys, we have chosen to compare the area of this component. It is important to note that the amount of magnesium carbonate was higher on the sputtered AZ61 alloy than on the AZ31 alloy. In a previous study [4] some correspondence was observed between the presence of β-phase (Mg17Al12) and the amount of magnesium carbonate formed on the surface after atmospheric exposure. The results of this work tend to support this behaviour. From the point of view of magnesium alloy protection mechanisms, the formation of a carbonate product layer, thicker than that observed in this work, provides better passivation of the surfaces and retards chloride-induced corrosion in the passivation zone [30].

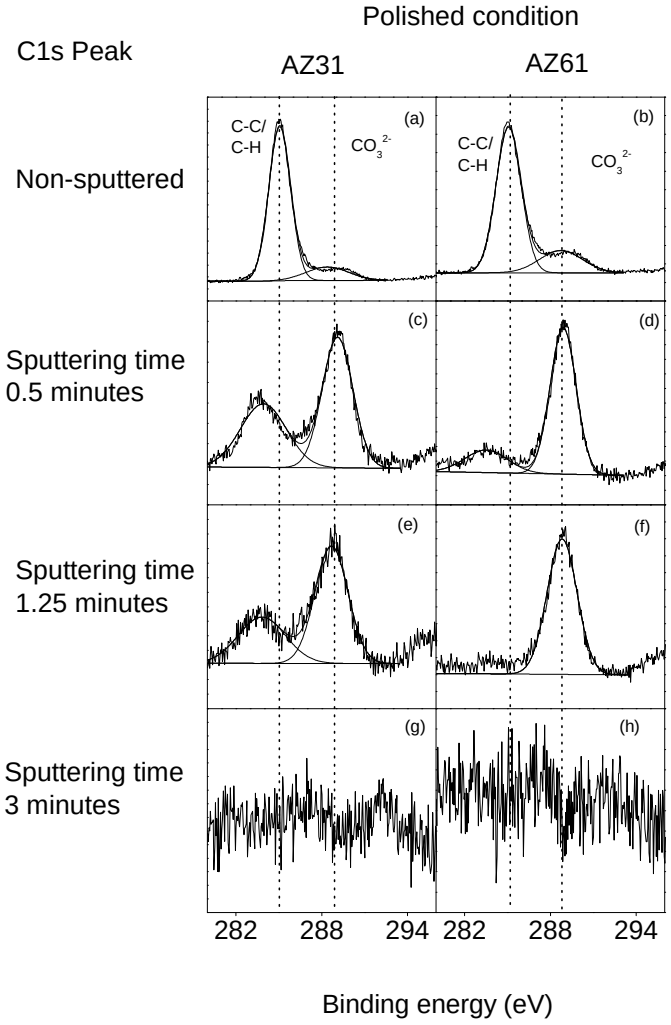

Figure 4. *XPS C1s spectra of the AZ31 and AZ61 alloy in polished condition*

3.5. Chemistry and structure of outer oxide surface layer formed on AZ31 and AZ61 alloys in as-received condition

From the point of view of the chemical composition of the oxide layer, attention is drawn to the presence of significant amounts of Ca on the non-sputtered surface of alloys AZ31 and AZ61 in as-received condition and their absence in polished condition (Table 3). It is also important to note the absence of significant amounts, within the detection limits of our XPS spectrometer, of other alloying elements such as Zn, Mn, Si and Fe on the surface of the studied alloys.

Table 3. *Atomic percentage observed by XPS on outer surface of alloys AZ31 and AZ61 in polished and as-received condition, and variation with sputtering time*

	Sputtering time (min)	%C	%O	%Mg	%Al	%Ca	O/(Mg+Al)	Al/(Mg+Al) x100
Polished condition								
AZ31	0	51	35	12	2	0	2.5	14
	5	0	41	54	5	0	0.7	8
	10	0	19	77	4	0	0.2	4
AZ61	0	37	47	13	3	0	2.9	19
	5	0	46	46	8	0	0.9	15
	10	0	23	70	7	0	0,3	9
As-received condition								
AZ31	0	51	30	16	2	1	1.7	11
	5	0	55	40	5	0	1.2	11
	10	0	54	40	6	0	1.2	13
	15	0	54	40	6	0	1.2	13
	20	0	51	43	6	0	1.0	12
	30	0	46	48	6	0	0.9	11
	40	0	40	53	7	0	0.7	12
AZ61	0	65	23	9	2	1	2.0	18
	5	0	60	28	12	0	1.5	30
	10	0	59	29	12	0	1.4	29
	15	0	57	32	11	0	1.3	25
	20	0	52	38	10	0	1.0	21
	30	0	44	49	7	0	0.8	12
	40	0	27	68	5	0	0.4	7

It is interesting to note that the Ca content observed in the XPS analysis of the outer surface of the as-received alloys tends to decline quickly with sputtering time (Table 3), probably because the presence of a significant calcium content in oxide form is limited to the outermost surface of the magnesium specimens [5,31]. This result is similar to that obtained by R. Souda et al. [32] who, working with MgO crystals including 210

ppm bulk Ca impurities, found that Ca ions were detected only in the outermost layer and that Ca enrichment did not take place in the deepest layers.

The Al/(Mg+Al) ratio determined by XPS after 10 minutes of sputtering is about 4 and 9 at% for the polished surfaces of alloys AZ31 and AZ61, respectively (Table 3). It should be noted that in as-received condition, and for the same sputtering time, this ratio is 29 at% for alloy AZ61, notably higher than in the polished condition.

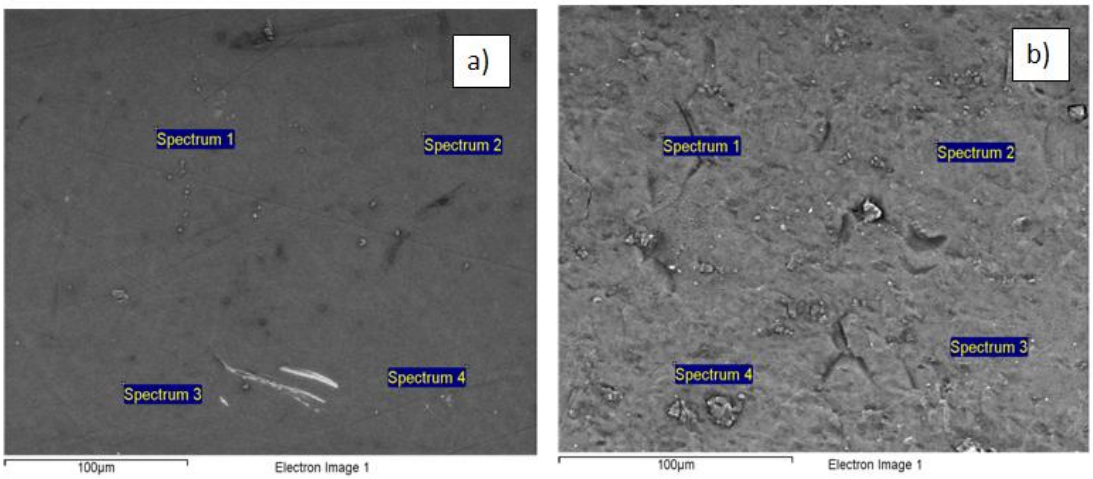

Figure 5. *SEM micrographs: (a) AZ61 alloy in polished condition, (b) AZ61 alloy in as-received condition.*

SEM examinations of the AZ61 alloy in as-received condition (Fig. 5b) revealed a rough surface covered with non-uniform features, very different to that of the polished surface (Fig. 5a). In EDX analyses obtained on the surface of the alloys in as-received condition, attention is drawn to the increase in the Al content and the decrease in the Mg content in spectra 1 and 4, compared to spectra 2 and 3 (Table 4, Fig. 5b). Furthermore, the Al percentage detected in spectra 1 and 4 is higher than its bulk content (6%). These figures tend to confirm, on the one hand, a non-uniform distribution of aluminium and magnesium, and on the other hand a surface enrichment of Al on the AZ61 alloy in as-received condition, as previously observed by XPS.

***Table 4**. EDX analyses of polished and "as received" surfaces of AZ61 alloys*

Sample	Spectrum	% Mg	% Al	%Zn
AZ61 in Polished Condition	1	93.51	5.61	0.88
	2	93.29	5.81	0.90
	3	93.29	5.64	1.06
	4	93.74	5.52	0.75
AZ61O in "as received condition"	1	91.75	7.50	0.75
	2	93.30	5.79	0.91
	3	93.36	5.76	0.88
	4	92.08	6.89	1.04

3.6. Oxide film thickness

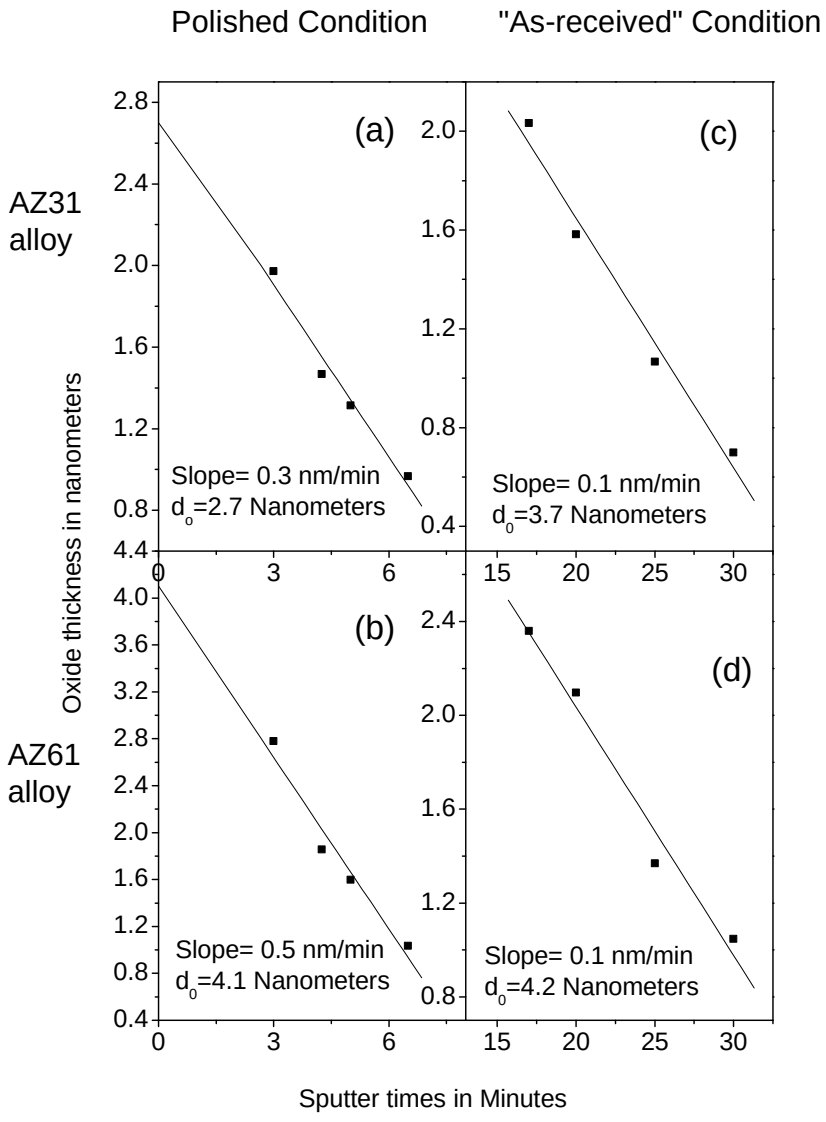

***Figure 6.** Oxide thickness obtained by XPS on AZ31 and AZ61 alloy in polished and as-received condition after sputtering.*

The thickness of the native oxide film on the surface of the magnesium specimens was calculated using the expression given by Strohmeier [33]:

$$d_o\ (nm) = \lambda_{oxide} \sin\theta \ln [I_{oxide} \times \lambda_{metal} \times N_m)/(I_{metal} \times \lambda_{oxide} \times N_o) + 1] \quad (1)$$

where d_o is the thickness of the magnesium oxide layer (in nm); θ is the photoelectron output angle; I_{metal} and I_{oxide} are the intensities of the magnesium components in the metallic state and as oxide from the Mg2p peak; λ_{metal} and λ_{oxide} are the mean free paths of photoelectrons in the substrate and the oxide layer; and N_m and N_o are the volume densities of magnesium atoms in metal and oxide. The values of λ_{metal} and λ_{oxide} are 3.0 [34] and 2.6 nm [35], respectively, [36], and an N_m/N_o ratio of 1.24 was used [37]. Figure 6 shows the oxide film thickness as calculated from Eq. 1 for the Mg2p peak after 3 min (Figs. 2c and 2d), 4.25 min (not shown), 5 min (Figs. 2e and 2f) and 6 min of sputtering (not shown) in the polished condition; and after 17 min (not shown), 20 min (Figs. 2s and 2t), 25 min (not shown), and 30 min of sputtering (Figs. 2n and 2v) in as-received condition. Following the approach proposed by McCafferty et al. [38], the oxide film thickness before sputtering was determined by extrapolation of the linear portion of Figure 6 (thicknesses after ion sputtering) back to zero sputter time.

Figures 6c-6d show the oxide film thickness as calculated from Eq. 1 for the Mg2p peak after 17 min (not shown), 20 min (Figs. 2s and 2t), 25 min (not shown) and 30 min of sputtering (Figs. 2u and 2v), for alloys AZ31 and AZ61 in as-received condition. With an oxide with non-uniform growth (island model), the oxide thickness and sputtering rate obtained can be used only as an estimate [33].

Figure 7 presents the low angle X-ray diffraction pattern for the AZ31 (a) and AZ61 alloys (b) in “as-received condition”. The diffractogram for the AZ31 and AZ61 alloys in polished condition were fairly similar to that acquired on the AZ31 alloys in “as-received condition” and are not shown. In contrast with the other samples (Fig. 7a), the diffractrogram of the AZ61 alloy in as “received condition” seems to show a small intensity peak of periclasa (MgO) (Fig. 7b) due to the formation of a thicker oxide layer during the manufacturing process.

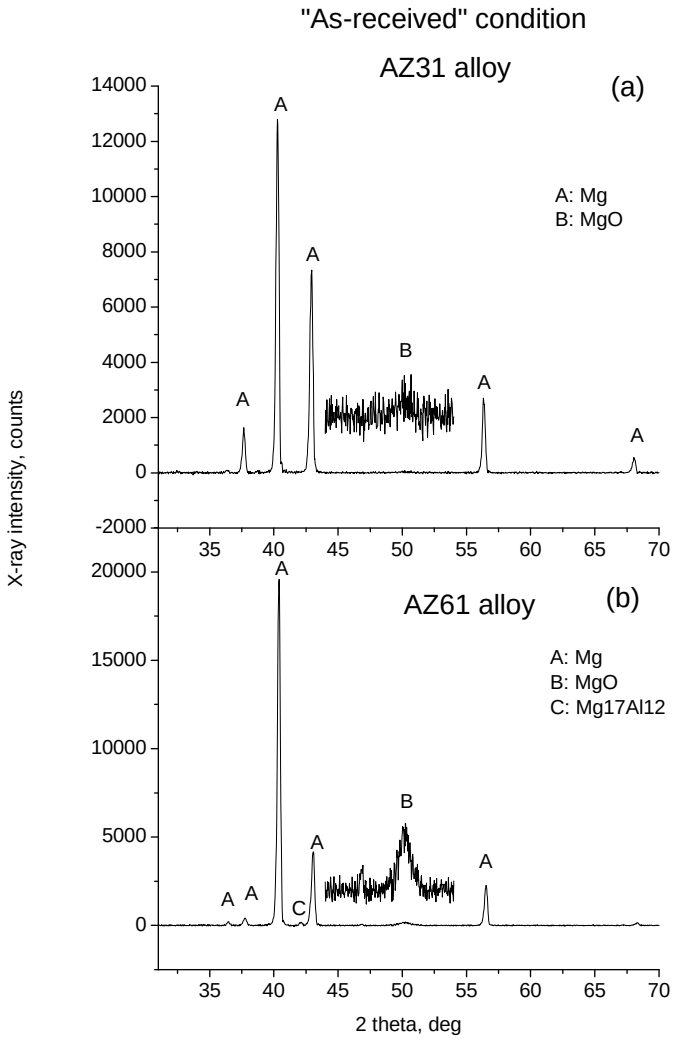

Figure 7. *Low angle XRD pattern for the AZ3 and AZ61 alloys in "as-received condition*

3.7. Corrosion results

Numerous studies in the literature support the use of impedance spectra to obtain information on the corrosion process. In the case of magnesium alloys, the diameter (R_{HF}) of the capacitive loop in the high frequency region of the diagram (Fig. 8) has been normally associated with the charge transfer resistance of the corrosion process. From the well-known Stern-Geary equation [39], it is expected an inverse proportionality between corrosion current (i_{corr}) and R_{HF} :

$$I_{corr} = B / R_{HF}$$

B being a constant. This relationship allows i_{corr} to be determined.

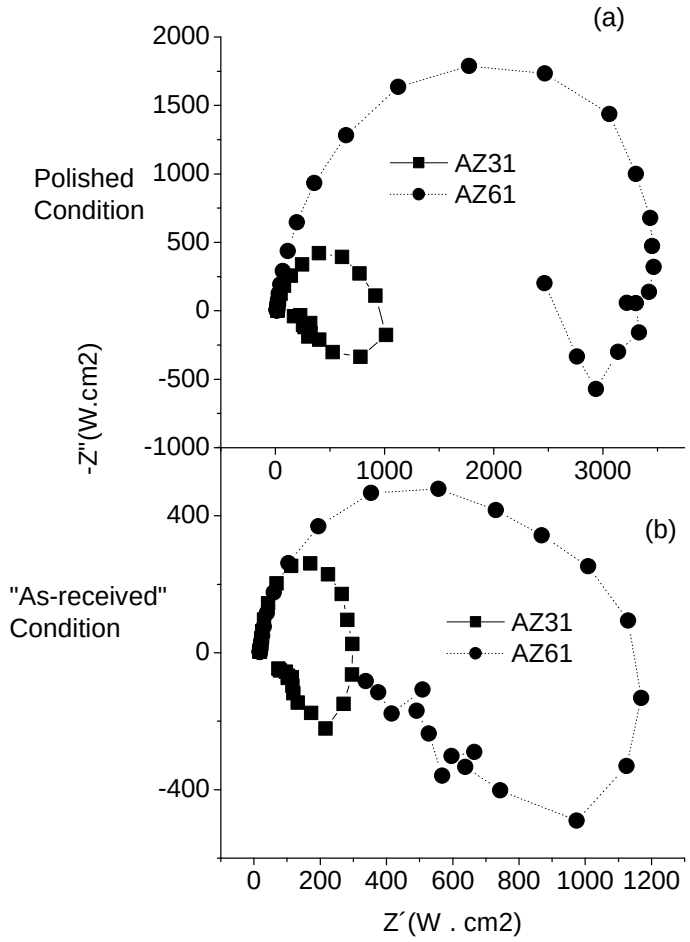

Figure 8. *Nyquist plots for the AZ31 and AZ61 alloy in polished and as-received condition.*

In this investigation, an empirical determination of the proportionality constant B from the correlation between electrochemical and gravimetric measurements has yielded values of around 65 mV for the AZ31 alloy and of around 120 mV for the AZ61 alloy. This difference in values of B should not interfere too much with our measurements aimed to a relative comparison of corrosion rates of similar corrosion systems. With the above values the instantaneous corrosion rates shown in Table 5 (column 3) have been estimated..

***Table 5**. Comparison of R_{HF} values with XPS features*

Specimens	EIS measurements		Special features (*) (Inferred from XPS results)
	RHF (Ω.cm2)	Corrosion rate (mm/y)	
As-received AZ31	300	4.9	B
Freshly polished AZ31	1000	1.5	A
As-received AZ61	1200	2.3	B, D
Freshly polished AZ61	4000	0.7	A, B, C

4. Discussion

4.1. Chemical composition of the native oxide film that forms spontaneously on the surface of AZ31 and AZ61 alloys after polishing

The metallic Mg at 49.7 eV could originate from either bulk metallic magnesium or islands of metallic magnesium beneath the oxide films, depending on the uniformity of this outer film [20]. XPS in combination with ion sputtering data may resolve this ambiguity. If the Mg2p emission at 49.7 eV was from metallic islands within the oxide film, the ratio of its intensity to that of the oxide peak would not vary significantly with ion sputtering, otherwise the intensity should increase as the sputtering time increases. The Mg2p spectra in Fig. 2 demonstrates that the ratio of the area of metallic Mg2p at 49.7 eV to that of the oxide Mg2p peak at 50.8 eV increases with sputtering time. This suggests that the emission at 49.7 eV is mainly from metallic magnesium beneath the magnesium oxide thin film, rather than from the surface islands of metallic magnesium, which is consistent with the layer by layer film growth mechanism discussed by Yao et al. [20]. Also, the rapid and continuous increase in the magnesium content and the reduction in the oxygen content after sputtering (Figs. 9a and 9b) tend to suggest that the MgO layer formed spontaneously in contact with the laboratory atmosphere on the surface of the AZ31 and AZ61 alloys as a result of the polishing process is a fairly homogeneous film [40].

Of relevance to understanding the corrosion behaviour of aluminium alloying elements is their chemical state, and particularly whether they are in a metallic state in solid solution or forming aluminium oxide particles in the outer region of the material. Alloy AZ61, which contains 6%Al (Table 1), could have accessed this aluminium in metallic or free form (Fig. 3h) for surface enrichment during the subsequent corrosion process. In alloy AZ31, which contains 3%Al (Table 1), the absence of a significant metallic

aluminium signal (Fig. 3g) suggests the absence of a significant amount of this element within the detection limits of the XPS spectrometer, perhaps because a large part of the Al is not in solid solution but present as aluminium oxide particulates. This difference seems to correspond with the significant increase in the Al content detected on the surface layers formed during the corrosion process when the alloy's aluminium content is increased above 4% , Nordlien et al [7] and Anik et al. [41].

It is interesting to note that the thickness of the oxide film on the AZ61 alloy is higher than that observed on the AZ31 specimens (Figure 6). Thickness differences (of nm order) in the native oxide layer formed spontaneously on metallic materials have been related with the presence of imperfections or heterogeneities where the film is more pervious to the movement of the reaction products [11, 42, 43]. In the commercial magnesium alloys tested in this work there also seems to be a direct relationship between the native oxide film thickness and the degree of microstructural complexity of the surface upon which it forms. Figure 1 shows a very significant presence of β intermetallic phase on the boundary of AZ61 (Fig. 1a) compared to its absence on AZ31 (Fig. 1b)

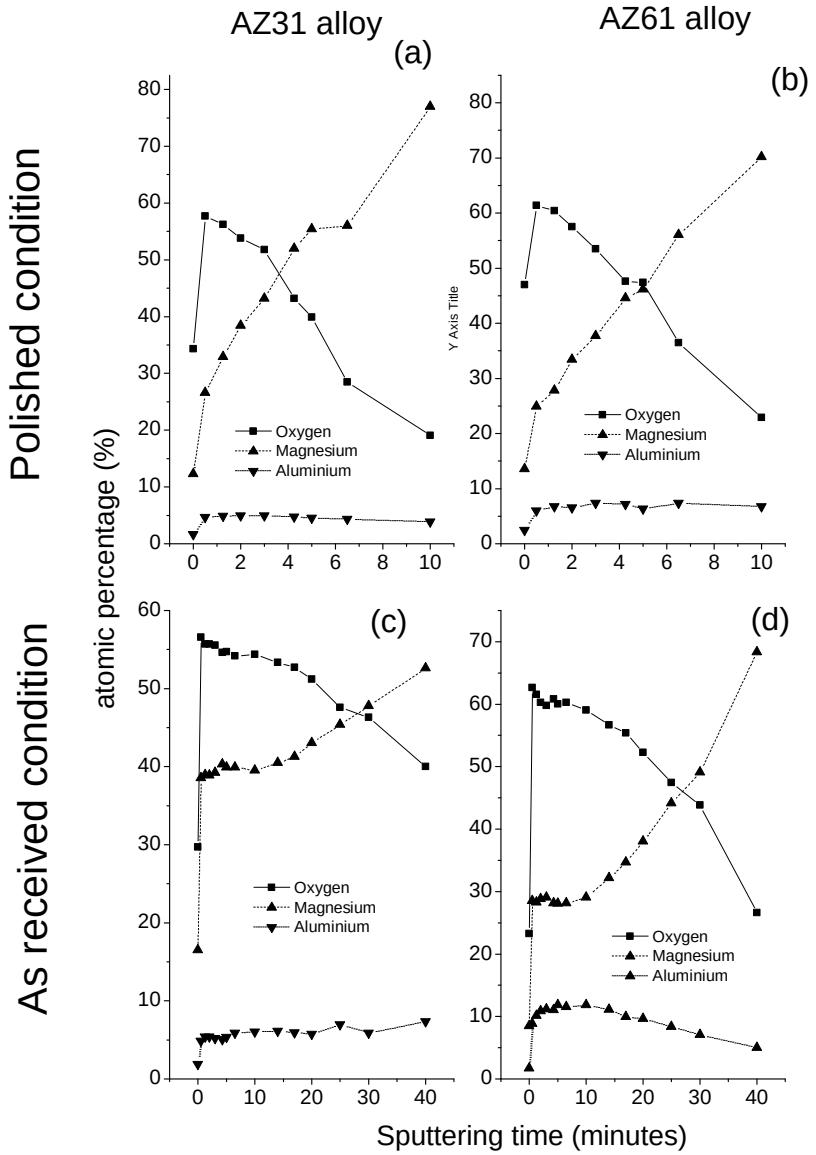

Figure 9. *Element percentages obtained by XPS on the outer surfaces of the AZ31 and AZ61 alloy in polished and as-received condition and after sputtering.*

4.2. Influence of surface condition in the chemistry of the nano layers formed on the outer surfaces of the Mg-Al alloys.

The O/(Mg+Al) atomic ratios obtained by XPS on the surface of alloys AZ31 and AZ61 for increasing sputtering times (Table 3) provide an approximation to the Mg-Al-O stoichometry of the surface oxide [44]. O/(Al+Mg) ratios of 1.2-1.5 are observed on the AZ61 and AZ31 alloys in as-received condition during the first 15 minutes of sputtering. These values are close to the theoretic value of 1.33 for spinel (MgAl2O4), although if this compound were to form its proportion in the oxide film would be

relatively small considering the Al/(Mg+Al)*100 ratios in Table 3, far from the theoretic value of 66 for spinel. Czerwinski [11] commented that during gradual oxidation of an AZ91 alloy, Al reacts to form MgAl2O4 spinel. By using XPS analyses in combination with ion sputtering, Shih et al. [45] have observed the presence of an admixture of Mg-Al oxides or spinel (MgAl2O4) in MgO when characterising the surface of the solution-treated AZ80 magnesium alloy.

Figures 9c and 9d show how the oxygen and magnesium contents observed on the alloys in as-received condition remain approximately stable during the first 15 minutes of sputtering before subsequently decreasing and increasing, respectively, after longer times. According to Nakano et al. [46], in films with a thin homogeneous layer the intensity of chemical compounds present in the outer layer should decrease linearly with sputtering time. However, the decay for the 3-D islands structure shows a progressively steeper slope with time. In contrast to the presence of a fairly homogenous MgO layer noted above for the alloys in polished condition, this data tends to suggest that the outer layer that grows on the alloys in as-received condition has a heterogeneous islands structure. In the hypothesis that all the Al included in the data in Table 3 were to be dedicated to the formation of spinel islands thick enough to avoid the magnesium signal coming through, around 25-30% of the alloy AZ61 surface would be covered by spinel, a percentage that would be approximately halved in the case of alloy AZ31.

It is interesting to note the reduction in the sputtering rate of the alloys in as-received condition (1 Å/min) compared to the alloys in polished condition (3-5 Å/min). It is important to remember that the sputtering rate is different for different materials [40]. Nenadovic et al. [47] observed that the sputtering yield of Al2O3 is close to four times lower than the sputtering yield of MgO at 4 KeV (sputtering energy used in our work). From the results of the present work it would be possible to speculate that the important segregation of Al to the surface to precipitate in the form of MgAl2O4 spinel-type oxide must have led to the reduction in sputtering rate values of the alloys in as-received condition.

4.3. Influence of surface conditions on the corrosion resistance of the Mg-Al alloys in 0.6 M NaCl solution

It seems likely that some of the differences that have been revealed in the composition and characteristics of oxide films formed on the alloys AZ31 and AZ61 may have an impact on the corrosion behavior. Paying attention to the uniformity of the oxide film,

its thickness and the percentage of surface covered by spinel, Table 5 (column 4) shows the occurrence of these special features as a function of surface conditions and type of alloy. As given in column 3 of Table 5, the highest corrosion rate corresponds to the as-received surface of alloy AZ31, which as a special feature shows the presence of spinel islands in the outermost surface of the oxide film. A small fraction of spinel does not seem to exert any relevant effect for corrosion protection. In the same alloy, but in the freshly polished condition, corrosion rate decreases significantly (by a factor of 3.3); the absence of spinel and the uniformity of the oxide film are now the special features to notice. These data tend to suggest that the growth of an additional layer of spinel islands on the surface of the as-received alloy, which modify the structure of the native oxide film, making it more defective, may decrease its protective properties. Comparison between corrosion rate values for alloys AZ31 and AZ61 both now in freshly polished condition shows a notably lower value for alloy AZ61 which presents a greater oxide film thickness. Finally, with the alloys in the as-received condition, corrosion rate for AZ61 alloy is about half that of alloy AZ31. XPS analysis has revealed as a special feature a larger fraction of AZ61 alloy surface covered by islands of spinel. One may speculate, that the outer surface of the AZ61 alloy in "as-received condition" may be more restrictive for the diffusion of magnesium atoms from the alloy substrate during the posterior corrosion process

5. Conclusions

Using XPS analysis, notable differences have been shown in the oxide films formed on the surface of AZ31 and AZ61 alloys in as-received and freshly polished conditions. Points to be noted are the degree of heterogeneity of the films coating as-received surfaces compared to the uniformity of the films formed on freshly polished surfaces; the greater thickness of the oxide film on the polished AZ61 alloy surface; and, in the case of alloy AZ61, the presence of a higher proportion of spinel with the magnesium oxide that mainly forms the oxide film.

The charge transfer values, R_{HF}, obtained from EIS measurements on the specimens after 1 hour of immersion in 0.6 NaCl solution have allowed possible relationships between surface characteristics and corrosion resistance to be explored. In the joint analysis of XPS and EIS data, attention is drawn to the increase in the R_{HF} value on freshly polished specimens compared to the as-received surfaces. This effect is especially seen on the AZ61 alloy.

Acknowledgment

We wish to express our gratitude to Prof. S. Feliu for several clarifying and stimulating discussions during the course of this work. Also, the authors gratefully acknowledge the financial support for this work from the Ministry of Science and Innovation of Spain (MAT 2009-13530)

References

[1] MC. Zhao, M. Liu, GL. Song, A. Atrens, Influence of the beta-phase morphology on the corrosion of the Mg alloy AZ91, Corros. Sci., 50 (2008) 1939-1953.

[2] GL. Song, ZQ Xu, The surface, microstructure and corrosion of magnesium alloy AZ31 sheet, Electrochim. Acta, 55 (2010) 4148-4161.

[3] S. Feliu Jr., M.C. Merino, R. Arrabal, A.E. Coy, E. Matykina, XPS study of the effect of aluminium on the atmospheric corrosion of the AZ31 magnesium alloy, Surf. Interface Anal., 41 (2009) 143- 150.

[4] S. Feliu Jr., A. Pardo, M.C. Merino, A.E. Coy, F. Viejo, R. Arrabal, Correlation between the surface chemistry and the atmospheric corrosion of AZ31, AZ80 and AZ91D magnesium alloys, Appl. Surf. Sci. 255 (2009) 4102-4108.

[5] S. Feliu Jr., J.C. Galván, A. Pardo, M.C. Merino, R. Arrabal, Native Air-Formed Oxide Film and its Effect on Magnesium Alloys Corrosion, The Open Corrosion Journal, 3 (2010) 80-91.

[6] S.Feliu Jr., C. Maffiotte, A. Samaniego, J. C. Galván, V. Barranco, Effect of naturally formed oxide films and other variables in the early stages of Mg-alloy corrosion in NaCl solution, Electrochim. Acta, in press ,

[7] J.H. Nordlien, K. Nisancioglu, S. Ono, N. Masuko, Morphology and structure of oxide films formed on MgAl alloys by exposure to air and water, J. Electrochem. Soc. 143 (1996) 2564-2572.

[8] J.H. Nordlien, K. Nisancioglu, S. Ono, N. Masuko, Morphology and structure of water-formed oxides on ternary MgAl alloys, J. Electrochem. Soc. 144 (1997) 461-466.

[9] O. Lunder, J.E. Lein, T. K. Aune, K. Nisancioglu, The role of Mg17Al12 phase in the corrosion of Mg alloy AZ91, Corrosion 45 (1989) 741-748.

[10] M. Santamaría, F.Di Quarto, S. Zanna, P. Marcus, Initial surface film on magnesium metal: A characterization by X-ray photoelectron spectroscopy (XPS) and photocurrent spectroscopy (PCS), Electrochim. Acta 53 (2007) 1314-1324.

[11] F. Cerwinski, The oxidation behaviour of an AZ91D magnesium alloy at high temperatures, Acta Mater. 50 (2002) 2639-2654.

[12] F. Reichel, L.P.H. Jeurgens, E.J. Mittemeijer, Modeling compositional changes in binary solid solutions under ion bombardment: Application to the Ar+ bombardment of MgAl alloys, Phys. Rev B. 73 (2006) ARTN 024103.

[13] S. Oswald, R. Reiche, Binding state information from XPS depth profiling: capabilities and limits. Appl. Surf. Sci. 179 (2001) 307-315

[14] W. Zhang, S. Jin, E. Ghali, R. Tremblay, Skin and bulk corrosion properties of die cast and thixocast AZ91D magnesium alloy in 0.05M NaCl solution, Can. Metall. Q. 45 (2006) 181-188.

[15] Y.L. Lee, C.S. Lin, Influence of Die-Chill Skin on the Formation of Stannate Conversion Coating on AZ91D Magnesium Alloy, J. Electrochemical Soc. 157 (2010) C187-C193.

[16] E. Aghion, N. Lulu, The effect of skin characteristics on the environmental behavior of die cast AZ91 magnesium alloy, J. Mater. Sci. 44 (2009) 4279-4285.

[17] G. L. Song, A. Atrens, M. Dargusch, Influence of microstructure on the corrosion of diecast AZ91D, Corros. Sci. 41 (1999) 249-273.

[18] B.L. Yu, J.Y. Uan, Correlating the microstructure of the die-chill skin and the corrosion properties for a hot-chamber die-cast AZ91D magnesium alloy, Metall. Mater. Trans. A. 36A (2005) 2245-2252.

[19] J.E. Gray-Munro, B. Luan, L. Huntington, The influence of surface microchemistry in protective film formation on multi-phase magnesium alloys, ,Appl. Surf. Sci. 254 (2008) 2871-2877.

[20] H.B. Yao, Y. Li, A.T.S. Wee, An XPS investigation of the oxidation/corrosion of melt-spun Mg, ,Appl. Surf. Sci. 158 (2000) 112-119.

[21] L.P.H. Jeurgens, M.S. Vinodh, and E.J. Mittemeijer, Quantitative analysis of multi-element oxide thin films by angle-resolved XPS: Application to ultra-thin oxide films on MgAl substrates, Appl. Surf. Sci. 253 (2006) 627-638.

[22] C.L. Liu, Y.C. Xin, X.B. Tian, P.K. Chu, Corrosion behavior of AZ91 magnesium alloy treated by plasma immersion ion implantation and deposition in artificial physiological fluids, Thin Solid Films 516 (2007) 422-427.

[23] H. M. Wang, Y. Li, F. H. Wang, Influence of cerium on passivity behavior of wrought AZ91 alloy, Electrochim. Acta 54 (2008) 706-713.

[24] X. M. Wang, X. Q. Zeng, G. S. Wu, S.S. Yao, Y.J. Lai, Surface analysis and oxidation behavior of Y-ion implanted AZ31 magnesium alloys, Appl. Surf. Sci. 253 (2007) 3574-3580.

[25] X. M. Wang, X.Q. Zeng, G.S. Wu, S.S. Yao, Y.J. Lai, Effects of tantalum ion implantation on the corrosion behavior of AZ31 magnesium alloys, J. Alloy. Comp. 437 (2007) 87-92.

[26] X.M. Wang, X.Q. Zeng, G.S. Wu, S. Yao, Y.J. Lai, The effects of cerium implantation on the oxidation behavior of AZ31 magnesium alloys, J. Alloy.Comp. 456 (2008) 384-389.

[27] X.M. Wang, X.Q. Zeng, G.S. Wu, S.S. Wu, S.S. Yao, B. Li, Oxidation kinetics of magnesium alloys treated by tantalum ions implantation, Nucl. Instr. Meth. Phys. Res. B 263 (2007) 401-406.

[28] L. Wang, T. Shinohara, B.P. Zhang, H, Iwai, Characterization of surface products on AZ31 magnesium alloy in dilute NaCl solution , J. Alloy. Comp. 485 (2009) 747-752.

[29] M. Jönsson, D. Persson, D. Thierry, Corrosion product formation during NaCl induced atmospheric corrosion of magnesium alloy AZ91D, Corros. Sci. 49 (2007) 1540-1558.

[30] L. Wang, T. Shinohara, B.P. Zhang, H, Iwai, Characterization of surface products on AZ31 magnesium alloy in dilute NaCl solution , J. Alloy. Comp. 485 (2009) 747-752.

[31] S. Feliu Jr., C. Maffiotte, J.C. Galván, A. Pardo, M. C. Merino, R. Arrabal, The Application of X-Ray Photoelectron Spectroscopy in Understanding Corrosion Mechanisms of Magnesium and Mg-Al Alloys, The Open Surface Science Journal, 3 (2011), 1-14.

[32] R. Souda, Y. Hwang, T. Aizawa, W. Hayami, K Oyoshi., S. Hishita, Ca segregation at the MgO(001) surface studied by ion scattering spectroscopy, Surf. Sci. 387 (1997) 136-141.

[33] B.R. Strohmeier, An ESCA method for determining the oxide thickness on Aluminium-alloys, Surf. Interface Anal. 15 (1990) 51-56

[34] S. Tanuma, C.J. Powell, D.R. Penn, Calculations of electron inelastic mean free paths. 2. Data for 27 elements over the 50-2000eV range, Surf. Interface Anal. 17 (1991) 911-926.

[35] A. Akkerman, T. Boutboul, A. Breskin, R. Chechik, A. Gibrekhterman, Y. Lifshitz, Inelastic electron interactions in the energy range 50 eV to 10 keV in insulators: Alkali halides and metal oxides, Phys. Stat. Sol (b) 198 (1996) 769-784.

[36] C.J. Powell, A. Jablonski, NIST Electron Inelastic-Mean-Free-Path Database, SRD 71, US Department of Commerce, National Institute of Standards and Technology, Gaithersburg, MD (2000)

[37] M. Liu, S. Zanna, H. Ardelean, I. Frateur, P. Schmutz, G.L. Song, A. Atrens, P. Marcus, A first quantitative XPS study of the surface films formed, by exposure to water, on Mg and on the Mg-Al intermetallics: Al_3Mg_2 and $Mg_{17}Al_{12}$, Corros. Sci. 51 (2009) 1115-1127.

[38] E. McCafferty, J.P. Wightman, An X-ray photoelectron spectroscopy sputter profile study of the native air-formed oxide film on titanium, J. Appl. Surf. 143 (1999) 92-100.

[39] M. Stern, A.L. Geary, Electrochemical polarization: I. A theoretical analysis of the shape of polarization curves,J. Electrochem. Soc. 104 (1957) 56-63.

[40] M. Liu, P. Schmutz, S. Zanna, A. Seyeux, H, Ardelean, G.L. Song, A. Atrens, P. Marcus, Electrochemical reactivity, surface composition and corrosion mechanisms of the complex metallic alloy Al_3Mg_2 , Corros. Sci. 52 (2010) 562-578

[41] M. Anik, G. Celikten, Analysis of the electrochemical reaction behavior of alloy AZ91 by EIS technique in H_3PO_4/KOH buffered K_2SO_4 solutions, ,Corros. Sci. 49 (2007) 1878-1894.

[42] N.S. McIntyre, C. Chen, Role of impurities on Mg surfaces under ambient exposure conditions , Corros. Sci. 40 (1998) 1697-1709.

[43] S. Feliu Jr, M.J. Bartolomé, Influence of alloying elements and etching treatment on the passivating films formed on aluminium alloys, Surf. Interface Anal. 39 (2007) 304-316.

[44] E. Panda, L.P.H., Jeurgens, E.J. Mittemeijer, Effect of in vacuo surface pre-treatment on the growth kinetics and chemical constitution of ultra-thin oxide films on Al-Mg alloy substrates, Surf. Sci. 604 (2010) 587-594.

[45] T.S. Shih, J.B. Liu, P.S. Wei, Oxide films on magnesium and magnesium alloys, Mater. Chem. Phys. 104 (2007) 497-504.

[46] T. Nakano, S. Sato, S. Baba, Structural analysis of Cu-In alloy films with XPS depth profiling by ion etching, Vacuum 74 (2004) 591-594.

[47] T. Nenadovic, B. Perraillon, Z. Bogdanov, Z. Djordjevic, M. Milic, Sputtering and surface-topography of oxides, Nucl. Instr. Meth. Phys. Res. B 48 (1990) 538-543.

Combined Effect of Composition and Surface Condition on Corrosion Behaviour of Magnesium Alloys AZ31 and AZ61

Alejandro Samaniego[a] , Irene Llorente[a] and Sebastián Feliu (Jr)[a].
Centro Nacional de Investigaciones Metalúrgicas CSIC, Avda. Gregorio del Amo 8, 28040 Madrid, Spain,

Corrosion Science 68 (2013) 66–71

Abstract

The work is an attempt to learn more about the role of several experimental variables in the corrosion of magnesium alloys in immersion tests carried out in 0.6 M NaCl. The effect of as-received and polished surface conditions, geometrical characteristics of the exposed area and different aluminium contents in the magnesium based alloys is considered. Results indicated that polished surfaces and AZ61 surfaces tend to develop corrosion slower than the respective as-received and AZ31 surfaces; these tendencies can change by prolonging exposure time. Filiform and localized corrosion are influenced by the presence of cut surfaces and small exposed areas, respectively.

Keywords: A. Magnesium; A. Alloy; B Weight loss; C. Pitting corrosion

1. Introduction

In the literature, different studies on the corrosion of magnesium alloys may yield unequal results in apparently similar experimental circumstances [1]. This casts doubts as to the true meaning of certain results, which could be clarified by means of a better knowledge of the factors that influence them and their relative importance.

In several investigations [2-8] it has become apparent the effect of certain combinations of variables relating to specimen preparation and testing conditions on the results obtained. The purpose of the present work has been to gain a better understanding of the influence of surface condition and specimen configuration variables on the corrosion behaviour of AZ31 and AZ61 magnesium based alloys in immersion corrosion tests carried out in 0.6 M NaCl solution. As the presence of chloride ion promotes the corrosion of magnesium alloys in aqueous solutions, a relatively high chloride concentration has been selected in order to accentuate possible effects.

Specifically, this study addresses the effect on the attack morphology and corrosion rate of AZ31 and AZ61 alloys of the: (a) configuration of the exposed surface area of the specimens; (b) surface condition at the start of the test; and (c) a change in the metallic composition using the two aforementioned commercial magnesium-aluminium alloys. Special attention has been paid to the possible repercussion of the confinement of the exposed area by means of a circular plastic gasket, as well as to the presence of cut edges on the square coupon specimens entirely exposed to the aggressive solution. Depending on the special circumstances of each case, examination of the corroded surfaces has shown substantially varied morphologies, which include uniform corrosion, filiform corrosion, and localized attack with the formation of pits and cavities.

2. Experimental

2.1. Materials

The chemical composition of the tested AZ31 and AZ61 magnesium alloys is given in Table 1. These alloys were manufactured in wrought condition and supplied in 3 mm thick plates by Magnesium Elecktron Ltd.

Table 1. *Chemical composition of AZ31 and AZ61 alloys (wt. %).*

Alloy	Al	Zn	Mn	Si	Fe	Ca	Mg
AZ31	3.1	0.73	0.25	0.02	0.005	0.0014	Bal.
AZ61	6.2	0.74	0.23	0.04	0.004	0.0013	Bal.

2.2. Surface conditions

The research compares the behaviour of specimens of the above alloys in the following two surface conditions: (a) specimens in as-received condition and (b) freshly polished specimens. In the as-received condition, the untreated surfaces were only cleaned with distilled water and dried with hot air. As these are commercial materials, precise information is not available on the various stages of their manufacturing, in particular about heat treatment and hot rolling operations with a probable influence on the as-received surface properties. For obtaining the freshly polished condition, the specimens were dry ground through successive grades of silicon carbide abrasive paper, from P600 to P2000, followed by finishing with 3 and 1 μm diamond paste, cleaned in distilled water and dried with hot air.

The difference between as-received and polished surfaces has been clearly evident in the roughness measurements carried out using atomic force microscopy (AFM). The as-received surfaces of alloys AZ31 and AZ61 yielded the highest roughness values, 198 and 116 nm RMS (root mean value), respectively, while the corresponding values for the polished surfaces were only 29 and 17 nm RMS.

2.3. Corrosion testing

Corrosion of the specimens was followed by measuring the volume of hydrogen evolved during the experiments [1,9]. Hydrogen was collected in a burette above the corroding sample using a similar procedure to that described in the literature [7,8]. It had been previously proved the existence of an acceptable correspondence between these estimates and gravimetric data, verification necessary considering recent literature [10, 11].

Corrosion weight loss rates were estimated from the hydrogen evolution versus time curves, each curve was fitted from 20-25 points distributed through 14 days of testing.

Specimen configuration

In general, square coupon specimens, with dimensions of 2 cm x 2 cm x 0.3 cm, have been used. All or part of the specimen surface has been exposed to the corrosion test. In the latter case the different configurations were: (i) specimens with a free surface area of 0.4, 0.8 or 9,0 cm^2 ,defined by the inner diameter of a circular plastic gasket; (ii) specimens with one of its two faces masked with epoxy resin; and (iii) specimens with a hole 0.3 cm in diameter drilled through them.

Tested specimens were suspended vertically in the 0.6 M NaCl solution and others were exposed in horizontal position.

2.4. Corrosion morphology observations

The attack morphology on the corroded surface was examined at low magnification. Photographic images were taken with an optical zoom camera.

The visual evolution of attack with immersion time was illustrated by series of photographs of specimens immersed horizontally, about 50 mm below the surface of the test solution, obtained with the photographic camera mounted above the solution.

3. Results

3.1. Morphology of the corroded surfaces

In this research, repeated tests have been carried out in order to analyse the corrosion attack morphologies developed on the 130 specimens that reasonably represented the effect of the different variables taken into consideration. These specimens belong proportionately to alloys AZ31 and AZ61 and to the as-received and polished surface conditions.

Particular attention has been paid to the three forms of corrosion ordinarily found in this research: uniform corrosion, localized corrosion and filiform corrosion. The latter term is applied when the dark thread-like filaments that characterize this type of morphology are clearly perceived. Filiform corrosion is usually initiated at different points on the metallic surface, and, at a rate which depends on the alloy type and surface preparation, gradually becomes converted into a dense mesh of indiscernible filaments. When this

occurs, the attack morphology becomes confused with that of uniform corrosion and is classified under this heading.

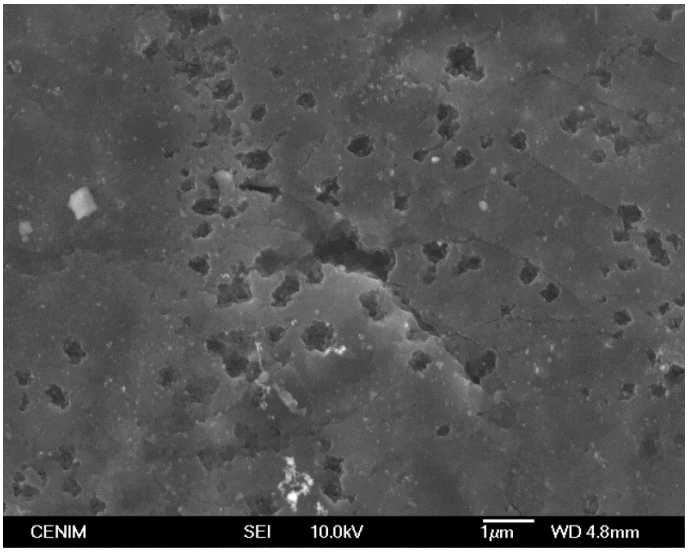

Fig. 1. *Presence of sub-micrometre pits on the corroded surface of the tested specimen.*

Macroscopic examination of the corroded specimens has often shown the presence of filiform-like attack together with areas of uniform corrosion. Localized forms of attack have been less abundant, but can nevertheless be observed at microscopic scale, as in Fig. 1, this revealing a large number of small pits of less than one micrometre diameter, or Fig. 2, with series of pits distributed on the filament grooves left on the corroded surface.

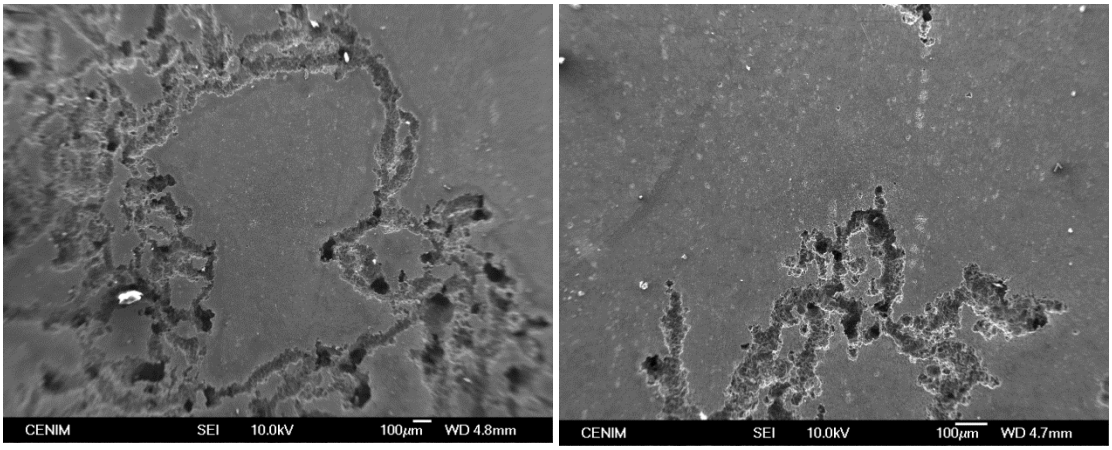

Fig. 2. *Holes of localised attack (dark spots) distributed on the filament grooves left by filiform corrosion after the removal of corrosion products.*

Full information on the combined effect of alloy type and surface condition is summarized below. The following nomenclature is used in the remainder of the paper to

designate the four dual combinations tested: AZ31-O, AZ31-P, AZ61-O, and AZ61-P, where the letters O and P, that accompany the alloy type, denote: O = original surface condition (e.g.,as-received condition); P = polished surface condition. The tested specimens normally exposed an area of 9 to 14 cm^2 to the corrosive solution, while the specimens labelled "small exposed area" exposed an area of 0.4 to 0.8 cm^2 limited by a circular gasket on the flat surface.

In general, the following trends have been disclosed when examining the attack morphologies on the specimens exposed to the 0.6 M NaCl solution:

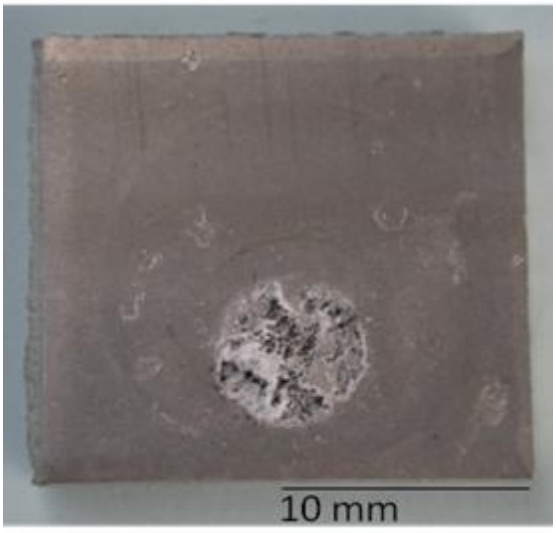

Fig. 3. *Pits and open cavities on the exposed circular area of ~0.4 cm^2.*

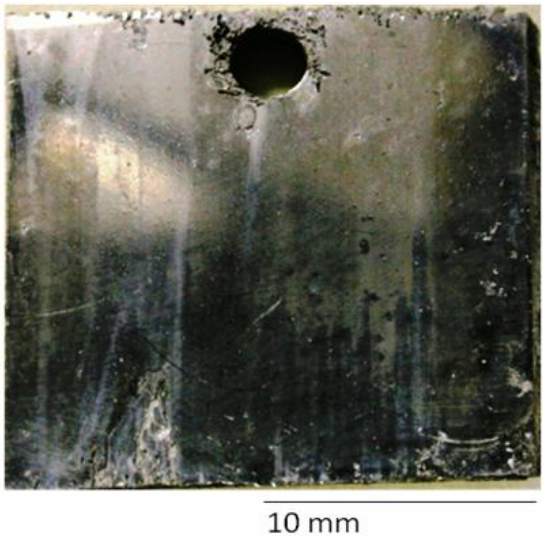

Fig. 4. *Uniform attack with some signs of filiform corrosion close to the drilled hole.*

AZ31-O: On the square specimens whose entire surface (~ 9-14 cm^2) was exposed to the saline solution, predominance of uniform attack and signs of filiform corrosion. In the case of the small exposed area, uniform attack is accompanied by pitting or cavities that occupy part of the surface. A typical example of this morphology is shown in Fig. 3.

AZ31-P: Large areas of uniform attack with the occurrence of filiform corrosion close to the shear cut specimen edges and the drilled hole. This morphology can be seen in Fig. 4. In the case of a small exposed area, some pits and cavities in the central zone of the exposed surface.

AZ61-O: Uniform attack and areas of filiform corrosion close to the specimen edges which can occupy 30-60% of the exposed surface. In the case of a small exposed area, numerous pits and some larger cavities in the central zone of the exposed surface.

Fig. 5. *Extensive areas of filiform corrosion. Specimen immersed vertically in the test solution.*

AZ61-P: Uniform attack on a large part of the exposed surface. In parallel, occurrence of filiform corrosion, generally initiated at the cut specimen edges (e.g. morphology in Fig. 5). In the case of the small exposed area, variety of localized forms, including pitting and some open cavities.

With an exposed area of ~0.4-0.8 cm^2, limited by a circular gasket, the presence of abundant corrosion cavities has normally been observed, while, on the specimens with an exposed area of ~9-14 cm^2 , it was usual the presence of clusters of filiform corrosion with hardly any sign of localized attack.

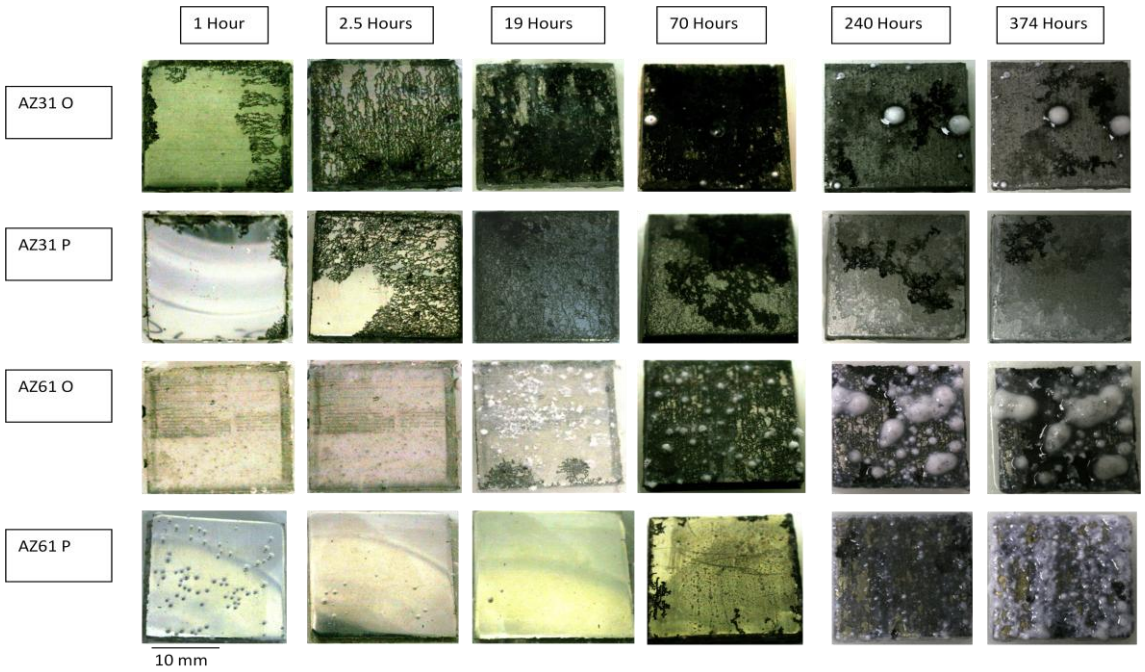

Fig. 6. *Photographic images of the evolution of corrosion morphology with immersion time for alloys AZ31 and AZ61 in the as-received (O) and polished (P) surface conditions. Specimens immersed horizontally about 50 mm below the surface of test solution.*

The series of photographs in Fig. 6 show that on the alloy AZ31 filiform corrosion is initiated almost immediately after immersion, especially on the as-received surface. The population of filaments expands in less than one day across the entire exposed surface. On the AZ61 alloy, the initiation and evolution of filiform corrosion is significantly slower than on AZ31, and clusters of propagating filaments do not appear until after 19 h of immersion on the as-received surface or 70 h on the polished surface. With increasing immersion time, expansion and densification of the mesh of filaments causes the corroding surface of both alloys to become darker and to take on the appearance of uniform corrosion, a development that occurs much faster with alloy AZ31 than with AZ61. The small points in Fig. 6 for AZ61-1hour correspond to hydrogen bubbles growing at and detaching from the polished surface. At longer times of test, white appearing large bubble like features are observed, e.g., on AZ61-374 hours, attributed to the growth of bubbles adhering to the surface accompanied by the precipitation of corrosion products. Also, after relatively long periods of immersion -around 200h for alloy AZ31 in the as-received surface condition and around 43h in the polished condition- the presence of arborescent forms that bear some analogy with the forms of filiform corrosion was observed, although differing from the initially formed by the greater thickness of the filaments and the almost nil tendence to expand with time.

4. Discussion

The triggering and degree of activity of the corrosion processes that take place on the metallic surface is normally related with defect sites present in the oxide film that covers the surface, stimulated by the adsorption of chloride ions in a saline medium and by the difference in potential between bare exposed alloy (in the defects) and the neighbouring oxide film. Microstructural features often promote the formation of points of attack due to the discontinuities that cause in the oxide film. In alloy AZ61 the aluminium is partly precipitated in the form of β phase, preferentially along the grain boundaries, which can cause micro-galvanic acceleration of corrosion of the α Mg matrix [9,12] (Fig.7 is an example of the intense attack that may suffer the AZ61 alloy) . On the contrary, this effect is irrelevant in the alloy AZ31 due to the practically nil presence of β phase. As will be seen later, microgalvanic corrosion can explain some of the differences in corrosion rate of the tested specimens.

Fig. 7. *Intense attack of the AZ61 alloy surface exposed in the as-received condition.*

Another factor that may influence surface activity is the presence of Al in the oxide layer that coats the Mg-Al alloys. Many studies [13-20] mention the beneficial effect of Al in determining the passivity of the exposed surface and resistance to local breakdown of the oxide film, decreasing the chance of chloride ions penetrating to the metal surface. In the present work this effect seems to be reflected in the corrosion of the polished AZ61 alloy specimens, where a large part of their surface retains for a quite

some time the initial shin, while soon the polished surface of the AZ31 alloy, with a notably lower Al content, appears affected by the corrosion (Fig. 6).

A significant improvement in the properties of the surface film is achieved when the bulk content of Al in the Mg-Al alloys exceeds a certain critical level situated around 4% [17,19]. Al content is below this level in alloy AZ31 and above it in alloy AZ61; therefore, a significant improvement in corrosion resistance due to the segregation of Al on the surface is only foreseeable in the latter alloy.

According to the literature, filiform corrosion is assumed to proceed on magnesium alloys under a relatively resistant oxide film from points where this film is no longer continuous [12,21,22,23]. Figs. 5 and 6 are representative images of the filament clusters encountered on the specimens tested in this work. The proliferation of filament populations close to the shear cut specimen edges is probably related with the high level of residual stresses in these regions; the tangled network of dislocations produced in the cold working process of cutting the metal plate must be a preferential site for attack initiation, with prevalence of the nucleation of filaments over other forms of corrosion.
The results of this research have also revealed a slightly lower tendency towards filiform corrosion on polished surfaces than on as-received surfaces, probably because polishing removes the original mill finished surface layer responsible for enhanced corrosion susceptibility [24,25].

4.1. Corrosion rate

In parallel with the analysis of the influence of experimental variables on the attack morphology. It is also interesting to establish their impact, if any, on the corrosion rate.
The addition of Al to Mg modifies the composition and structure of the surface oxide film, improving its resistance to the aggressive attack of Cl^- ions. In contrast with this beneficial action of Al, it is also possible that, in certain circumstances, a negative effect of Al on the corrosion of Mg-Al alloys be prevalent in the final result due to a pronounced microgalvanic action by the β phase [9]. For this reason, higher Al containing Mg alloys, with appreciable amounts of β phase, may corrode faster than alloys of lower Al content if the protective effect of the preexisting surface oxide film is lost.

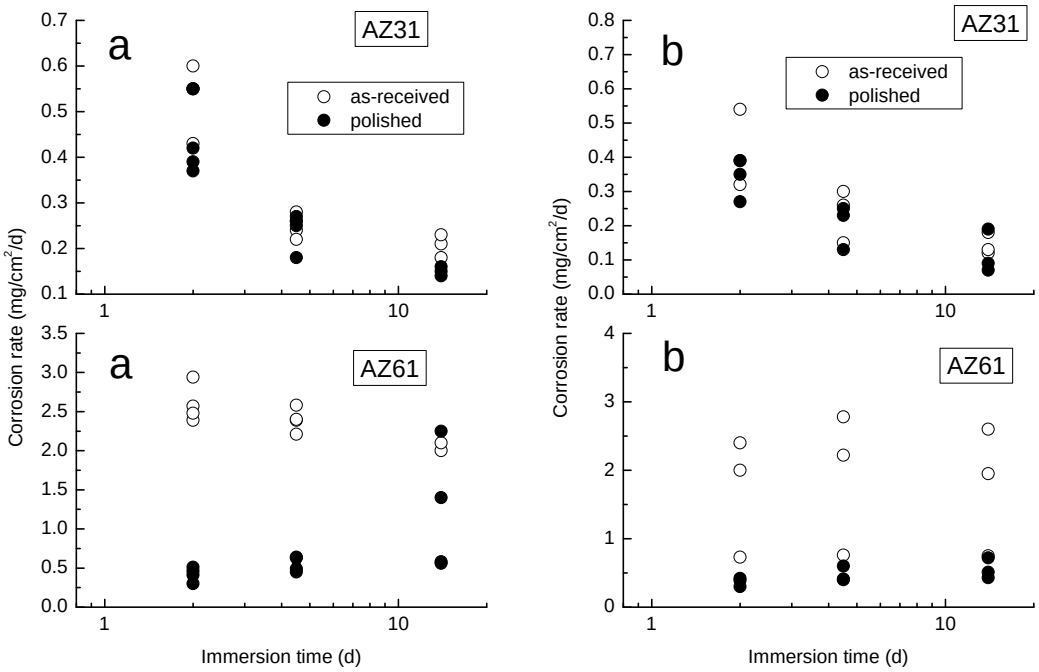

Fig. 8. *Instantaneous corrosion rate (mg/cm^2/d) as a function of immersion time in 0.6M NaCl solution. (a) Square specimens placed vertically exposing the entire surface (~10.4 cm^2) and (b) Square specimens placed horizontally exposing only the upper surface (~4 cm^2). Open points= surface in the as-received condition; solid points= surface in the polished condition.*

Values of the instantaneous corrosion rates evaluated from the slope of hydrogen evolution versus time curves, at immersion times of 2, 4.5 and 14 days are presented in Fig.8. In Fig.8a results refer to specimens immersed vertically and in Fig.8b to specimens immersed horizontally with their top side exposed. Notable aspects include: (i) the marked reduction in the corrosion rate with immersion time for the AZ31-O and AZ31-P specimens; (ii) the less defined or no tendency for the corrosion rate to decrease with immersion time for the AZ61-O specimens; and (iii) the slight tendency to increase corrosion rate with time for the AZ61-P specimens. In general, the results in Fig.8 reveal no special effect of orientation of the specimens within the solution.

If we take as a reference the corrosion rate values determined after two days of immersion, little differences are seen between the data for AZ31-O, AZ31-P and AZ61-P specimens, but the differences are large if compared with the data for AZ61-O specimens, which show three or four times higher corrosion rates. This special behaviour of AZ61-O specimens may be explained by the negative effect of the presence of a not very compact and little protective oxide film in the as-received surface

condition in conjunction with an accelerated microgalvanic corrosion process due to the significant β phase fraction in the AZ61 alloy.

In the early stages of the immersion test attention is drawn to the notably lower corrosion rate on the polished AZ61 specimens compared to the specimens of the same alloy in the as-received surface condition (Fig. 8). This difference may be due to the strong protective effect of the oxide film that forms spontaneously on the polished AZ61 alloy surface, much more perfect and protective than the film on the as-received surface. As long as these properties do not noticeably deteriorate with testing time, said film will prevent or slow microgalvanic corrosion on the AZ61-P specimens.

The reduction in corrosion rate of the AZ31 alloy specimens with immersion time up to the 14 days duration of test (Fig.8) suggests a progressive accumulation of corrosion products on the metallic surface. The corrosion rate also tends to decrease on the AZ61 alloy specimens in the as-received condition, but much more slowly than on the AZ31 alloy specimens, perhaps because the effect of the accumulation of corrosion products is now partly countered by the micro-galvanic corrosion process present on the two-phase AZ61 alloy.

The fact that corrosion rate grows on the polished AZ61 specimens during the 14 days of testing (Fig. 8) suggests a progressive deterioration, due to the action of Cl^- ions, of the protective oxide film that initially coats the polished surface of this alloy.

5. Conclusions

1. The initial surface conditions of AZ31 and AZ61 alloys exposed to 0.6 M NaCl solution has been seen to exert an influence on the corrosion results, with a tendency, especially evident in the AZ61 alloy, for polished surfaces to develop corrosion slower than the as-received surfaces.

2. In the early stages of immersion test, surfaces of AZ61 developed corrosion slower than AZ31 surfaces, behavior attributed to the high protective effect of the pre-existing native oxide film formed on the polished surface of the AZ61 alloy.

3. After several days' immersion, the corrosion rate of AZ61 specimens in as-received surface condition significantly exceeded that of the AZ31 alloy, a phenomenon

explained by the combination of a poorly protective oxide film and an accelerated microgalvanic corrosion on AZ61 alloy.

4. There was an effect of cut surface. Square specimens exposed to the aggressive solution have shown great susceptibility to the development of filament populations in regions close to the shear cut edges.

5. The morphology of most of the corroded surfaces have been predominated by areas of uniform and filiform corrosion. Pits and other forms of localized corrosion have been found mainly in specimens exposing a small area delimited by a circular gasket.

Acknowledgments

We wish to express our gratitude to Professor S. Feliu for several clarifying and stimulating discussions during the course of this work. The authors also gratefully acknowledge the financial support for this work from the Spanish Ministry of Science and Innovation (MAT 2009-13530)

References

[1] Z.M. Shi, M. Liu, A. Atrens, Measurement of the corrosion rate of magnesium alloys using Tafel extrapolation, Corros. Sci. 52 (2010) 579-588.
[2] S. Feliu Jr., C. Maffiotte, J.C. Galván, V. Barranco, Atmospheric corrosion of magnesium alloys AZ31 and AZ61 under continuous condensation conditions, Corros Sci. 53 (2011) 1865-1872.
[3] S. Feliu Jr., C. Maffiotte, A. Samaniego, J.C. Galván, V. Barranco, Effect of naturally formed oxide films and other variables in the early stages of Mg-alloys in NaCl solution, Electrochim. Acta 56 (2011) 4554-4565.
[4] M. Kühlein, U. Galovsky, Influence of testing parameters on the corrosion rate of magnesium alloys, Materials and Corrosion, 55 (2004) 444-448.
[5] G. Song, Z. Xu, The surface, microstructure and corrosion of magnesium alloy AZ31 sheet, Electrochim. Acta, 55 (2010) 4148-4161.
[6] M. Zidoune, M.-H. Grosjean, L. Roué, J. Huot, R. Schulz, Comparative study on the corrosion behavior of milled and unmilled magnesium by electrochemical impedance spectroscopy, Corros. Sci. 46 (2004) 3041-3055.
[7] Z.M. Shi, A. Atrens, An innovative specimen configuration for the study of Mg corrosion, Corros. Sci. 53 (2011) 226-246.
[8] R.L. Xin, B. Li, Q. Liu, Influence of texture on corrosion rate of AZ31 Mg alloy in 3.5 wt% NaCl, Mater. Design., 32 (2011) 4548-4552.
[9] G.L. Song, A. Atrens, Understanding magnesium corrosion – A framework for improved alloy performance, Advanced Engineering Materials 5 (2003) 837-858.
[10] N.I. Zainal Abidin, A.D. Atrens, D. Martin, A. Atrens, The corrosion of high purity Mg, Mg2Zn0.2Mn, ZE41 and AZ91 in Hank's solution at 37ºC, Corros. Sci. 53 (2011) 3542-3556.

[11] Z. Qiao, Z. Shi, N. Hort, N.I. Zainal Abidin, A. Atrens, Corrosion behavior of nominally high purity Mg ingot produced by permanent mold direct chill casting, Corros. Sci. 61 (2012).
[12] M. Liu, P. Schmutz, P.J Uggowitzer, G.L. Song, A Atrens, The influence of yttrium (Y) on the corrosion of Mg-Y binary alloys, Corros. Sci. 52 (2010) 3687-3701.
13. G.L. Song, A. Atrens, Corrosion mechanisms of magnesium alloys, Adv. Eng. Mater. 1 (1999) 11-33.
[14] R. Lindstrom, J.E. Svensson, L.G. Johansson, The influence of carbon dioxide on the atmospheric corrosion of some magnesium alloys in the presence of NaCl, J. Electrochem. Soc. 149 (2002) B103-B107.
[15] S. Feliu Jr., M.C. Merino, R. Arrabal, A.E. Coy, E. Matykina, XPS study of the effect of aluminium on the atmospheric corrosion of the AZ31 magnesium alloy, Surf. Interface Anal. 41 (2009) 143-150.
[16] M. Liu, P.J. Uggowitzer, A.V. Nagasekhar, P. Schmutz, M. Easton, G.L. Song, A. Atrens, Calculated phase diagrams and the corrosion of die-cast Mg-Al alloys, Corros. Sci. 51 (2009) 602-619.
[17] J.H. Nordlien, K. Nisancioglu, S. Ono, N. Masuko, Morphology and structure of oxide films formed on MgAl alloys by exposure to air and water, J. Electrochem. Soc. 143 (1996) 2564-2572.
[18] A. Pardo, M.C. Merino, A.E. Coy, R. Arrabal, F. Viejo, E. Matykina, Corrosion behaviour of magnesium/aluminium alloys in 3.5 wt% NaCl, Corros. Sci. 50 (2008) 823-834.
[19] M. Jönsson, D. Persson, R. Gubner, The initial steps of atmospheric corrosion on magnesium alloy AZ91D, J. Electrochem. Soc., 154 (2007) C 684-C691.
[20] N. Hara, Y. Kobayashi, D. Kagaya, N. Akao, Formation and breakdown of surface films on magnesium and its alloys in aqueous solutions, Corros. Sci., 49 (2007) 166-175.
[21] O. Lunder, J.E. Lein, S.M. Hesjevic, T.K. Aune, K. Nisancioglu,Corrosion morphologies on magnesium alloy AZ-91, Werkst. Korros. 45 (1994) 331-340.
[22] P. Schmutz, V. Guillaumin, R.S. Lillard, G.S. Frankel, Influence of dichromate ions on corrosion processes on pure magnesium, J. Electrochem. Soc., 150 (2003) B99-B110.
[23] G. Williams, R. Grace, Chloride-induced filiform corrosion of organic-coated magnesium, Electrochim. Acta, 56 (2011) 1894-1903.
[24] A.J. Kayes, M.J. Robinson, S. Impey, The influence of cleaning and surface treatment on filiform corrosion of aluminium alloys, JCSE (The journal of Corrosion Science and Engineering) Vol. 2, paper 1, published 12th November 1999.
[25] P. Premendra, W. Loven, H. Terrin, J.H.W.. deWit, L. Katgerman, Consequences of hot rolling of recycled AA5050 on filiform corrosion. Material Science Forum, Vols. 519-521 (20006) 687-692.

Corrosion Product Layers on Magnesium Alloys AZ31 and AZ61: Characterisation and Protective ability.

A. Samaniego[a], I. Llorente[a,] A.A. El-Hadad[b], and S. Feliu (Jr)[a].

[a] Centro Nacional de Investigaciones Metalúrgicas CSIC, Avda. Gregorio del Amo 8, 28040 Madrid, Spain,

[b] Physics Department, Faculty of Science, Al-Azhar University,Nasr City 11884, Cairo, Egypt.

Abstract:

Chemical composition of the corrosion product layers formed on magnesium alloys in 0.6M NaCl was studied. The chemical nature of the layers was quantified by X-ray photoelectron spectroscopy (XPS), scanning electron microscopy (SEM) and energy dispersive analysis of X-ray (EDX). Corrosion behavior was investigated by Electrochemical Impedance Spectroscopy (EIS) and hydrogen evolution measurement. An inhibitive effect from the corrosion product layers was observed from EIS, principally in the case of AZ31, as confirmed by hydrogen evolution tests. A link was found between carbonate enrichment in the corrosion product layer, concomitant with the increase in the protective properties observed by EIS.

Keywords: A. Magnesium; B. XPS; B. SEM; B. EIS; C. Passive films

1. Introduction

Magnesium (Mg) and its alloys continue to have great technological interest, growing in use over the last two decades [1]. From a practical point of view, Mg is the lowest density structural metal, making it attractive for use in the transportation and electronics industries, where light weighting is increasingly important. However, Mg is one of the most chemically active metals, with inadequate resistance to atmospheric and aqueous corrosion [2, 3]. None the less, the observation of corrosion upon Mg that has occurred for over 100 years indicates that corrosion of Mg is localised, and not uniform as may be expected from the Pourbaix diagram which thermodynamically predicts Mg^{2+} for pH values below about 11 [2]. As a result, there is anecdotal evidence that Mg is capable of sustaining some level of corrosion protection, be it by imperfect passive films, or protective films that may arise as a result of corrosion itself [4-7]. This is particularly true for the family of Mg-Al alloys, which make up the predominant tonnage of Mg-alloy usage to date [8-10].

There remains a need for more complete understanding of the factors that influence the corrosion propagation upon Mg-alloys. Recent works in this area have placed a focused on careful surface analysis, including methods such as XPS, XRD, and even FIB-SEM and cross sectional TEM, to observe and characterise surface products and films. The present work aims to contribute to this knowledge, using two commercial Mg-alloys with differing wt % Al additions, AZ31 (nominally 3 wt. % Al - 1 wt. % Zn) and AZ61 (nominally 6 wt.% Al - 1 wt.% Zn).

Corrosion of Mg alloys depends upon circumstances such as: (i) alloy composition and microstructure [3, 11, 12] and (ii) properties of the film developed in the medium to which they are exposed [13]. With regard to the latter, studies have paid attention to the formation of corrosion product layers precipitated on the surface of the Mg and its alloys immersed in aqueous solutions [14-17]. It is appreciated that the outer layer of corrosion products from aqueous exposure consists mainly of brucite ($Mg(OH)_2$), the formation of which is predictable because Mg dissolution favors the production of OH^- ions from the cathodic reaction [5,6,18]. The structure of the surface film has been described as a mixed layer of $MgO/Mg(OH)_2$ [19,20], or a single layer of $MgO_x(OH)_y$ nH_2O [21], or, a bilayer formed by an inner layer of MgO and outer layer of $Mg(OH)_2$.[16, 22]. Some studies performed at ambient atmospheric exposure have detected the presence of Mg-carbonate ($MgCO_3$) on the outer layer of the film [16, 19, 20, 23].

During Mg dissolution, Mg^{2+} ions diffuse to react with the hydroxyl ions OH^- to form the porous layer of $Mg(OH)_2$ on top of the inner barrier film formed by MgO [24]. In contact with a NaCl solution, the adsorbed chloride ions on the surface of magnesium alloys tend to transform $Mg(OH)_2$ into soluble $MgCl_2$ [25, 26] and therefore creates more film free areas where magnesium is corroded.

In our previous work [19, 20, 26], it has been observed that the chemical composition of the corrosion product layer formed during atmospheric exposure [20] or under inside a high humidity conditions [19, 26] may affect the subsequent corrosion behaviour of Mg alloys. Using XPS, notable differences in surface chemistry have been revealed in the corrosion product layer formed on the surface of commercially pure Mg, AZ31, AZ80 and AZ91D - stored at room temperature. Correlation between XPS analysis and gravimetric measurements indicated a coincidence of lower corrosion associated with a higher proportion of magnesium carbonate measured at the surface [20].

In dilute NaCl solutions, Wang et al [27] commented that the formation of a carbonate product layer provides better passivation of the magnesium alloy surfaces and slows down chloride-induced corrosion. According to Liu et al [28], the relatively strong inhibition of the corrosion of AM60 magnesium alloy in 0.01 M NaCl solution may be attributed to the reaction between the dissolved CO_2 and the surface film of $Mg(OH)_2$ to form magnesium compounds containing carbonate, which are more protective, while in more concentrated electrolytes (0.62 M and 1.0 M NaCl solutions) the adsorption of a higher concentration of chloride ions on the surface of the magnesium alloys induced the breakdown of naturally air formed film and the continuous attack of the specimen. A possible reaction for the carbonate compound formation could be described as [29,30]:

$$5Mg(OH)_2(s) + 4HCO_3^-(aq) + 4H^+ \rightarrow Mg_5(CO_3)_4(OH)_2.8\ H_2O \quad (1)$$

As such, the objective of this research is (i) to study the differences in chemical composition of the corrosion products layers that form on the surface AZ31 and AZ61 after immersion in 0.6M NaCl, and (ii) to correlate and discuss chemical and physical characteristics of the product layers and the relative corrosion these alloys in 0.6M NaCl.

In the literature, different studies on the corrosion of magnesium alloys may yield unequal results in apparently similar experimental circumstances [31]. In a previous

investigation [8] it has become apparent the effect of certain combinations of variables relating to specimen preparation and testing conditions on the results obtained. Specifically, the presence of abundant pits, cavities and other forms of localized corrosion were observed in specimens of 0.4-0.8 cm^2, while on the specimens with an exposed area of ~ 9-14 cm^2, it was usual the presence of clusters of filiform corrosion with hardly any sign of localized attack. This casts doubts as to the true meaning of our previous electrochemical impedance measurements [24] obtained using an electrochemical cell with an exposed area of 0.8 cm^2 limited for a circular gasket, which could be clarified by means of better knowledge of the factors that influence them. With this idea, the EIS results of this research have been measured with an exposed area of 9 cm^2, increased by a factor of around ten compared with our previous study [24].

Concerning the composition of Mg-alloys, it is generally assumed that the presence of aluminium in solid solution improves the corrosion resistance of magnesium alloys exposed to aqueous solutions containing chlorides. Many studies [6, 13, 19, 29, 32-35] mention the beneficial effect of aluminium, which can be an essential factor in determining the passivity of the surface, improving the resistance to local breakdown of the oxide film and decreasing the chance of chloride ions penetrating to the surface. However, when aluminium content is higher than 3% according to the phase diagram [36], β-phases precipitates may appear and micro galvanic couples may take places. In this study, AZ31 and AZ61 are used as the base material. The microstructure of the AZ31 alloy is formed practically by an α-matrix with Al in solid solution (Fig. 1a), while a large part of the Al in the microstructure of the AZ61 alloy is precipitated in the form of β-phase (Fig. 1b).

2. Experimental

The chemical composition of the Mg alloys AZ31 and AZ61 are listed in Table 1. Specimens were tested in the wrought condition, supplied in 3 mm thick plates by Magnesium Elecktron Ltd, UK. The research herein compares the behaviour of specimens of each of the above alloys in the two following conditions: a) the "as-received" surface condition, meaning that the surface of the samples was untreated and had only been cleaned with distilled water and dried with hot air, and, b) freshly polished specimens, ground with successive grades of silicon carbide paper to P2000 and followed by finishing with 3 and 1 μm diamond paste, cleaned in distilled water and dried with hot air. The following nomenclature is used in the remainder of the paper to designate the four dual combinations tested: AZ31-O, AZ31-P, AZ61-O, and AZ61-P,

where the letters O and P, that accompany the alloy type, denote: O = original surface condition (i.e. as-received); P = polished surface condition.

Table 2 *EDX result of corrosion products on the surface of the investigated alloys.*

Alloy	Al	Zn	Mn	Si	Fe	Ca	Mg
AZ31	3.1	0.73	0.25	0.02	0.005	0.0014	Bal.
AZ61	6.2	0.74	0.23	0.04	0.004	0.0013	Bal.

Photoelectron spectra were recorded using a Fisons MT500 spectrometer equipped with a hemispherical electron analyser (CLAM 2) and a Mg K_α X-ray source operated at 300 W. The samples were fixed on small flat discs on a *XYZ* manipulator and placed in the analysis chamber. The residual pressure in this ion-pumped analysis chamber was maintained below 10^{-8} torr during data collection. The spectra were collected for 20–90 min depending on the peak intensities, at a pass energy of 20 eV, which is typical for high-resolution conditions. The intensities were estimated by calculating the area under each peak after smoothing and subtraction of the S-shaped background and fitting the experimental curve to a combination of Lorentzian and Gaussian lines of variable proportions. Although specimen charging was observed, it was possible to determine accurate binding energies (BEs) by making references to the adventitious C 1s peak at 285.0 eV. The atomic ratios were calculated from the peak intensity ratios and the reported atomic sensitivity factors [37]. The measurements were performed at take-off angles of 45° with respect to the sample surface. The sampled areas were 1 x 1 mm^2.

For the acquisition of concentration profiles (distribution of elements as a function of specimen thickness) the surface was sputtered by argon ion bombardment (AIB). This was performed using an EXO5 ion gun incorporated in the equipment, which was provided with a scanning unit to track the beam operating at a voltage of 5 kV, an intensity of 10 mA and a pressure of 1 x 10^{-7} torr. The sample current was 1 μA during bombardment. In a previous study [38], it was estimated that the sputtering rate for native oxide films on Mg and Mg alloys was about 0.15 nm/min. This value is close to the sputtering rates obtained by Yao et al. [39] for Mg in air.

Specimens were examined by scanning electron microscopy (SEM) using a JEOL 840A unit operating with Rontec EDR288 software for EDX spectra acquisition and image digitalisation.

X-ray diffraction (XRD) measurements were carried out with a Bruker AXS D8 diffractometer in grazing incidence condition. In the setup used, a X-ray Co tube is equipped with a Goebel mirror optics to obtain a parallel and monochromatic X-ray beam. A current of 30 mA and a voltage of 40 KV were employed as tube setting. XRD data were collected with a beam incidence angle of 1º and 2θ scan between 20 and 110º with a step size of 0.03ºand a counting time of 4 s/step.

For the hydrogen evolution determinations, the corrosion of magnesium alloys during solution immersion was estimated by determining the volume of hydrogen evolved during the corrosion process. Samples for hydrogen collection were cut into square coupons with dimensions of 2cm x 2cm x 0.3cm and vertically immersed in 700 ml of quiescent 0.6M NaCl for 14 days in a beaker open to laboratory air at 25 ± 2 °C. The entire specimen surface was exposed to the electrolyte. Evolved hydrogen was collected in a burette above an inverted funnel placed centrally above specimen. All these experiments were run simultaneously and each sample was subjected to essentially the same temperature and exposure history. The experimental difficulties and limitations of such test was recently documented [40]. For the gravimetric determination of corrosion, the specimens were weighed before exposure and then after testing were pickled in chromic acid to remove the corrosion products, rinsed with isopropyl alcohol, dried in hot air and reweighed in order to calculate the mass loss per unit of surface area.
Electrochemical impedance measurements were conducted in 0.6 M NaCl during 14 days of exposure at room temperature (25ºC) using an AUTOLAB PGSTAT30, with frequency response analyser. The frequency ranged from 100 kHz to 1 mHz with 5 points/decade and a sinusoidal potential signal of 10 mV. A typical three-electrode setup was employed, using Ag/AgCl (Sat.) and graphite as the reference and counter electrodes, respectively. The exposed area of the working electrode was 9 cm^2.
The pH values were measured during the galvanic corrosion process by immersing an electrode in the solution with the electrode tip held 10 mm above the sample.

3. Results

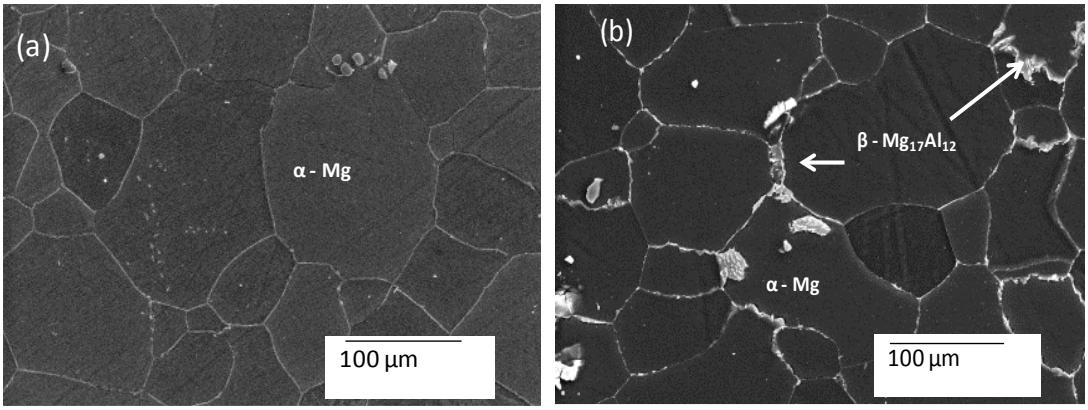

Figure 1. *Micrographs of a) AZ31 b) AZ61magnesium alloys.*

3.1. Charge transfer resistance measurements or corrosion rate.

3.1.1 Electrochemical impedance measurements

The Nyquist diagrams (Fig. 2) obtained in monitoring the evolution of the corrosion on the AZ31-O, AZ31-P, AZ61-O and AZ61-P specimens immersed in 0.6 M NaCl show the presence of a capacitive loop at high frequencies (HF) and an inductive loop at low frequencies (LF). In the literature about the corrosion of magnesium alloys is normal to associate the diameter of the capacitive loop in the HF frequency region with the charge transfer resistance (R_t) of the corrosion process [17, 41, 42], value which is inversely related to the corrosion current (i_{corr}) through the well known Stern-Geary equation [43]. In a previous investigation [9], an empirical determination of the proportionality constant B from the correlation between electrochemical and gravimetric measurements yielded values of around 65 mV for the AZ31 alloy and of around 120 mV for the AZ61 alloy.

Fig. 3a shows the evolution of R_t deduced as function of immersion time in 0.6M NaCl solution. Taking R_t values for the AZ31 alloy specimens measured after 1 hour of immersion as reference, exposure for 14 days increase the size of the HF loop of the Nyquist diagram, and thus the R_t value associated with it (Fig. 3a); so that after 14 days testing the R_t values for the AZ31 specimens in both surface conditions are about 4 times greater than those obtained in the initial stages of testing (Fig. 3a). It should be noted also in Fig. 3a the different behaviour shown by the AZ61 specimens during the first two days of testing depending on their initial surface condition (as-received or

polished). In accordance with a previous study [24], the high R_t values for the polished surface suggest a special protective effect of the native oxide film formed on it, while this effect is not manifested in the alloy AZ31.

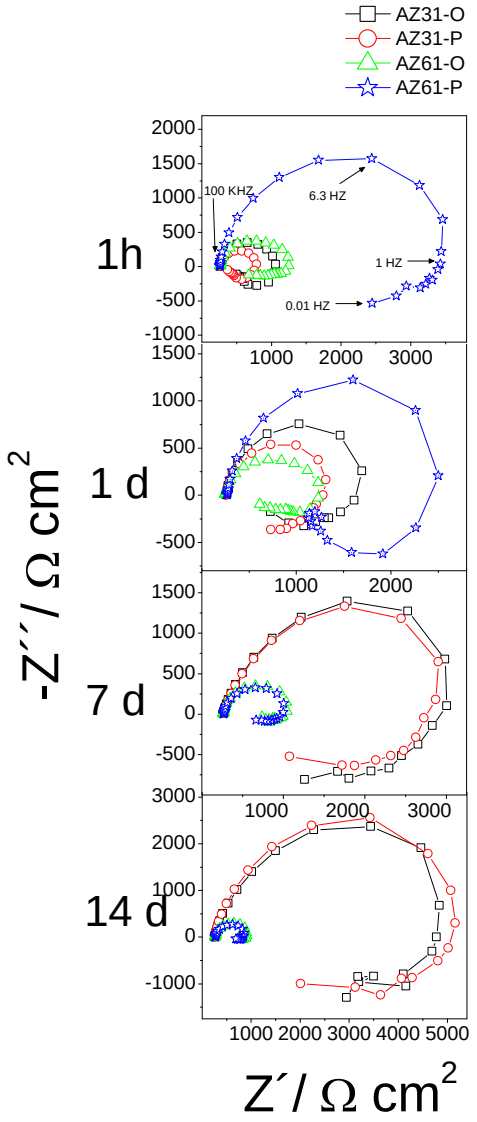

Figure 2. *Variation in Nyquist plots for AZ31-O, AZ31-P, AZ61-O and AZ61-P specimens with immersion time.*

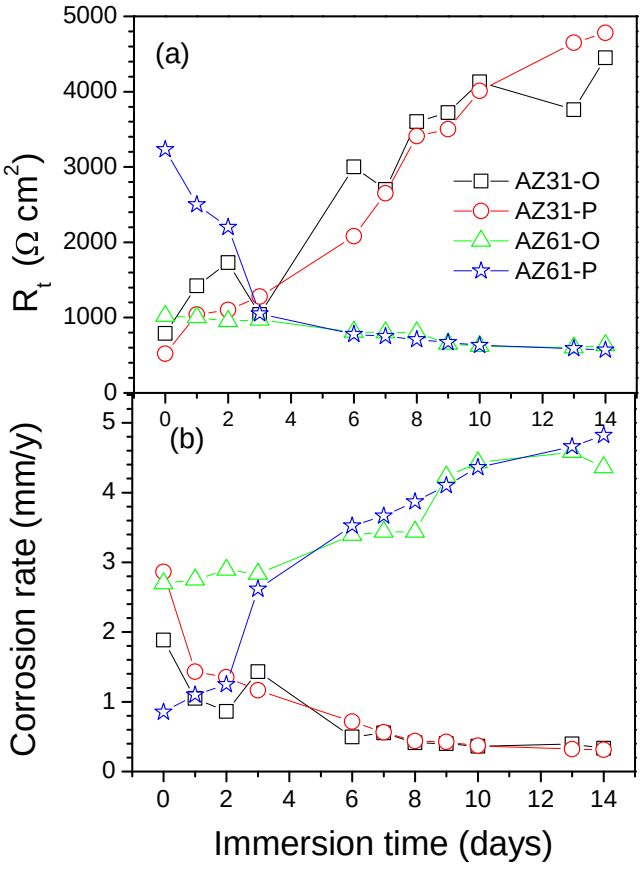

Figure 3. *Variations of corrosion as a function of alloy type, surface condition and immersion time: (a) R_t values ; (b) corresponding corrosion rates.*

If we take as a reference the R_t values determined with an exposed area of 0.8 cm^2 [24] after 14-15 days of immersion, little differences are seen with the data for the AZ61 alloys with an exposed area of 9cm^2 but the differences are large if compared with the data for AZ31 specimens which show five or six times higher Rt values. This special behaviour of AZ31 specimens may be explained by the negative effect of the pits and

other forms of localized corrosion observed in specimens exposing a small area [8] which countered the positive effect of the accumulation of protective corrosion products.

R_t data together with Stern-Geary equation have enabled electrochemical calculations of corrosion rate and amount of corroded metal. For determination of the amount of corroded metal over an extended period of time, i_{corr} values have been converted into weight losses by applying Faraday´s law and integrating the weight changes for individual exposure periods over the considered interval. This way, the results depicted in Fig. 3b were determined, which show the instantaneous corrosion rate variations with time over 14 days immersion. On the other hand, Fig. 4 shows the average corrosion rates of the specimens after 14 days of exposure to the 0.6 M NaCl solution.

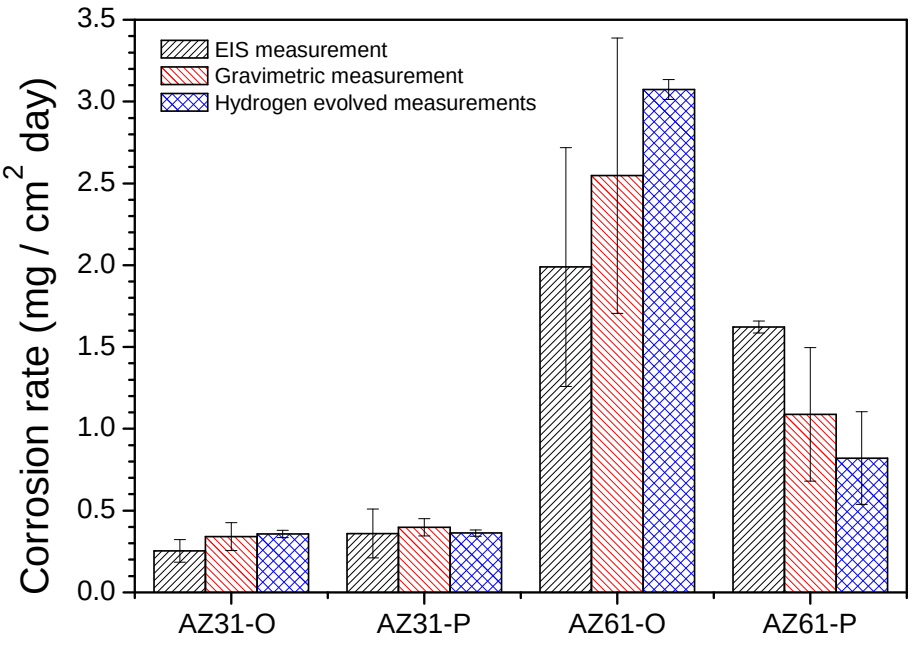

Figure 4. *Comparison of corrosion rates (mm/y) obtained from EIS with weight loss and hydrogen evolution measurements after 14 days immersion in 0.6M NaCl.*

3.1.2. Hydrogen evolution measurements

Fig. 5 is instructive in showing the differences in the hydrogen volume data between alloys AZ31 and AZ61 over 14 days of immersion in 0.6 M NaCl. It is interesting to note that similar trends regarding the corrosion behaviour are deduced from these hydrogen evolution determinations that from the electrochemical ones.

Fig. 4, which compares the amounts of corroded metal determined by hydrogen evolution, gravimetric and electrochemical measurements, also gives us an idea of the degree of similarity between these three types of determinations.

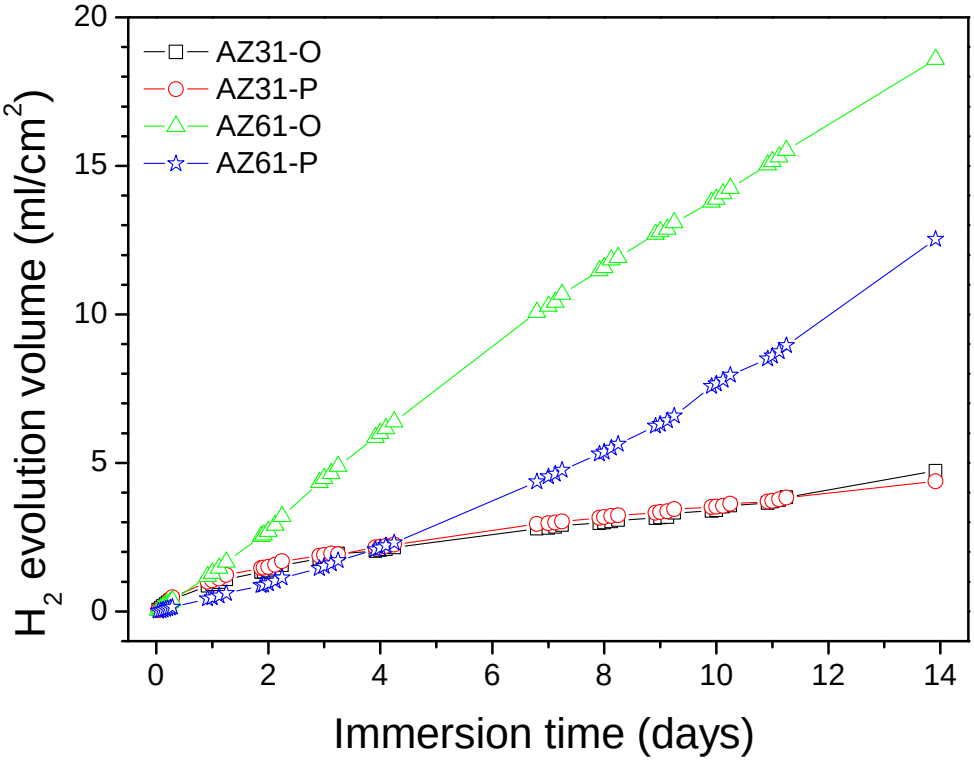

Figure 5. *Variation in H_2 evolution volume values as a function of surface conditions and alloy type over 14 days immersion in 0.6M NaCl.*

3.1.3. pH measurements

Fig. 6 displays the pH values for the AZ31 and AZ61 alloy specimens as a function of immersion time. In the case of AZ31 specimens, little variation of the pH values is observed with immersion time. In contrast with AZ31 specimens, it is interesting to note the rapid increase of the pH values after periods of immersion around 1h for AZ61-O specimen and around 3 days in the AZ61-P specimen. One point emerging in the set of pH values (Fig. 6) is the clear tendency for AZ61 specimens to present after 3 days higher values than the AZ31 specimens for the same immersion time. However, it should be stressed that these values corresponds to the pH of the bulk solution which may differ significantly from the pH changes that occur directly above the metallic substrate surface during immersion in the 0.6M NaCl solution.

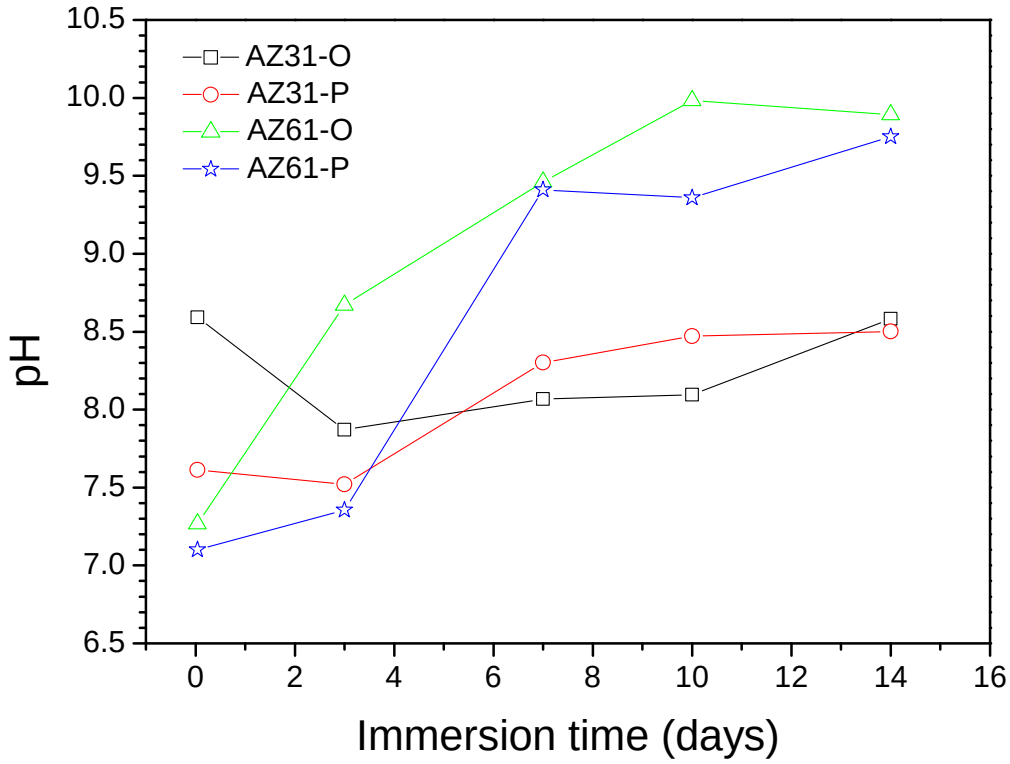

Figure 6. *Variation in pH values as a function of surface conditions and alloy type over 14 days immersion in 0.6M NaCl.*

3.2. Characterisation of the corrosion layer

3.2.1 Morphology and micro composition of the corrosion layer formed on the surface of the AZ31 and AZ61 magnesium alloys after immersion in NaCl 0.6M solution.

Fig. 7 compares the SEM micrographs of the surface of the tested materials after 14 days of immersion in 0.6M NaCl solution. The surface of the AZ31-O (Fig 7a) and AZ31-P (Fig. 7b) specimens is completely covered with a rather uniform and continuous corrosion film. On the surface of the AZ61-O specimen (Figs. 7c), attention is drawn to the presence of a large number of needles-like clusters oriented nearly perpendicular to the specimen surface in the dark inner corrosion layer with a "sand rose" [44] or "sunflower" [45] morphology [46] much less compact and probably protective than that formed on the surface of the other specimens.

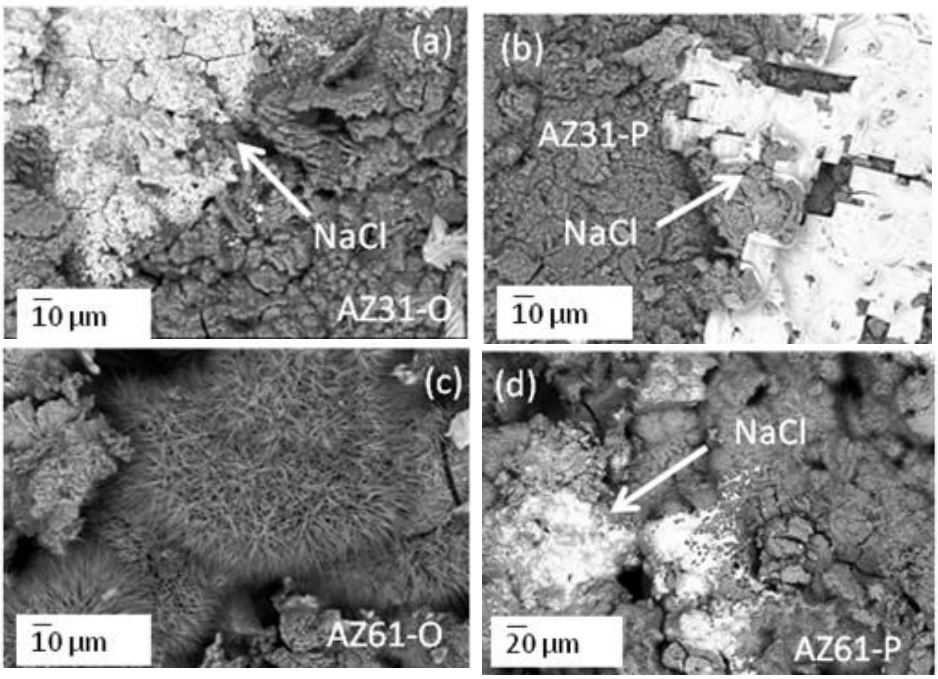

Figure 7. *SEM surface morphologies for AZ31-O (a), AZ31-P (b), AZ61-O (c) and AZ61-P (d) specimens after immersion in 0.6M NaCl solution for 14 days.*

A rather significant presence of top white areas, where crystals of NaCl have precipitated on the surface of the corrosion layer formed on the AZ31-O, AZ31-P and AZ61-P specimens (Fig 7a, Fig 7b and 7d, respectively), is noted. In contrast, these white areas have practically disappeared on the surface of the corrosion layer formed on the AZ61-O specimens (Fig 7c). The coupons were not chemically cleaned, only rinsed with distilled water to ensure that the surface remained unchanged. This cleaning method could allow corrosion products and salt residues to remain attached to the surface [47].

Table 2 *EDX result of corrosion products on the surface of the investigated alloys.*

	Composition (at%)				
Specimen	O	Mg	Al	Cl	Na
AZ31-O	61	34	1	2	2
AZ31-P	58	33	0.5	4.5	3
AZ61-O	59	34	0	7	0
AZ61-P	59	30	0	11	0

Table 2 gives the atomic composition obtained by EDX analysis focused only on the dark corrosion layers formed on the surface of the AZ31-O, AZ31-P, AZ61-O and AZ61-P specimens (Fig.6). These analyses do not reveal any significant enrichment of aluminum on the surface of the corrosion layer. The Cl/Na ratios (1-1.5) detected by EDX in the dark corrosion layer formed on the surface of the AZ31-O and AZ31-P specimens are consistent with the presence of crystals of NaCl. In contrast, it is interesting to note the absence of Na on the EDX analyses of the dark corrosion layer formed on the surface of the AZ61-O and AZ61-P specimens. This data tends to suggest that the Cl detected in these layers is mainly associated with the presence of $MgCl_2$.

3.2.2. Low Angle X-ray diffraction

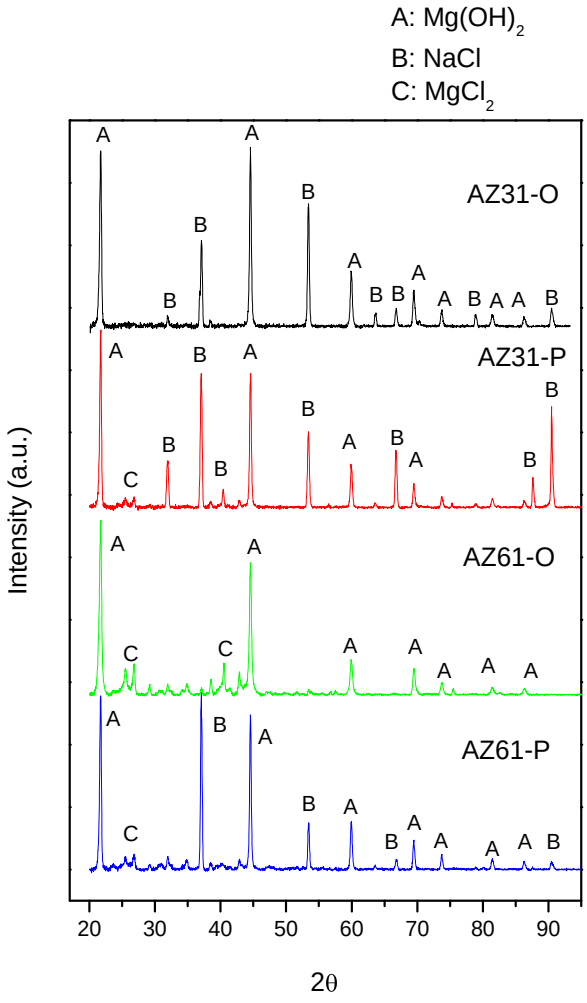

***Figure 8**. Low-angle XRD pattern of tested alloys exposed to 0.6M NaCl solution for 14 days*

Fig. 8 shows low-angle XRD patterns for the corrosion products layer produced after immersion in 0.6M NaCl for 14 days. The diffractograms revealed brucite, $Mg(OH)_2$, as the main corrosion product. Some peaks of $MgCl_2$ were also detected which exhibited higher intensity for the AZ61-O specimen. In agreement with the SEM observations (Fig 7), significant evidence of NaCl is observed in the XRD diffractograms of the corrosion layer formed on the AZ31-O, AZ31-P and AZ61-P specimens after immersion in 0.6M NaCl for 14 days, but not on the AZ61-O specimen (Fig. 8).

3.2.3. Changes in the surface chemistry of the corrosion layers formed on the surface of the AZ31 and AZ61 alloys after immersion in 0.6M NaCl

Table 3. *Atomic percentage observed by XPS in the surface of the corrosion layer formed on alloys exposed to 0.6M NaCl solution for 15 days.*

Specimen	Elements (at.%)						
	C	O	Mg	Al	Cl	Na[a]	CO_3^{2-} (obtained from the fitting of the C 1s peak and the C atomic percentage)
Non sputtered surface							
AZ31-O	42	15	8	2	15	18	18
AZ31-P	40	9	6	3	19	23	18
AZ61-O	35	41	13	0	5	6	7
AZ61-P	36	35	10	0	8	11	9
After 10 min of sputtering							
AZ31-O	27	25	10	2	16	20	17
AZ31-P	24	20	9	3	19	25	18
AZ61-O	20	48	16	0	7	9	6
AZ61-P	27	37	14	0	8	14	10

Table 3 compares the elemental composition obtained by XPS on the non-sputtered surfaces and after 10 minutes of sputtering of the corroded surfaces of the AZ31-O, AZ31-P, AZ61-O and AZ61-P specimens after immersion for 15 days in 0.6 M NaCl. On the AZ31-O and AZ31-P specimens, attention is drawn to the important increase in the Cl and Na content observed on the surface of the corrosion layer respect to the corresponding of the AZ61 alloys. In contrast to the AZ61 specimens, the surface of the corrosion layer on the AZ31 specimens after 10 minutes of sputtering shows an excess of Na over the Cl, content (Table 3). Probably, because of the higher intensity of the Cl2p peak observed by XPS in the surface of the AZ31 alloy after the immersion test,

the effect from its respective chlorine Auger induced peak ($ClKL_1L_{23}$) at a binding energy of 1072.0 eV is a significant increase in the area of the Na1s spectrum. Also, an important increase in the Magnesium and Oxygen content is observed in the AZ61 alloys compared with the outer surface of the AZ31 alloys.

Fig. 9 shows a comparison of the high-resolution C1s spectra obtained in the non-sputtered surface (Figs 9a-9d) and after 10 minutes of sputtering (Figs 9e-9h) of the corrosion layer formed on the AZ31 y AZ61 specimens after immersion for 15 days in 0.6 M NaCl. The C1s spectra obtained on the non-sputtered surface of the corrosion layer formed on the AZ61-O specimen (Fig 9c) may be fitted using two components at different binding energies: at 285.0 eV, which may be associated with the presence of C-C/C-H groups, and a less intense component, about 4.5-5.0 eV higher, which is associated with the presence of magnesium carbonate [39]. The first component, C-C/C-H groups, appears on the surface (<3 nm in thickness) of almost any metal in contact with the atmosphere at room temperature, irrespective of its composition. In the spectra obtained on the non-sputtered surface of the corrosion layer formed on the AZ31-O (Fig. 9a) and AZ31-P specimens (Fig. 9b), the C1s peaks splitting at the high binding energy side may be associated to differential charge effects. The component at 285.0 eV may be associated to C-C/C-H groups in the relatively conducting dark corrosion layer next to the metallic substrate and the component at approximately 287.0 eV may be associated with the presence of similar groups on the more isolating white NaCl crystals of the outer surface (Figs 7a and 7b). Likewise, a shift of about 3 eV is seen in the binding energy, accompanied by an increase in the intensity of the component that appears at the highest binding energies of close to 293.0 eV, which may be attributed to the presence of significant amounts of magnesium carbonate which charges appreciably in contact with the NaCl crystals (non-conducting). On the non-sputtered surface of the corrosion layer formed on the AZ61-P specimen condition there is a notable decrease in the intensity of the second and fourth components (Fig. 9d) compared to the AZ31 specimens (Figs. 9a and 9b). We speculate that these differences maybe related with a decrease in the surface fraction of the dark inner corrosion layer covered by the white NaCl crystal in the case of the AZ61-P specimen (Fig. 7d) in comparison with the AZ31-O (Fig 7a) and AZ31-P (Fig 7b) ones.

After 10 minutes of sputtering the intensity of the magnesium carbonate components significantly increased and become higher than the intensity of C-C/C-H groups in the case of the AZ31-O (Fig. 9e) or AZ31-P (Fig. 9f) specimens. No such increment is seen on AZ61 specimens (Figs. 9g and 9h).

In contrast with the C1s peak (Fig.9), it is interesting to note that the O1s (Fig.10), Mg2p, Cl2p, Na1s and Al 2s high resolution XPS peaks (Fig. 11) seem not to be significantly affected by differential charging effects. The O1s high resolution spectra obtained on the corrosion layer formed on the AZ61-O specimen (Fig 10a) shows the most intense component at a binding energy of 532.0 eV associated with the presence of oxygen in the form of $Mg(OH)_2$ and another less intense at 533.6 eV which may be attributed to magnesium carbonate [48]. As was previously observed in the C1s peak (Fig.9), it is important to note the significant increase in the intensity of the component which appears at the highest binding energies (magnesium carbonate) in the O1s spectra observed in the corrosion layer formed on the AZ31-O specimen (Fig. 10b) compared with that of the AZ61-O specimen (Fig. 10a).

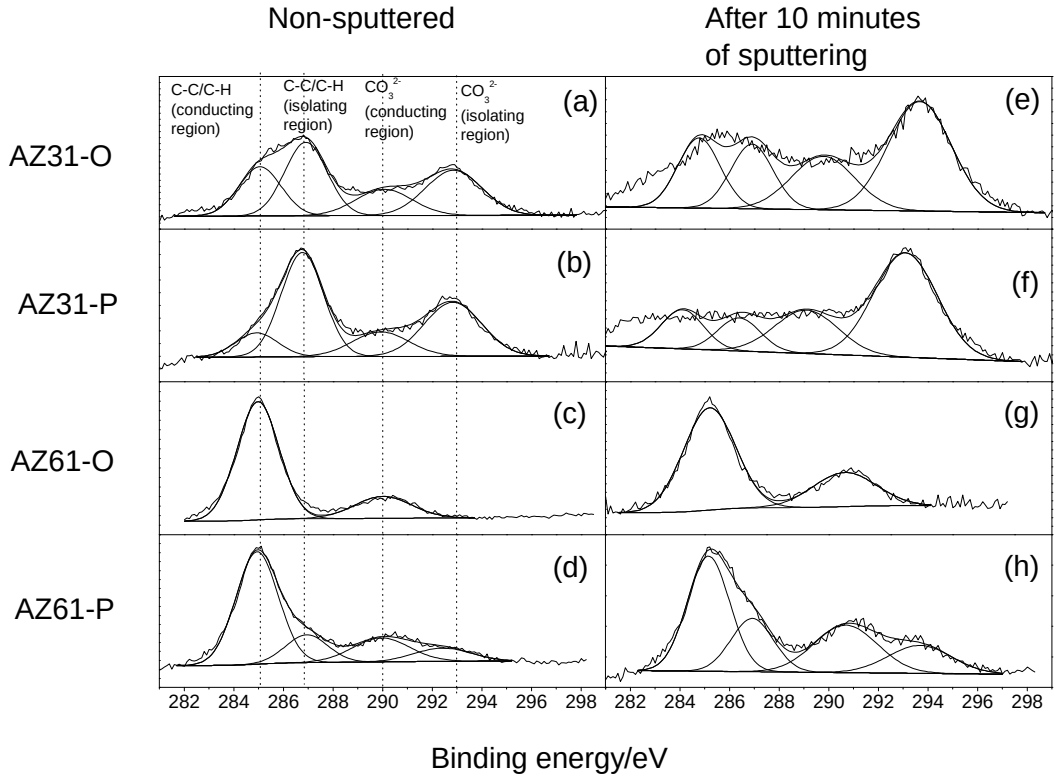

Figure 9. *High-resolution C 1s spectra obtained before (a-d) and after 10 min of argon sputtering (e-h) on the tested alloys exposed to 0.6M NaCl solution for 14 days.*

Fig 11 shows the Mg 2p (a), Al2s (b), Cl2p (c) and Na 1s (d) XPS high resolution spectra on the non-sputtered surface of the corrosion layer formed on the AZ31-O specimen. These spectra are representative of the similar Mg 2p, Al 2s, Cl2p and Na1s spectra obtained on the surface of the corrosion layers formed on the other AZ31 and AZ61 samples studied. In the Mg 2p spectrum (Fig. 11a) only one component appears that is associated with the presence of Magnesium in Mg^{2+} (51.0 eV) form [49, 50]. In

the Al 2s spectrum (Fig.11b) there is a 119.5eV component characteristic of aluminium in ionic state (Al^{3+} type). The Cl2p high resolution spectrum (Fig. 11c) may be fitted to one doublet with a binding energy of 198.2 eV associated with the presence of Cl^-. Finally, the Na1s spectrum (Fig. 11d) may be fitted to one component at 1071.7 eV associated with the presence of sodium (Na^+) ions.

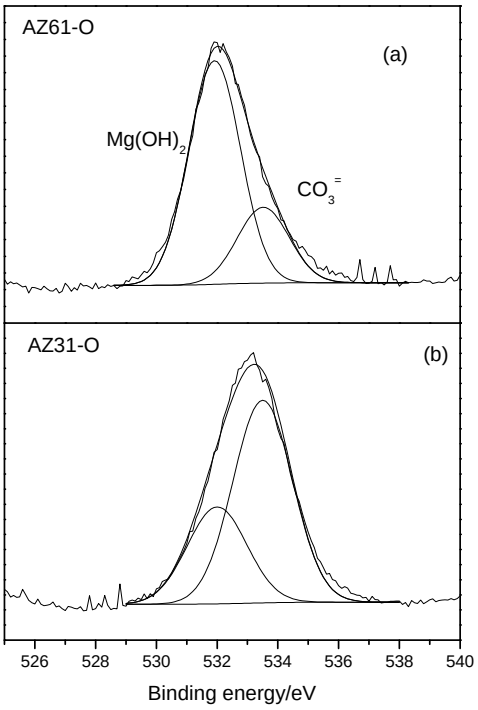

Figure 10. *High-resolution O 1s spectra obtained before (a) and after 10 min of argon sputtering (b) on the AZ31-O alloys exposed to 0.6M NaCl solution for 14 days.*

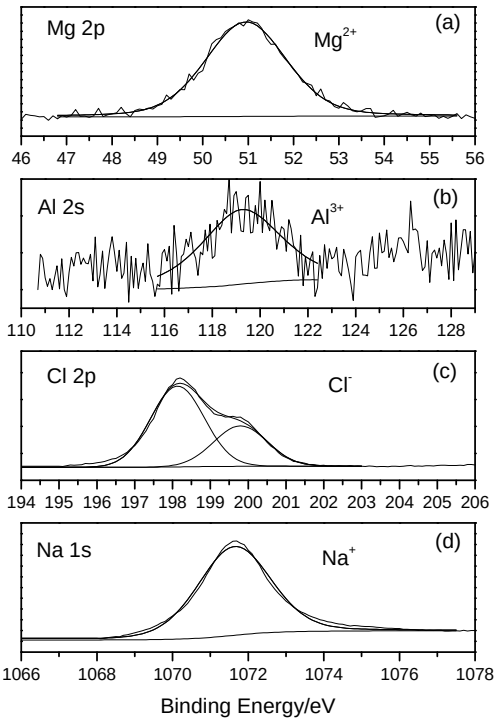

Figure 11. *High-resolution Mg2p (a), Cl2p (b), Na1s (c) and Al2s (d) spectra obtained on non-sputtered surface of the AZ31-O alloys exposed to 0.6M NaCl solution for 14 days.*

Table 3 compares the atomic percentages of carbonate on the surface of the corrosion layers formed on the AZ31 and AZ61 alloys exposed to the NaCl solution. The atomic percentages of carbonate were obtained from the area of the CO_3^{2-} components used in the fitting of the C1s spectra (Fig. 9) and the atomic percentages of C obtained by XPS on the surface of the corrosion layer formed on the AZ31 and AZ61 alloys (Table 3). It is important to note, the significant increase in the amount of carbonates observed by X-ray photoelectron spectroscopy (XPS) on the non-sputtered surface of the corrosion layer formed on the AZ31 samples, increased by a factor of around 2, compared with the AZ61 alloys. Similar differences are obtained after 10 min of sputtering.

In contrast with XPS data, no evidence of carbonate is observed by XRD (Fig.8). It is reasonable that corrosion products composed of carbonates formed on the samples in solution NaCl 0.6M may be amorphous and not crystalline structure.

4. Discussion

4.1. Influence of type of alloy on surface chemistry, morphology and protectiveness of the corrosion layer.

When magnesium and its alloys are immersed in saline solutions, corrosion takes place with hydrogen evolution and release of OH^- ions and, as a consequence, the pH of the liquid adjacent to the metallic surface increases [51] The final interfacial pH comes from the balance between corrosion rate with formation of OH^- ions and the rate of removal of these ions by diffusion and convection. For example, with high corrosion rates the final pH can reach values of 10.5-11, but with lower corrosion rates the final pH will be less than 10.5.

It seems likely that many of the differences in the contents of magnesium hydroxide and carbonate observed on the surface of the specimens obey to differences in the corrosion rate of the tested specimens. In this paper, according Fig. 4, specimens of alloy AZ61 showed three or four times higher corrosion rates than those of alloy AZ31.

In general, with increasing pH, and as the solution becomes saturated by Mg^{2+} during the corrosion process, it takes place the precipitation of a layer of $Mg(OH)_2$ on the exposed surface. If CO_2 is also present in the solution, a decreasing concentration of Mg^{2+} ions tends to favors the precipitation of $MgCO_3$ compared to $Mg(OH)_2$, so $Mg(OH)_2$ deposition may not take place over a wide range of pH values. In this case it is understandable that the precipitated corrosion products are mainly formed of magnesium hydroxi-carbonate type compounds. The results of several studies have suggested compositions close to $Mg_2(OH)_2CO_3.3H_2O$ (artenite) or $Mg_5\ (CO_3)_4\ (OH)_2.\ 5H_2O$ (hydromagnesite) for the precipitated corrosion products [23].

Data in Table 3 show that the outermost portion of the corrosion layer on AZ61-O and AZ61-P specimens after 15 days immersion in 0.6M NaCl is constituted mainly by $Mg(OH)_2$ with a small proportion of magnesium carbonate (Figs.9c, 9d, 9g, 10a and Table 3). Instead, the AZ31 specimens have shown an increase in carbonate accompanied by a decrease in $Mg(OH)_2$, so that both contents approaches (Figs 9a, 9b,

9e, 9f, 10b and Table 3). The differences in the contents of magnesium hydroxide and carbonates observed on the surface of the various specimens may be related to differences in the corrosion rate. From the corrosion rates determined after 14 days of immersion (Fig.4), it follows that AZ61-O and AZ61-P specimens show three or four times higher corrosion rates than AZ31-O and AZ31-P specimens.

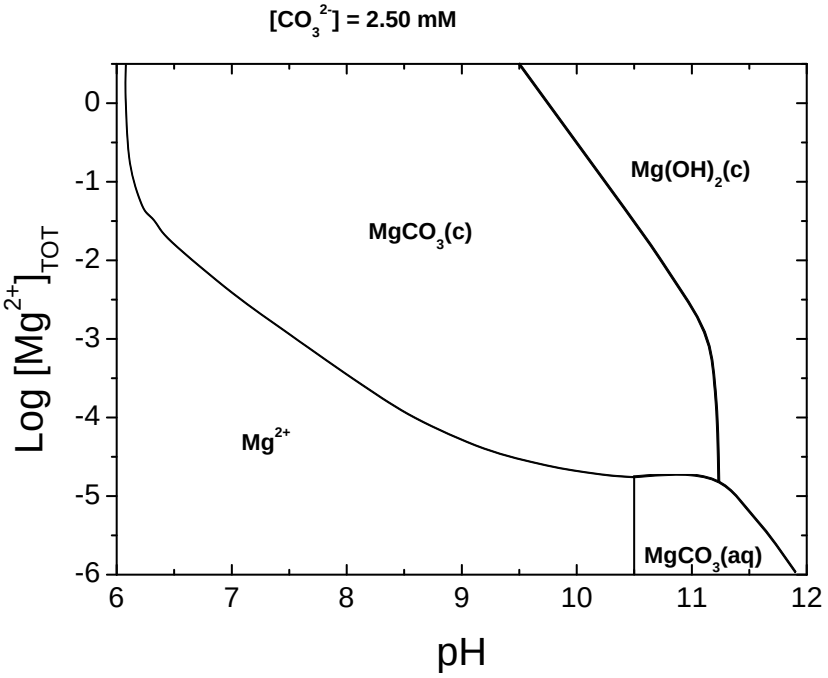

Figure 12. *Equilibrium predominance diagram of various magnesium species calculated using MEDUSA [53] for a concentration of 2.50 mM CO_3^{2-}. $MgCO_3$ (aq) is a soluble complex. The reaction equations corresponding boundaries are:*
$CO_3^{2-} + Mg^{2+} = MgCO_3$ (c) $\log K_s = 8.029$
$Mg^{2+} = 2\,H^+ + Mg(OH)_2$ (c) $\log K_s = 16.84$
$CO_3^{2-} + Mg^{2+} = MgCO_3$ (aq) $\log K_s = 2.98$

Using the MEDUSA software package [52-54] an equilibrium thermodynamic diagram showing the predominance of various magnesium species with the variation in Mg^{2+} ion concentration with pH (for a fixed CO_3^{2--} concentration of 2.5 mM (which is of the order of the CO_2 content in air-saturated water)) was determined and is shown in Fig. 12. In the AZ61-O and AZ61-P specimens it is likely that the higher magnesium dissolution and production of OH^- ions from the cathodic reaction increases the pH allowing the preferential formation of magnesium hydroxide. In contrast, the notably lower corrosion rates of the AZ31-O and AZ31-P specimens and significant decrease of pH promotes the preferential formation of magnesium hydroxi-carbonate type compounds.

4.2. Protectiveness of the corrosion layer formed on the surface of the AZ31 and AZ61 alloys in the 0.6M NaCl solution

It is natural that the surface of the specimens after the corrosion test exhibits different morphologies, influenced in some way by the microstructure of the alloys and characteristics of the corrosion products deposited on it.

Although 0.6 M NaCl solution favours a rapid attack of the magnesium alloys to form $Mg(OH)_2$ and hydroxicarbonates, the resulting surface layer is only semi-protective due to its numerous cracks and flaky-like structure. Compounds which are present in the alloy structure in form of eutectic or intermetallic phase can cause an increase of areas where breaks of the corrosion products layer abounds and where more intensive corrosion processes can take place. In the Mg-Al alloys the attack can be initiated at points close to beta phase which, acting as a galvanic cathode, accelerates alpha phase corrosion.

The discontinuities in the corrosion products layer motivate the constant exposure of fresh metal and even the possible appearance of new crystalline forms, often as needle or flower-like crystals. Conglomerates of needle-shaped crystals has been found over localized corrosion areas, e.g. inside pinholes on the surface [55]. In the present work, this form of crystallization has been observed on the AZ61specimens but not in those of the AZ31 alloy.

Evidently, the porous morphology of the clusters of needle-like crystals is not appropriate for an effective contribution to the protection offered by virtually continuous layers of corrosion products.

Electrochemical impedance results have provided additional information on the effect of experimental variables on the corrosion resistance of the specimens tested. One point emerging from the R_t values in Fig. 3 is the clear trend of the AZ61-P specimen to present in the first three days of immersion higher values than the other tested specimens for the same immersion times. This higher resistance is in agreement with previous results [8, 9, 24] which attributed it to a particularly protective effect of the pre-existing native oxide film formed on the polished surface of the AZ61 alloy. Comparison of the R_t values for the two tested alloys have shown another difference: after the first day of immersion, R_t values for the AZ61 specimens showed a rather moderate tendency to decrease with time throughout the 14 days testing (Fig. 3) but

with alloy AZ31 the reverse tendency predominated, so the values of R_t for the two alloys tend to accentuate their divergence.

The above results are logically linked to changes experienced by the specimen surfaces during exposure to the 0.6M NaCl solution. In this respect, it is to be highlighted the marked tendency of the AZ61-P specimen for R_t to decrease from the start of testing, suggesting a weakening of the protective action of the film covering the metallic surface, probably due to progressive deterioration of the air-formed film in contact with the aggressive 0.6 M NaCl solution. Since the films formed in an aqueous environment are not equal to the films formed in air, once a specimen is placed in solution the pre-existing film on its surface can be transformed and replaced by a thicker corrosion products layer. However, in the case of the AZ61-P specimen, the presence of $Mg(OH)_2$ as a major component of the corrosion products layer cannot compensate the weakening of the protective action of the pre-existing film. In contrast, on alloy AZ31 the initial oxide film is less protective and its effect disappears relatively soon; instead, the corrosion products layer takes a leading role and to its growth and consolidation is attributable the marked tendency for R_t to increase. In this alloy, XPS analysis has revealed an appreciable content of magnesium carbonate, suggesting a positive effect of these species on the corrosion resistance. These results are in line with the protective role of the carbonate products observed by Wang et al [27] after immersion of AZ31 and AZ91 magnesium alloys in dilute NaCl solution.

5. Conclusions

Using XPS analysis, notable differences have been shown in the chemical composition of the surface corrosion products layer formed on Mg-Al alloys from immersion in the 0.6M NaCl. Attention is drawn to the carbonate enrichment of the surface corrosion layers formed on the AZ31 specimens exposed for 15 days. A carbonate contents about two times higher has been found in surface layers formed on AZ31 compared to the AZ61 alloy.

In the early stages of immersion, the notably higher rate of corrosion for AZ61 specimens in as-received surface condition compared with that of AZ31 alloy, may promote a rise in the interfacial pH, and hence promote the precipitation of magnesium hydroxide type species. Because of the high protective effect of the initial native oxide film formed on the polished surface of the AZ61 alloy, longer immersion periods are

needed to observe similar trends. On the other hand, the lower corrosion rate of the exposed AZ31 alloy motivates a significant decrease in magnesium dissolution and pH, likely contributing to the preferential formation of more protective magnesium compounds containing carbonate.

After several days´ immersion, the charge transfer resistance values obtained from EIS measurements testing show the protective capacity of the corrosion products layer formed depending on alloy type and surface conditions of the specimens. The combined XPS and EIS data validate the protective action of the carbonate enriched layer of corrosion products.

Acknowledgments

We would like to express our gratitude to Professor S. Feliu for numerous clarifying and stimulating discussions during the course of this research. The authors also gratefully acknowledge the financial support for this project from the Spanish Ministry of Economy and Competitiveness (MAT 2009-13530)

References

[1] B.L. Mordike, T. Ebert. Magnesium-Properties-applications-potential. Mater. Sci. Eng., A 302 (2001) 37–45
[2] E. Ghali, W. Dietzel, K.U. Kainer, General and localized corrosion of magnesium alloys: A critical review. J.Mater. Eng. Perform. 13 (2004) 7-23.
[3] G.L Makar and J. Kruger. Corrosion of magnesium. Int. Mater. Rev. 38 (1993) 138-153.
[4] O. Lunder, J. E. Lein, S. M. Hesjevik, T. K. Aune, K. Nisancioglu, Corrosion morphologies on magnesium alloy AZ 91. Werkst. Korros., 45 (1994) 331-340.
[5] P. Schmutz, V. Guillaumin, R. S. Lillard, J. A. Lillard, and G. S. Frankel, Influence of dichromate ions on corrosion processes on pure magnesium. J. Electrochem. Soc. 150 (2003) B99-B110.
[6] M. Taheri, R.C. Phillips, J.R. Kish, G.A. Botton, Analysis of the surface film formed on Mg by exposure to water using a FIB cross-section and STEM-EDS. Corros. Sci. 59 (2012) 222-228.
[7] G. Williams, H.N. McMurray, Localized corrosion of magnesium in chloride-containing electrolyte studied by a scanning vibrating electrode technique. J. Electrochem. Soc. 155 (2008) C340-C349.
[8] A. Samaniego, I. Llorente, S. Feliu Jr, Combined effect of composition and surface condition on corrosion behaviour of magnesium alloys AZ31 and AZ61. Corros. Sci. 68 (2013) 66–71.
[9] S. Feliu Jr, C. Maffiotte , A. Samaniego, J. C. Galván, V. Barranco. Effect of the chemistry and structure of the native oxide surface film on the corrosion properties of commercial AZ31 and AZ61 alloys, Appl. Surf. Sci. 257 (2011) 8558–8568.
[10] J.R. Kish, Y.Hu, J. Li, W. Zheng, J.R. McDermid. Examination of Focused Ion Beam-Sectioned Surface Films Formed on AM60B Mg Alloy in an Aqueous Saline Solution. Corrosion 68 (2012) 468-474.
[11] J.A. Boyer. The corrosion of magnesium and of the magnesium aluminum alloys containing manganese. Report 248.
[12] E. Ghali, W. Dietzel, K.U. Kainer, Testing of general and localized corrosion of magnesium alloys: A critical review. J. Mater. Eng. Perform. 13 (2004) 517-529.

[13] A. Pardo, M.C. Merino, A.E. Coy, R. Arrabal, F. Viejo, E. Matykina, Corrosion behaviour of magnesium/aluminium alloys in 3.5 wt% NaCl, Corros. Sci. 50 (2008) 823-834.
[14] G. Baril, N. Pebere, The corrosion of pure magnesium in aerated and deaerated sodium sulphate solutions, Corros. Sci. 43 (2001) 471-484.
[15] A. Pardo, M.C. Merino, A.E. Coy, F. Viejo, R. Arrabal, S. Feliu Jr., Influence of microstructure and composition on the corrosion behaviour of Mg/Al alloys in chloride media, Electrochim. Acta 53 (2008) 7890-7902.
[16] M. Santamaria, F.Di Quarto, S. Zanna, P. Marcus, Initial surface film on magnesium metal: A characterization by X-ray photoelectron spectroscopy (XPS) and photocurrent spectroscopy (PCS), Electrochim. Acta 53 (2007) 1314-1324.
[17] N. Pebere, C. Riera, F. Dabosi, Investigation of magnesium corrosion in aerated sodium-sulfate solution by electrochemical impedance spectroscopy, Electrochim. Acta 35 (1990) 555-561.
[18] G. Baril, G. Galicia, C. Deslouis, N. Pebere, B. Tribollet, V. Vivier, An impedance investigation of the mechanism of pure magnesium corrosion in sodium sulfate solutions, J. Electrochem. Soc. 154 (2007) C108-C113.
[19] S. Feliu Jr., M.C. Merino, R. Arrabal, A.E. Coy, E. Matykina, XPS study of the effect of aluminum on the atmospheric corrosion of AZ31 magnesium alloy, Surf.Interface Anal. 41 (2009) 143–150.
[20] S. Feliu Jr., A. Pardo, M.C. Merino, A.E. Coy, F. Viejo, R. Arrabal, Correlation between the surface chemistry and the atmospheric corrosion of AZ31, AZ80 and AZ91D magnesium alloys, Appl. Surf. Sci. 255 (2009) 4102–4108.
[21] K. Asami, S. Ono, Quantitative X-ray photoelectron spectroscopy characterization of magnesium oxidized in air, J. Electrochem. Soc. 147 (2000) 1408–1413.
[22] J. H. Nordlien, S. Ono, N. Masuko, K. Nisancioglu, A TEM investigation of naturally formed oxide films on pure magnesium, Corros. Sci. 39 (1997) 1397–1414.
[23] R. Lindström, L.G. Johansson, G.E. Thompson, P. Skeldon, J.E. Svensson, Corrosion of magnesium in humid air, Corros. Sci. 46 (2004) 1141–1158.
[24] S. Feliu Jr., C. Maffiotte, A. Samaniego, J.C. Galván, V. Barranco, Effect of naturally formed oxide films and other variables in the early stages of Mg-alloy corrosion in NaCl solution, Electrochim. Acta 56 (2011) 4554-4565.
[25] L. Wang, T. Shinohara, B.P. Zhang, Influence of chloride, sulfate and bicarbonate anions on the corrosion behavior of AZ31 magnesium alloy , J. Alloys Compd. 496 (2010) 500-507.
[26] S. Feliu Jr, C. Maffiotte, J.C. Galvan, V. Barranco, Atmospheric corrosion of magnesium alloys AZ31 and AZ61 under continuous condensation conditions, Corros. Sci. 53 (2011) 1865-1872.
[27] L. Wang, T. Shinohara, B.P. Zhang, XPS study of the surface chemistry on AZ31 and AZ91 magnesium alloys in dilute NaCl solution, Appl. Surf. Sci. 256 (2010) 5807-5812.
[28] W. Liu, F. Cao, A. Chen, L. Chang, J. Zhang and C. Cao, Effect of chloride ion concentration on electrochemical behavior and corrosion product of AM60 Magnesium alloy in aqueous solutions, Corrosion 68 (2012) Article Number: 045001.
[29] L. Wang, T. Shinohara, B.P. Zhang, H. Iwai, Characterization of surface products on AZ31 magnesium alloy in dilute NaCl solution J. Alloys Compd. 485 (2009) 747-752.
[30] R. Lindström, J.E. Svensson, L.G. Johansson. The influence of carbon dioxide on the atmospheric corrosion of some magnesium alloys in the presence of NaCl. J. Electrochem. Soc. 149 (4) (2002) B103–B107.
[31] Z.M. Shi, M. Liu, A. Atrens, Measurement of the corrosion rate of magnesium alloys using Tafel extrapolation, Corros. Sci. 52 (2010) 579-588.
[32] G.L. Song, A. Atrens, Corrosion mechanisms of magnesium alloys, Adv. Eng. Mater. 1 (1999) 11-33.
[33] J.H. Nordlien, K. Nisancioglu, S. Ono, N. Masuko, Morphology and structure of oxide films formed on MgAl alloys by exposure to air and water, J. Electrochem. Soc. 143 (1996) 2564-2572.
[34] M. Jönsson, D. Persson, R. Gubner, The initial steps of atmospheric corrosion on magnesium alloy AZ91D, J. Electrochem. Soc. 154 (2007) C684-C691.
[35] N. Hara, Y. Kobayashi, D. Kagaya, N. Akao, Formation and breakdown of surface films on magnesium and its alloys in aqueous solutions, Corros. Sci. 49 (2007) 166-175.
[36] ASM Handbook Committee, Alloy Phase Diagrams ASM International, Ohio, USA, 1992.
[37] C.D. Wagner, L.E. Davis, M. V. Zeller, J.A. Taylor, R.H. Raymond, L.H. Gale, Empirical atomic sensitivity factor for quantitative analysis by electron spectroscopy for chemical analysis, Surf. Interface Anal. 3 (1981) 211-225.

[38] S. Feliu Jr., J.C. Galván, A. Pardo, M.C. Merino, R. Arrabal, Native Air-Formed Oxide Film and its Effect on Magnesium Alloys Corrosion, Open Corrosion Journal, 3 (2010) 80-91.
[39] H.B. Yao, Y.Li, A.T.S. Wee, An XPS investigation of the oxidation/corrosion of melt-spun Mg, Appl. Surf. Sci. 158 (2000) 112-119.
[40] N.T. Kirkland, N. Birbilis, M.P. Staiger, Assessing the corrosion of biodegradable magnesium implants: a critical review of current methodologies and their limitations, Acta Biomater. 8 (2012) 925-936.
[41] G.L. Makar, J. Kruger, Corrosion studies of rapidly solidified magnesium alloys, J. Electrochem. Soc. 137 (1990) 414-421.
[42] S. Mathieu, C. Rapin, J. Hazan, P. Steinmetz, Corrosion behaviour of high pressure die-cast and semi-solid cast AZ91D alloys, Corros. Sci. 44 (2002) 2737-2756.
[43] M. Stern, A. L. Geary, Electrochemical polarization .1. A theoretical analysis of the shape of polarization curves J. Electrochem. Soc. 104 (1957) 56-63.
[44] C. Henrist, J.P. Mathieu, C. Vogels, A. Rulmont, R. Cloots, Morphological study of magnesium hydroxide nanoparticles precipitated in dilute aqueous solution, J. Cryst. Growth 249 (2003) 321–330.
[45] Y.Y. Gao, H.H. Wang, Y.L. Su, Q. Shen, D.J. Wang, Influence of magnesium source on the crystallization behaviors of magnesium hydroxide, J. Cryst. Growth 310 (2008) 3771–3778.
[46] S.S. Pathak, M.D. Blanton, S. K. Mendon, J.W. Rawlins. Investigation on dual corrosion performance of magnesium-rich primer for aluminum alloys under salt spray test (ASTM B117) and natural exposure Corros. Sci. 52 (2010) 1453-1463.
[47] C. A. Walton, H.J. Martin, M.F. Horstemeyer, P. T. Wang, Quantification of corrosion mechanisms under immersion and salt- spray environments on an extruded AZ31 magnesium alloys, Corros. Sci. 56 (2012) 194-208.
[48] N.C. Hosking, M.A. Ström, P.H. Shipway, C.D. Rudd, Corrosion resistance of zinc-magnesium coated steel, Corros. Sci. 49 (2007) 3669-3695.
[49] M. Liu, P. Schmutz, S. Zanna, A. Seyeux, H. Ardelean, G.L. Song, A. Atrens, P. Marcus, Electrochemical reactivity, surface composition and corrosion mechanisms of the complex metallic alloy Al_3Mg_2, Corros. Sci. 52 (2010) 562-578.
[50] M. Liu, S. Zanna, H. Ardelean, I. Frateur, P. Schmutz, G.L. Song, A. Atrens, P. Marcus, A first quantitative XPS study of the surface films formed, by exposure to water, on Mg and on the Mg-Al intermetallics: Al3Mg2 and Mg17Al12, Corros. Sci. 51 (2009) 1115-1127.
[51] J.Y. Uan, B.L. Yu, X.L. Pan, Morphological and microstructural characterization of the aragonitic $CaCO_3$/Mg,Al- Hydrotalcite coating on Mg-9 Wt Pct Al-1 Wt Pct Zn alloy to protect against corrosion, Metall. Mater. Trans. A 39 (2008) 3233-3245.
[52] X.B. Chen, N. Birbilis, T.B. Abbot, A review of corrosion resistant conversion coatings for magnesium and its alloys, Corrosion 67 (2011) Article Number: 03005.
[53] X.B. Chen, N. Birbilis, T.B. Abbott, A simple route towards a hydroxyapatite-$Mg(OH)_2$ conversion coating for magnesium, Corros. Sci. 53 (2011) 2263-2268.
[54] <http://www.kemi.kth.se//medusa>
[55] T. Tanski, K. Labisz, L.A. Dobrzanski, Effect of Al additions and heat treatment on corrosion properties of Mg-Al based alloys, Journal of Achievements in Materials and Manufacturing Engineering, 44/1 (2011) 64-72.

Discusión Capítulo II

Caracterización de la película de óxidos superficiales y la capa de productos de corrosión de las aleaciones AZ31 y AZ61

Estos estudios se centraron fundamentalmente en aleaciones del sistema Mg-Al-Zn; más concretamente en las aleaciones AZ31 y AZ61. En primer lugar se realizó un extenso estudio sobre la influencia de los óxidos superficiales en la reacción de corrosión de las dos aleaciones, en dos condiciones superficiales diferentes (pulido y estado de recepción). Se escogieron estas aleaciones por su contenido de aluminio. En la aleación AZ31, con un 3% de aluminio, se predijo una mínima presencia de fase β, la cual fue confirmada mediante microscopía electrónica de barrido, pudiéndose considerar la existencia de esta segunda fase, prácticamente inexistente. En contraposición, la aleación AZ61, presentó una cantidad significativa de fase β, aunque esta se encuentra dispersa en los límites de grano de la aleación sin formar una red continua, a diferencia de lo que ocurre en otras aleaciones con un contenido superior de aluminio, como la aleación AZ91. También se ha reportado que concentraciones superiores al 4% de Al en las aleaciones de Mg aumentan significativamente la resistencia a la corrosión de la aleación [70, 76]. Mediante la elección de estas aleaciones se pudo estudiar este efecto en profundidad, ya que el contenido de aluminio en estas aleaciones se encuentra a ambos lados de este límite.

- **Morfología de corrosión:** en ambas aleaciones, inicialmente se observó corrosión filiforme y, al aumentar el grado de ataque, se detectaron grandes áreas de corrosión generalizada.

- **Caracterización de la película de óxidos superficiales e influencia sobre la corrosión:** mediante espectroscopia fotoelectrónica de rayos X (XPS) se observaron diferencias importantes en las películas superficiales formadas espontáneamente sobre las superficies pulidas y en estado de recepción de ambas aleaciones. Las superficies en estado de recepción presentaron una cantidad de heterogeneidades y defectos muy superior a las pulidas. Destacó la presencia de espinelas en la superficie de las aleaciones en estado de recepción cuya presencia no fue observada en las aleaciones en

estado pulido. La cantidad de espinelas fue significativamente superior en el caso de la aleación AZ61 que en el de la AZ31.

En condiciones de pulido, al comparar la influencia del tipo de aleación sobre las películas superficiales formadas espontáneamente en contacto con la atmósfera, se detectó un mayor espesor y homogeneidad en la fina capa de los óxidos superficiales formados sobre la aleación AZ61 que sobre la aleación AZ31. Este mayor espesor y homogeneidad fue asociado a un aumento importante en la resistencia a la corrosión, muy superior al observado en la aleación AZ31. Esta influencia fue estudiada tanto por espectroscopia de impedancia electroquímica (EIS), como por medidas de pérdida de peso o desprendimiento de hidrógeno. El efecto fue monitorizado con el tiempo, revelando una influencia importante durante los primeros días de exposición. Se pudo concluir que transcurrida aproximadamente una semana de exposición en NaCl 0,6 M, el efecto beneficioso de los óxidos desapareció y los valores de resistencia a la transferencia de carga alcanzaron valores muy similares a los obtenidos para otros estados superficiales. La desaparición de esta protección con el tiempo, se asoció a la destrucción de estas películas protectoras por acción de los aniones cloruro presentes en el medio.

- **Caracterización e influencia de los productos de corrosión sobre la velocidad de corrosión:** se caracterizaron los productos de corrosión formados sobre estas aleaciones durante inmersión en soluciones de cloruro sódico y su influencia sobre la corrosión. Notables diferencias fueron observadas entre las dos aleaciones estudiadas. Los productos de corrosión formados sobre la aleación AZ31 presentaron un enriquecimiento significativo en la concentración de carbonatos presentes en comparación con los observados sobre la aleación AZ61 (aproximadamente el doble). La tendencia de la velocidad de corrosión de las aleaciones con el tiempo fue analizada tanto por EIS como por medidas de desprendimiento de hidrógeno. La aleación AZ31, en ambas condiciones superficiales, presentó una tendencia a disminuir la velocidad de corrosión al aumentar el tiempo de inmersión, mientras que la AZ61 en estado de recepción, mostró una velocidad de corrosión prácticamente constante con el tiempo. Este diferente comportamiento fue asociado a la diferente concentración de carbonatos presentes en la capa de productos de corrosión formados en la superficie de las aleaciones.

Debido a la mayor protección ofrecida por las películas de óxidos presentes sobre la aleación AZ61 en estado pulido, inicialmente la velocidad de corrosión presentó un valor reducido. Sin embargo, al transcurrir alrededor de 4 días, aumentó de forma drástica, manteniéndose constante con el tiempo. Este cambio de tendencia se asoció a la ruptura de la capa de óxidos protectores durante la exposición a un medio tan agresivo como el NaCl 0,6 M.

La diferente composición de los productos de corrosión se asoció a la presencia de fase β en la aleación AZ61 y su influencia en el pH. En esta aleación, el pH interfacial con la segunda fase, es mayor durante la corrosión, lo que puede promover la precipitación de especies del tipo hidróxido de magnesio. Sin embargo, al no existir segunda fase en la aleación AZ31, no existe este incremento localizado de pH, lo que permitiría la formación preferente de precipitados con altos contenidos de carbonato, de mayor carácter protector.

Capítulo III

Estrategias para mejorar la resistencia a la corrosión del magnesio y aleaciones del sistema Mg-Al-Zn.

Introducción

Existen múltiples estrategias para intentar proteger las aleaciones de magnesio de la corrosión. De una manera general estos métodos se pueden clasificar en tres grandes grupos [25, 71, 107]:

- **Producción de aleaciones de alta pureza y generación de nuevas aleaciones:** desde la década de 1940 se sabe que existe un límite de tolerancia a las impurezas [35]; gracias a las técnicas de procesado y purificación se obtienen aleaciones por debajo de estos límites. Por otro lado, también se generan nuevas aleaciones con mejor comportamiento a la corrosión [24].

- **Modificación de la micro-estructura a través del procesado:** por ejemplo, la solidificación por enfriamiento rápido ayuda a disminuir el efecto negativo de la impurezas y homogeniza la aleación, evitando la formación de fases secundarias [34, 108].

- **Generación de capas superficiales protectoras y recubrimientos:** En este grupo entrarían multitud de técnicas que buscan obtener capas superficiales que ejerzan un efecto barrera y protejan la aleación. Estarían incluidos técnicas como el anodizado, electroplating, electroless, tratamientos de conversión superficial, revestimientos de hidruro, recubrimientos orgánicos, depósitos en fase vapor, recubrimientos por proyección térmica, láser, pinturas o modificación/generación de películas pasivas, entre otros.

Pese a la gran cantidad de posibilidades, hoy en día, las estrategias más utilizadas en la lucha contra la corrosión son los recubrimientos por conversión [23, 109], los recubrimientos electroquímicos (plating y electroless [110, 111]) y, en menor medida, estudios que involucran la generación de nuevas aleaciones [24].

La mayor parte de los estudios realizados en esta tesis con el fin de disminuir la velocidad de corrosión, se caracterizan por su sencillez, bajo coste y cortos tiempos de duración, aunque también se realizaron estudios adicionando elementos aleantes

alternativos sobre magnesio puro y la aleación AZ31, donde se obtuvieron buenos resultados.

Resultados Capítulo III

Los resultados obtenidos durante la elaboración de esta tesis doctoral, relacionados con este tema, se muestran en esta sección en forma de publicaciones. Los artículos publicados fueron los siguientes:

A study on the relationships between corrosion properties and chemistry of thermally oxidised surface films formed on polished commercial magnesium alloys AZ31 and AZ61. S. Feliu Jr., A. Samaniego, V. Barranco, A.A. El-Hadad, I. Llorente, C. Serra, J.C. Galván. Applied Surface Science, 295 (2014) 219-230.
http://dx.doi.org/10.1016/j.apsusc.2014.01.033

The effect of low temperature heat treatment on surface chemistry and corrosion resistance of commercial magnesium alloys AZ31 and AZ61 in 0.6 M NaCl solution. S. Feliu Jr., A. Samaniego, V. Barranco, A.A. El-Hadad, I.Llorente, P. Adeva. Corrosion Science, 80 (2014) 461-472.
http://dx.doi.org/10.1016/j.corsci.2013.11.065

The effect of $NaHCO_3$ treatment time on the corrosion resistance of commercial magnesiumalloys AZ31 and AZ61 in 0.6 M NaCl solution. S. Feliu Jr., A. Samaniego, A.A. El-Hadad, I. Llorente. Corrosion Science, 67 (2013) 204-216
http://dx.doi.org/10.1016/j.corsci.2012.10.020

Poisoning the corrosion of magnesium. N. Birbilis, G. Williams, K. Gusieva, A. Samaniego, M.A. Gibson, H.N. McMurray. Electrochemistry Communications, 34 (2013) 295-298.
http://dx.doi.org/10.1016/j.elecom.2013.07.021

En revisión en Corrosion Science:

Exploring the possibility of protective surface oxides upon Mg alloy AZ31 via lutetium additions. A. Samaniego, K. Gusieva, I. Llorente, S. Feliu Jr. and N. Birbilis

A study on the Relationships Between Corrosion Properties and Chemistry of Thermally Oxidised Surface Films Formed on Polished Commercial Magnesium Alloys AZ31 and AZ61

Sebastián Feliu (Jr)[a], Alejandro Samaniego[a], Violeta Barranco[b], A.A. El-Hadad[c], Irene Llorente[a] , Carmen Serra[d] and J.C. Galván[a]

[a]Centro Nacional de Investigaciones Metalúrgicas CSIC, Avda. Gregorio del Amo 8, 28040 Madrid, Spain.
[b]Instituto de Ciencias de Materiales de Madrid, ICMM, Consejo Superior de Investigaciones Científicas, CSIC, Sor Juana Inés de la Cruz, 3, Cantoblanco, 28049, Madrid, Spain.
[c]Physics Department, Faculty of Science, Al-Azhar University,Nasr City 11884, Cairo, Egypt.
[d]Servicio de Nanotecnologia y Análisis de Superficies, CACTI, Universidade de Vigo, 36310 Vigo, Spain

Applied Surface Science, 295 (2014) 219-230.

Abstract

This paper studies the changes in chemical composition of the thin oxide surface films induced by heating in air at 200ºC for time intervals from 5 minutes up to 60 minutes on the freshly polished commercial AZ31 and AZ61 alloys with a view to better understanding their protective properties. This thermal treatment resulted in the formation of layers enriched in metallic aluminium at the interface between the outer MgO surface films and the bulk material. A strong link was found between the degree of metallic Al enrichment in the subsurface layer (from 10 to 15 at %) observed by XPS (X-ray photoelectron spectroscopy) in the AZ61 treated samples and the increase in protective properties observed by EIS (Electrochemical Impedance Spectroscopy) in the immersion test in 0.6M NaCl. Heating for 5 to 60 minutes in air at 200ºC seems to be an effective, easy to perform and inexpensive method for increasing the corrosion resistance of the AZ61 alloy by approximately two or three times.

Keywords: Magnesium alloys, Thermal treatments; Surface segregation; corrosion; X-ray photoelectron spectroscopy (XPS),

1. Introduction

Chosen materials for this study are Mg-Al alloys, which have aroused great scientific and technological interest over the last two decades. From a practical point of view magnesium is the structural metal of lowest density, which makes it highly attractive for use in the automotive, aerospace, IT, and electronics industries where weight plays a decisive role. However, as magnesium is one of the most chemically active metals, insufficient resistance to atmospheric and aqueous corrosion sometimes limits its applications. Thus it is desirable to have as complete as possible information on the factors that influence the corrosion of these magnesium base materials. This work seeks to contribute to such information.

Many researchers have carried out studies to find relationships between changes in the alloy microstructure (amount and distribution of β-phase precipitates) with long term heat treatments (T4 (solution treatment) or T6 (aging treatment)) [1-10] and changes in corrosion resistance. In the literature a great deal of attention has been paid to the role of the β-phase in the corrosion mechanism of magnesium/aluminium alloys. A generally accepted idea is that this phase acts as an effective cathode and/or barrier against corrosion, depending on its size and distribution [1].

In our previous studies [11-14], we have observed that the properties of the thin oxide/hydroxide native oxide surface film (only a few nanometres thick) may affect the corrosion properties of magnesium alloys in the atmosphere [11, 12] or in NaCl solution [13,14]. XPS analysis has revealed notable differences in the native oxide films formed in air on the surface of AZ31 and AZ61 alloys in as-received and freshly polished conditions. In the joint analysis of XPS and EIS data, attention has been drawn to the increase in the corrosion resistance value on the AZ61 alloy in freshly polished conditions, which showed a higher thickness and greater uniformity of the native oxide film. Following up the idea that the thin native oxide film may provide resistance to magnesium corrosion initiation and its propagation [1,13,14], in the present research studies have been carried out into the possibility of improving its corrosion resistance by short heat treatments at 200ºC. As Jeurgens et al. noted [15], the thermal oxidation of metallic alloys at low temperatures (e.g. at $T < 600$ K) and for short times has only scarcely been investigated. The detailed chemical composition and constitution of the oxide films formed on such alloy surfaces at low temperatures for short heating times are unknown. Furthermore, there is no comprehensive knowledge of the effect of the concurrent processes of chemical segregation and preferential oxidation on both the

developing oxide-film microstructure and the induced compositional changes in the alloy subsurface.

Czerwinski [16] studied the oxidation behaviour of AZ91D Mg alloy at different temperatures. His results showed that AZ91D exhibited protective oxidation only at a temperature of 197ºC, while at higher temperatures the behaviour was non-protective and associated with the formation of oxide nodules and their coalescence into a loose fine-grained structure. On the basis of these results, this study has selected a low-temperature heat treatment process at 200ºC to study the possibility of improving the protective properties of the native oxide film formed on AZ31 and AZ61 Mg alloy surfaces.

One of the main obstacles to characterise the thermally oxidised film formed on the surface of magnesium alloys after heating at low temperatures (200ºC) is its small thickness. As Czerwinski [16] reported, the maximum oxide thickness achieved during heating (as converted from weight gain data) was equal to 64 nanometres for 197ºC. This film thickness is too small to produce a sufficient signal for conventional materials characterisation techniques (Optical microscopy, SEM/EDX, XRD or TEM) [13]. The use of the XPS surface analysis technique makes it possible to reduce the analysed thickness to only 3 nm and supplies information on the oxidation state of the detected element.

The objectives of this research are as follows:

1. To study the chemical changes in the native oxide surface film of AZ31 and AZ61 alloys induced by short heat treatments at 200ºC in order to try to find relationships between the chemistry of the thin oxide films, the nature of the alloy and the heating time.

2. To contribute to better understanding the effect of the chemistry and structure of the thin films (approximate thickness of 1-3 nanometers) formed on the surface of commercial Mg-Al alloys and their corrosion resistance in saline solutions.

2. Experimental

The chemical compositions of the tested magnesium alloys, AZ31 and AZ61, are listed in Table 1. They were manufactured in wrought condition and supplied in 3 mm thick plates by Magnesium Elecktron Ltd. Freshly polished specimens were dry ground through successive grades of silicon carbide abrasive papers from P600 to P2000 followed by finishing with 3 and 1 μm diamond paste, rinsed in water and dried with hot air. Due to the high affinity of magnesium to the ambient atmosphere, it was attempted to keep to a minimum (around 1 h) the exposure time to the atmosphere prior to characterisation of the specimens.

Table 1. *Chemical composition of Mg-Al alloys (wt%)*

Alloy	Al	Zn	Mn	Si	Cu	Fe	Ni	Ca	Zr	Others
AZ31	3.1	0.73	0.25	0.02	<0.001	0.005	<0.001	0.0014	<0.001	<0.30
AZ61	6.2	0.74	0.23	0.04	<0.001	0.004	<0.001	0.0013	<0.001	<0.30

The two alloys were oxidised in the same conditions in a thermogravimetric analyser (TGA) (TA instruments Q600 SDT) using cylindrical specimens of 4 mm in diameter by 2 mm in height (weighing approximately 44 mg). The apparatus was capable of accommodating a specimen with a maximum weight of 0.5 g and had a measurement accuracy of 0.1 μg. The reaction temperature was monitored by a Pt/Pt–Rh thermocouple. Weight change kinetics were measured in air under isothermal conditions at a temperature of 200ºC. The heating rate before reaching the isothermal condition was 50ºC/min.

The simple thermal treatment consisted of horizontal exposure of 2 cm x 2 cm square specimens of AZ31 and AZ61 alloys in a convective stove at 200°C in air for 5, 20, and 60 minutes.

XPS analysis of the samples was performed using a Thermo Scientific K-Alpha ESCA instrument equipped with aluminium $K_{\alpha 1,2}$ monochromatized radiation at 1486.6 eV X-ray source. The system is fitted with a charge compensation dual-beam source to minimize surface charging. Photoelectrons were collected from a take-off angle of 90° relative to the sample surface. The measurement was performed in a constant analyser energy mode with a 100 eV pass energy for survey spectra and 20 eV pass energy for high-resolution spectra. Composition–depth profiling was performed by sequential XPS

surface analysis and sputter etching using 3 keV argon ion flux. Our previous results [13] on AZ31 and AZ61 alloys in polished condition, where we observed a sputtering rate of 5 Å/min, leads us to believe that this is approximately the rate which is obtained on specimens with the bombardment conditions and spectrometer used in this study. Survey scans and detailed scans of Mg 2p, Al 2s, C 1s and O 1s photoelectron emissions were recorded for each sample. The intensities were estimated by calculating the area under each peak after smoothing and subtraction of the S-shaped background and fitting the experimental curve to a combination of Lorentzian and Gaussian lines of variable proportions. Binding energies (BEs) were referenced to the adventitious C1s peak at 285.0 eV. The atomic ratios were computed from the peak intensity ratios and the reported atomic sensitivity factors [17]. The sampled areas were 1 x 1 mm^2.

Electrochemical impedance measurements were conducted with the specimens immersed in 0.6 M NaCl after 1 hour, 1 day, 7, 14, 21 and 28 days of exposure at room temperature (25ºC). An AUTOLAB potentiostat, model PGSTAT30, with frequency response analyser software was used. The frequency ranged from 100 kHz to 1 mHz with 5 points/decade, whereas the amplitude of the sinusoidal potential signal was 10 mV with respect to the open circuit potential. A typical three-electrode setup was employed: Ag/AgCl and graphite were used as reference and counter electrodes, respectively, and the material under study (metal sheet) was the working electrode.

For the hydrogen evolution determinations, the corrosion of magnesium alloys during solution immersion was estimated by determining the volume of hydrogen evolved during the corrosion process. Samples for hydrogen collection were cut into square coupons with dimensions of 2 × 2 x 0.3 cm and vertically immersed in 700 ml of quiescent 0.6M NaCl for 14 days in a beaker open to laboratory air at 25 ± 2 °C. The entire specimen surface was exposed to the electrolyte. Evolved hydrogen was collected in a burette above an inverted funnel placed centrally above specimen. All these experiments were run simultaneously and each sample was subjected to essentially the same temperature and exposure history. The experimental difficulties and limitations of such test was recently documented [18]. For the gravimetric determination of corrosion, the specimens were weighed before exposure and then after testing were pickled in chromic acid to remove the corrosion products, rinsed with isopropyl alcohol, dried in hot air and reweighed in order to calculate the mass loss per unit of surface area.

3. Results

3.1. Thermogravimetric analysis

Figure 1 compares the weight change kinetics curves obtained for alloys AZ31 and AZ61 after heating at 200ºC in an air environment. It is interesting to note that the mass change values are similar in the case of the two alloys (Fig. 1) and that some mass loss is observed during the first 35 minutes of exposure, followed by an approximately steady state region and then a slight increase in weight. Liu et al [19], studying the oxidation of pure Mg and Mg-Gd-Y-Zr alloys at 300ºC, attributed the mass loss at the start of the mass change measurements as due to the dehydration and disintegration of the external $Mg(OH)_2$ layer formed during mechanical polishing.

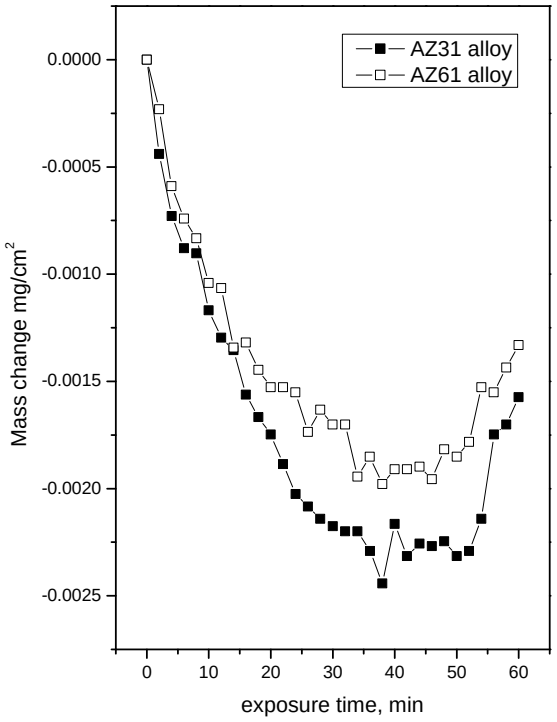

Figure 1. *Evolution of mass change values obtained in the polished AZ31 and AZ61 alloys as a function of the time of heating at 200ºC in an air environment.*

3.2. Microstructural characterization

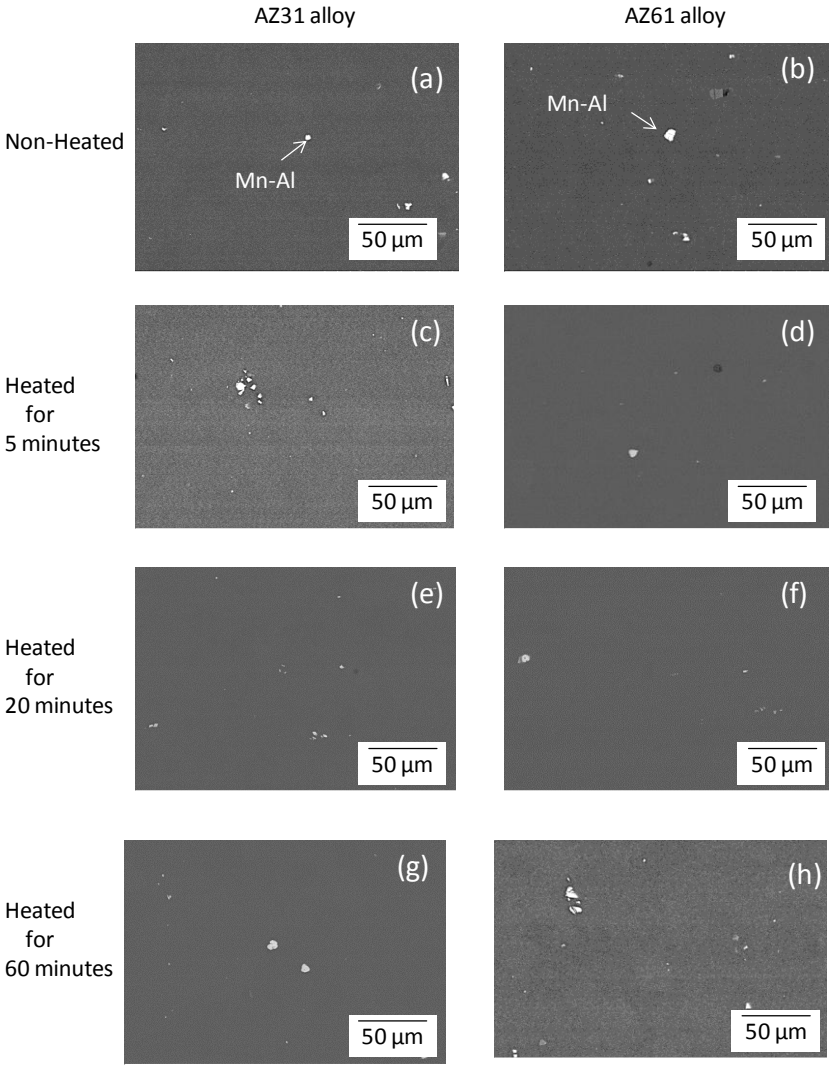

Figure 2. *SEM micrographs (BSE mode) morphologies for AZ31 (a, c, e, g) and AZ61 magnesium alloys (b, d, f, h) non-heated (a, b), heated for 5 min (c, d), heated for 20 min (e, f) and heated for 60 min (g, h), respectively*

Figure 2 compares the size and amount of the precipitates on the surface of the non-heated and heated for different times AZ31 and AZ61 specimens. A small amount of precipitates is observed for the non-heated AZ31 alloy (Fig. 2a) and AZ61 alloy (Fig. 2b). The backscattered electrons produce a sharp contrast between the bright particles and the magnesium-rich matrix. By comparing Fig. 2a with Figs. 2c, 2e and 2g for AZ31 alloy and Fig. 2b with Figs. 2d, 2f and 2h in the case of the AZ61 alloy, it is apparent that the size and amount of the precipitates on the surface do not change significantly with the treatment time.

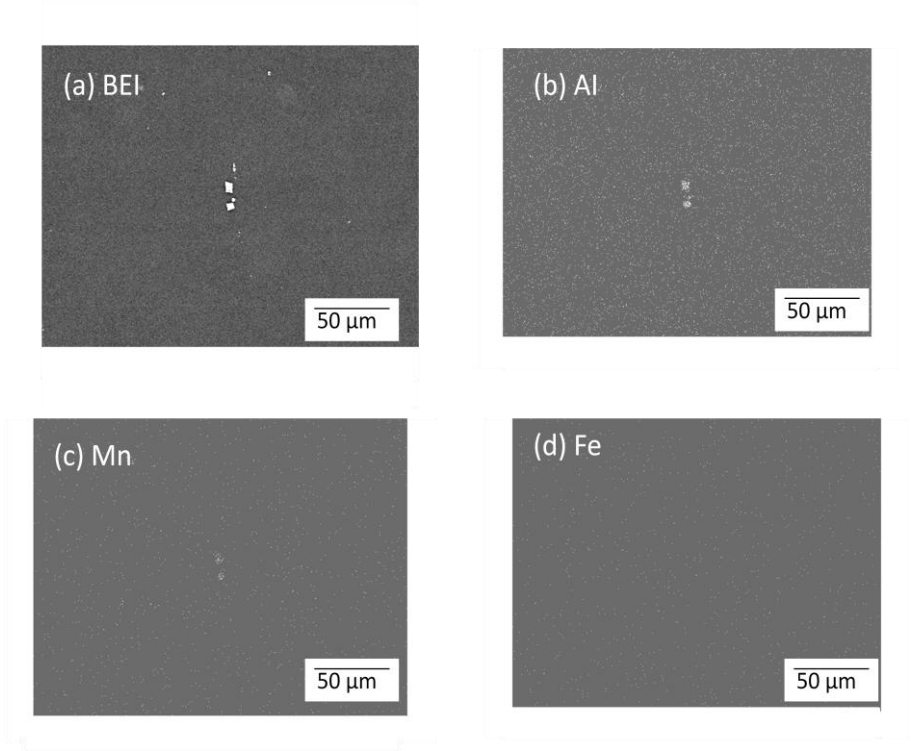

Figure 3. *Morphology (a) and elemental maps of Al (b), Mn (c) and Fe (d) for the non-heated AZ31 alloy surface.*

Fig. 3 shows elemental mapping results of the non-heated AZ31 alloy surface. Fig. 3a-3d respectively shows the surface morphology (backscattering electron imaging: BEI) and elemental maps of Al, Mn and Fe. The elemental mapping results indicate that the bright particles contain Al and Mn (Figs. 3b and 3c). In contrast, it is interesting to note that no iron is detected on the particles or on the matrix (Fig. 3d).

Figure 4 compares the surface microstructures for the non-heated and heated for different times AZ31 and AZ61 specimens. The microstructure of the AZ31 alloy is formed practically by an α-matrix with Al in solid solution (Fig. 4a), while a large part of the Al in the microstructure of the AZ61 alloy is precipitated in the form of β-phase (Fig. 4b). As commented earlier for the Al-Mn precipitates, no significant differences in the grain morphology and size are observed in both alloys after different periods of heat treatment (Figs 4c, 4e and 4g for AZ31 alloy and 4d, 4f and 4h for AZ61 alloy) compared with the non-heated alloy (Figures 4a and 4b).

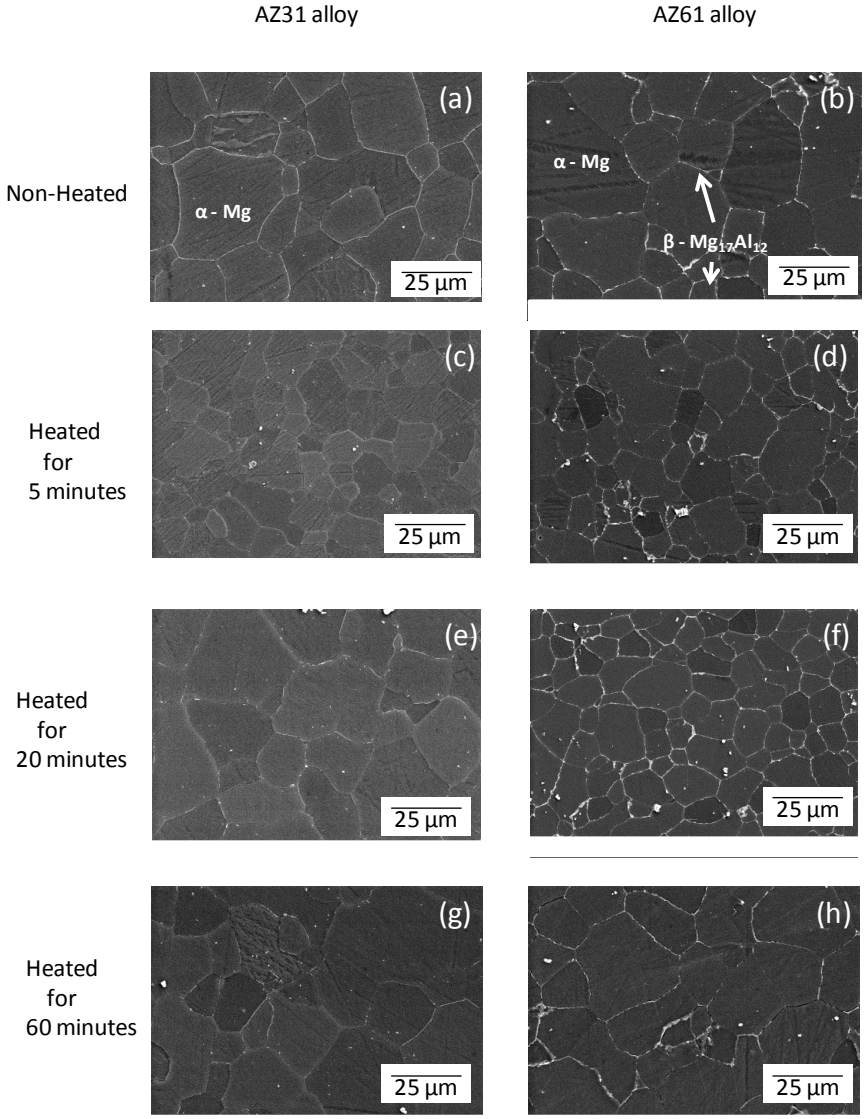

Figure 4. *Microstructure. for AZ31 (a, c, e, g) and AZ61 magnesium alloys (b, d, f, h) non-heated (a, b), heated for 5 min (c, d), heated for 20 min (e, f) and heated for 60 min (g, h), respectively.*

3.3. Changes in the chemistry of the surface films formed on AZ31 and AZ61 alloys with the heating treatment

Figure 5 shows the high resolution spectra for C1s peak obtained on the non-sputtered surfaces of the AZ31 alloy: non-heated (a) and heated for 60 minutes (b) and of the AZ61 alloy: non-heated (c) and heated for 60 minutes (d), with those corresponding to the same surfaces after 2 minutes of sputtering (e-h), 5 minutes of sputtering (i-l) and 10 minutes of sputtering (m-p). The XPS spectra obtained for other heat treatment times are fairly similar and are not shown. Throughout the work, in order to avoid repeating

similar results, only those necessary to support the corresponding facts are displayed. The spectra can be fitted using two components at different binding energies: at 285.0

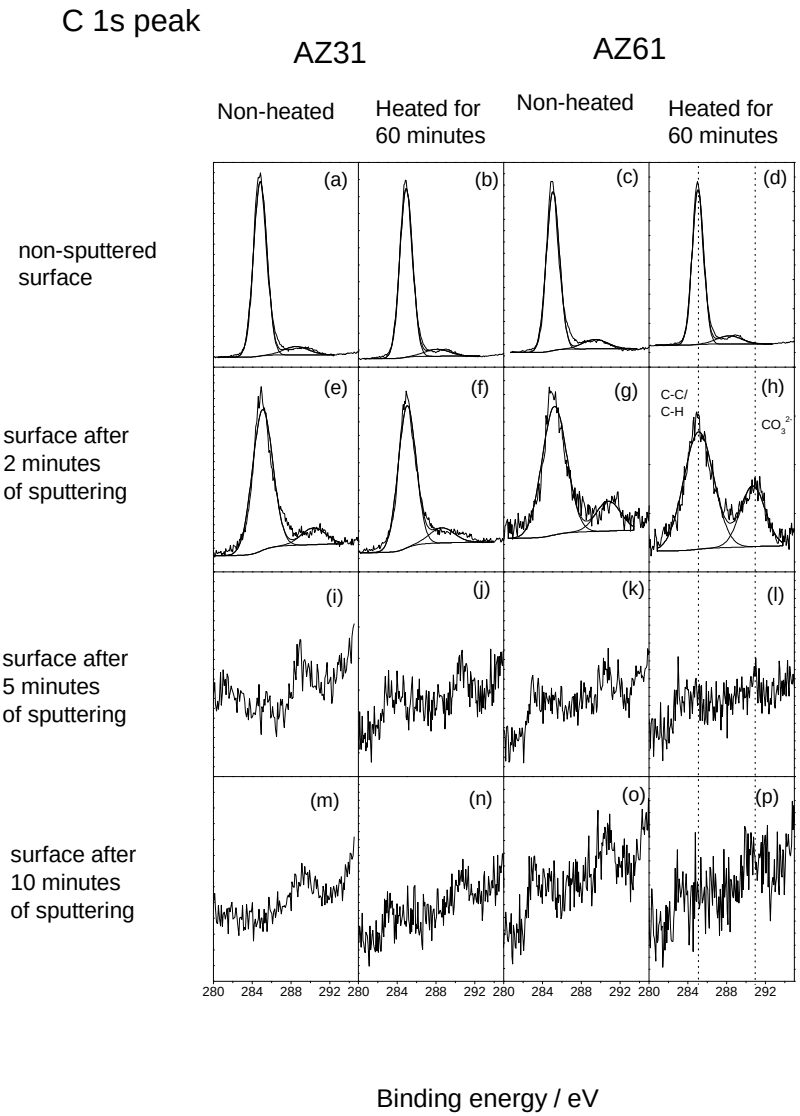

Figure 5. *Variation of the C1s high resolution peak obtained by XPS on the surface of the AZ31 and AZ61 alloys non-heated and heated for 60 minutes as a function of the time of sputtering.*

eV, which may be associated with the presence of C–C/C–H groups; and a less intense component about 4.5–5.0 eV higher which is associated with the presence of magnesium carbonate [20]. The first component, C–C/C–H groups, appears on the outer surface (<3 nm in thickness) of almost any metal in contact with the atmosphere at room temperature, irrespective of its composition. Magnesium carbonate formation can be explained by the diffusion of CO_2 from the environment and its reaction with the oxide film on the freshly polished surface [21]. After 2 minutes of sputtering, the intensity of the magnesium carbonate component observed on the surface of the AZ61 alloy (Fig.

5g and 5h) was higher than on the AZ31 alloy (Fig. 5e and 5f). In a previous study [12] some correspondence was observed between the presence of β-phase ($Mg_{17}Al_{12}$) and the amount of magnesium carbonate formed on the surface after atmospheric exposure. The results of this work tend to support this behaviour. From the point of view of magnesium alloy protection mechanisms, the formation of a carbonate product layer, thicker than that observed in this work, provides better passivation of the surfaces and retards chloride-induced corrosion in the passivation zone [22]. It is interesting to note that the magnesium carbonate content observed in the XPS analysis of the outer surface of the alloys (Fig. 5a-5h) tends to decline quickly with sputtering time (Fig. 5i-5p), probably because its presence is limited to the outermost surface of the magnesium specimen.

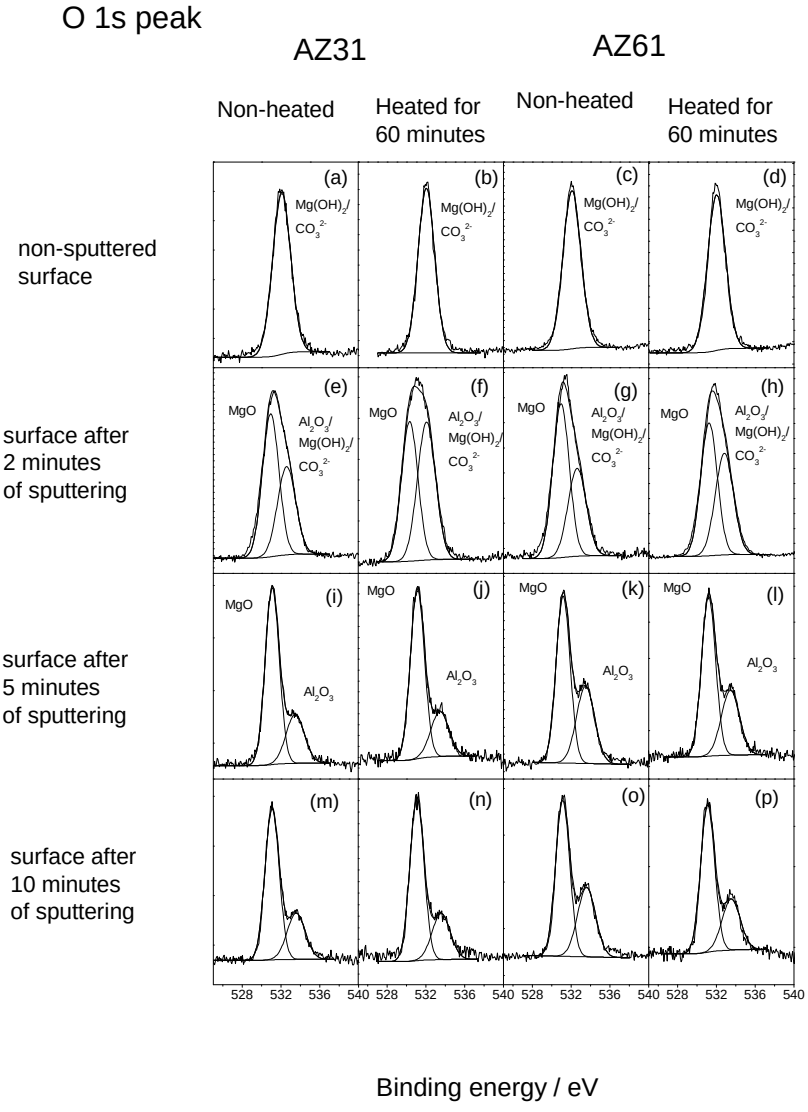

***Figure 6**. Variation of the O1s high resolution peak obtained by XPS on the surface of the AZ31 and AZ61 alloys non-heated and heated for 60 minutes as a function of the time of sputtering.*

High-resolution O1s spectra of the oxide films formed on the surface of the AZ31 and AZ61 alloys non heated and heated for 60 minutes as a function of the time of sputtering are presented in Figures 6a-6p. The spectra obtained on the non-sputtered surface (Figs. 6a-6d) are fairly similar, containing one single component at a binding energy of 532.2 eV associated with the presence of magnesium carbonate or magnesium hydroxide form [23]. After 2 minutes of sputtering, a higher or similar intensity second component appears at a binding energy of approximately 531.0 eV associated with the presence of oxygen in the form of magnesium oxide [23] (Fig. 6e-6h). After 5 minutes of sputtering, the spectra show the most intense component at a binding energy of 531.0 eV and another less intense component at a binding energy of 533.2 eV related to Al_2O_3 (Fig 6j-.6l). The O1s spectra obtained after 10 minutes of sputtering (Figs 6m-6p) were similar to those acquired after 5 minutes (Figs 6j-6l).

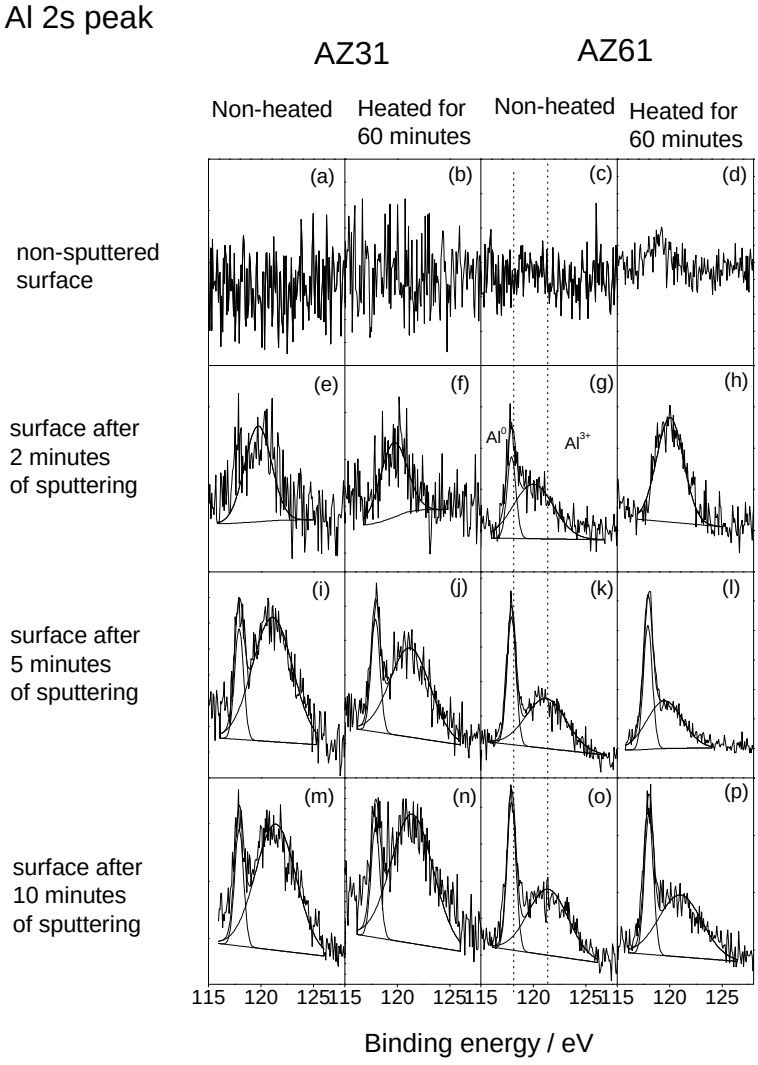

Figure 7. *Variation of the Al2s high resolution peak obtained by XPS on the surface of the AZ31 and AZ61 alloys non-heated and heated for 60 minutes as a function of the time of sputtering.*

Due to strong overlap between the second bulk plasmon of the metallic Mg2p peak and the Al2p peak observed in our measurements, we have measured the Al2s peak instead of the Al2p peak [24]. Figure 7 compares the high resolution spectra for Al2s peak obtained on the non-sputtered surfaces of the AZ31 alloy: non-heated (a) and heated for 60 minutes (b) and of the AZ61 alloy: non-heated (c) and heated for 60 minutes (d), with those corresponding to the same surfaces after 2 minutes of sputtering (e-h), 5 minutes of sputtering (i-l) and 10 minutes of sputtering (m-p). No appreciable aluminium signal is detected on the spectra obtained on the non-sputtered surfaces (Figs. 7a-7d). After 2 minutes of sputtering, the spectra obtained on the AZ31 alloy non-heated (Fig.7e) and heated for 60 minutes (Fig. 7f), as well as on the AZ61 alloy heated for 60 minutes (Fig. 7h), contain one single component at a binding energy of approximately 120.0 eV associated with the presence of aluminium in the form of Al^{3+} . The spectra obtained on the non-heated AZ61 alloy after 2 minutes of sputtering (Fig. 7g) show the most intense component at a binding energy of 118.0 eV, associated with the presence of metallic aluminium (Al^0), and a less intense component at a binding energy of 120.0 eV. After 5 minutes of sputtering (Figs. 7i-7l) the intensity of the metallic aluminium (Al^0) signal tends to rise and the intensity of the aluminium oxide (Al^{3+}) signal tends to decline quickly. No appreciable changes in the shape of the spectra have been observed after 10 minutes of sputtering between the non-heated alloys (Figs. 7m and 7o) and heated for 60 minutes (Figs. 7n and 7p). Attention is drawn to the significant increase in the metallic to oxide height (intensity) ratio in the Al2s peak obtained on the AZ61 alloy surface after 5 (Figs. 7k and 7l) or 10 minutes of sputtering (Figs. 7o and 7p) compared to that corresponding to the AZ31 alloy (Figs. 7i, 7j, 7m and 7n). This difference in trend suggests that a large part of the Al is in metallic state in solid solution in the AZ61 alloy, and as aluminium oxide particulates in the layers close to the outermost surface in the case of the AZ31 alloy [13].

Figure 8 compares the evolution with sputtering time of the high resolution spectra Mg2p peak obtained on the AZ31 alloy surface non-heated (a, e, i, m) and heated for 60 minutes (b, f, j, n) with those obtained on the AZ61 alloy surface non-heated (c, g, k, o) and heated for 60 minutes (d, h, l, p). The spectra obtained on the non-sputtered surface (Figs. 8a-8d) contain one single component at a binding energy of 50.8 eV associated with the presence of magnesium in the form of magnesium hydroxide/carbonate [20]. After 2 minutes of sputtering, a higher intensity second component appears at a binding energy of 49.7 eV, associated with the presence of magnesium in metallic state on the surface of the non-heated AZ31 and AZ61 alloys (Figs. 8e and 8g). Attention is drawn to the different shape of the spectra obtained on alloys AZ31 or AZ61 heated for 60

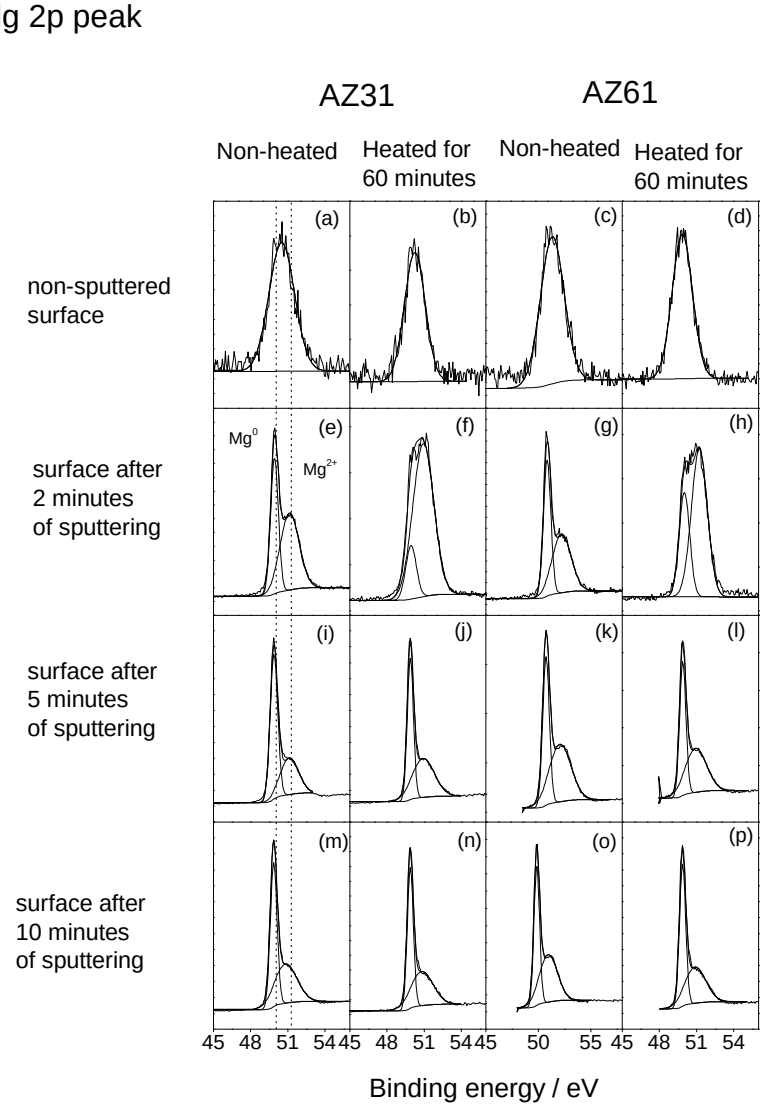

Figure 8. *Variation of the Mg2p high resolution peak obtained by XPS on the surface of the AZ31 and AZ61 alloys non-heated and heated for 60 minutes as a function of the time of sputtering.*

minutes after 2 min of sputtering (Figs 8f and 8h, respectively), with a higher intensity of the Mg^{2+} component respect to the Mg^0 component which could be explained by the formation of a thicker magnesium oxide layer after the heat treatment. After 5 minutes of sputtering, the intensity of the Mg^0 component observed in the heated samples (Figs 8j and 8l) increased significantly and no differences are observed in the Mg^{2+} to Mg^0 component height (intensity) ratio in the Mg2p peak compared to the non heated samples (Figs. 8i and 8k). No appreciable changes between the samples non-heated and heated for 60 minutes have been observed in the shape of the spectra after 10 minutes of sputtering (Figs. 8m - 8p). The fact that O, Al^{3+} and Mg^{2+} signals do not cease to be present on the surface of the specimens after long sputtering times (Figs. 6i-6p, 7i-7p

and 8i-8p) may be due to the presence of residues of Al_2O_3 and MgO that cannot be removed by the incident argon ions.

Figure 9 compares the variation in the $Al^0/(Al^0+Mg^0)$ x 100 atomic ratio obtained by XPS on the AZ31 and AZ61 alloy surfaces as a function of heating and sputtering times. This ratio was calculated from the area of the Al^0 and Mg^0 components in the fitting of the Al2s (Fig. 7) and Mg2p (Fig. 8) spectra and the atomic percentages of Al and Mg obtained by XPS on the surface of the alloys (not shown). It is interesting to note that the fraction of area occupied by the intermetallic precipitate of β- phase in the grain boundaries of alloy AZ61 is very small (Figs. 4b, 4d, 4f and 4h). Thus, the XPS results (which refer to an analysis area of 1mm x 1mm) give an average surface chemistry which is dominated to a large extent by the effect of the α-phase.

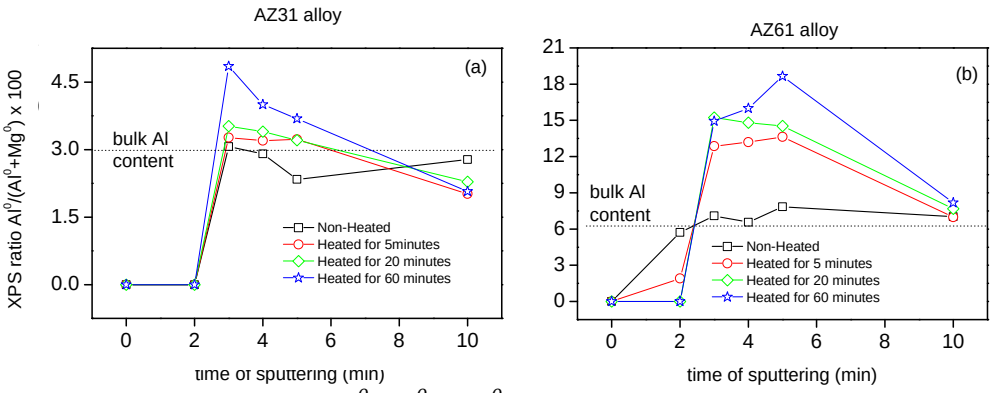

Figure 9. *Variation in the $Al^0/(Al^0+Mg^0)$ x 100 atomic ratio obtained by XPS on the surface of the AZ31 and AZ61 alloys as a function of the time of heating and time of sputtering.*

Strong Al enrichment develops in the alloy subsurface region upon sputter-cleaning, as experimentally confirmed in Ref. [15] . However, the fact that the $Al/(Al^0+Mg^0)$ x 100 atomic ratio obtained by XPS on the non-heated AZ31 and AZ61 alloy surfaces are practically identical to that of the aluminium content in the bulk of these materials (Table 1) and remain approximately stable during the 10 minutes of sputtering (Fig. 9) suggest that this is not the origin of the phenomenon observed in our study.

3.4.Electrochemical measurements

3.4.1. Charge transfer resistance measurements and corrosion rate.

The evolution of the corrosion process on the heat-treated AZ31 and AZ61 alloys immersed in 0.6 M NaCl solution has been monitored by means of impedance measurements. The Nyquist diagrams (Fig. 10) show the presence of a capacitive loop in the high frequency (HF) region and an inductive loop at low frequencies (LF). Many studies in the literature [25-27], support the use of the charge transfer resistance (R_{CT}), deduced from HF capacitive loop, to obtain information on the corrosion rate of magnesium alloys. It is normal to associate the diameter of this capacitive loop with the charge transfer resistance of the corrosion process [25, 26, 28], which is inversely related to the corrosion current (i_{corr}) through the well known Stern-Geary equation [29]:

$$i_{corr} = \frac{B}{R_{CT}} \quad (1)$$

The R_{CT} values, corresponding to the HF capacitive loop, were derived from the impedance data in the range of 10^5 to 10 Hz. With the help of Zview software fitting method [30] the results were adequately fitted using an equivalent circuit formed by the charge transfer resistance and a constant phase element in parallel.

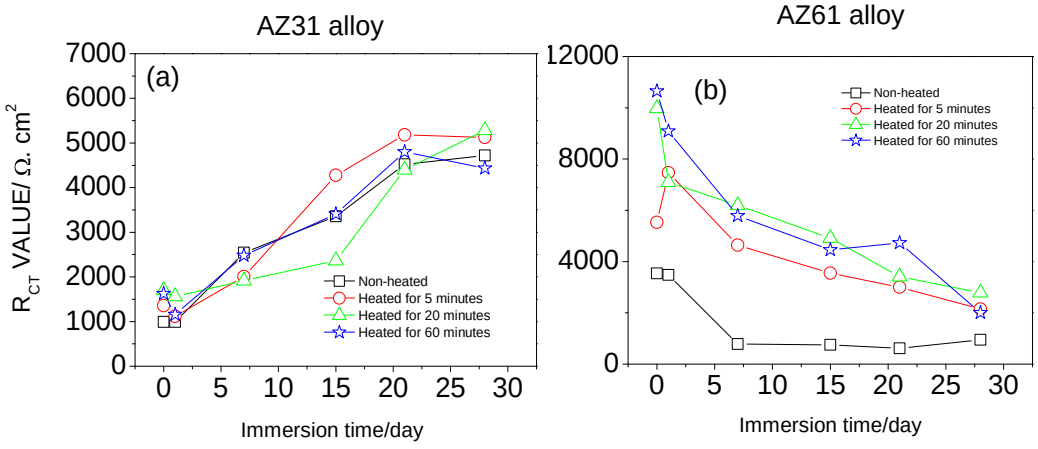

Figure 11. *Variation in R_{CT} values as a function of alloy type and of time of heating over 28 days immersion in 0.6M NaCl*

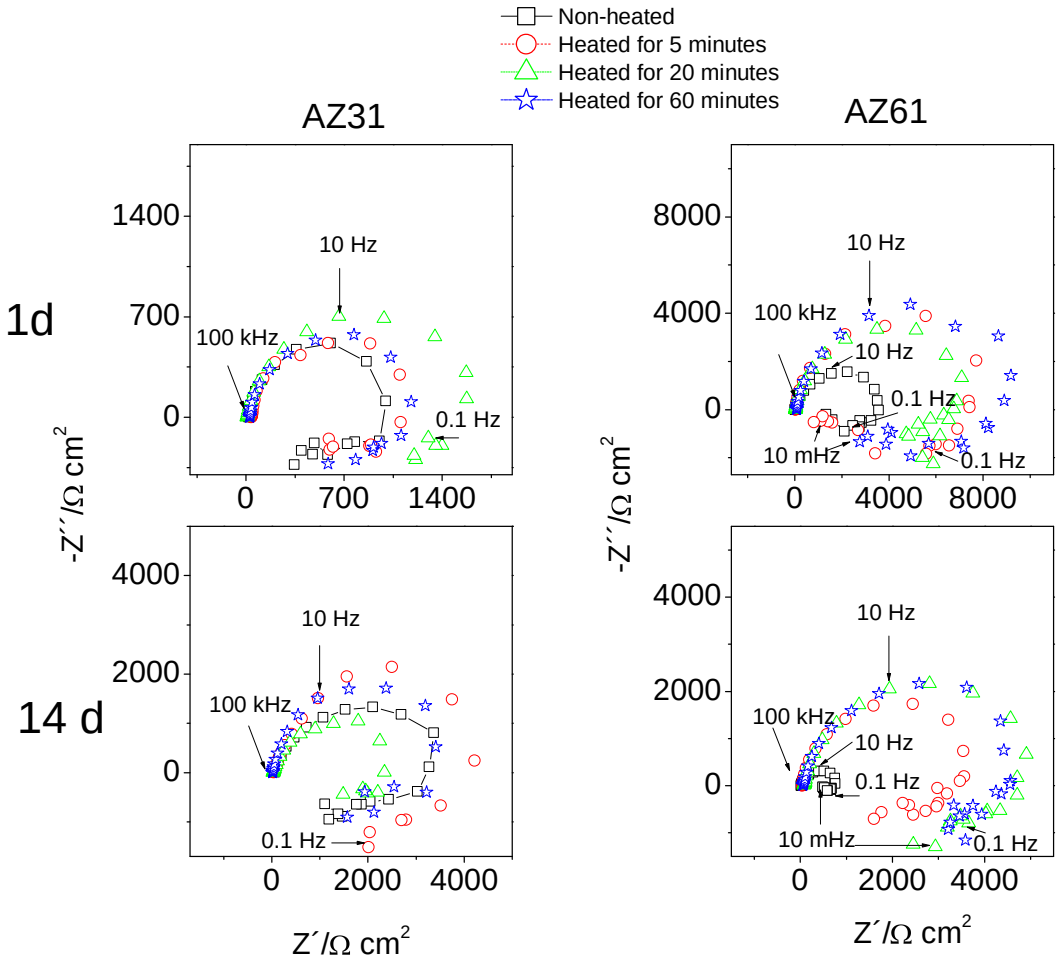

Figure 10. *Variation in Nyquist plot for AZ31 and AZ61 alloys with immersion time (hours or days on the Y-axis) and times of heating.*

Fig. 11 shows the evolution of the charge transfer resistance (R_{CT}) with immersion time in the 0.6M NaCl solution.

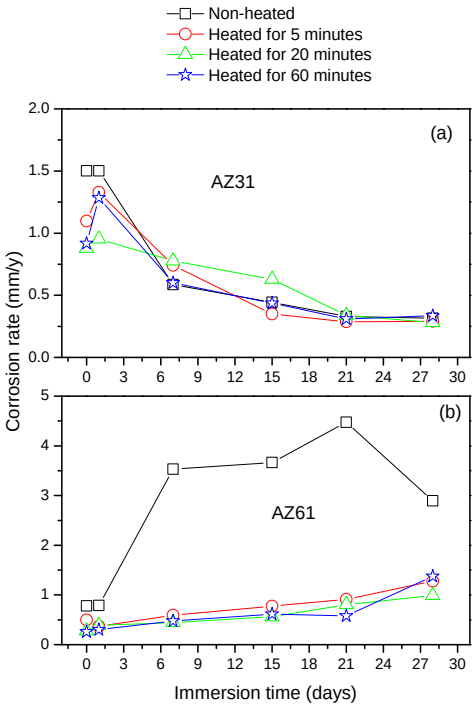

Figure 12. *Variation in corrosion rates (mm/y) obtained from EIS as a function of the time of heating and alloy type over 28 days immersion in 0.6M NaCl*

.

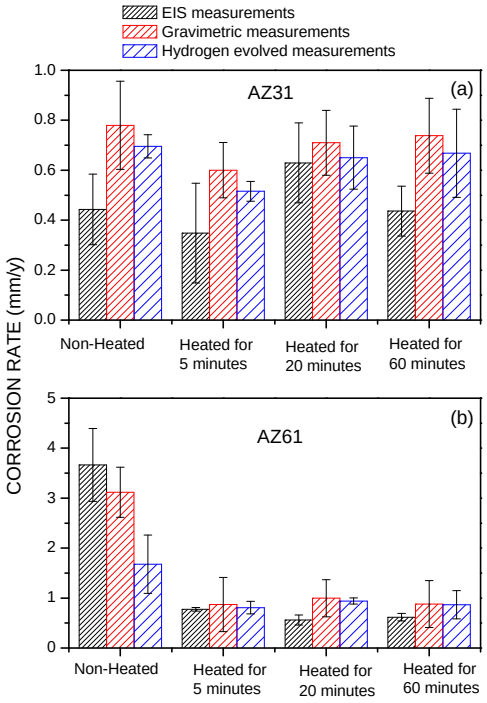

Figure 13. *Comparison of corrosion rates (mm/y) obtained from EIS with weight loss and hydrogen evolution measurements after 14 days immersion in 0.6M NaCl*

Corrosion rates in Fig.12, showing the instantaneous corrosion rate variations with time, were obtained from R_{CT} values represented in Fig. 11, by means of the Stern-Geary equation (1), in which the constant of proportionality B (i.e., about 65 mV for the AZ31 alloy and about120 mV for the AZ61 alloy) had been empirically determined by the correlation between electrochemical and gravimetric measurements [13]. Corrosion current densities in mA/cm^2 were converted to corrosion rates, mm/y, by applying Faraday's law and the resulting equation:

$$\text{corrosion rate} = 22.85\, i_{corr} \quad (2)$$

Cumulative weight loss after an extended period of time was determined by integration of the weight changes for individual exposure periods. This way, the results of EIS measurements in Fig. 13, showing the average corrosion rates of the specimens after 14 days of exposure to the 0.6 M NaCl solution, were determined.

Regarding the inductive loop observed at LF, several processes can induce this behaviour in the corrosion of magnesium and its alloys. In the literature [31-35] it is mainly attributed to the relaxation of adsorbed species, such as Mg^{2+} or $MgOH^{+}$ on the electrode surface and, also, to the possible dissolution of partially protective surface films although it is not always easy to find a definitive explanation to these inductive loops [31].

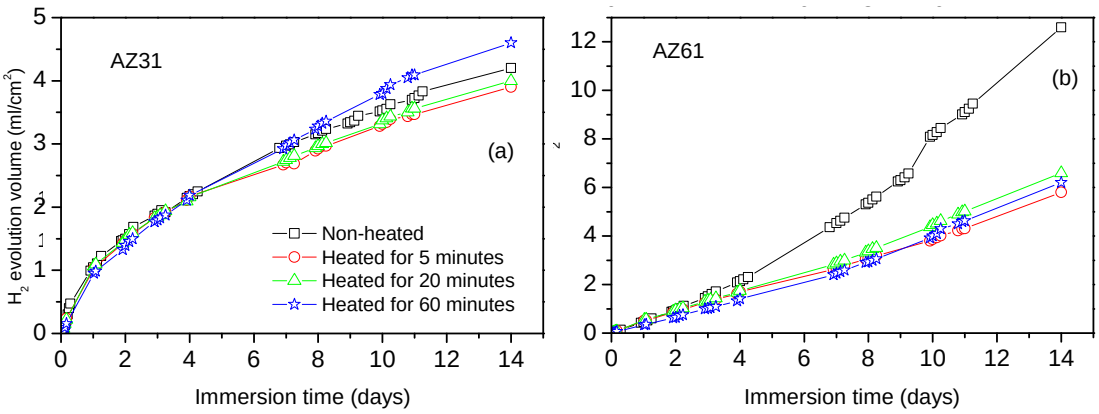

Figure 14. *Variation in H_2 evolution volume values as a function of the time of heating and alloy type over 14 days immersion in 0.6M NaCl.*

Because the inductive loops are not directly related to the rate of corrosion, their interpretation is considered immaterial as to provide kinetic information about the corrosion process.

Fig. 14 is instructive in showing the differences in the hydrogen volume data between heat treated AZ31 and AZ61 alloys over 14 days of immersion in 0.6 M NaCl. It is interesting to note that similar trends regarding the corrosion behaviour are deduced from these hydrogen evolution determinations that from the electrochemical ones.

Fig. 13, which compares the amounts of corroded metal determined by hydrogen evolution, gravimetric and electrochemical measurements, also gives us an idea of the degree of similarity between these three types of determinations.

4. Discussion

4.1. Changes in chemical composition of the thin oxide films grown on AZ31 and AZ61 alloys by themal oxidation at 200ºC

As can be seen in figure 1, the time interval of 35-60 minutes of heating at 200ºC was characterised by a very small weight gain, around only 0.6 μg/cm^2, similar for the two alloys, which corresponds approximately to an oxide film thickness of 17 Å. This data is consistent with the small increase in the thickness of the MgO film on the surface of the alloys as seen by XPS after 60 minutes of heating and commented above. It is generally accepted that the growth of compact MgO films is controlled by solid sate diffusion through adherent oxide areas followed by the reaction with oxygen at the oxide/gas interface. Hence, a lack of easy-paths for fast Mg transport could be a possible explanation of highly protective behaviour [16]. Since the diffusivity of Mg within the MgO lattice is expressed by [36]:

$$D_L = 1.0 \times 10^{-6} \exp(- 150000/ RT) \ \ m^2 / s$$

at 473 K the value of D is as low as 2.67 x 10^{-23} m^2/s justifying negligible weight. Similarly, in previous work [13] with the same alloys in 0.6M NaCl solution, we observed that the homogeneous and continuous native oxide film formed on freshly polished samples had a possible inhibiting effect on the diffusion of magnesium atoms during the corrosion process.

In general, the XPS analyses of the AZ61 heated samples show an important aluminium enrichment, mainly as metallic aluminium, at the interface between the surface oxide and the bulk of the alloy compared to the Al content on the non-heated alloy or in the bulk alloy (Fig. 9b). The relative $Al^0/(Al^0+Mg^0)$ x 100 atomic ratio determined by XPS for the heated samples is 2-3 times higher than for the Al alloying bulk content or non-heated AZ61 alloys. This behaviour suggests the possibility of a considerably higher diffusion rate of Al than the Mg throughout the heat treatment. This idea could be sustained if the diffusivity values for Al in MgO are much higher than those corresponding to the diffusion of Mg. Recent data in the literature [37, 38] suggest

diffusion coefficients for Al about ten orders of magnitude higher than for Mg, which tends to support this possibility.

4.2. Relationship between the chemistry of thin oxide films grown on the surface of magnesium alloys by themal oxidation and their corrosion resistance in saline solutions

It seems likely that some differences revealed in the composition characteristics of oxide films formed on alloy AZ31 and AZ61 surfaces after the heat treatment may have an impact on the corrosion behaviour of the specimens in saline solutions. In this respect, attention is drawn to: (a) very thin MgO layer, only few nanometers thick, grown on the surface of polished commercial AZ31 and AZ61 alloys with the heat treatment conditions used in this study and (b) metallic Al enrichment in the subsurface layers of the thermally treated AZ61 alloy.

As pointed out in early studies by Pilling and Bedworth [39], due to the large difference in densities between the oxide and metal, expressed by the MgO to Mg volume ratio of 0.81, oxide scale should not form a compact layer. Justified by our gravimetric and XPS results it may be inferred that a minimal formation of magnesium oxide occurs during the heating treatment. In a previous study [13] it was seen that the freshly polished AZ61 and AZ31 alloys showed better corrosion resistance than the alloys in as-received condition, probably due to the formation of a homogeneous, uniform passive thin layer on the polished surface. It is interesting to note that heating at 200ºC avoids the adverse effect of the growth of thick MgO oxide layers at higher temperatures which may break the compact structure of the initial native oxide film impairing their diffusion barrier properties in a NaCl aqueous environment.

Jeurgens et al. [15] have investigated the growth kinetics and the evolution of the chemical composition and constitution of the initial oxide film grown on Mg-based MgAl surfaces by dry thermal oxidation, and observed that within the grown oxide films adjacent to the alloy/oxide interface the interstitial sites were preferentially occupied by Al cations. In the present study, attention is drawn to the preferential increase in the metallic component compared to the oxide component in the Al signal in the subsurface layer as a result of the heat treatment. It is speculated that the homogeneous, uniform and compact native oxide layer present on the surface of the alloys inhibits significantly the oxidation or solid state diffusion of the Al alloying element within the exposure times and temperature chosen in our study reducing the

adverse effects on the protective properties associated to the growth of Al_2O_3 or $MgAl_2O_4$ type species [13].

In addition to the uniformity and compactness effects, the chemical composition of the thin oxide layers on surface of the AZ61 alloy after the thermal treatment also plays a fundamental part in the observed corrosion rate. Figures.11b, 12b, 13b and 14b reveal that metallic aluminium enrichment of the subsurface layers with heat treatment exerts an important effect in the evolution of R_{CT} and corrosion values for the AZ61 alloy during the first 14 days of the immersion test in solution of NaCl 0.6M. The findings of the present work suggest that the higher the amount of aluminium in the subsurface of the heated alloy better is corrosion resistance in saline solution. Many studies mention the beneficial effect of Al [11, 40-45], which may become the essential factor in determining the passivity of the surface, improving the resistance to local breakdown of the oxide and reducing the chance of chloride ions penetrating as far as the metal surface It is logical to relate a decrease in the corrosion rate with the strengthening of the thin magnesium oxide film spontaneously formed on the metallic surface of magnesium alloys by the Al enrichment induced by the heat treatment. Any increase in the percentage of passivating points or aluminium hydroxide areas on the metallic surface will reduce the tendency (stimulated by the presence of Cl- ions) for metallic ions to pass from the reactive bare surface into the aqueous solution.

Finally, in the case of the AZ31 specimens, it is interesting to note the absence of significant variations in the corrosion rate, (Figs.12a and 13a) or in the volumes of hydrogen evolved (Fig. 14a) as a function of the heating time, where the XPS analyses (Figs.9a) has revealed Al contents on the heated specimens similar to those observed on the non-heated alloy or in the bulk alloy (Table 1). This fact tends to support the idea that the aluminium incorporation in the magnesium oxide film that covers the surface of the magnesium alloys after the heat treatment plays a fundamental part in the observed corrosion rate.

5. Conclusions

XPS analysis has been used to characterise the subtle changes in the chemical composition of native films formed in air on the surface of AZ31 and AZ61 alloys as a result of heating at a temperature of 200ºC for a time of between 5 minutes and 1 hour. Attention is drawn to the metallic aluminium enrichment on the subsurface layers of the

AZ61. Close to two or three times higher metallic aluminium contents have been found in these layers compared to the bulk content.

The native oxide film formed on the surface of polished AZ31 and AZ61 alloys seems to significantly inhibit the growth of magnesium oxide- or Al^{3+} enriched surface layers during thermal treatment in air at 200ºC and periods of 60 minutes.

Charge transfer values (R_{CT}), obtained from EIS measurements in an interval between 1 h and 28 days of immersion in 0.6M NaCl solution, have allowed the establishment of relationships between the chemical composition of the thin surface films formed as a result of the heating treatment and the corrosion resistance of the alloys. There is a notable rise in the R_{CT} values of the AZ61 alloy in NaCl as a result of the prior heating process, even for the earliest stages (only 5 minutes). This effect is less evident in the AZ31 alloy.

Combined analysis of XPS and EIS data suggests a favourable effect for corrosion resistance of: a) metallic Al enrichment in the subsurface of the thermally treated alloy; and b) the absence of significant changes in the uniformity, homogeneity and compactness of the native oxide film formed on the surface of polished commercial AZ31 and AZ61 alloys during thermal oxidation of the alloys at 200ºC in air.

Acknowledgments

The authors express their gratitude to Prof. S. Feliu for several clarifying and stimulating discussions during the course of this work. They also gratefully acknowledge financial support for this work from the Ministry of Economy and Competitivity of Spain (MAT 2009-13530 and MAT2012-30854).

References

[1] M.C. Zhao, M. Liu, G.L. Song, A. Atrens, Influence of the beta-phase morphology on the corrosion of the Mg alloy AZ91, Corros. Sci. 50 (2008) 1939-1953.
[2] M.C. Zhao, M. Liu, G.L. Song, A. Atrens, Influence of homogenization annealing of AZ91 on mechanical properties and corrosion behavior, Adv. Eng. Mater. 10 (2008) 93-103.
[3] C.L. Liu, Y.C. Xin, G.Y. Tang, P.K. Chu, Influence of heat treatment on degradation behavior of bio-degradable die-cast AZ63 magnesium alloy in simulated body fluid, Mater. Sci. Eng., A 456 (2007) 350-357.
[4] T. Beldjoudi, C. Fiaud, L. Robbiola, Influence of homogenization and artificial aging heat-treatments on corrosion behavior of Mg-Al alloys, Corrosion 49 (1993) 738-745.
[5] G.L. Song, A.L. Bowles, D.H. StJohn, Corrosion resistance of aged die cast magnesium alloy AZ91D, Mater. Sci. Eng., A 366 (2004) 74-86.

[6] N.N. Aung, W. Zhou, Effect of heat treatment on corrosion and electrochemical behaviour of AZ91D magnesium alloy, J. Appl. Electrochem. 32 (2002) 1397-1401.
[7] J.D. Majumdar, U. Bhattacharyya, A. Biswas, I. Manna, Studies on thermal oxidation of Mg-alloy (AZ91) for improving corrosion and wear resistance, Surf. Coat. Technol. 202 (2008) 3638-3642.
[8] W. Zhou, T. Shen, N.N. Aung, Effect of heat treatment on corrosion behaviour of magnesium alloy AZ91D in simulated body fluid, Corros. Sci. 52 (2010) 1035-1041.
[9] L.Q. Zhu, W.P. Li, D.D. Shan, Effects of low temperature thermal treatment on zinc and/or tin plated coatings of AZ91D magnesium alloy, Surf. Coat. Technol. 201 (2006) 2768-2775.
[10] H.Y. Hsiao, P. Chung, W.T. Tsai, Baking treatment effect on materials characteristics and electrochemical behavior of anodic film formed on AZ91D magnesium alloy, Corros. Sci. 49 (2007) 781-793.
[11] S. Feliu Jr., M.C. Merino, R. Arrabal, A.E. Coy, E. Matykina, XPS study of the effect of aluminium on the atmospheric corrosion of the AZ31 magnesium alloy, Surf. Interface Anal. 41 (2009) 143-150.
[12] S. Feliu Jr., A. Pardo, M.C. Merino, A.E. Coy, F. Viejo, R. Arrabal, Correlation between the surface chemistry and the atmospheric corrosion of AZ31, AZ80 and AZ91D magnesium alloys, Appl. Surf. Sci. 255 (2009) 4102-4108.
[13] S. Feliu Jr., C. Maffiotte, A. Samaniego, J.C. Galvan, V. Barranco, Effect of the chemistry and structure of the native oxide surface film on the corrosion properties of commercial AZ31 and AZ61 alloys, Appl. Surf. Sci. 257 (2011) 8558-8568.
[14] S. Feliu Jr., C. Maffiotte, A. Samaniego, J.C. Galvan, V. Barranco, Effect of naturally formed oxide films and other variables in the early stages of Mg-alloy corrosion in NaCl solution, Electrochim. Acta 56 (2011) 4554-4565.
[15] L.P.H. Jeurgens, M.S. Vinodh, E.J. Mittemeijer, Initial oxide-film growth on Mg-based MgAl alloys at room temperature, Acta Mater. 56 (2008) 4621-4634.
[16] F. Czerwinski, The oxidation behaviour of an AZ91D magnesium alloy at high temperatures, Acta Mater. 50 (2002) 2639-2654.
[17] C.D. Wagner, L.E. Davis, M.V. Zeller, J.A. Taylor, R.H. Raymond, L.H. Gale, Empirical atomic sensitivity factors for quantitative-analysis by electron-spectroscopy for chemical-analysis, Surf. Interface Anal. 3 (1981) 211-225.
[18] N.T. Kirkland, N. Birbilis, M.P. Staiger, Assessing the corrosion of biodegradable magnesium implants: a critical review of current methodologies and their limitations, Acta Biomater. 8 (2012) 925-936.
[19] J.W. Liu, Y. Li, F.H. Wang, The High Temperature Oxidation Behavior of Mg-Gd-Y-Zr Alloy, Oxid. Met. 71 (2009) 319-334.
[20] H.B. Yao, Y. Li, A.T.S. Wee, An XPS investigation of the oxidation/corrosion of melt-spun Mg, Appl. Surf. Sci. 158 (2000) 112-119.
[21] M. Jönsson, D. Persson, D. Thierry, Corrosion product formation during NaCl induced atmospheric corrosion of magnesium alloy AZ91D, Corros. Sci. 49 (2007) 1540-1558.
[22] L. Wang, T. Shinohara, B.P. Zhang, XPS study of the surface chemistry on AZ31 and AZ91 magnesium alloys in dilute NaCl solution, Appl. Surf. Sci. 256 (2010) 5807-5812.
[23] J.S. Liao, M. Hotta, S. Motoda, T. Shinohara, Atmospheric corrosion of two field-exposed AZ31B magnesium alloys with different grain size, Corros. Sci. 71 (2013) 53-61.
[24] L.P.H. Jeurgens, M.S. Vinodh, E.J. Mittemeijer, Quantitative analysis of multi-element oxide thin films by angle-resolved XPS: application to ultra-thin oxide films on MgAl substrates, Appl. Surf. Sci. 253 (2006) 627–638.
[25] N. Pebere, C. Riera, F. Dabosi, Investigation of magnesium corrosion in aerated sodium-sulfate solution by electrochemical impedance spectroscopy, Electrochim. Acta 35 (1990) 555-561.
[26] S. Mathieu, C. Rapin, J. Hazan, P. Steinmetz, Corrosion behaviour of high pressure die-cast and semi-solid cast AZ91D alloys, Corros. Sci. 44 (2002) 2737-2756.
[27] G. Baril, N. Pebere, The corrosion of pure magnesium in aerated and deareated sodium sulfate solutions, Corros. Sci. 43 (2001) 471-484.
[28] G.L. Makar, J. Kruger, Corrosion studies of rapidly solidified magnesium alloys, J. Electrochem. Soc. 137 (1990) 414-421.
[29] M. Stern, A. L. Geary, Electrochemical polarization .1. A theoretical analysis of the shape of polarization curves J. Electrochem. Soc. 104 (1957) 56-63.
[30] ZView software, Version 3.1c (Scribner Associates Inc), Southern Pines, NC, USA
[31] R. Pinto, M.G.S. Ferreira, M.J. Carmezim, M.F. Montemor, The corrosion behaviour of rare-earth containing magnesium alloys in borate buffer solution, Electrochim. Acta 56 (2011) 1535-1545.

[32] P. Cordoba-Torres,M. Keddam, R.P. Nogueira, On the intrinsic electrochemical nature of the inductance in EIS, a monte Carlo simulation of the two consequitive-step mechaninsm: the flat surface 2 D case, Electrochim. Acta, 54 (2008) 518-523.
[33] G. Baril, G. Galicia, C. Deslouis, N. Pébere, B. Tribollet, V. Vivier, An impedance investigation of the mechanism of pure magnesium corrosion in sodium sulfate solutions, J. Electrochem. Soc. 154 (2007) C 108- C 113.
[34] M. Anic, G. Celiklen, Analysis of the electrochemical reaction behavior of alloy AZ91 by EIS technique in $H_3 PO_4$ / KOH buffered $K_2 SO_4$ solutions, Corros. Sci., Vol. 49 (2007) 1878-1894.
[35] F. Mansfeld, J.C.S. Fernandes, Impedance spectra for aluminium 7075 during the early stages of immersion in sodium chloride, Corros. Sci. 34 (1993) 2105-2108.
[36] C. Lea, C. Molinari, Magnesium diffusion, surface segregation and oxidation in Al-Mg alloys, J. Mater. Sci. 19 (1984) 2336-2352.
[37] J.A. Van Orman, K.L. Crispin, Diffusion in oxides, Rev. Mineral. Geochem. 72 (2010) 757–825.
[38] B.H. Zhang, X.P. Wu, Diffusion of aluminium in MgO: A thermodynamic approach study Chin. Phys. B 22 (2013) 056601.
[39] N.B. Pilling, R.E. Bedworth, The oxidation of metals at high temperatures, J. Inst. Met. 29 (1923) 529-582.
[40] R. Lindstrom, J.E. Svensson, L.G. Johansson, The influence of carbon dioxide on the atmospheric corrosion of some magnesium alloys in the presence of NaCl, J. Electrochem. Soc. 149 (2002) B 103-107.
[41] M. Liu, P.J. Uggowitzer, A.V. Nagasekhar, P. Schmutz, M. Easton, G. L. Song, A. Atrens, Calculated phase diagrams and the corrosion of die-cast Mg-Al alloys, Corros. Sci. 51 (2009) 602-619.
[42] J.H. Nordlien, K. Nisancioglu, S. Ono. N. Masuko, Morphology and structure of oxide films formed on MgAl alloys by exposure to air and water, J. Electrochem. Soc. 143 (1996) 2564-2572.
[43] A. Pardo, M.C. Merino, A.E. Coy, R. Arrabal, F. Viejo, E. Matykina, Corrosion behaviour of magnesium/aluminium alloys in 3.5 wt.% NaCl, Corros. Sci. 50 (2008) 823-834.
[44] M. Jönsson, D. Persson, R. Gubner, The initial steps of atmospheric corrosion on magnesium alloy AZ91D, J. Electrochem. Soc. 154 (2007) C 684-691.
[45] N. Hara, Y. Kobayashi, D. Kagaya, N. Akao, Formation and breakdown of surface films on magnesium and its alloys in aqueous solutions, Corros. Sci. 49 (2007) 166-175.

The Effect of Low Temperature Heat Treatment on Surface Chemistry and Corrosion Resistance of Commercial Magnesium Alloys AZ31 and AZ61 in 0.6 M NaCl Solution.

Sebastián Feliu (Jr)[a] , Alejandro Samaniego[a], Violeta Barranco[b], A.A. El-Hadad[c], Irene Llorente[a], P. Adeva[a].

[a]Centro Nacional de Investigaciones Metalúrgicas CSIC, Avda. Gregorio del Amo 8, 28040 Madrid, Spain.
[b]Instituto de Ciencias de Materiales de Madrid, ICMM, Consejo Superior de Investigaciones Científicas, CSIC, Sor Juana Inés de la Cruz, 3, Cantoblanco, 28049, Madrid, Spain
[c] Physics Department, Faculty of Science, Al-Azhar University,Nasr City 11884, Cairo, Egypt.

Corrosion Science, 80 (2014) 461-472.

Abstract

This paper studies the differences in chemical composition of the oxide surface layers induced by heating in air at 200ºC for time intervals from 5 minutes up to 60 minutes on commercial AZ31 and AZ61 magnesium alloys with a view to a better understanding of their protective properties. A strong link was found between the aluminium enrichment observed in the surface of the oxide layer and the decrease in the protective properties of the heat treated AZ31 alloy. In contrast, no significant changes have been observed in the case of the heat treated AZ61 alloy.

Keywords: A. Magnesium; B. XPS; B. SEM; C. Passivity; C. Segregation.

1. Introduction

The chosen study materials are Mg-Al alloys, which have aroused great scientific and technological interest over the last two decades. From a practical point of view magnesium is the structural metal of lowest density, which makes it highly attractive for use in the automotive, aerospace, IT and electronics industries, where weight plays a decisive role. However, as magnesium is one of the chemically most active metals, insufficient resistance to atmospheric and aqueous corrosion sometimes limits its applications. Thus it is desirable to have as complete as possible information on the factors that influence the corrosion of these materials. This work seeks to contribute to such information.

Many researchers have carried out studies to find relationships between changes in the alloy microstructure (amount and distribution of β-phase precipitates) with long term heat treatments (T4 (solution treatment) or T6 (aging treatment)) [1-12] and changes in corrosion resistance. In the literature a great deal of attention has been paid to the role of the β-phase in the corrosion mechanism of magnesium/aluminium alloys. A generally accepted idea is that this phase acts as an effective cathode and/or barrier against corrosion, depending on its size and distribution [1].

Oxide film formation and properties like protectiveness may be sensitive to the conditions in which the film grows. Laboratory tests normally refer to the behaviour of surfaces that have been mechanically polished prior to testing in order for metallographic observation and to remove the impurities and oxidation/corrosion product layers formed during the manufacturing and subsequent storage of the alloy. However, it is of particular technological interest to obtain information on the chemical composition of the surface in as-received condition (untreated surface), because these alloys are normally used with most of the surface intact and the cost of polishing treatment limits its industrial application [13]. The literature contains controversial views relating to the effect of skin characteristics on the corrosion performance of magnesium alloys [13]. Song et al. [14] reported that the skin of die cast AZ91D showed better corrosion resistance than the interior. The opposite conclusion was obtained by Yu and Uan [15] and Zhang et al [16]. Recently, Song and Xu [17] have observed an improvement in the corrosion performance of AZ31B Mg alloy sheet by surface polishing.

In a previous study [18], XPS analysis revealed notable differences in the chemical composition, structure and thickness of the external oxide films on the surface of AZ31 and AZ61 alloys in as-received and freshly polished conditions. In the joint analysis of XPS and EIS data, attention was drawn to the significant decrease in the corrosion resistance value of the alloys in as-received conditions In immersion test in saline solution, during the initial stages of testing, considerable higher corrosion rates were obtained in as-received specimens compared to the freshly polished surfaces. The formation of an additional thin (thickness of just a few nanometres) and non-uniform external oxide layer (in the form of islands) composed by a mixture of spinel ($MgAl_2O_4$) and MgO as a result of the manufacturing process seemed to diminish the protective properties compared to the more perfect and uniform films formed on freshly polished surface. An economic and simple method to generate on a material a protective barrier against the effects of aggressive environments is to expose it to a thermal treatment in an oxygen rich atmosphere [19]. Following up the idea that the initial external oxide film plays an important role in the resistance to magnesium corrosion initiation and its propagation [1,18,20], in the present research it is studied the possibility of improving its protective properties by short time low temperature heat treatments in air.

From a scientific point of view, Jeurgens et al. [21] noted that the thermal oxidation of metallic alloys at low temperatures (e.g. at $T < 600$ K) and for short times has only scarcely been investigated. The detailed chemical composition and constitution of the oxide films formed on such alloy surfaces at low temperatures for short heating times are unknown and there is no comprehensive knowledge of the effect of the concurrent processes of chemical segregation and preferential oxidation on the developing oxide-film.

Czerwinski [22] studied the oxidation behaviour of AZ91D Mg alloy at different temperatures. The results showed that AZ91D exhibited protective oxidation only at a temperature of 197ºC, while at higher temperatures the behaviour was non-protective and associated with the formation of oxide nodules and their coalescence into a loose fine-grained structure. On the basis of these results, we have selected a low-temperature heat treatment process at 200ºC to study the possibility of improving the protective properties of the external oxide film on the surface of AZ31 and AZ61 Mg alloy in as-received condition.

Thus, special objective of this research is to study the effect of the type of alloy and heating time at 200ºC on the chemistry of the outer thin films formed on the surface of magnesium alloys after short heat treatments and their corrosion resistance in saline solution.

2. Experimental

The chemical compositions of the tested magnesium alloys, AZ31 and AZ61, determined in wet conditions, are listed in Table 1. They were fabricated in wrought condition and supplied in 3 mm thick plates by Magnesium Elecktron Ltd, UK, Manchester. This research compares the behaviour of specimens of the above alloys in the two following surface conditions: specimens in as-received condition, which means that the surface of the samples was untreated and had only been cleaned with distilled water and dried with hot air, and freshly polished specimens, which were dry ground with successive grades of silicon carbide abrasive paper from P600 to P2000 followed by finishing with 3 and 1 μm diamond paste, cleaned in water and dried with hot air. The following nomenclature is used in the remainder of the paper to designate the four dual combinations tested: AZ31-O, AZ31-P, AZ61-O, and AZ61-P, where the letters O and P, that accompany the alloy type, denote: O = original surface condition (i.e. as-received); P = polished surface condition.

***Table 1**. Chemical composition of AZ31 and AZ61 alloys (wt. %).Average values for four replicates measurements.*

Alloy	Al	Zn	Mn	Si	Fe	Mg
AZ31	3.175 ± 0.005	0.735 ± 0.005	0.250 ± 0.001	0.0200 ± 0.001	0.0050 ± 0.0001	Bal
AZ61	6.200 ± 0.005	0.740 ± 0.005	0.230 ± 0.001	0.0400 ± 0.001	0.0040 ± 0.0001	Bal

The two alloys were oxidised in identical conditions in a thermogravimetric analyser (TGA) (TA instruments Q600 SDT) using cylindrical specimens of 4 mm in diameter by 2 mm in height (weight approximately 100 mg). The apparatus was capable of accommodating a specimen with a maximum weight of 0.5 g and had a measurement accuracy of 0.1 μg. The reaction temperature was monitored by a Pt/Pt–Rh thermocouple. Weight change kinetics were measured in air under isothermal conditions at a temperature of 200°C. The heating rate before reaching the isothermal condition was 50°C/min. For reference, thermogravimetric measurements of weight change versus time are also shown for freshly polished AZ31 and AZ61 alloys in an air environment.

In this case, the as-received specimens were dry ground through successive grades of silicon carbide abrasive papers from P600 to P2000 followed by finishing with 3 and 1 μm diamond paste, rinsing in water and drying with hot air.

The thermal treatment was very simple, consisting of the horizontal exposure of 2 cm x 2 cm square specimens of the AZ31 and AZ61 alloys in a convective stove at 200°C in air for 5, 20 and 60 minutes.
The tested specimens were examined by scanning electron microscopy (SEM) using a Hitachi S-4800 equipped with an Oxford energy dispersive X-ray microanalysis system (EDX).

Photoelectron spectra were recorded using a Fisons MT500 spectrometer equipped with a hemispherical electron analyser (CLAM 2) and an Mg Kα X-ray source operated at 300 W. The specimens were fixed on small flat discs supported on an XYZ manipulator placed in the analysis chamber. The residual pressure in this ion-pumped analysis chamber was maintained below 10^{-8} torr during data acquisition. Spectra were collected for 20-90 min, depending on the peak intensities, at a pass energy of 20 eV, which is typical of high-resolution conditions. The intensities were estimated by calculating the area under each peak after smoothing and subtraction of the S-shaped background and fitting the experimental curve to a combination of Lorentzian and Gaussian lines of variable proportions. Although specimen charging was observed, it was possible to determine accurate binding energies (BEs) by referencing to the adventitious C 1s peak at 285.0 eV. The atomic ratios were computed from the peak intensity ratios and reported atomic sensitivity factors [23]. The measurements were performed at take-off angles of 45° with respect to the specimen surface. The sampled areas were 1 x 1 mm^2.

Potentiodynamic polarization curves were measured in 0.6 M NaCl solution at room temperature. A common three-electrode electrochemical cell was used, with a saturated Ag/AgCl electrode as the reference electrode and a graphite carbon electrode as the counter electrode. Prior to polarization, the specimens remained at open circuit for 30 min to reach a steady value. Scans were obtained from 150mV below OCP to and scanned upwards at a rate of 1 mV/s. Two sets of electrochemical tests were conducted in each experimental condition and repeatable results were achieved.

Electrochemical impedance measurements were conducted in 0.6 M NaCl after 1 hour, 1 day, 7, 14, 21 and 28 days of exposure at room temperature (25°C). An AUTOLAB potentiostat, model PGSTAT30, with frequency response analyser (FRA) software was

used. The frequency ranged from 100 kHz to 1 mHz with 5 points/decade, whereas the amplitude of the sinusoidal potential signal was 10 mV with respect to the open circuit potential in a steady state. The electrochemical system used for this purpose included graphite electrode (counter electrode), saturated Ag/AgCl electrode (reference electrode) and metal sheet (working electrode).

Also, the corrosion of the magnesium alloys was estimated by determining the volume of hydrogen evolved during the corrosion process. Samples for hydrogen gas collection were cut into square coupons with dimensions of 2 cm × 2 cm x 0.3 cm and horizontally immersed in 700 ml of quiescent test for 11 days in a beaker open to laboratory air at 20 ± 2 °C. The hydrogen evolved during the corrosion experiment was collected in a burette by a funnel above the corroding sample, as described by Song et al [14, 24, 25]. The experiments were run simultaneously and each sample was subjected to essentially the same temperature and exposure history.

The morphology of the attack on the corroded surface was examined at low magnification and a camera was used to take the photographic images. Once the test was finished, the corroded specimens were pickled in chromic acid to remove the corrosion products, then rinsed with isopropyl alcohol and dried in hot air in order to study the corrosion morphology

3. Results

3.1. Thermogravimetric analysis

Figure 1 compares the evolution in weight gain values with heating time at 200°C in air on the AZ31-O, AZ31-P, AZ61-O and AZ61-P specimens. AZ31-O specimen presents a linear increase in weight gain values with time, whereas AZ61-O specimen shows much lower weight gain. The oxide film on the AZ31-O specimen must surely be discontinuous and porous, possessing low protective properties; the oxygen should have free access to the reaction surface. Instead, the good oxidation resistance exhibited by the AZ61-O specimen indicates the presence of a protective film, in this case suggesting the building of a very compact film.

Fig. 1 also shows that the polished AZ31 and AZ61 specimens present much lower increases in weight gain than the corresponding specimens in the as-received condition, difference attributable to the uneven and probably defective oxide film present on the

as-received surfaces compared with the continuity of the oxide film formed on the polished surfaces.

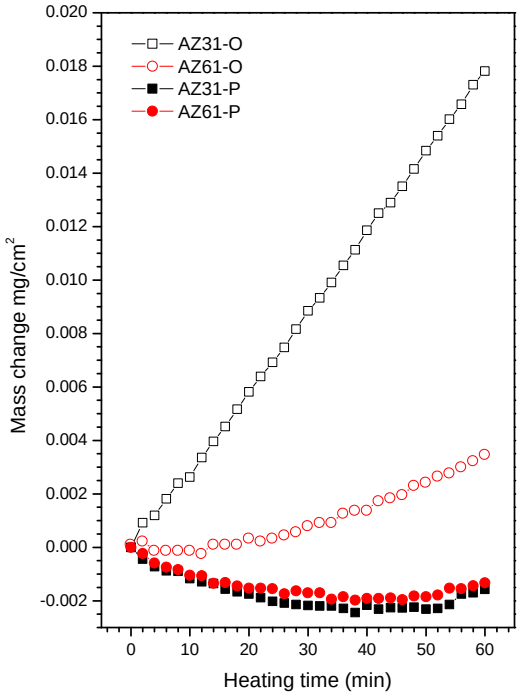

Fig. 1. *Evolution of weight gain values obtained in the AZ31 and AZ61 in as-received conditions alloys as a function of the time of heating at 200ºC in air compared with those of the same alloys in polished condition.*

About the thermo gravimetric (TG) curves for the polished specimens, that show weight loss, similar behaviour are found, occasionally, in the literature for the magnesium alloys exposed to air at relatively high temperatures. Czerwinski's results [22] have shown this behavior during the oxidation of AZ91 magnesium alloy at temperatures lower than 397ºC, but do not discuss the reason for such proceed. Also, Shih et al. [26] observed weight loss in the TG analysis of pure magnesium, which relate to the dehydration of brucite formed at low temperature on the metal surface. For our part, an adequate explanation for the weight loss in Fig.1 does not seem possible at present.

3.2. Morphology and microcomposition of the oxide layer formed on the surface of the AZ31 and AZ61 magnesium alloys after the heat treatment for different times.

Figure 2 compares the surface morphologies on the non-heated and heated for different times AZ31-O and AZ61-O specimens. As can be seen, the metallic surface of the non-heated AZ31-O specimen appears to be covered by a large number of white precipitated particles (Fig. 2a), whereas in the surface of the non-heated AZ61-O these particles are

not apparently visible (Fig. 2b). After 5 minutes of the heat treatment, attention is drawn to the significant presence of black zones on the surface of the oxide layer formed on the AZ61-O specimen (as marked by circles in Fig. 2d). In contrast, these black zones are hardly observed on the surface of the oxide layer formed on the AZ31-O specimen (Fig. 2c). By comparing Fig. 2d with Fig 2f and 2h for the AZ61-O specimen, it is apparent that the fraction of the surface covered by the black zones decreases gradually with the heating time.

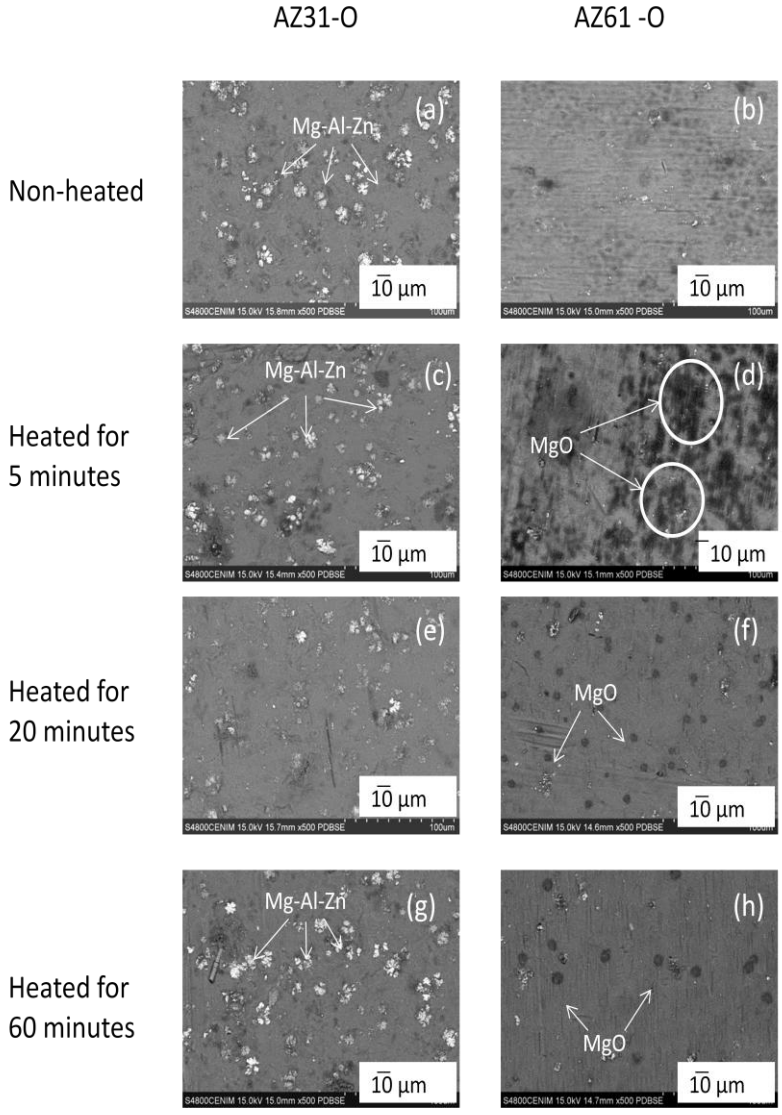

Fig. 2. *SEM surface morphologies for AZ31 (a, c, e, g) and AZ61 magnesium in as-received conditions alloys (b, d, f, h) non-heated (a, b) and heated for 5 min (c, d), 20 min (e, f) and 60 minutes (g,h) at 200ºC in air, respectively.*

EDX analysis of the AZ31-O specimen surface after heating for 60 minutes was performed for points labelled in Fig. 3 in order to investigate possible differences in composition between the white precipitated particles and the larger darker regions

associated with the α-Mg matrix. Atomic percentages and Al/(Al+Mg) ratios of the white particles obtained by EDX are presented in Table 2 and compared with the measurements made in the darker regions. In EDX analyses obtained on the white particles, attention is drawn to the increase in the Al, Zn and Mn content and the decrease in the Mg content compared to the darker regions.

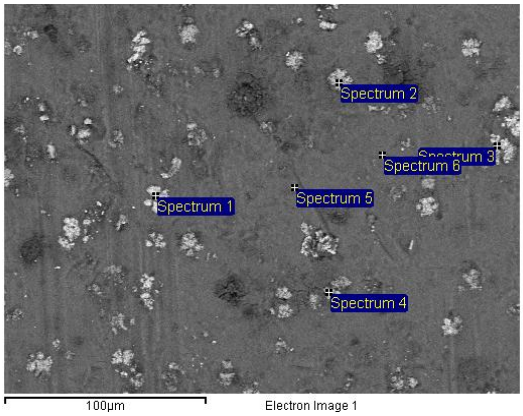

Fig. 3. *Micrograph illustrating locations of points for EDX spot analysis of the AZ31 magnesium in as-received condition alloy heated for 60 min at 200ºC in air. Spectrum 1, 2, 3 and 4 (white oxide nodules) and Spectrum 5 and 6 (Dark layer).*

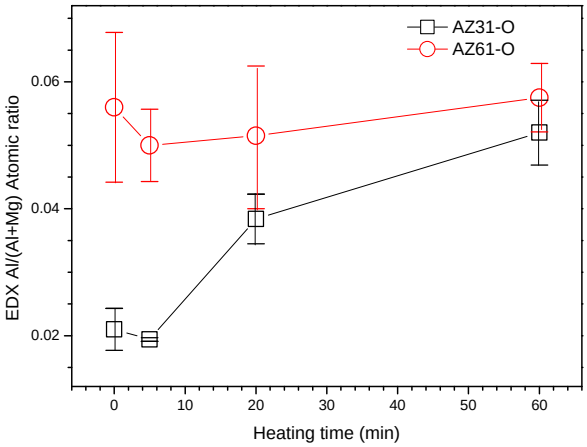

Fig. 4. *Variation in the Al/(Al+Mg) atomic ratio of the dark layer obtained by EDX on the surface of the AZ31-O and AZ61-O specimens as a function of the time of heating.*

Table 2. *Measurements of atomic composition by EDX on the surface of the AZ31-O heated for 60 minutes*

Element	White spots EDX (Average values from spectrum 1, 2, 3 and 4) (at.%)	Dark layer EDX[a] (Average values from spectrum 5 and 6) (at.%)
O	37.28 ± 5.12	13.27 ± 0.11
Mg	20.26 ± 7.68	81.73 ± 0.45
Al	13.86 ± 5.88	3.91 ± 0.43
Mn	1.75 ± 0.16	0.02 ± 0.03
Zn	26.49 ± 5.70	1.02 ± 0.11
Al/(Mg+Al)	0.41 ± 0.19	0.046 ± 0.005

Fig. 4 compares the variation in the Al/(Al+Mg) atomic ratio of the darker regions obtained by EDX on the surface of the AZ31-O and AZ61-O specimens as a function of the heating time. No significant differences in these ratios were observed in the AZ61-O specimen after different heating times compared with the non-heated specimen (Fig. 4). In contrast with the AZ61-O specimen, significantly higher Al/(Al+Mg) atomic ratio than the non-heated AZ31-O specimen and after 5 minutes of heat treatment were observed in the AZ31-O specimens heated for 20 and 60 minutes

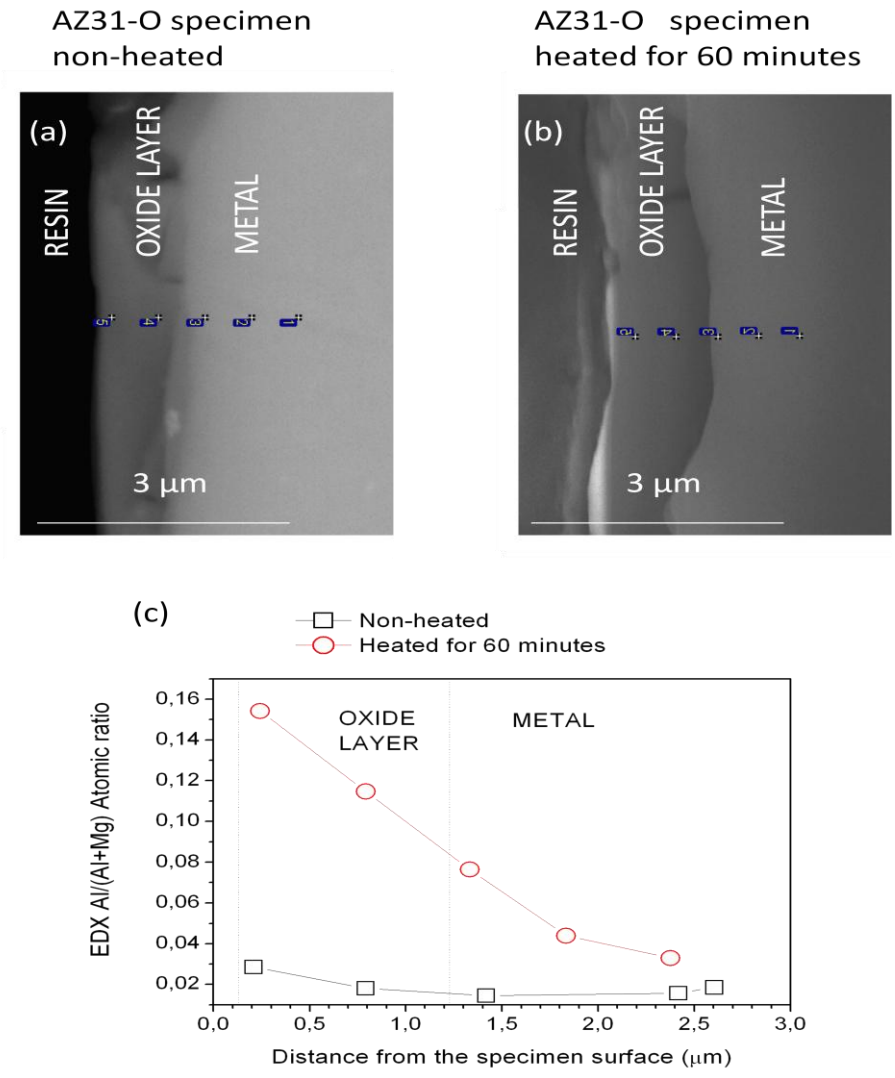

Fig. 5. *SEM morphology and variation in the Al/(Al+Mg) atomic ratio obtained by EDX on the cross section of the AZ31-O specimen non-heated (a) and heated for 60 minutes (b) at 200ºC in air.*

3.3. Changes in the chemistry of thermally oxidised films formed on AZ31 and AZ61 alloys in as-received condition with heating time

Fig.5 compares SEM images on the cross sections of the surface of the AZ31-O specimen non-heated (a) and heated for 60 minutes (b) and the Al/(Al-Mg) atomic ratios obtained by EDX (c). Fig. 5 c clearly reflects the trend towards an increase in Al concentration when approaching the oxidized surface. The enrichment far exceeds the concentration of Al in the bulk AZ31 alloy, as the Al content is increased from 3% to about 16% in the metal oxide film. On the other hand, in the non-heated specimen the Al concentration does not exceed 3% in any of the measurement points, which altogether supports the idea of an effect of heat treatment on the Al enrichment.

Figure 6 compares the atomic percentages of O, Mg, Al and Zn obtained by XPS on the surface of the AZ31-O and AZ61-O specimens and their variation with heating time. It is worth noting that after the heat treatment there was a marked decrease in the magnesium content (Fig. 6b) and an increase in oxygen and aluminium content (Figs. 6b and 6c respectively) on the surfaces of the AZ31-O specimens in comparison to the results obtained on the surfaces of the AZ61-O specimens.

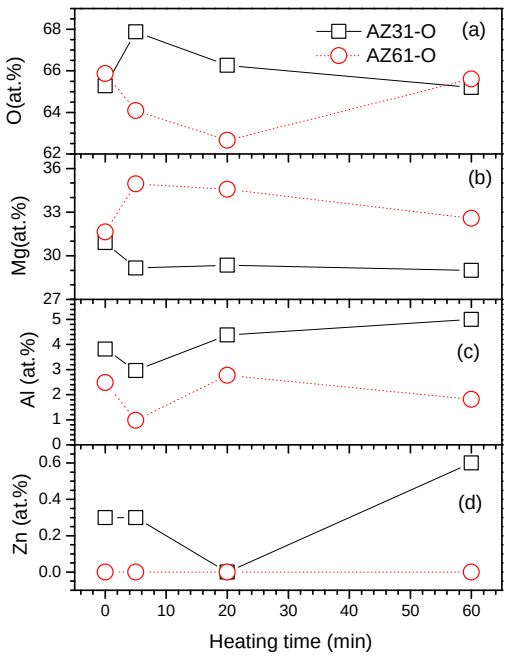

Fig. 6. *Variation in the Oxygen (a), Magnesium (b), Aluminium (c) and Zinc (d) atomic percentages obtained by XPS on the surface of the AZ31-O and AZ61-O specimens as a function of the time of heating*

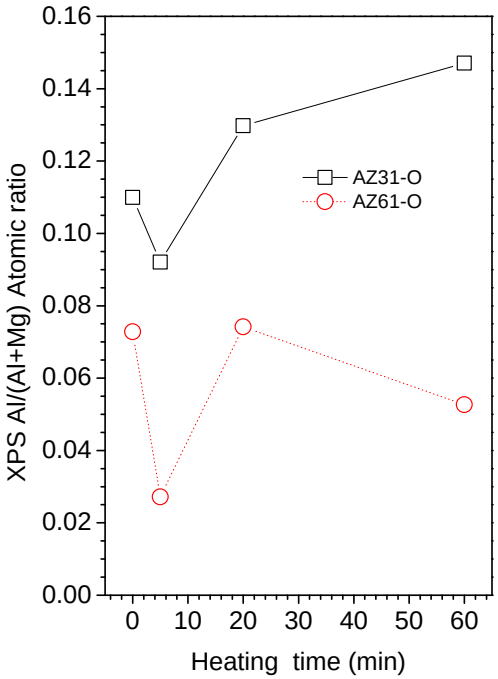

Fig. 7. *Variation in the Al/(Al+Mg) atomic ratio obtained by XPS on the surface of the AZ31-O and AZ61-O specimens as a function of the time of heating.*

Figure 7 compares the Al/(Al-Mg) atomic ratios obtained by XPS on the surface of the non-heated AZ31-O and AZ61-O specimens with those resulting from the heat treatment at a temperature of 200°C for different times. The Al/(Mg+Al) ratio determined by XPS is about 0.11 for the non-heated AZ31-O specimen surface (Fig. 6), which is much higher than the 0.03 value in the bulk alloys (Table 1). Heat treatment times of 60 minutes promotes an increase in this ratio on the surface of the AZ31-O specimen (Fig. 7). On the other hand, an important decrease is detected in the Al/(Mg+Al) ratio in the surface of the AZ61-O specimen heated for 5 minutes (Fig. 7), which suggests the preferential growth of a magnesium-rich film (magnesium oxides or hydroxides) that covers the non-heated surface. Longer heating times (20 and 60 minutes) lead to an increase in the Al/(Mg+Al) ratio on the AZ61-O (Fig. 7) that may be related with the enrichment in Al of the outer oxide layer formed at the shortest heating times. This significant aluminium enrichments detected by XPS on the surface of the AZ61-O specimen heated for 20 and 60 minutes respect to the AZ61-O specimen heated for 5 minutes (Fig. 7) are consistent with the decrease in the fraction of the surface covered by the black zones observed by SEM (Figs. 2d, 2f and 2h). In contrast, it is interesting to note the absence of significant variations of the Al/(Al+Mg) ratios detected by EDX in the oxide layer formed on the surface of the AZ61-O specimens with the heating time (Fig.4). It is worth mentioning that, while XPS gives the composition information of the very top surface oxide layer (thicknesses of only few nanometers), EDX gives information of the bulk of this layer (thicknesses of several micrometers).

Figure 8 shows the O1s (a) Mg 2p (b) Al 2s (c) and $Zn2p_{3/2}$ (d) XPS high resolution spectra obtained on the surface of the AZ31-O specimen after 5 minutes of heating. These spectra are representative of the similar spectra obtained on the surface of non-heated AZ31 and AZ61 alloys and after other heating times. The O1s spectrum (Fig. 8a) show the most intense component at a binding energy of 531.2 eV, associated to the presence of oxygen in the form of magnesium oxide, MgO [27-29], and another less intense component at a binding energy of 533.2 eV, which may be attributed to the presence of oxygen in magnesium hydroxide or $Al(OH)_3$.[30]. The Mg 2p spectrum (Fig. 8b) presents one single component associated to the presence of magnesium in the form of magnesium oxide or hydroxide (51.0 eV). [31, 32]. The Al 2s spectrum (Fig. 8c) may be fitted to one component at 119.5 eV due to the presence of Al^{3+}. Finally, The $Zn2p_{3/2}$ high resolution spectrum (Fig. 8d) may be fitted to one component with a binding energy of 1022.0 eV associated with the presence of Zn^{2+}.

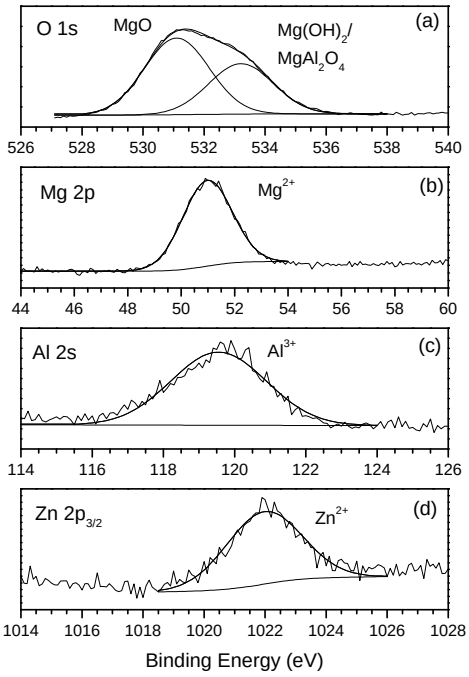

Fig. 8. *High resolution O1s (a), Mg2p (b), Al2s (c) and Zn2p$_{3/2}$ (d) XPS peaks obtained by XPS on the surface of the AZ31 alloy after 5 minutes of heating.*

3.4. Electrochemical measurements

3.4.1. Open circuit potentials

Fig.9 shows that the open circuit potential of the AZ31-O and AZ61-O specimens shifts towards more negative values than the non-heated specimens of reference. However, this effect is lost after 28 days immersion when the corrosion potentials of the heated specimens are increased to the potential of the non-heated ones.

3.4.2. Potentiodynamic polarization curves

Representative polarization curves of the specimens immersed in the saline solutions are displayed in Fig. 10. In many of the specimens tested the anodic branches almost coincide and are typically non-lineal. The differences between specimens are more apparent from the cathodic branches. In the AZ31-O specimens, the tendency of the cathodic branches of the heated specimens to show lower current intensities compared with the non-heated specimens suggests a protective effect of the heat treatment (Table 3)

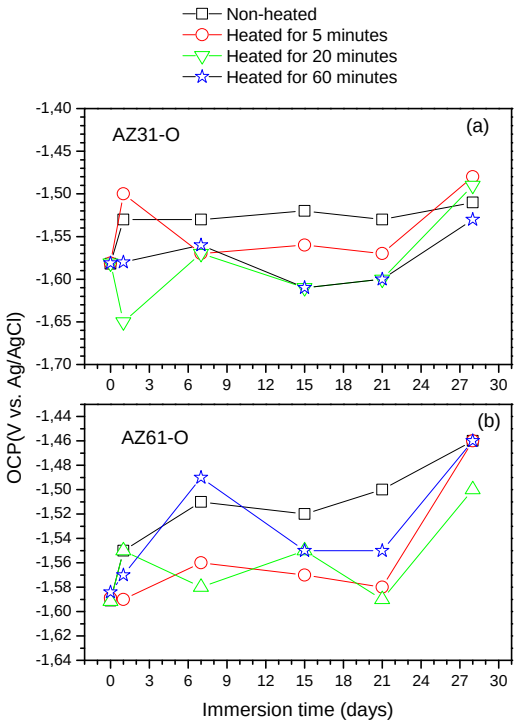

Fig. 9. *Variation of open circuit potential (OCP) values as a function of the time of heating and alloy type over 28 days immersion in 0.6 M NaCl.*

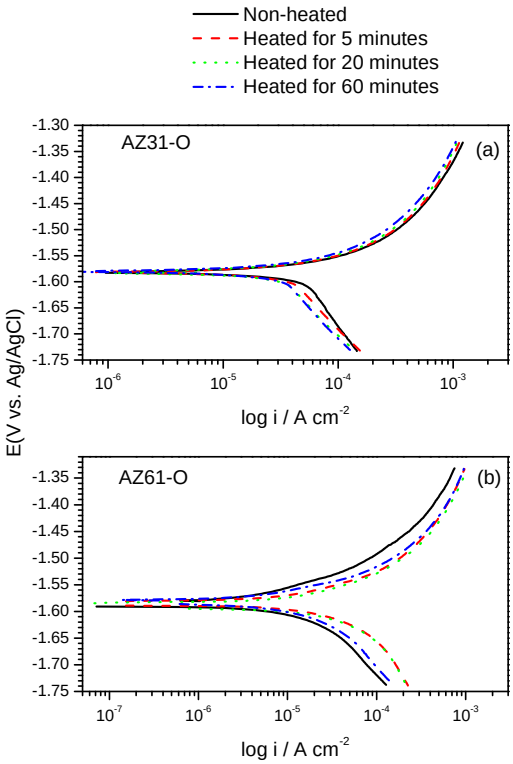

Fig. 10. *Variation of polarization curves for AZ31-O (a) and AZ61-O (b) as a function of heating in 0.6M NaCl.*

Table 3. *Data from polarization curves.*

Specimens	Ecorr ($V_{Ag/AgCl}$)	i_{corr} (10^{-5} A/cm^2)	Tafel slopes β_c (mV decade^{-1})
		AZ31-O	
Non-heated	-1.57	4.5	-230
Heated for 5 minutes	-1.57	3.5	-380
Heated for 20 minutes	-1.57	2.5	-380
Heated for 60 minutes	-1.57	2.1	-270
		AZ61-O	
Non-heated	-1.59	1.2	-270
Heated for 5 minutes	-1.59	3.5	-330
Heated for 20 minutes	-1.59	6	-260
Heated for 60 minutes	-1.58	2.6	-200

3.4.3. Electrochemical impedance measurements

The evolution of the corrosion process of the heat treated AZ31-O and AZ61-O specimens was monitored by means of impedance measurements with the specimens immersed in 0.6 M NaCl solution.

Nyquist diagrams in Fig. 11 show the presence of two capacitive loops, one at high frequencies (HF) and an inductive loop at low frequencies. In the literature about the corrosion of magnesium alloys is normal to associate the diameter of this capacitive loop in the HF region with the charge transfer resistance (R_t) of the corrosion process [33-35]. For the inductive behavior observed, an interpretation of this part of the impedance plot is immaterial in studies of electrochemical corrosion in which the kinetic information is estimated from the capacitive arc.

The R_t values corresponding to the HF capacitive loop were derived from the impedance data in the range 10^5 to 10 Hz using ZView software fitting method [36]. Corrosion current (i_{corr}) is inversely related to R_t through the Stern-Geary [37] equation:

$$i_{corr} = \frac{B}{R_t} \quad (1)$$

where the proportionality constant B can be usually calculated from both the anodic and cathodic Tafel slopes. However, due to the uncertainty in the β_a values from the polarization curves in this work, it was decided to use the constant B obtained empirically from the correlation between R_t measurements and weight loss data. Our previous investigation [18], yielded B values of around 65 mV for the AZ31 alloy and of around 120 mV for the AZ61 alloy.

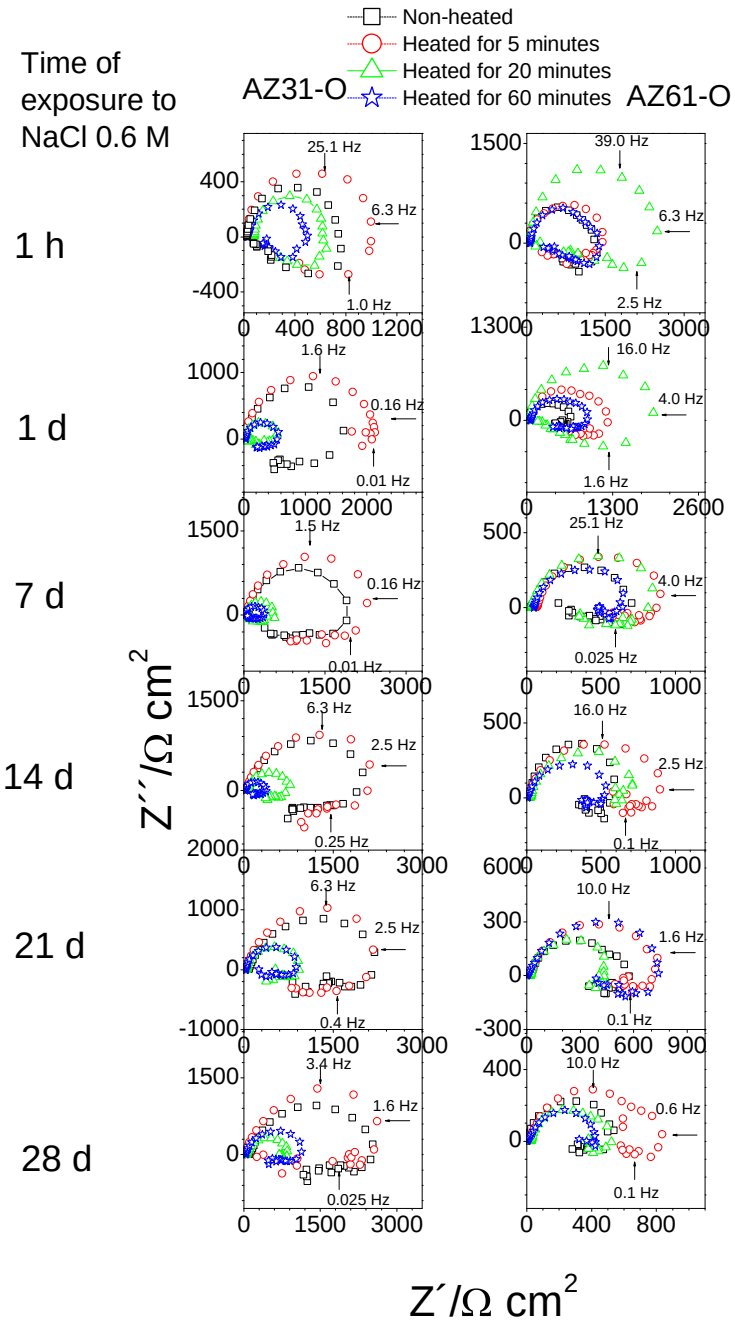

Fig. 11. *Variation in Nyquist plot for AZ31-O and AZ61-O specimens with immersion time (hours or days on the Y-axis) and with times of heating.*

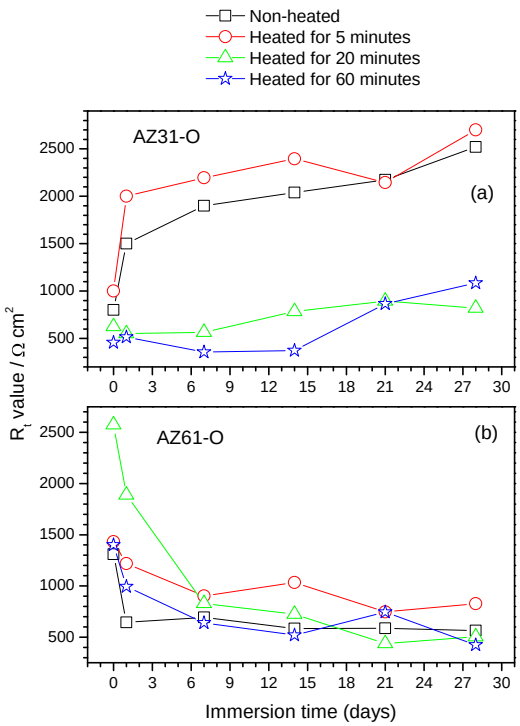

Fig. 12. *Variation in R_t values for AZ31-O (a) and AZ61-O (b) as a function of the time of heating and alloy type over 28 days immersion in 0.6M NaCl.*

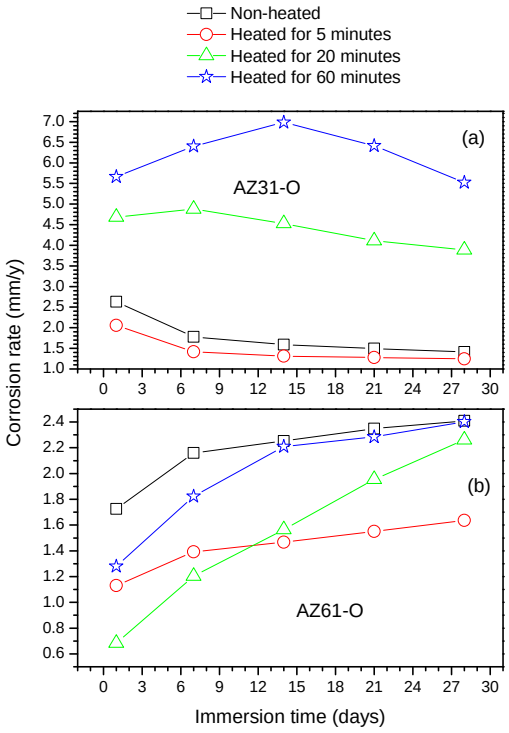

Fig. 13. *Variation in corrosion rates (mm/y) for AZ31-O (a) and AZ61-O (b) obtained from EIS as a function of the time of heating and alloy type over 28 days immersion in 0.6M NaCl.*

Fig. 12 shows the evolution of the R_t values deduced from the capacitive loop at high frequencies in function of immersion time in 0.6M NaCl solution. The corrosion current densities (mA/cm^2) values obtained from Eq. (1) were converted to corrosion rates (mm/y) in Fig.13 by considering Faraday's law and the resulting equation:

$$\text{corrosion rate} = 22.85\, i_{corr} \qquad (2)$$

The results show the corrosion rate variations with time over 28 days immersion. Taking the values for the non-heated or heated for 5 minutes AZ31-O specimens as reference, heat treatment for 20 and 60 minutes increases markedly the corrosion rate values (Fig. 13 a), while in the case of AZ61-O specimens (Fig. 13 b), little effect or a moderate decrease in the corrosion rate is observed.

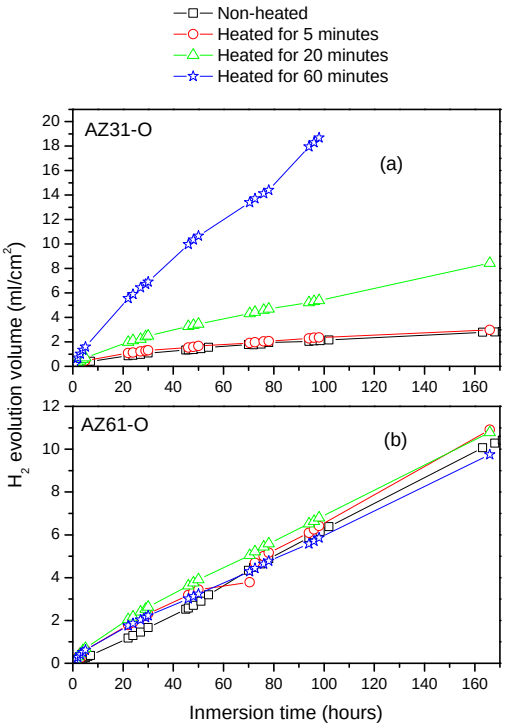

Fig. 14. *Variation in H_2 evolution volume values for AZ31-O (a) and AZ61-O (b) as a function of the times of heating and alloy type over 14 days immersion in 0.6M NaCl.*

Fig. 14 is instructive in showing the differences in the hydrogen volume data between alloys AZ31 and AZ61 over 7 days of immersion in 0.6 M NaCl. It is interesting to note that similar trends regarding the corrosion behaviour are deduced from these hydrogen evolution that from the electrochemical ones.

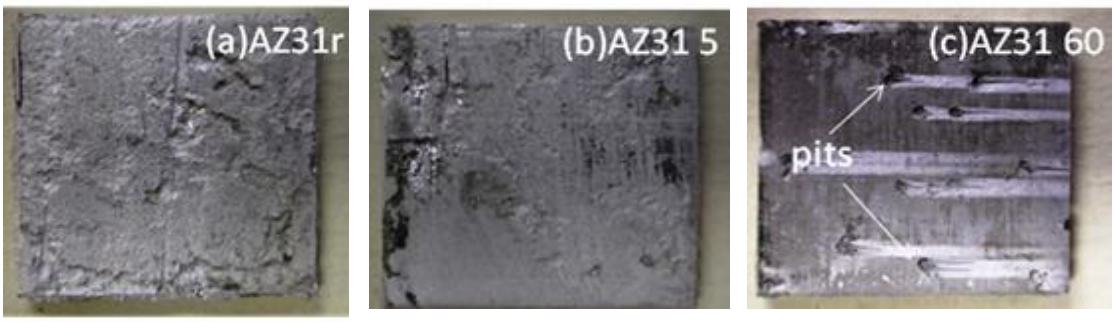

Fig. 15. *Representative macroscopic surface appearance of corroded AZ31-O specimens after 14 days of immersion in NaCl 0.6M and after corrosion product removal. (a) non-heated alloy (b) heated for 5 minutes and (c) AZ31 alloy heated for 60 minutes at 200ºC in air.*

Fig. 15 compares the macroscopic surface appearance of the corroded non-heated (a) and heated for 5 (b) and 60 minutes AZ31-O specimens (c) after 7 days of immersion in NaCl 0.6M and after corrosion product removal. In the test samples one can observe uniform attack on large areas of the exposed surface of the non-heated AZ31-O specimen or heated for 5 minutes (Fig. 15a and b). However, after 60 minutes (Figs. 15c) of heat treatment, some wide pits seem to cover the specimen surface. The appearance of deep craters and pits on the surface of corroded magnesium alloy specimen after heat treatment has been observed by Zhou et al [8] and Neill et al [38]. In general, there is a qualitative agreement between the presence or absence of pits on the surface of the corroded specimens (Fig. 15) and the corrosion data (Fig. 13a).

4. Discussion

4.1. Changes in chemical composition of the oxide layers grown on the surface of AZ31 and AZ61 alloys in as-received condition after heat treatment at 200°C

Figure 1 shows that the polished AZ31 and AZ61 specimens present much lower increases in weight gain during heat treatment than the corresponding specimens in the as-received surface condition. As can be seen in figure 1, 35-60 minutes of heating at 200ºC produces a very small weight gain, around only 0.6 μg/cm^2, which is similar for the two alloys. It is generally accepted that the growth of compact MgO films is controlled by solid sate diffusion through adherent oxide areas followed by the reaction with oxygen at the oxide/gas interface, hence a lack of easy-paths for fast Mg transport could be a possible explanation for a highly protective behaviour [22]. From Eq. (3) [39]:

$$D_L = 1.0 \times 10^{-6} \exp\left(\frac{-150000}{RT}\right) \text{ m}^2/\text{s} \qquad (3)$$

Diffusivity (D_L) of Mg within the MgO lattice at 473 K is as low as 2.67 x 10^{-23} m^2/s justifying negligible weight gain.

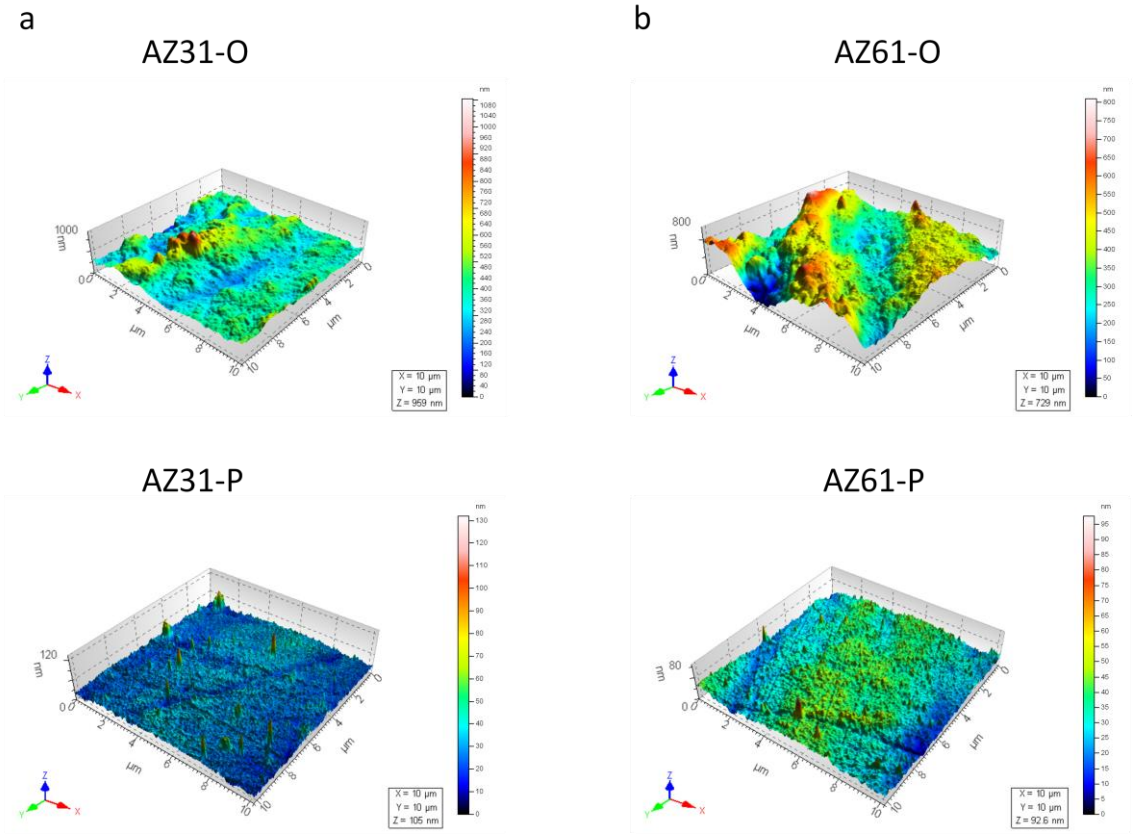

Fig. 16. *AFM images of the surfaces in the original (O) and polished (P) surface conditions for: (a) AZ31 alloy and (b) AZ61 alloy.*

Table 4. *Roughness values obtained with atomic force microscope. The values are average of four determinations.*

ORIGINAL SURFACE	RMS (nm)	AFTER POLISHING	RMS (nm)
AZ31	123.1	AZ31	7.3
AZ61	109.6	AZ61	5.6

This behavior is not detected in the case of the AZ31-O and AZ61-O specimens (Fig. 1) which tends to suggest that the increase in weight gain with the heat treatment is dependent of the initial surface condition of the studied alloys. As Table 4 shows, roughness values of the AZ31-O and AZ61-O specimens are more than ten times greater than for the AZ31-P and AZ61-P specimens. Nanometric scale details of the typical surface roughness exhibited by the tested specimens are given in Fig 16. The difference in weight gain with heating time between the as-received and polished surfaces (Fig. 1) may be in agreement with the very heterogeneous and likely defective surface layer present on the as-received surfaces (Fig. 16) compared to the continuity of the oxide films formed on the polished specimens. Similarly, in previous work [18, 20,

40] with the same alloys in 0.6M NaCl saline solution, an inhibiting effect of the homogeneous and continuous native oxide surface film formed on freshly polished samples was observed.

One point emerging from the set of the weight gain values (Fig. 1) is the clear tendency for AZ31-O specimen to present higher values than the AZ61-O specimen throughout the heat treatment.

It is important to note the close relationships between the difference in increases in weight gain values with heating time for AZ31-O and AZ61-O specimens and the differences in chemical composition observed by XPS and EDX in the oxide films formed on the surface of these alloys during heat treatment. Thus, figure 1 shows a very significant increase in the weight gain values and the EDX (Fig.4) and the XPS data (Fig.7) indicates an increase in the aluminium contents, while for the AZ61 alloy the increase in weight gain values is relatively small (Fig. 1) and only a slight increase in aluminium is detected on its surface (Figs. 4 and 7).This relationship appears to suggest that some common factor is acting on the mechanisms that determine both magnitudes. One immediate idea is that they may be directly related with the ease of diffusion of aluminium atoms towards the aforementioned surface. Moreau et al [41] have found that the volume diffusion coefficient for aluminium in magnesium can be determined using:

$$D_L = 3.39 \times 10^{-4} \exp\left(\frac{-135000}{RT}\right) \quad m^2/s \qquad (4)$$

which gives a value of 4.112×10^{-19} m^2/s at 200ºC. On the other hand, diffusivity of Al in the grain boundaries of the magnesium alloys is as high as 9.263×10^{-12} m^2/s at 200ºC [42]. The obtained values show that the volume diffusion coefficient is approximately 7 orders of magnitude less than the diffusion coefficient for the grain boundary. At 200ºC the process of Al surface segregation is controlled by grain boundary diffusion.

The microstructure of the non-heated AZ31 alloy is formed practically by an α matrix with Al in solid solution surrounded by grain boundary free of precipitates of β phase (Fig.17a). In contrast, the aluminium is distributed, forming part of the chemical composition of the β-phase precipitates in the grain boundary of the AZ61 alloy (Fig.17b). Available literature [43, 44] mentions that the presence of stable intermetallics at the grain boundary reduces the activity of atom diffusion along the

grain boundary. It is likely that blockage of the grain boundaries in the AZ61 alloy due to preferential precipitation of β phase inhibits the diffusion of aluminium solute along the grain boundary of the magnesium matrix at 200ºC compared to the AZ31 alloy. Also, this can probably explain the initial presence of the called" white spots" with high Al content on the surface of the AZ31-O specimen as a result of the manufacturing process and their absence on the AZ61-O specimen (Fig. 2).

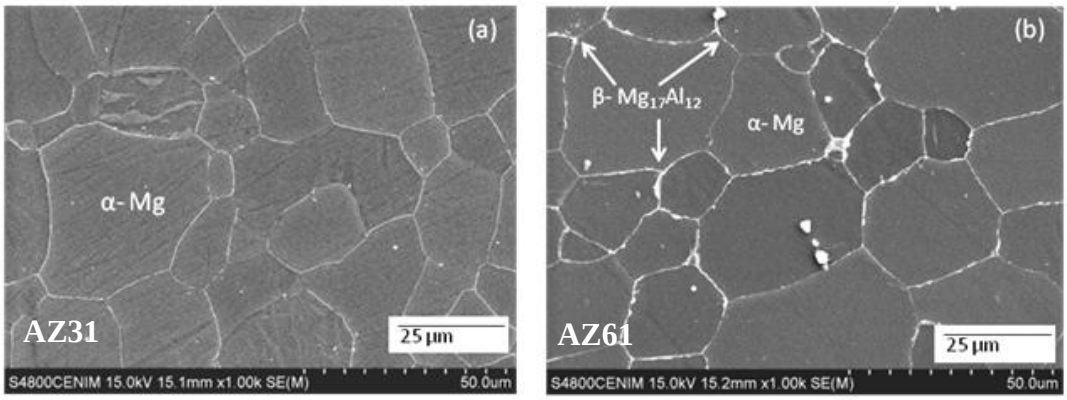

Fig.17. *SEM micrographs: (a) AZ31 alloy and (b) AZ61 alloy.*

The EDX (Fig.4 and 5c) and XPS analyses (Fig.7) suggests a considerable superficial aluminium species enrichment of the AZ31 alloy that had been heat treated. Growth of the oxide film requires the motion of reactants for some transport mechanism. In Mg-Al Alloys, diffusion rates of Mg and Al ions may influence their concentration in the oxide film formed on the alloy surface. According to Van Orman et al.[45], in the MgO (periclase) trivalent cations diffuse rapidly compared to divalent cations, behavior arising from the coulombic attraction between trivalent cations and cation vacancies; for this reason diffusion of Al^{3+} can be one order of magnitude faster than Mg^{2+} at the same conditions. This could favor the increases in Al concentration highlighted in the paper.

The above behavior agrees in the literature with Nordlien et al. results [46], which mention a sharp increase in the concentration of Al in the surface of the Mg-Al alloys.

In the case of the AZ61-O specimens, it is apparent that the fraction of the surface covered by black areas increases significantly after 5 minutes of heating (Fig. 2d). In the commercial magnesium alloys tested in this work there seems to be a direct relationship between the formation of MgO on the AZ61-O specimen during the initial stages of the heating process and the degree of microstructural complexity of the surface upon which

it forms. Fig. 14 shows a very significant presence of β intermetallic phase on the boundary of AZ61 (Fig. 17b) compared to its absence on AZ31 (Fig. 17a), suggesting that the two-phase nature of the alloy may play a significant role in the early stages of oxide formation [47].

4.2. Relationship between the chemistry of the oxide layers formed on the surface of magnesium alloys as a result of the heat treatment and their corrosion resistance in saline solutions.

It seems likely that some of the differences that have been revealed in the composition and characteristics of the oxide layers formed on the surfaces of the AZ31-O and AZ61-O specimens as a result of the heat treatment may have an impact on their corrosion behaviour. As commented earlier, the more significant features that have been observed on the oxide layer, depending on the type of alloy and heat treatment time, have been (a) the aluminium enrichment of the surface of the AZ31-O alloy after prolonged heat treatment time and (b) the absence of similar enrichments in the AZ61-O alloy.

Electrochemical impedance results (Figs. 12 and 13) and hydrogen evolution versus time curves (Fig.14) have provided information on the effect of experimental variables on the corrosion resistance of the specimens tested. For times of more than 1 hour up to the end of the immersion test, it is clear the trend of the AZ31-O specimen heated for 20 and 60 minutes to present lower R_t and higher corrosion rates than the other tested specimens for the same immersion times (Fig.12a and 13a). Many studies mention the beneficial effect of Al [46, 48-53], which may become the essential factor in determining the passivity of the surface, improving the resistance to local breakdown of the oxide and reducing the chance of chloride ions penetrating as far as the surface. In the literature [54], it is presumed that the Al_2O_3 component forms a continuous skeletal structure in an amorphous matrix, so that the film properties become predominantly determined by the protective properties of Al_2O_3, very superior to that of $Mg(OH)_2$. Curiously in our study, an opposite effect seems to be observed. Comparing the corrosion data (Figs 12a, 13a and 14a) with the chemical composition determined by EDX (Fig 4) and XPS (Fig 7) on the surface of the oxide layers resulting from the heat treatment, one can clearly see a tendency towards an increase in the corrosion rate (Fig.13a) values and an in the hydrogen volumes evolved (Fig. 14a) as the Al/(Al+Mg) ratio increases (Figs 4 and 7). This correspondence suggests an influence of the said enrichment in aluminium oxide/hydroxide of the surface of oxide layer as a result of the heat treatment on the corrosion process in posterior immersion in 0.6 M NaCl. Although

the presence of the Al_2O_3 component can serve as diffusion barrier in compact scale, it seems likely that the aluminium surface enrichment observed in our study after the heating process had a heterogeneous island structure without any special effect for corrosion protection [20]. The atomic ratio Al/(Mg+Al) determined by EDX on the surface of the AZ31-O alloy after 20 and 60 minutes of heating reached values of 0.04 and 0.06, which are two or three times higher than those non-heated or heated for 5 minutes specimens (Fig.4). It is probable that this surface enrichment in aluminium over prolonged heating periods contributes to a significant decrease in the aluminium content of the primary α-Mg matrix in the region close to the sheet surface. According with Song et al [5], Zhou et al [8] and Asmussen et al [55] it may be speculated that the development of an alloy layer of low Al content immediately beneath the oxide film makes the α matrix more active causing an increase in the corrosion rate.

Finally, in the case of the AZ61-O specimens, it is interesting to note the absence of significant variations in the corrosion rate, (Fig.13b) or in the volumes of hydrogen evolved (Fig. 14b) as a function of the heating time, where the EDX and XPS analyses (Figs.4 and 7, respectively) have revealed Al contents on the heated specimens similar to those observed on the non-heated alloy or in the bulk alloy (Table 1). This fact tends to support the idea that the aluminium incorporation in the magnesium oxide film that covers the surface of the magnesium alloys after the heat treatment plays a fundamental part in the observed corrosion rate.

5. Conclusions

SEM/EDX and XPS analyses have revealed notable differences in the oxide films formed on the surface of AZ31 and AZ61 alloys in as-received condition as a result of their heating in air at a temperature of 200°C for a time of 5 minutes to 1 hour. SEM and EDX analyses shows a larger fraction of the AZ31 alloy surface covered by precipitates, mainly composed by a mixture of Al_2O_3 and ZnO, than the AZ61 alloy surface. XPS analysis has revealed considerable superficial aluminium species enrichment of the AZ31 alloy owing to the heat treatment. Close to four times higher aluminium oxide contents have been found in these layers compared to the bulk content. Curiously, this phenomenon has not been detected in the AZ61 alloy subjected to identical treatment, which has higher aluminium content in the bulk composition

It seems likely that the heterogeneous structure associated with the second-phase played a decisive role in the enrichment phenomenon. The practically nil presence of β-phase

on the AZ31 alloy favours the diffusion of aluminium atoms along the grain boundaries towards the outer surface, where they precipitate in the form of Al_2O_3. This result contrast with the presence of β-phase on the AZ61 alloy, preferentially along the grain boundaries, which may act as a barrier for diffusion of aluminium towards the outermost surface through the heating treatment.

EIS measurements in the interval of between 1 h and 28 days of immersion in 0.6M NaCl solution have allowed to relate the chemical composition of the oxide films formed as a result of the heating treatment with the corrosion resistance of the alloys. It is to point out the notable increase in corrosion rate of the AZ31 alloy after 20 or 60 minutes of heat treatment compared to same alloy non-treated or only treated for 5 minutes. In contrast, no significant changes have been observed in the case of the heat treated AZ61 alloy

Acknowledgment

We wish to express our gratitude to Prof. S. Feliu for several clarifying and stimulating discussions during the course of this work. Also, the authors gratefully acknowledge the financial support for this work from the Ministry of Science and Innovation of Spain (MAT 2009-13530)

References

[1] M.C. Zhao, M. Liu, G.L. Song, A. Atrens, Influence of the beta-phase morphology on the corrosion of the Mg alloy AZ91, Corros. Sci. 50 (2008) 1939-1953.
[2] M.C. Zhao, M. Liu, G.L. Song, A. Atrens, Influence of homogenization annealing of AZ91 on mechanical properties and corrosion behavior, Adv. Eng. Mater. 10 (2008) 93-103.
[3] C.L. Liu, Y.C. Xin, G.Y. Tang, P.K. Chu, Influence of heat treatment on degradation behavior of bio-degradable die-cast AZ63 magnesium alloy in simulated body fluid, Mater. Sci. Eng., A 456 (2007) 350-357.
[4] T. Beldjoudi, C. Fiaud, L. Robbiola, Influence of homogenization and artificial aging heat-treatments on corrosion behavior of Mg-Al alloys, Corrosion 49 (1993) 738-745.
[5] G.L. Song, A.L. Bowles, D.H. StJohn, Corrosion resistance of aged die cast magnesium alloy AZ91D, Mater. Sci. Eng., A 366 (2004) 74-86.
[6] N.N. Aung, W. Zhou, Effect of heat treatment on corrosion and electrochemical behaviour of AZ91D magnesium alloy, J. Appl. Electrochem. 32 (2002) 1397-1401.
[7] J.D. Majumdar, U. Bhattacharyya, A. Biswas, I. Manna, Studies on thermal oxidation of Mg-alloy (AZ91) for improving corrosion and wear resistance, Surf. Coat. Technol. 202 (2008) 3638-3642.
[8] W. Zhou, T. Shen, N.N. Aung, Effect of heat treatment on corrosion behaviour of magnesium alloy AZ91D in simulated body fluid, Corros. Sci. 52 (2010) 1035-1041.
[9] L.Q. Zhu, W.P. Li, D.D. Shan, Effects of low temperature thermal treatment on zinc and/or tin plated coatings of AZ91D magnesium alloy, Surf. Coat. Technol. 201 (2006) 2768-2775.

[10] H.Y. Hsiao, P. Chung, W.T. Tsai, Baking treatment effect on materials magnesium alloy, Corros. Sci. 49 (2007) 781-793.
[11] Y. Zhao, G.S. Wu, J. Jiang, H.M. Wong, K.W.K. Jeung, P.K. Chu, Improved corrosion resistance and cytocompatibility of magnesium alloy by two stage cooling in thermal treatment, Corros. Sci. 59 (2012) 360-365.
[12] N.N. Aung, W. Zhoy, Effect of grain size and twins on corrosion behavior of AZ31B magnesium alloy, Corros. Sci. 52 (2010) 589-594.
[13] E. Aghion, N. Lulu, The effect of skin characteristics on the environmental behavior of die cast AZ91 magnesium alloy, J. Mater. Sci. 44 (2009) 4279-4285.
[14] G. L. Song, A. Atrens, M. Dargusch, Influence of microstructure on the corrosion of diecast AZ91D, Corros. Sci. 41 (1999) 249-273.
[15] B.L. Yu, J.Y. Uan, Correlating the microstructure of the die-chill skin and the corrosion properties for a hot-chamber die-cast AZ91D magnesium alloy, Mater. Trans. A. 36A (2005) 2245-2252.
[16] W. Zhang, S. Jin, E. Ghali, R. Tremblay, Skin and bulk corrosion properties of die cast and thixocast AZ91D magnesium alloy in 0.05M NaCl solution, Can. Metall. Q. 45 (2006) 181-188.
[17] G.L. Song, Z.Q. Xu, The surface, microstructure and corrosion of magnesium alloy AZ31 sheet, Electrochim. Acta 55 (2010) 4148-4161.
[18] S. Feliu Jr., C. Maffiotte, A. Samaniego, J.C. Galvan, V. Barranco, Effect of the chemistry and structure of the native oxide surface film on the corrosion properties of commercial AZ31 and AZ61 alloys, Appl. Surf. Sci. 257 (2011) 8558-8658.
[19] M.F. Lopez, J.A. Jimenez, A. Gutierrez, XPS characterization of surface modified titanium alloys for use as biomaterials, Vacuum 85 (2011) 1076-1079.
[20] S. Feliu Jr., C. Maffiotte, A. Samaniego, J.C. Galvan, V. Barranco, Effect of naturally formed oxide films and other variables in the early stages of Mg-alloy corrosion in NaCl solution, Electrochim. Acta 56 (2011) 4454-4565.
[21] L.P.H. Jeurgens, M.S. Vinodh, E.J. Mittemeijer, Initial oxide-film growth on Mg-based MgAl alloys at room temperature, Acta Mater. 56 (2008) 4621-4634.
[22] F. Czerwinski, The oxidation behaviour of an AZ91D magnesium alloy at high temperatures, Acta Mater. 50 (2002) 2639-2654.
[23] C.D. Wagner, L.E. Davis, M.V. Zeller, J.A. Taylor, R.H. Raymond, L.H. Gale, Empirical atomic sensitivity factors for quantitative-analysis by electron-spectroscopy for chemical-analysis, Surf. Interface Anal. 3 (1981) 211-225.
[24] G. Song, A. Atrens, D. Stjohn, J. Naim, Y. Li, The electrochemical corrosion of pure magnesium in 1 N NaCl, Corros. Sci. 39 (1997) 855-875.
[25] G.L. Song, A. Atrens, X.L. Wu, B. Zhang, Corrosion behaviour of AZ21, AZ501 and AZ91 in sodium chloride, Corros. Sci. 40 (1998) 1769-1791
[26] T.S. Shih, J.B. Liu, P.S. Wei, Oxide films on magnesium and magnesium alloys, Mater. Chem. and Phys. 104 (2007) 497-504.
[27] H.B. Yao, Y. Li, A.T.S. Wee, An XPS investigation of the oxidation/corrosion of melt-spun Mg, Appl. Surf. Sci. 158 (2000) 112–119.
[28] V. Fournier, P. Marcus, I. Olefjord, Oxidation of magnesium, Surf. Interface Anal. 34 (2002) 494-497.
[29] J. Kim, K.C. Wong, P.C. Wong, S.A. Kunlich, J.B. Metson, K.A.R. Mitchell, Characterization of AZ91 magnesium alloy and organosilane adsorption on its surface, Appl. Surf. Sci. 253 (2007) 4197-4207.
[30] N.C. Hosking, M.A. Ström, P.H. Shipway, C.D. Rudd, Corrosion resistance of zinc-magnesium coated steel, Corros. Sci. 49 (2007) 3669-3695.
[31] M. Liu, P. Shmutz, S. Zanna, A. Seyeux, H. Ardelean, G. Song, A. Atrens, P. Marcus, Electrochemical reactivity, surface composition and corrosion mechanisms of the complex metallic alloy Al_3Mg_2, Corros. Sci. 52 (2010) 562-578.
[32] M Liu, S Zanna, H Ardelean, I Frateur, P Schmutz, G Song, A Atrens, P Marcus, A first quantitative XPS study of the surface films formed, by exposure to water, on Mg and on the Mg-Al intermetallics: Al_3Mg_2 and $Mg_{17}Al_{12}$, Corros. Sci. 51 (2009) 1115-1127.
[33] N. Pebere, C. Riera, F. Dabosi, Investigation of magnesium corrosion in aerated sodium-sulfate solution by electrochemical impedance spectroscopy, Electrochim. Acta, 35 (1990) 555-561.
[34] G.I. Makar, J. Kruger, Corrosion studies of rapidly solidified magnesium alloys, J. Electrochem. Soc. 137 (1990) 414-421.

[35] S. Mathieu, C. Rapin, J. Hazan, P. Steinmetz, Corrosion behaviour of high pressure die-cast and semi-solid cast AZ91D alloys, Corros. Sci. 44 (2002) 2737-2756.
[36] ZView software, Version 3.1c (Scribner Associates Inc), Southern Pines, NC, USA
[37] M. Stern, A. L. Geary, Electrochemical polarization1. A theoretical analysis of the shape of polarization curves, J. Electrochem. Soc. 104 (1957) 56-63.
[38] W.C. Neil, M. Forsyth, P.C. Howlett, C.R. Hutchinson, B.R.W. Hinton, Corrosion of heat treated magnesium alloy ZE41, Corros. Sci. 53 (2011) 3299-3308.
[39] C. Lea, C. Molinari, Magnesium diffusion, surface segregation and oxidation in Al-Mg alloys, J. Mater. Sci. 19 (1984). 2336-2352.
[40] A. Samaniego, I. Llorente, S. Feliu Jr., Combined effect of composition and surface condition on corrosion behaviour of magnesium alloys AZ31 and AZ61, Corros. Sci. 68 (2012) 66-71.
[41] G. Moreau , J.A. Cornet , D. Calais, Acceleration de la diffusion chimique sous irradiation dans le systeme aluminium-magnesium, J. Nucl.Mater. 38 (1971) 197-202.
[42] K.N. Braszczynska-Malik. Discontinuous and continuous precipitation in magnesium-aluminium type alloys, J. Alloys Compd 477 (2009) 870-876.
[43] B. Kim, B. Kang, Y. Park, I. Park, Influence of Pd addition on the creep behavior of AZ61 magnesium alloy, Mater. Sci. Eng., A 528 (2011) 5747-5753.
[44] A. Srinivasan, J. Swaminathan, M.K. Gunjan, U.T.S. Pillai, B.C. Pai, Effect of intermetallic phases on the creep behavior of AZ91 magnesium alloy, Mater. Sci. Eng., A 527 (2010) 1395-1403.
[45] J.A. Van Orman, K.L. Crispin, Diffusion in oxides, Rev. Mineral. Geochem. 72 (2010) 757–825.
[46] J.H. Nordlien, K. Nisancioglu, S. Ono. N. Masuko, Morphology and structure of oxide films formed on MgAl alloys by exposure to air and water, J. Electrochem. Soc. 143 (1996) 2564-2572.
[47] S.J. Splinter, N.S. McIntyre, The initial interaction of water-vapor with mg-al alloy surfaces at room-temperature, Surf. Sci. 314 (1994) 157-171
[48] S. Feliu Jr., M.C. Merino, R. Arrabal, A.E. Coy, E. Matykina, XPS study of the effect of aluminium on the atmospheric corrosion of the AZ31 magnesium alloys, Surf. Interface Anal. 41 (2009) 143-150.
[49] R. Lindstrom, J.E. Svensson, L.G. Johansson, The influence of carbon dioxide on the atmospheric corrosion of some magnesium alloys in the presence of NaCl, J. Electrochem. Soc. 149 (2002) B 103 - B 107.
[50] M. Liu, P.J. Uggowitzer, A.V. Nagasekhar, P. Schmutz, M. Easton, G. L. Song, A. Atrens, Calculated phase diagrams and the corrosion of die-cast Mg-Al alloys, Corros. Sci. 51 (2009) 602-619.
[51] A. Pardo, M.C. Merino, A.E. Coy, R. Arrabal, F. Viejo, E. Matykina, Corrosion behaviour of magnesium/aluminium alloys in 3.5 wt% NaCl, Corros. Sci. 50 (2008) 823-834.
[52] M. Jönsson, D. Persson, R. Gubner, The initial steps of atmospheric corrosion on magnesium alloy AZ91D, J. Electrochem. Soc. 154 (2007) C684-C691.
[53] N. Hara, Y. Kobayashi, D. Kagaya, N. Akao, Formation and breakdown of surface films on magnesium and its alloys in aqueous solutions, Corros. Sci. 49 (2007) 166-175.
[54] J.H.Nordlien, S. Ono, N. Masuko, K. Nisancioglu**,** A TEM investigation of naturally formed oxide films on pure magnesium, Corros. Sci. 39 (1997) 1397-1414.
[55] R.M. Asmussen, P. Japuki, M. Danaie, G.A. Botton, D.W. Shoesmith, Tracking the corrosion of magnesium sand cast AM50 alloy in chloride environments, Corros. Sci. 75 (2013) 114-122.

The Effect of $NaHCO_3$ Treatment Time on the Corrosion Resistance of Commercial Magnesium Alloys AZ31 and AZ61 in 0.6 M NaCl Solution.

Sebastián Feliu (Jr)[a], Alejandro Samaniego[a], A.A. El-Hadad[a] and Irene Llorente[a].

[a]Centro Nacional de Investigaciones Metalúrgicas CSIC, Avda. Gregorio del Amo 8, 28040 Madrid, Spain.

Corrosion Science 67 (2013) 204–216

Abstract

This paper studies the chemical composition and structure of the conversion coatings formed during immersion on saturated aqueous $NaHCO_3$ solution treatment on the surface of as-received commercial AZ31 and AZ61 magnesium alloys with a view to a better understanding of their protective properties. The great uniformity and the significant increase in the amount of aluminium oxides and hydroxides observed on the surface of the conversion coating of the AZ61 alloy after 10 or 60 minutes of treatment (about 30% higher Al atomic contents) seems to improve the corrosion resistance

Keywords: A. Magnesium; B. XPS; B. SEM; C. Passivity; C. segregation.

1. Introduction

Materials chosen for the study are Mg-Al alloys which have aroused a great deal of scientific and technological interest over the past two decades. From a practical point of view, magnesium has the lowest density of all structural metals, making it highly attractive for use in the automotive, aerospace, IT and electronics industries, as well as in the development of new biomaterials for orthopaedic and cardiovascular applications, where weight plays a decisive role. However, as magnesium is one of the most chemically active metals, insufficient resistance to atmospheric and aqueous corrosion sometimes limits its applications. Therefore it is desirable to have the most complete information possible on the factors that influence the corrosion of these magnesium base materials. This work seeks to contribute to such information.

In our previous studies [1-3], we observed that the chemical composition of the corrosion layer formed during atmospheric exposure [1] or under continuous condensation conditions [2, 3] may affect the corrosion behaviour of magnesium alloys. Using XPS analysis, notable differences have been shown in the naturally formed films on the surface of commercially pure magnesium and AZ31, AZ80 and AZ91D magnesium alloys stored at room temperature. In the joint XPS analysis and gravimetric measurements, attention was drawn to the coincidence of increased corrosion resistance of the magnesium alloy and higher amount of magnesium carbonate measured on their surface. Wang et al [4] commented that the formation of a carbonate product layer provides better passivation of the magnesium alloy surfaces and slows down chloride-induced corrosion in the passivation zone. Following the idea that the amount of carbonate on the surface film may provide resistance to the initiation and propagation of magnesium corrosion, the present study investigates the possibilities of improving corrosion resistance by chemical treatment of the alloys with a saturated aqueous $NaHCO_3$ solution.

Today's eco-awareness coupled with the rapid growth of Mg die-casting applications in the automotive industry motivates the search for environmentally friendly treatments which enhance the corrosion resistance of magnesium alloy surfaces. Among the various surface treatments, chemical conversion treatments are easy to perform and cost-effective [5]. Additionally, these chemical conversion coatings may be used as a pre-treatment to improve the adhesion or corrosion resistance of subsequent paint or organic layers to the surface of the magnesium alloy substrate [6]. There are many studies in the literature on the conversion treatment of Mg alloys in aqueous HCO_3^-

/CO_3^{2-} carbonate solutions [6-13], which are often based on the analysis of the results obtained using conventional techniques in material characterization (SEM/EDX, FTIR,TEM or DRX). It is far more unusual, to find studies about the effects of the thin films on the external surface of the conversion coating (thicknesses of about 3nm) formed in contact with aqueous HCO_3^-/CO_3^2 solutions [12,13]. It seems of particular scientific/technological interest to obtain information on the chemical composition of this outer thin film because surface enrichments of the alloying elements may significantly affect the corrosion susceptibility of the conversion coating. The present work seeks to contribute to the knowledge on the effect of the concurrent processes of chemical segregation and preferential precipitation on the development of the conversion coating.

Although coating by chemical conversion in carbonic acid solution is a relatively clean method, it takes 2 to 24 hours to form on Mg alloy substrates [6, 8-13]. Therefore, some fundamental studies on this type of coatings should aim to reduce the treatment time [12].

The objectives of this research are as follows:

1. To study the chemical changes on the surface of the conversion coating formed on the AZ31 and AZ61 alloys induced by treatments with saturated aqueous $NaHCO_3$ solution in an attempt to find relationships between the chemistry of these outer thin films, the type of alloy and the duration of treatment.

2. To contribute to better understanding of the relationship between the surface chemistry of the conversion coatings and their corrosion resistance in saline solutions.

2. Material and methods

The chemical compositions of the tested magnesium alloys, AZ31 and AZ61, are listed in Table 1. They were manufactured and supplied in 3 mm thick plates by Magnesium Elecktron Ltd. The surfaces of the samples were untreated, having been cleaned only with distilled water and dried with hot air.

The carbonate coating was formed chemically at room temperature, based on previous work by Al-Abdullat [14]. The substrates were immersed into 4 litres of aqueous

$NaHCO_3$ solution at a concentration of 9 mass%, or saturation. The surface treatment was allowed to proceed for a given time at laboratory temperature, followed by rinsing with distilled water and then air dried.

Table 1. *Chemical composition of Mg-Al alloys (wt%)*

Alloy	Al	Zn	Mn	Si	Cu	Fe	Ni	Ca	Zr	Others
AZ31	3.1	0.73	0.25	0.02	<0.001	0.005	<0.001	0.0014	<0.001	<0.30
AZ61	6.2	0.74	0.23	0.04	<0.001	0.004	<0.001	0.0013	<0.001	<0.30

Photoelectron spectra were recorded using a Fisons MT500 spectrometer equipped with a hemispherical electron analyser (CLAM 2) and an Mg Kα X-ray source operated at 300 W. The samples were fixed on small flat discs supported on an *XYZ* manipulator placed in the analysis chamber. The residual pressure in this ion-pumped analysis chamber was maintained below 10^{-8} torr during data acquisition. The spectra were collected for 20–90 minutes, depending on the peak intensities, at a pass energy of 20 eV, which is typical of high-resolution conditions. The intensities were estimated by calculating the area under each peak after smoothing and subtraction of the S-shaped background and fitting the experimental curve to a combination of Lorentzian and Gaussian lines of variable proportions. Although specimen charging was observed, it was possible to determine accurate binding energies (BEs) by referencing to the adventitious C1s peak at 285.0 eV. The atomic ratios were computed from the peak intensity ratios and the reported atomic sensitivity factors [15]. The measurements were performed at take-off angles of 45° with respect to the sample surface. The sampled areas were 1 x 1 mm^2.

Two etching reagents were used: (a) nital 2%, 2 ml HNO_3 + 98 ml H_2O, to reveal the constituents and general microstructure of non-treated alloy AZ61, and (b) 4.6 g picric acid + 10 ml acetic acid + 70 ml ethanol + 10 ml H_2O to reveal the grain boundaries of non-treated alloy AZ31.

The tested specimens were examined by scanning electron microscopy (SEM) using a JEOL JXA 840A unit operating with Rontec EDR288 software for EDX spectra acquisition and image digitalisation.

The corrosion of magnesium and its alloys was estimated by determining the volume of hydrogen evolved during the corrosion process. Samples for hydrogen gas collection, to

characterise corrosion rate during solution immersion, were cut into square coupons with dimensions of 2 cm × 2 cm x 0.3 cm, and vertically immersed in 700 ml of quiescent test solution for 30 days in a beaker open to laboratory air at 20 ± 2 °C. All of the specimen surface has been exposed to the corrosion test. The hydrogen evolved during the corrosion experiment was collected in a burette by a funnel above the corroding sample, as described by Song et al [16-18]. All these experiments were run simultaneously and each sample was subjected to essentially the same temperature and exposure history

The morphology of the attack on the corroded surface was examined at low magnification and a camera was used to take the photographic images. Once the test was finished, the corroded specimens were stripped to eliminate corrosive products remaining on the surface, then rinsed with isopropyl alcohol and dried in hot air in order to study the corrosion morphology.

Electrochemical impedance measurements were conducted in 0.6 M NaCl during 14 days of exposure at room temperature (25ºC). An AUTOLAB potentiostat, model PGSTAT30, with frequency response analyser (FRA) software was used. The frequency ranged from 100 kHz to 1 mHz with 5 points/decade, whereas the amplitude of the sinusoidal potential signal was 10 mV with respect to the open circuit potential. A typical three-electrode setup was employed: Ag/AgCl and graphite were used as reference and counter electrodes, respectively, and the material under study was the working electrode. The exposed area of the working electrode was 9 cm^2.

3. Results

3.1. XPS analysis of the chemical composition of the surface of the AZ31 and AZ61 magnesium alloys after $NaHCO_3$ treatment for different times

In Fig.1 the evolution of the atomic percentages of C, O, Mg, Al and Zn obtained by XPS on the surfaces of the AZ31 and AZ61 alloys were compared to the treatment times in saturated $NaHCO_3$ solution. It is worth noting that after 30 minutes of treatment there was a marked decrease in the oxygen and aluminium content (Figs. 1b and 1d respectively) and an increase in carbon content on the surfaces of the AZ31 and AZ61 alloys (Fig. 1a) in comparison to the results obtained after other treatment times.

Fig. 2 compares the high resolution C1s spectra obtained on the surface of the AZ31 alloy after 10 minutes (a), 30 minutes (b), 60 minutes (c) and 360 minutes (d), with the AZ61 alloy treated for similar treatment times (Figs. 2e-2h). The spectra can be fitted using two components at different binding energies: at 285.0 eV, which may be associated with the presence of C-C/C-H groups; and a less intense component about 4.5–5.0 eV higher which is associated with the presence of magnesium carbonate [19]. The first component, C-C/C-H groups, appears on the outer surface (<3 nm in thickness) of almost any metal in contact with the atmosphere at room temperature, irrespective of its composition. On the surfaces of the AZ31 and AZ61 alloys there is a notable increase in the intensity of the second component on the sample treated for 30 minutes (Figs. 2b and 2f) compared to other immersion times (10, 60 and 360 minutes).

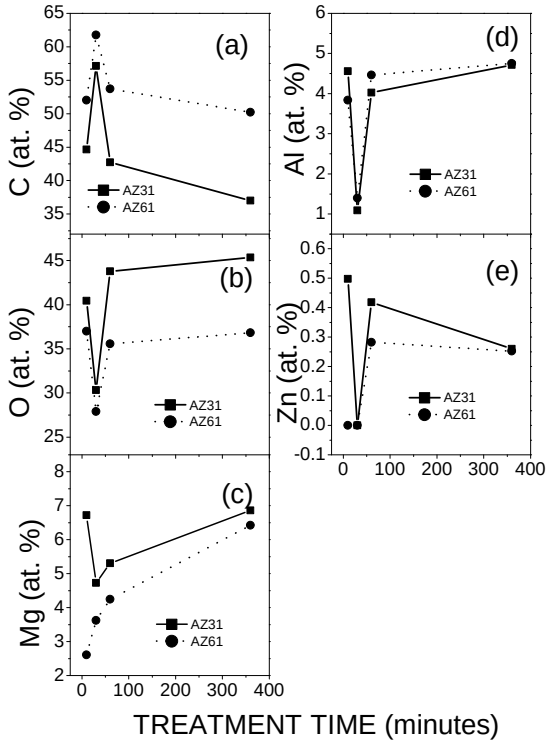

Figure 1. *Variation in the carbon (a), oxygen (b), magnesium (c), aluminium (d), and zinc (e) atomic percentages obtained by XPS on the surface of the AZ31 and AZ61 alloys as a function of the treatment time in $NaHCO_3$ saturated solution.*

Fig. 3 compares the variation in the atomic percentages of sodium (a) carbonate (b) and Al/(Al+Mg) x 100 atomic ratio(c) obtained by XPS on the surface of the AZ31 and AZ61 alloys as a function of the treatment time. The atomic percentages of carbonate were obtained from the area of the second component used in the fitting of the C1s spectra (Fig. 2) and the atomic percentages of C obtained by XPS on the surfaces of the AZ31 and AZ61 alloys after the treatment (Fig.1). Comparison of the evolution of the

sodium (Fig. 3a) and carbonate (Fig 3b) contents with the immersion time shows that they are directly related. Different behaviour is observed when one compares the evolution of the carbonate (Fig. 3b) and Al/(Al+Mg) x 100 atomic ratio (Fig. 3c), where one can appreciate a tendency for the carbonate content to increase as the Al/(Al+Mg) x 100 atomic ratio decreases on the outer surface of the conversion coating.

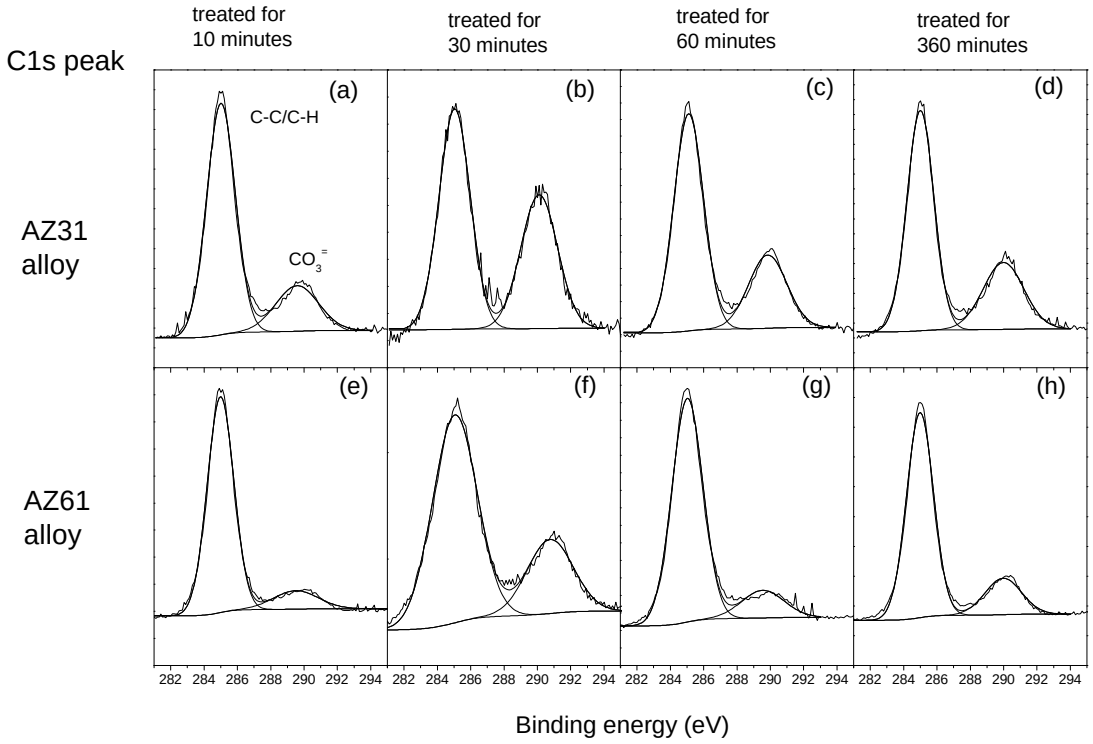

Figure 2. *Variation in the C1s high resolution peak obtained by XPS on the surface of the AZ31 and AZ61 alloys as a function of the treatment time in $NaHCO_3$ saturated solution.*

Fig 4 shows the O1s (a), Mg (b), Al2s (c), Zn $2p_{3/2}$ (d) and Na 1s (e) XPS high resolution spectra on the surface of the AZ31 alloy after 10 minutes of treatment. These spectra are representative of the similar O1s, Mg 2p, Al 2s, Zn $2p_{3/2}$ and Na1s spectra obtained on the surface of the conversion coatings formed on the AZ31 and AZ61 alloys after other treatment times. The O1s high resolution spectra may be fitted with two components (Fig. 4a). The first is situated at approximately 531.0 eV and is normally interpreted as oxygen in the form of magnesium oxide/aluminium oxide [19-21]. At 533.2-533.4 eV a more prominent peak is observed, which is attributed to the presence of $MgCO_3$ and/or $Mg(OH)_2$ and/or $Al(OH)_3$ [22]. In the Mg 2p spectrum (Fig. 4b) only one component appears that is associated with the presence of Magnesium in Mg^{2+} (51.0 eV) form [23]. In the Al 2s spectrum (Fig. 4c) there is a 119.5eV component characteristic of aluminium in ionic state (Al^{3+} type). The $Zn2p_{3/2}$ high resolution spectrum (Fig. 4d) may be fitted to one component with a binding energy of 1022.0 eV

associated with the presence of Zn^{2+}. Finally, the Na1s spectrum (Fig. 4e) may be fitted to one component at 1071.7 eV associated with the presence of sodium (Na^{+}) ions.

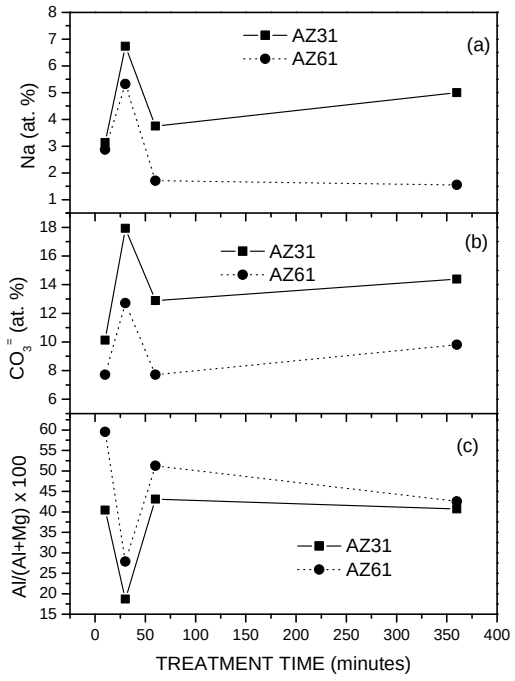

Figure 3. *Variation in the atomic percentage of sodium (a) carbonate (b) and Al/(Al+Mg) x 100 (c) obtained by XPS on the surface of the AZ31 and AZ61 alloys as a function of the treatment time in $NaHCO_3$ saturated solution.*

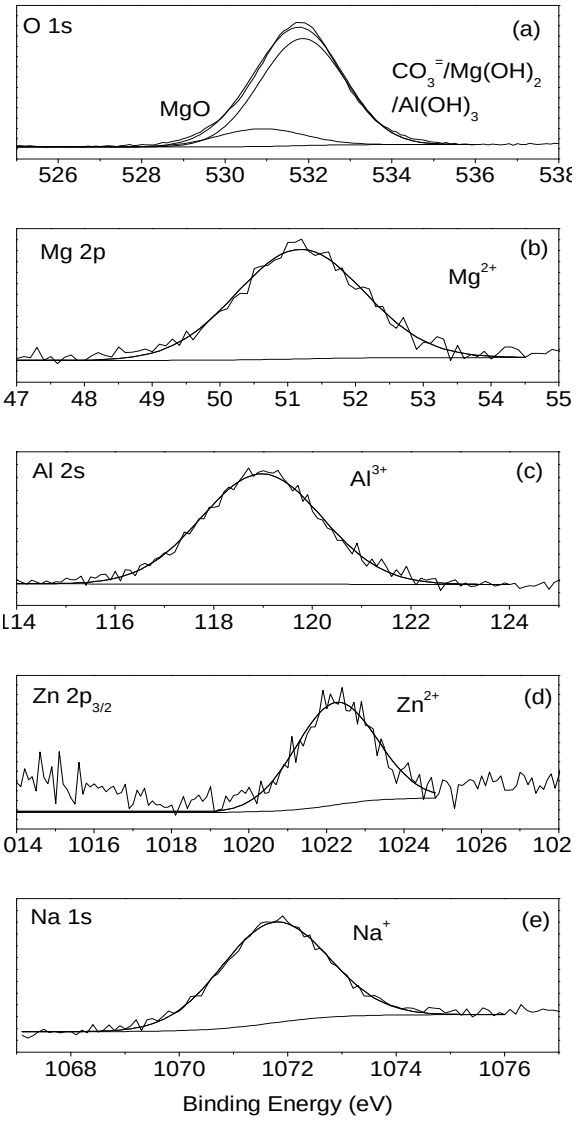

Figure 4. *High resolution O1s (a), Mg 2p (b), Al 2s (c), Zn $2p_{3/2}$ (d) and Na 1s (e) XPS peaks obtained on the surface of the AZ31 alloy after 10 minutes of treatment in $NaHCO_3$ saturated solution.*

3.2. Morphology and microcomposition of the conversion coating formed on the surface of the AZ31 and AZ61 magnesium alloys after $NaHCO_3$ treatment for different times.

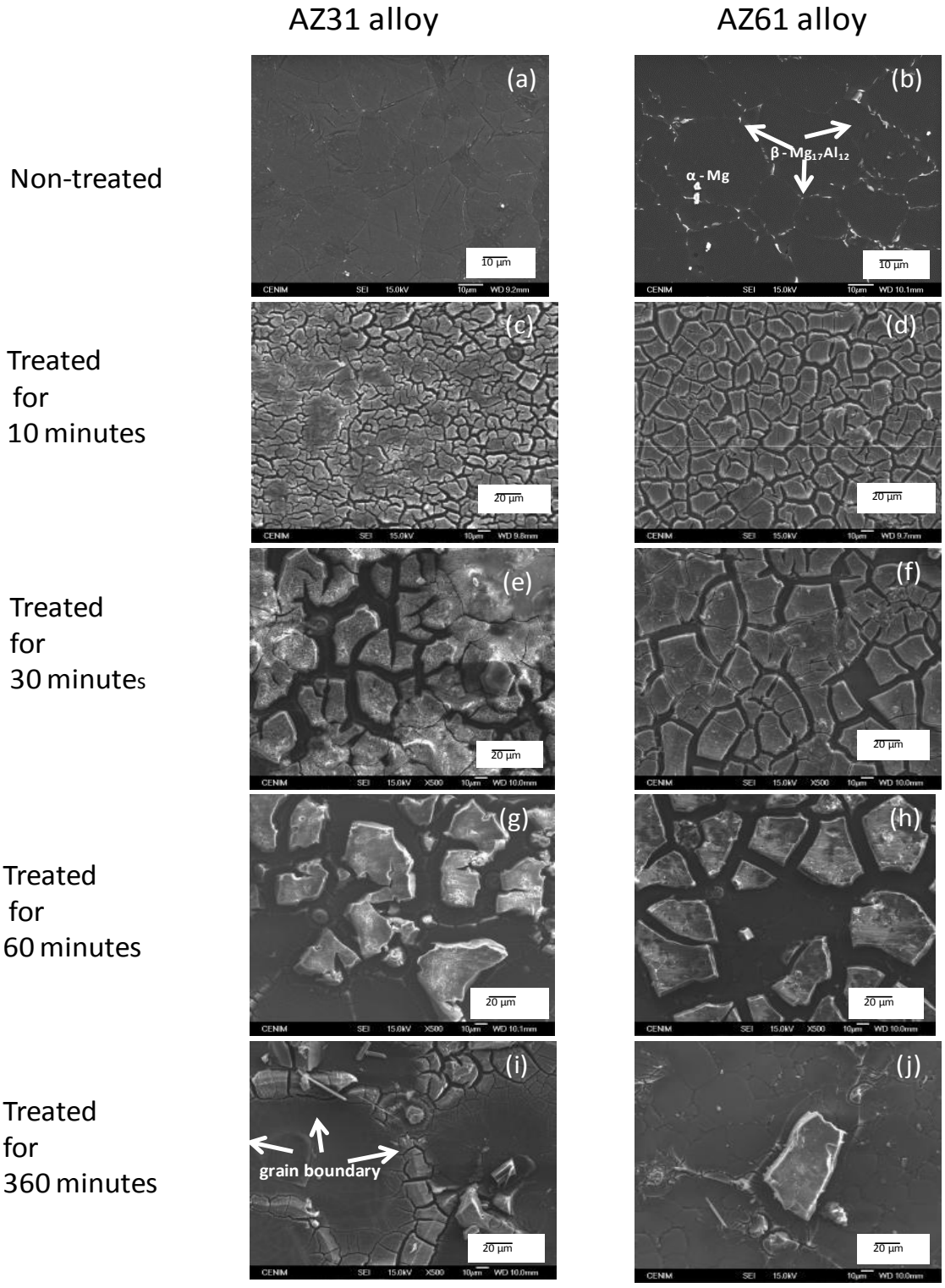

Figure 5. *SEM surface morphologies for AZ31 (a, c, e, g, i) and AZ61 magnesium alloys (b, d, f, h, j) non-treated (a, b) and treated for 10 min (c, d), 30 min (e, f), 60 min (g, h) and 360 minutes (i, j) in saturated $NaHCO_3$ solution, respectively.*

Figure 5 compares the surface microstructures on the non-treated AZ31 and AZ61 magnesium alloys and treated in $NaHCO_3$ saturated solution for different times. As can be seen, the microstructure of the non-treated AZ31 alloy is formed almost entirely of the α-matrix (Fig. 5a), whereas in the microstructure of alloy AZ61 a considerable part of the aluminium has precipitated in the form of β-phase at the grain boundaries (Fig. 5b). After ten minutes of treatment (Figs. 5c and 5d), the metallic surface appears to be completely covered by a clear and cracked coating with "dry-mud" morphology. In conversion coating treatments for magnesium alloys, this surface morphology is commonly observed [9,24-28]. The cracks may possibly be due to hydrogen being released via the chemical reaction during the conversion treatment and/or the dehydration of the surface layer after treatment [25,29,30]. A dark, inner film between the outer thick layer and the magnesium alloy substrate appears to be formed from the earliest stages of treatment (Fig. 6). By comparing Fig. 5c with Figs. 5e, 5g and 5i for AZ31 alloy and Fig. 5d with Figs. 5f, 5h and 5j in the case of the AZ61 alloy, it is apparent that the fraction of the surface covered by the thick outer layer decreases with the treatment time. It is important to note that, from the early stages of the treatment, micro-cracks appear on the inner layer of the conversion coating formed on the surface of the AZ31 alloy (Figs. 6a and 6b). In contrast when the AZ61 alloy is treated for 10

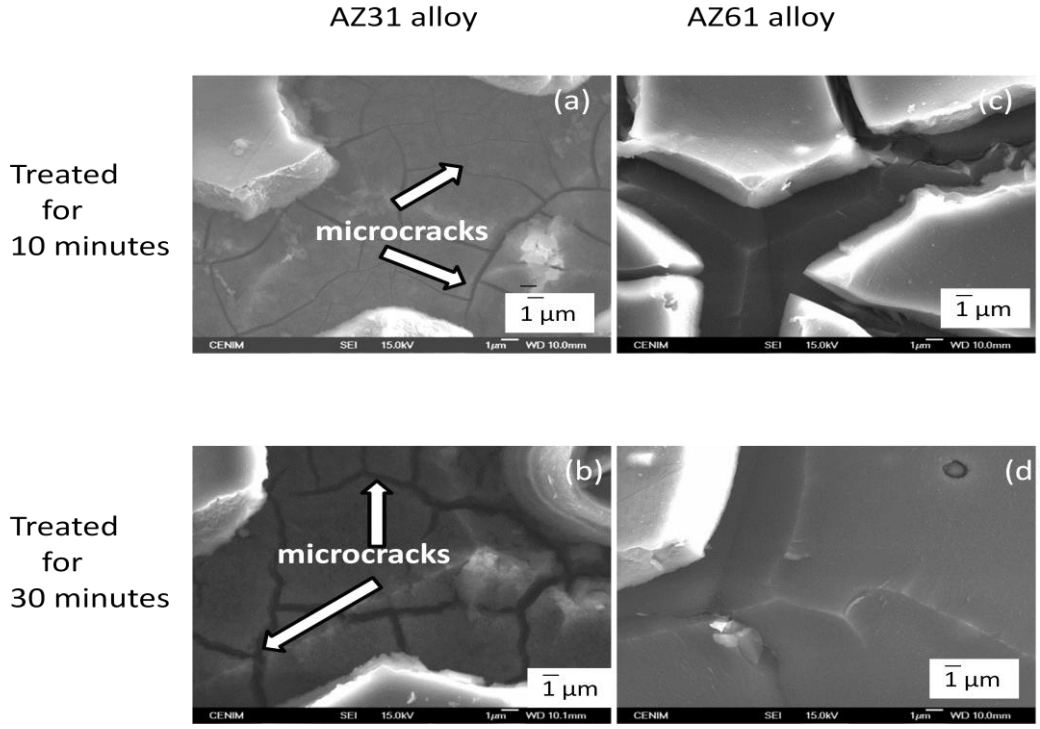

Figure 6. *SEM micrographs of the conversion coating formed on the surface of AZ31 (a, b) and AZ61 alloys (c, d) and after treatment for 10 min (a, c) and 30 min (b, d) showing the presence of micro-cracks on the inner layer.*

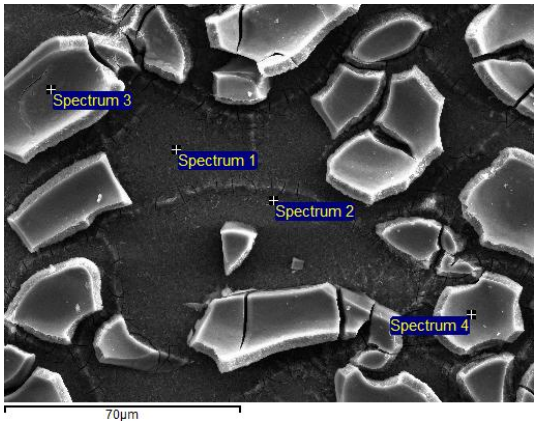

Figure 7. *Micrograph illustrating locations of points for EDX spot analysis of the coatings formed on AZ31 magnesium alloy treated for 10 min in saturated NaHCO3 solution. Spectrum 1 and 2 (inner layer) and Spectrum 3 and 4 (Outer layer).*

and 30 minutes (Figs. 6c and 6d) the dark film looks smoother, more uniform and there are no visible micro-cracks. After 60 and 360 minutes of immersion, wider cracks are seen on the inner layer of the conversion coating formed on AZ31 alloy (Figs 5g and 5i) and the nucleation and growth of theses cracks seems to start around the grain boundaries areas (as marked by arrowheads in Fig 5i). EDX analysis of the conversion coating formed on the AZ31 alloy surface after immersion for 10 minutes was performed in order to investigate possible differences in composition between the two previously mentioned layers. Atomic percentages and Al/(Al+Mg) ratios of the inner and outer layers obtained by EDX are presented in Table 2 and compared with surface measurements made with XPS (over an average analysis of 1mm x 1mm). It is worth mentioning that, while XPS analysis gives the composition information of the very top surface layer, EDX gives information of the bulk material. The amount of Al (4%) detected by EDX on the inner layer formed on the surface of the AZ31 alloy (Figure 7, Spectra 1 and 2) is similar to the alloy bulk content (Table1). It is probable that the penetration of the EDX analysis clearly exceeds the thickness of the inner layer. In contrast, it is interesting to note the similarity between the atomic composition determined by EDX on the outer layer (Fig. 7, spectra 3 and 4) and that detected by XPS on the outermost surface (Table 2) with a sampled area of approximately $1mm^2$. Attention should be drawn to the fact that, apart from the significant decrease observed by SEM in the fraction of surface covered by the outer layer with the time of treatment (Fig. 5), the surface chemical composition determined by XPS after 10 minutes, which appears almost completely covered by the outer layer (Figs 5c and 5d), is practically the same as that observed after 360 minutes (Figure 1), with the inner layer becoming dominant (Figs 5i and 5j). It seems reasonable to suppose that the chemical composition of these layers is similar.

Figure 8 compares SEM images and EDX quantitative analysis for the cross-section of the coating formed on AZ61 alloy treated for 10 min (a) and 60 minutes (b) in saturated $NaHCO_3$ solution. It is interesting to note that the thickness of the conversion coating on the AZ61 alloy treated for 10 min seems to be higher than that observed after 60 minutes. We speculate that these thickness differences (of µm order) may be related with the increase in imperfections or growth defects with the treatment time which can generate highly localized stress development, distortion of the structure and possible failures in the coating.

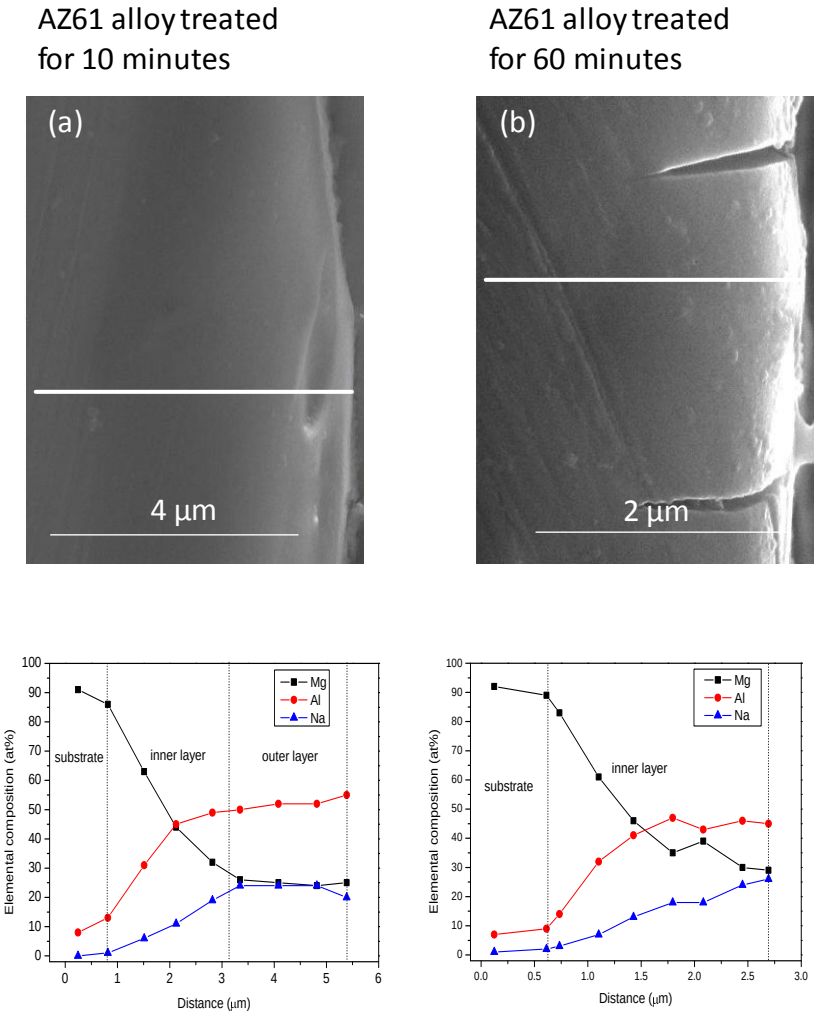

Figure 8. *SEM morphology and EDX quantitative analysis for the cross-section of the coating formed on AZ61 alloy treated for 10 min (a) and 60 minutes (b) in saturated $NaHCO_3$ solution.*

The EDX analysis of the AZ61 alloy treated for 10 minutes (Fig 8a) shows how the magnesium, aluminium and sodium contents observed on the outer layer remain stable. In contrast to the presence of a fairly homogeneous layer noted above, on the inner layer there is a notable decrease in aluminium and sodium contents and an increase in

magnesium content toward the substrate. The composition of coating of the AZ61 alloy treated for 60 minutes (Fig 8b) seems to be fairly similar to that of the inner layer on the alloy treated for 10 minutes (Fig 8a).

3.3 Protective properties of $NaHCO_3$ surface treatment.

3.3.1. Hydrogen evolution measurements as a function of immersion time in NaCl 0.6M solution.

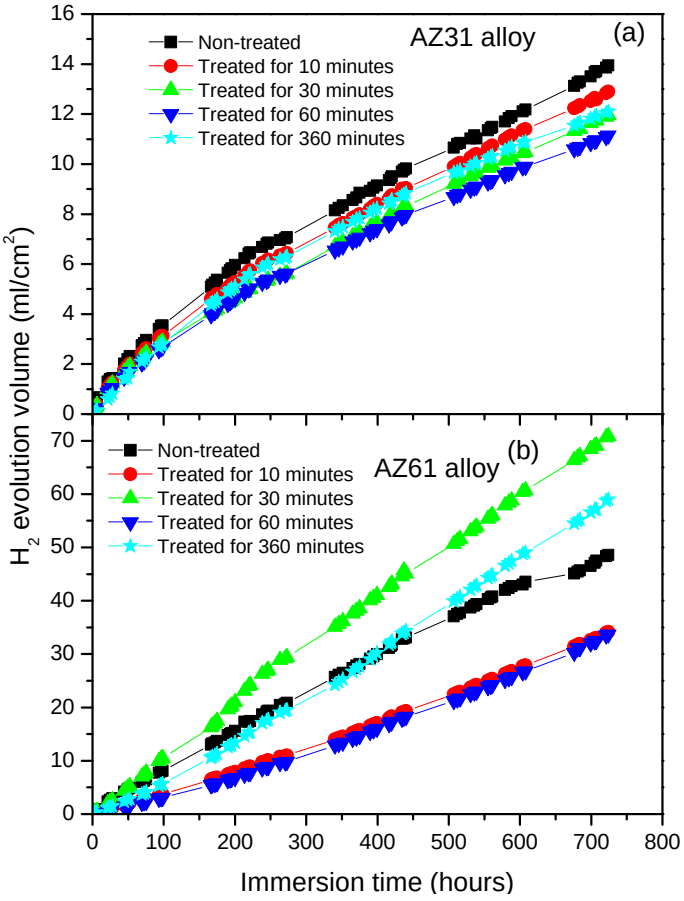

***Figure 9**. Hydrogen evolution curves for the various treatment times and alloys during immersion in 0.6M NaCl for 700 hours.*

Figure 9 compares the hydrogen evolution versus time curves (direct measure of the corrosion rate) for the AZ31 alloy non-treated and after 10, 30, 60 and 360 minutes of $NaHCO_3$ treatment (Fig. 9a) and those corresponding to the AZ61 alloy (Fig. 9b) during immersion in 0.6M NaCl for 700 hours. No significant differences in these curves were observed in the AZ31 alloy after different treatment times compared with the non-treated alloy (Figure 9a). In contrast with the AZ31 alloy, significantly lower hydrogen evolution data than the non-treated AZ61 alloy were observed in the AZ61 alloy

$NaHCO_3$ treated for 10 and 60 minutes (Figure 9b). It is interesting to highlight that the hydrogen volume values found in the AZ61 alloy treated with $NaHCO_3$ for 10 and 60 minutes were reduced by about 50% over 10 days testing and by 30% over 30 days testing. Treatment periods of 30 and 360 minutes increase the hydrogen volume data to similar or higher values than those obtained from non-treated AZ61 alloy (Fig. 9b).

***Table 2**. Measurements of atomic composition by EDX and XPS on the surface of the AZ31 treated for 10 minutes.*

Element	Inner layer EDX[a] (Average values from spect. 1 and 2) (at%)	Outer layer EDX[a] (Average values from spect. 3 and 4) (at%)	Average analysis area of 1mm x 1mm XPS[b] (at%)
Mg	96	38	41
Al	4	35	28
Na	0	27	30
Al/(Mg+Al)	4	48	41

[a] All values from SEM after removal of signals from carbon and oxygen
[b] All values from XPS after removal of signals from carbon, oxygen and zinc

Fig. 10 shows the macroscopic surface appearance of the corroded non-treated AZ61 alloy, treated samples after 700 hours of immersion in NaCl 0.6M and after corrosion product removal. In the test samples one can observe uniform attack on large areas of the exposed surface of the non-treated AZ61 alloy (Fig. 10a), after 30 minutes of $NaHCO_3$ treatment (Fig. 10c) and after 360 minutes of $NaHCO_3$ treatment (Fig. 10e) and it is worth noting that there are areas in which the metal has disappeared, mainly around the edges. However, after 10 (Fig. 10b) and 60 (Fig. 10d) minutes of $NaHCO_3$ treatment, no metal disappeared from the borders of the AZ61 alloy when compared with the other samples. Likewise it is interesting to note the predominance of non-corroded areas which appear to occupy more than 50% of the exposed surface (Figs 10b and 10d). In general, there is a qualitative agreement between the largest fraction of the corrosion area of the samples (Fig. 10) and the hydrogen evolution data (Fig. 9b).

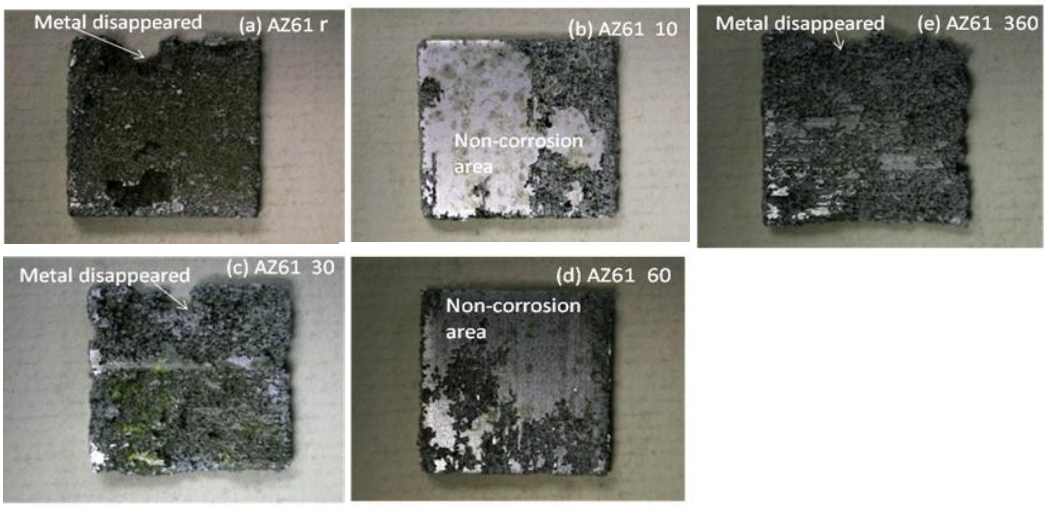

Figure 10. *Representative macroscopic surface appearance of corroded AZ61 samples after 700 hours of immersion in NaCl 0.6M and after corrosion product removal. (a) untreated alloy, (b) AZ61 alloy treated with $NaHCO_3$ for 10 minutes, (c) AZ61 alloy treated with $NaHCO_3$ for 30 minutes, (d) AZ61 alloy treated with $NaHCO_3$ for 60 minutes and (e) AZ61 alloy treated with $NaHCO_3$ for 360 minutes.*

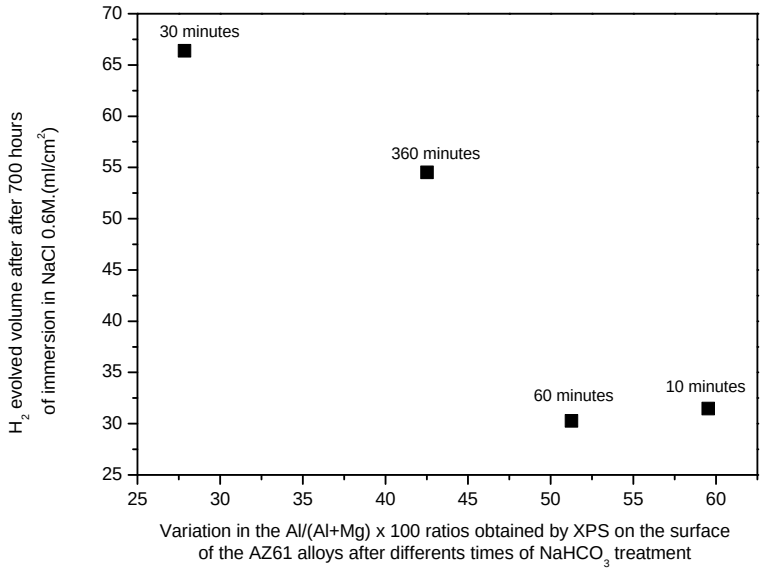

Figure 11*. Variation in the Al/(Al+Mg) x 100 ratio obtained by XPS on the surface of the AZ61 alloys after different $NaHCO_3$ treatment times as a function of hydrogen evolved after immersion in 0.6M NaCl for 700 hours.*

Fig. 11 shows a representation of the tendency for the Al/(Al+Mg) x 100 ratio obtained by XPS on the surface of the AZ61 alloys after different times of $NaHCO_3$ treatment to increase as the H_2 evolved volume after 700 hours of immersion decreases, suggesting a relationship between the Al/(Al+Mg) x 100 ratio obtained by XPS on the outer surface of the conversion coatings and the reaction kinetics in the corrosion process after immersion in NaCl 0.6M.

3.3.2. *Electrochemical impedance measurements as a function of immersion time in NaCl 0.6M solution.*

The evolution of the corrosion process on the treated AZ31 and AZ61 alloys immersed in 0.6 M NaCl solution has been monitored by means of impedance measurements. Nyquist diagrams (Fig. 12) show the presence of a capacitive loop at high frequencies (HF) and an inductive loop at low frequencies (LF). In the literature about the corrosion of magnesium alloys, the diameter (R_{HF}) of the capacitive loop in the high frequency region of the diagram has normally been associated with the charge transfer resistance of the corrosion process [31]. From the well-known Stern-Geary equation [32], inverse proportionality is expected between the corrosion current (i_{corr}) and R_{HF}:

$$I_{corr} = \frac{B}{R_{HF}}$$

where B is a proportionality constant specific for each particular system.

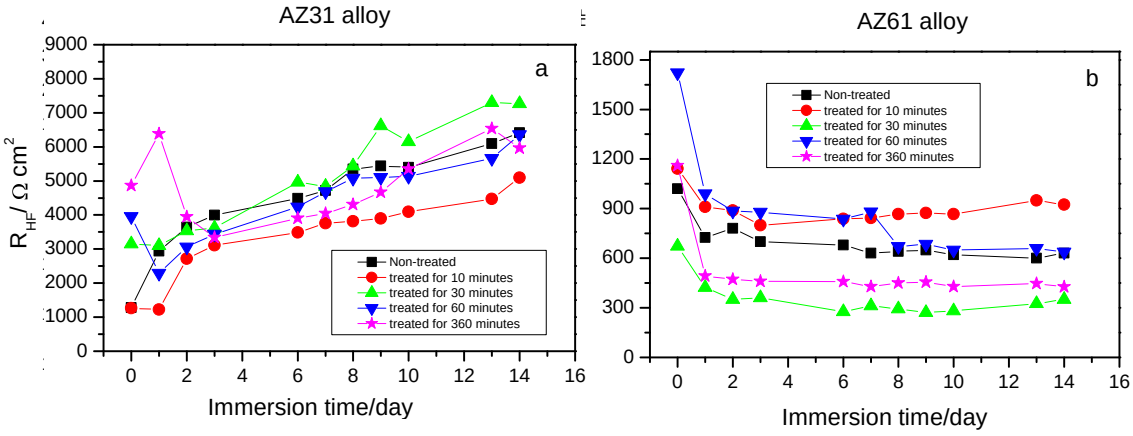

***Figure 13**. Variation in RHF values as a function of alloy type and treatment time over 14 days immersion in 0.6M NaCl.*

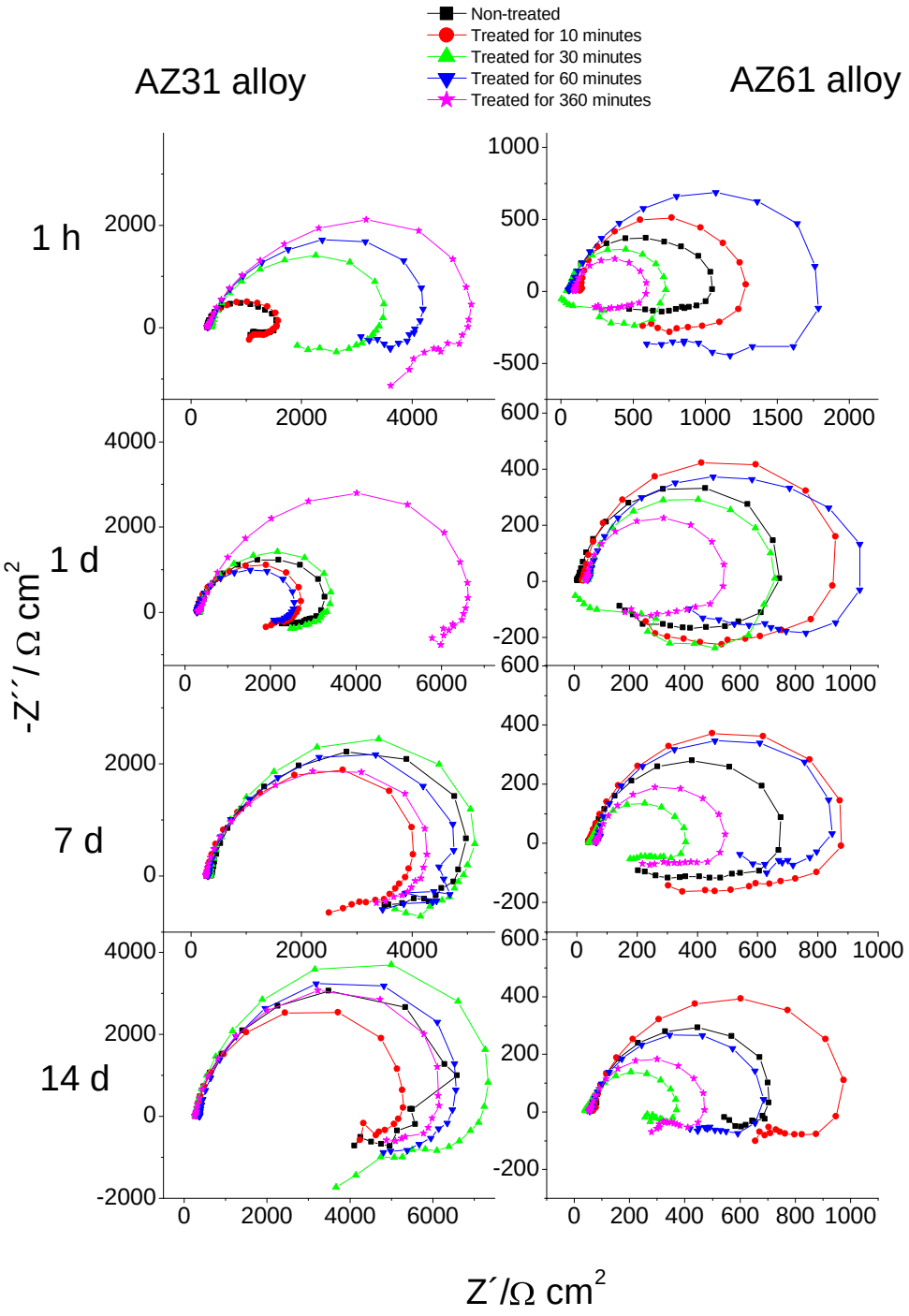

Figure 12. *Variation in Nyquist plot as a function of alloy type and treatment time over 14 days immersion in 0.6M NaCl.*

4. Discussion

4.1. Influence of the type of alloy on the conversion coatings surface morphology

After 360 minutes of treatment, the importance of the role played by the presence or absence of β-phase precipitates on the grain boundaries of the alloy in the growth mechanisms of the conversion coating can be perfectly established. In Fig. 5i, which represents the visual appearance of the AZ31 alloy treated for 360 minutes, one can see that the inner layer is not uniform, and that there are areas without apparent cracks coexistent with other areas with visible cracks, particularly located at grain boundaries. In contrast, the conversion coating formed on the AZ61 alloy treated for 360 minutes (Fig. 5j) is far more perfect and uniform. The formation of porous, non-uniform coatings with cracks and particularly poor coverage at the grain boundaries during chemical conversion treatment of aluminium alloys has been reported by Lunder et al [33] and would appear to be a result of the galvanic coupling grain boundary/matrix when the grain boundaries apparently became preferred anodic sites and the matrix acts as a cathode.

As shown in Fig. 5b, the aluminium is distributed, forming part of the chemical composition of the β-phase precipitates in the grain boundary of the AZ61 alloy. The notable difference between the electro-chemical potentials of the β and α phases suggests that during the conversion treatment the anodic reaction is supported by hydrogen evolution at the cathodic β phase contributing significantly to increase the pH in the vicinity of this phase and preferential precipitation of carbonates on the top of the β phase. Available literature mentions that the cathodic reaction took place at β phase and gaseous hydrogen appeared to be generated, which caused local pH rise in the vicinity of β phase and resulted in the preferential precipitation of phosphate-type protective films [29] or molybdates [34] on the β phase of AZ91D alloys at the very early stages of the chemical conversion treatment, which may reduce the potential difference between the α and β phases. It is likely that quick blockage of the grain boundaries in the AZ61 alloy due to preferential precipitation of carbonates on the β phase, leaves the metal surface in a less active state, motivating the growth of a more perfect, uniform, protective conversion layer than that which results on the AZ31 alloy.

4.2. Influence of the immersion time on the surface chemistry of the conversion

The properties of the thin oxide/hydroxide film formed on the surface of the magnesium alloys often determine the protective behavior of the conversion coatings. Assuming the hypothesis that the performance of the coating relies upon the chemistry of the oxide film that cover the alloy before the treatment, its characterization is of considerable importance. In a previous study [35], XPS was used to characterize the differences in the oxide films formed on the surface of AZ31 and AZ61 alloys in as-received and freshly polished conditions. The findings revealed the presence of a significant fraction of the as-received alloy surface covered by islands of spinel (<3 nm in thickness) formed as a result of the manufacturing process. Also, 5 minutes of sputtering (equivalent to about 2.5 nm of thining) seemed to be sufficient to eliminate the signal of water and OH^- adsorbed groups that may be accumulated in the original oxide film during ambient storage or cleaning procedure [31]. In immersion test in saline solution, during the initial stages of testing, considerable higher corrosion rates were obtained as-received specimens compared to the freshly polished surfaces. The degree of heterogeneity of the films coating as-received surfaces seemed to decrease their protective capacity compared to the more perfect and uniform of the films formed on freshly polished surface. In the present work, it would be possible to speculate that the very defective and heterogeneous surface layer initially present on the alloys in "as-received condition" barely affects the coating growth process.

The enrichment in sodium, aluminium and carbonate compounds observed by XPS as a function of time (Fig. 3.) may be related to the pH changes that occur directly above the metallic substrate surface during immersion in the $NaHCO_3$ saturated solution. Using the XPS data, and taking into account the potential-pH diagrams of Al and Mg-water system [36], we can speculate on the formation mechanism of the conversion coating [37]**.** The possible film formation reactions as proposed by Chen et al [13] are listed as follows :

$$2Mg^{2+} + 7OH^- + Al^{3+} \rightarrow Mg_2Al(OH)_7 \downarrow$$

$$Mg^{2+} + 8OH^- + 2Al^{3+} + xH_2O \rightarrow MgAl_2(OH)_8 \cdot xH_2O \downarrow$$

$$5Mg^{2+} + 2OH^- + 4 \quad + 5H_2O \rightarrow Mg_5(CO_3)_4(OH)_2 \cdot 5H_2O$$

The atomic ratio Al/(Mg+Al) determined by XPS on the surface of the AZ31 and AZ61 alloys after 10 minutes of treatment reach values of 40% and 60% respectively (Fig 3c), which are far superior to the bulk content of the AZ31 and AZ61 alloys, with about 3%

and 6% Al. This surface enrichment in aluminium could be related to the stronger stability of the aluminium hydroxide compared to the magnesium hydroxide when the pH is close to neutral, as may be the case at the beginning of the immersion test [17, 36]. After immersion times of 30 minutes one can observe a clear increase in the carbonate content (Fig. 3b) accompanied by a decrease in the Al/(Al+Mg) ratio (Fig. 3c).

In a solution with a pH of above 9, aluminium hydroxide is not stable as it easily turns into soluble AlO_2^- [17, 36]. Magnesium carbonate, however, is stable at this pH level. After 60 minutes immersion, the XPS data shows a notable increase in the Al/(Al+Mg) ratio, which maintains values of approximately 50% in immersions of up to 360 minutes (Fig. 3b). It is probable that the conversion coating formed over prolonged immersion periods contributes to a significant decrease in the magnesium dissolution process and the production of OH^- ions from the cathodic reaction, decreasing the pH and allowing the formation of an aluminium hydroxide film by means of a precipitation reaction. In general this data is in keeping with the evolution of the pH values measured directly above the surfaces of an AZ91 alloy with an immersion time in a Ca^{2+}/HCO_3^- aqueous solution observed by Uan et al [38], who observed that the pH values directly above the surfaces of samples increased rapidly from ~ 5.5 to 10.4 in 0.5 hours of immersion and subsequently, the pH values decreased from pH ~ 10.4 to pH ~ 8.5 after 3 hours of immersion.

During the test we can highlight the direct, linear relationship between the atomic percentages of sodium and carbonate obtained by XPS on the surface of the AZ31 and AZ61 alloys (Figs. 3a and 3b respectively), suggesting formation of mixtures of carbonates of sodium and magnesium as the principal constituents of the layers formed during exposure to aqueous solutions of sodium bicarbonate.

4.3. Protectiveness of the chemical conversion coatings on the surface of the AZ31 and AZ61 alloys in the 0.6M NaCl solution

It seems likely that some of the differences that have been revealed in the composition and characteristics of the chemical conversion coatings formed on the AZ31 and AZ61 alloys may have an impact on corrosion behaviour. As commented earlier, the more significant changes that have been observed on the conversion coatings, depending on the type of alloy and the treatment times, have been (a) the initial presence of a network of cracks on the inner layer of the conversion coating, (b) a higher concentration of

aluminium oxides and hydroxides on the surface chemical conversion coating and (c) higher concentration of carbonate.

If, as a reference, we take hydrogen evolution versus time curves obtained during the immersion test in NaCl 0.6M in the non-treated AZ31 alloy, minor difference is observed between these data and the data obtained from the samples with the same alloy treated with $NaHCO_3$ (Fig. 9a). In the literature there are references to the formation of thick layers of corrosion products on the Mg and its alloys immersed in saline solution whose growth has little effect on the corrosion rate due to its high porosity [39-41]. The presence of micro-cracks (Figs. 6a and 6b) or visible cracks in the layer formed on the AZ31 alloy (Fig. 5j) may have the effect of decreasing its compactness, thereby helping the diffusion of Cl^- species and not seeming to exert any relevant effect on corrosion protection. Despite the notable enrichment in aluminium oxides and hydroxides observed by XPS on the surface of the chemical conversion coating in the case of the samples treated for 10, 60 or 360 minutes, or in the carbonates seen on the samples treated for 30 minutes (Figs 3b and 3c), there has been no evidence of significant variation in their protective properties. This suggests that surface enrichment of aluminium cannot counteract the negative effect of the presence of a very defective layer of conversion coating in this alloy.

In contrast to the findings with the AZ31 alloy, there are some $NaHCO_3$ treatment times which significantly improve the protective properties of the AZ61 alloy in comparison with the non-treated same alloy (Fig. 9b). Simple microscopic observation revealed that the inner layer that forms on the surface of the AZ61 alloy (Figs. 6c and 6d) is far more perfect, uniform and without the presence of visible of micro-cracks, compared to that formed on the AZ31 alloy (Figs. 6a and 6b). It seems likely that the uniformity of the conversion layer may slow down the corrosion process by physically blocking the active sites on the metal surface (presence of β-phase). It may also diminish the rate at which Cl^- ions are transported through the micro-channels in the conversion coating

In addition to the uniformity effect, the chemical composition of the conversion layer on the AZ61 alloy also plays a fundamental part in the observed corrosion rate. Many studies mention the beneficial effect of Al [2, 42-47], which may become the essential factor in determining the passivity of the surface, improving the resistance to local breakdown of the oxide and reducing the chance of chloride ions penetrating as far as the surface. In our study, this effect seems to be observed in the lower values of hydrogen volume evolved in the samples treated with $NaHCO_3$ for 10 and 60 minutes

compared to those non-treated or treated for 30 and 360 minutes over 30 days by immersion in 0.6 M NaCl (Fig. 9b). Comparing these results with the chemical composition obtained by XPS on the surface of the conversion layers resulting from the treatment, one can clearly see a tendency towards a decrease in the hydrogen volumes evolved as the Al/(Al+Mg) ratio increases. This correspondence suggests that the enrichment of the aluminium oxide/hydroxide on the surface of the conversion layer as a result of the treatment probably controls the corrosion process in posterior immersion in 0.6 M NaCl. In the literature [49], it is presumed that the Al_2O_3 component forms a continuous skeletal structure in an amorphous matrix, so that the film properties become predominantly determined by the protective properties of Al_2O_3, very superior to that of $Mg(OH)_2$. Curiously, despite the different values of coating thickness (Fig 8), no significant differences in the value of hydrogen volume evolved are observed when comparing these results for the samples treated for 10 and 60 minutes (Fig. 9b). The relationship that can exist between corrosion and surface chemistry of the coating could perhaps explain this fact.

Finally, in the case of the AZ61 alloys, it is interesting to note that the highest volumes of hydrogen evolved correspond to the alloy treated for 30 minutes (Fig. 9b), where the XPS analysis has revealed as a distinctive characteristic the higher carbonate content on the surface of the chemical conversion coating (Fig. 3), a fact which seems to suggest that the magnesium carbonate component does not provide effective protection to the AZ61 alloy in solutions containing chloride concentrations of 0.6M.

4.4. Information from Nyquist plots

Fig. 13 shows the evolution of the polarization resistance versus immersion time in the exposure of the alloys to the 0.6 M NaCl solution. Comparing the R_{HF} values for the specimens treated with the bicarbonate bath with the corresponding reference values for the untreated specimens it is observed the existence of a beneficial effect of the treatment, particularly during the initial stages of the corrosion test.

In the first hour of immersion in the 0.6 M NaCl solution, the AZ31 specimens pre-treated with $NaHCO_3$ for 30, 60 and 360 minutes show R_{HF} values about 3 to 5 times higher than those for the untreated ones (Fig. 13a). After the first day corrosion, the R_{HF} values obtained with the untreated and treated AZ31 specimens converged to relatively similar values which tend to increase with time, suggesting some blocking of the surface by the precipitation of corrosion products.

One point emerging from the set of R_{HF} values for alloy AZ61 (Fig 13b) is the rather moderate tendency for this alloy treated for 10 or 60 minutes to present during the subsequent corrosion test higher values than the same alloy treated for 30 or 360 minutes, behavior which is in agreement with the hydrogen evolution curves reported above. No significant changes were observed in the R_{HF} values with exposure time, possibly due to the attainment in this case of a sort of balance between protection afforded by the corrosion products layer and the microgalvanic corrosion process in this biphasic alloy.

In general, the expected beneficial effect of the conversion coating, indicated by R_{HF} values clearly exceeding the reference ones, has been shown in this investigation during the first hours or days of corrosion testing. However this effect tends to be quickly lost after a few days of corrosion testing, where many of the R_{HF} values fall below the reference values, indicating an only slightly durable protective action of the studied coating in presence of the highly aggressive 0.6 M NaCl solution.

It seems likely that the improvement factor of corrosion resistance for the $NaHCO_3$ treated surfaces should be significantly better if the corrosion tests were carried out in milder corrosive environments. In this sense, it remains to be explored the effectiveness of the $NaHCO_3$ conversion treatment in the case of Mg alloys exposed to other environments than the NaCl solution, representative of the variable conditions of service that may be encountered in practice.

4. CONCLUSIONS

1) XPS analysis has been used to quantify the chemical changes on the surface of the carbonate coatings produced by immersion of AZ31 and AZ61 alloys in a $NaHCO_3$ solution for a time between 10 and 360 minutes. Attention is drawn to the considerable surface enrichment in mixtures of carbonates of magnesium and sodium and aluminium hydroxide in the layers formed as a result of the treatment. Close to ten times higher aluminium contents have been measured in the surface of these coatings compared to the bulk of the alloy.

2) The degree of enrichment in sodium, aluminium and carbonate compounds observed by XPS seems to be function of the treatment time and may be related to changes in the pH that occur directly above the metallic substrate during the treatment. Significant increase in the amount of aluminium hydroxides are observed on the surface of the conversion coating formed on the AZ61 alloy after 10 or 60 minutes (about 30% higher Al contents) compared to other treatment times (30 and 360 minutes).

3) Combined analysis of XPS, EIS and hydrogen evolution data suggests a favourable effect for corrosion resistance of: a) the amount of aluminium hydroxides observed on the external surface of the conversion coating and b) the absence of significant cracks or discontinuities on the inner layer of the conversion coating.

Acknowledgments

We wish to express our gratitude to Professor S. Feliu for several clarifying and stimulating discussions during the course of this work. The authors also gratefully acknowledge the financial support for this work from the Spanish Ministry of Science and Innovation (MAT 2009-13530)

References

[1] S. Feliu Jr., A. Pardo, M.C. Merino, A.E. Coy, F. Viejo, R. Arrabal, Correlation between the surface chemistry and the atmospheric corrosion of AZ31, AZ80 and AZ91D magnesium alloys, Appl. Surf. Sci. 255 (2009) 4102-4108.
[2] S. Feliu Jr., M.C. Merino, R. Arrabal, A.E. Coy, E. Matykina, XPS study of the effect of aluminium on the atmospheric corrosion of the AZ31 magnesium alloys, Surf. Interface Anal. 41 (2009) 143-150.
[3] S. Feliu Jr, C. Maffiotte, J.C. Galvan, V. Barranco, Atmospheric corrosion of magnesium alloys AZ31 and AZ61 under continuous condensation conditions, Corros. Sci. 53 (2011) 1865-1872.
[4]. L. Wang, T. Shinohara, B.P. Zhang, XPS study of the surface chemistry on AZ31 and AZ91 magnesium alloys in dilute NaCl solution, Appl. Surf. Sci. 256 (2010) 5807-5812.
[5] H.H. Elsentriecy, K. Azumi, H. Konno, Improvement in stannate chemical conversion coatings on AZ91 D magnesium alloy using the potentiostatic technique, Electrochim. Acta 53 (2007) 1006-1012.
[6].J.K. Lin, J.Y. Uan, Formation of Mg,Al-hydrotalcite conversion coating on Mg alloy in aqueous HCO_3^-/CO_3^{2-} and corresponding protection against corrosion by the coating, Corros. Sci. 51 (2009) 1181-1188.
[7] B.L. Yu, X.L. Pan, J.Y. Uan, Enhancement of corrosion resistance of Mg-9wt% Al- 1 wt% Zn alloy by Calcite ($CaCO_3$) conversion hard coating, Corros. Sci. 52 (2010) 1874-1878.
[8] J.K. Lin, C.L. Hsia, J.Y. Huan, Characterization of Mg,Al- hydrotalcite conversion film on Mg alloy and Cl^- and CO_3^{2-} anion-exchangeability of the film on a corrosive environment, Scr. Mater. 56 (2007) 927-930.
[9] A.A. Zuleta, E Correa, C. Villada, M. Sepulveda, J.G. Castaño, F. Echevarria, Comparative study of different environmentally friendly (Chromium-free) methods for surface modification of pure magnesium, Surf. Coat. Technol. 205 (2011) 5254-5259.
[10] M. Carboneras, L.A. Hernandez-Alvarado, Y.E. Mireles, L.S. Hernandez, M.C. Garcia-Alonso, M.L. Escudero, Chemical conversion treatments to protect biodegradable magnesium in applications as temporary implants for bone repair, Rev. Metal. Madrid 46 (2010) 86-92.
[11] J. Wang, D. Li, X. Yu, X. Jing, M. Zhang, Z. Jiang, Hydrotalcite conversion coating on Mg alloys and its corrosion resistance, J. Alloys Compd. 494 (2010) 271-274.
[12] J.K. Lin, K.L. Jeng, J.Y. Uan, Crystallization of a chemical conversion layer that forms on AZ91D magnesium alloy in carbonic acid, Corros. Sci. 53 (2011) 3832-3839.
[13] J. Chen, Y. Song, D. Shan, E.H. Han, In situ growth of Mg-Al hydrotalcite conversion film on AZ31 magnesium alloy, Corros. Sci. 53 (2011) 3281-3288.
[14] Y. Al-Abdullat, S. Tsutsumi, N. Nakajima, M. Ohta, H. Kuwahara, K. Ikeuchi, Surface modification of magnesium by $NaHCO_3$ and corrosion behaviour in Hank´s solution for new biomaterial applications, Mater. Trans. 42 (2001) 1777-1780.
[15] C.D. Wagner, L.E. Davis, M. V. Zeller, J.A. Taylor, R.H. Raymond, L.H. Gale. Empirical atomic sensitivity factor for quantitative analysis by electron spectroscopy for chemical analysis, Surf. Interface Anal. 3 (1981) 211-225.
[16] G. Song, A. Atrens, D. Stjohn, J. Naim, Y. Li, The electrochemical corrosion of pure magnesium in 1N NaCl, Corros. Sci. 39 (1997) 855-875.
[17] G.L. Song, A. Atrens, X.L. Wu, B. Zhang, Corrosion behaviour of AZ21, AZ501 and AZ91 in sodium chloride, Corros. Sci. 40 (1998) 1769-1791
[18] G.L. Song, A. Atrens, M. Dargusch, Influence of microstructure on the corrosion of diecast AZ91D, Corros. Sci. 41 (1998) 249-273.
[19] H.B. Yao, Y. Li, A.T.S. Wee, An XPS investigation of the oxidation/corrosion of melt-spun Mg, Appl. Surf. Sci. 158 (2000) 112–119.
[20] V. Fournier, P. Marcus, I. Olefjord, Oxidation of magnesium, Surf. Interface Anal. 34 (2002) 494-497.
[21] J. Kim, K.C. Wong, P.C. Wong, S.A. Kunlich, J.B. Metson, K.A.R. Mitchell, Characterization of AZ91 magnesium alloy and organosilane adsorption on its surface, Appl. Surf. Sci. 253 (2007) 4197-4207.
[22] N.C. Hosking, M.A. Ström, P.H. Shipway, C.D. Rudd, Corrosion resistance of zinc-magnesium coated steel, Corros. Sci. 49 (2007) 3669-3695.
[23] M. Liu, P. Shmutz, S. Zanna, A. Seyeux, H. Ardelean, G. Song, A. Atrens, P. Marcus, Electrochemical reactivity, surface composition and corrosion mechanisms of the complex metallic alloy Al_3Mg_2, Corros. Sci. 52 (2010) 562-578.

[24] K. Brunelli, M. Dabalà, I. Calliari, M. Magrini, Effect of HCl pre-treatment on corrosion resistance of cerium-based conversion coatings on magnesium and magnesium alloys, Corros. Sci. 47 (2005) 989-1000.
[25] L. Yang, J. Li, C. Lin, M. Zhang, J. Wu, Study of molybdenum/lanthanum-based composite conversion coatings on AZ31 magnesium alloy, Appl. Surf. Sci. 257 (2011) 2838-2842.
[26] Y.F. Jiang, H.T. Zhou, S.M. Zeng, Microstructure and properties of oxalate conversion coating on AZ91D magnesium alloy, Trans. Nonferrous Met. Soc. China 19 (2009) 1416-1422.
[27] Z. Yong, J. Zhu, C. Qiu, Y. Liu, Molybdate/phosphate composite conversion coating on magnesium alloy surface for corrosion protection, Appl. Surf. Sci. 255 (2008) 1672-1680.
[28] S. Zhang, Q. Li, B. Chen, X. Yang. Preparation and corrosion resistance studies of nanometric sol-gel-based CeO_2 film with a chromium-free pretreatment on AZ91D magnesium alloy, Electrochim. Acta 55 (2010) 870-877.
[29] K.Z. Chong, T.S. Shih, Conversion coating treatment for magnesium alloy by a permanganate-phosphate solution, Mater. Chem. Phys. 80 (2003) 191-200.
[30] W. Zhou, D. Shan, E.H. Han, W.Ke, Structure and formation mechanism of phosphate conversion coating on die-cast AZ91D magnesium alloy, Corros. Sci. 50 (2008) 329-337.
[31] S. Feliu Jr., C. Maffiotte, A. Samaniego, J.C. Galvan, V. Barranco, Effect of naturally formed oxide films and other variables in the early stages of Mg-alloy corrosion in NaCl solution, Electrochim. Acta 56 (2011) 4454-4565.
[32] M. Stern, A.L. Geary, Electrochemical polarization: I. A theoretical analysis of the shape of polarization curves, J. Electrochem. Soc. 104 (1957) 56-63.
[33] O. Lunder, J.C. Walmsley, P. Mack, K. Nisancioglu, Formation and characterization of a chromate conversion coating on AA6060 aluminium, Corros. Sci. 47 (2005) 1604-1624.
[34] H.H. Elsentriecy, K. Azumi, Electroless Ni-P deposition on AZ91D magnesium alloy prepared by molybdate chemical conversion coatings, J. Electrochem. Soc. 156 (2009) D70-D77.
[35] S. Feliu Jr., C. Maffiotte, A. Samaniego, J.C. Galvan, V. Barranco, Effect of the chemistry and structure of the native oxide surface film on the corrosion properties of commercial AZ31 and AZ61 alloys, Appl. Surf. Sci. 257 (2011) 8558-8568.
[36] M. Pourbaix, Atlas of Electrochemical Equilibria in Aqueous Solutions, Pergamon Press, Oxford (1966).
[37] H. Ardelean, I. Frateur, P. Marcus, Corrosion protection of magnesium alloys by cerium, zirconium and niobium-bases coatings, Corr. Sci. 40 (2008) 1907-1918.
[38] J.Y. Uan, B.L. Yu, X.L. Pan, Morphological and microstructural characterization of the aragonitic $CaCO_3$/Mg,Al- Hydrotalcite coating on Mg-9 Wt Pct Al-1 Wt Pct Zn alloy to protect against corrosion, Metall. Mater. Trans. A 39 (2008) 3233-3245.
[39] G. Baril, N. Pébère, The corrosion of pure magnesium in aerated and deaerated sodium sulphate solution, Corros. Sci. 43 (2001) 471–484.
[40] M. Santamaria, F.Di. Quarto, S. Zanna, P. Marcus, Initial surface film on magnesium metal: A characterization by X-ray photoelectron spectroscopy (XPS) and photocurrent spectroscopy (PCS), Electrochim. Acta 53 (2007) 1314–1324
[41] A. Pardo, M.C. Merino, A.E. Coy, F. Viejo, R. Arrabal, S. Feliu Jr. , Influence of microstructure and composition on the corrosion behavior of Mg/Al alloys in chloride media, Electrochim. Acta 53 (2008) 7890–7902.
[42] R. Lindstrom, J.E. Svensson, L.G. Johansson, The influence of carbon dioxide on the atmospheric corrosion of some magnesium alloys in the presence of NaCl, J. Electrochem. Soc. 149 (2002) B 103 - B 107.
[43] M. Liu, P.J. Uggowitzer, A.V. Nagasekhar, P. Schmutz, M. Easton, G. L. Song, A. Atrens, Calculated phase diagrams and the corrosion of die-cast Mg-Al alloys, Corros. Sci. 51 (2009) 602-619.
[44] J.H. Nordlien, K. Nisancioglu, S. Ono. N. Masuko, Morphology and structure of oxide films formed on MgAl alloys by exposure to air and water, J. Electrochem. Soc. 143 (1996) 2564-2572.
[45] A. Pardo, M.C. Merino, A.E. Coy, R. Arrabal, F. Viejo, E. Matykina, Corrosion behaviour of magnesium/aluminium alloys in 3.5 wt% NaCl, Corros. Sci. 50 (2008) 823-834.
[46] M. Jönsson, D. Persson, R. Gubner, The initial steps of atmospheric corrosion on magnesium alloy AZ91D, J. Electrochem. Soc. 154 (2007) C684-C691.
[47] N. Hara, Y. Kobayashi, D. Kagaya, N. Akao, Formation and breakdown of surface films on magnesium and its alloys in aqueous solutions, Corros. Sci. 49 (2007) 166-175.
[48] J.H.Nordlien, S. Ono, N. Masuko, K. Nisancioglu**,** A TEM investigation of naturally formed oxide films on pure magnesium, Corros. Sci. 39 (1997) 1397-1414.

Poisoning the Corrosion of Magnesium

N. Birbilis[a], G. Williams[b], K. Gusieva[a], A. Samaniego[a,c], M.A. Gibson[a,d], H.N. McMurray[b]

[a]Department of Materials Engineering, Monash University, VIC, Australia
[b]Materials Research Centre, Swansea University, Swansea, UK
[c]Department of Materials Engineering, CENIM, Madrid, Spain
[d]CSIRO Division of Process Science and Engineering, VIC, Australia

Electrochemistry Communications 34 (2013) 295–298

Abstract

Despite possessing excellent specific properties, rapid corrosion of magnesium is a significant barrier in its widespread use. Alloying Mg to enhance mechanical properties nominally increases susceptibility to corrosion from microstructural heterogeneity. Furthermore, alloying Mg nominally accelerates cathodic kinetics and hence also accelerates corrosion. To date, no alloying additions to Mg suggest that a reduction in corrosion rate can be imparted, however we reveal for the first time that alloying additions of arsenic can impart significant corrosion resistance to Mg via retarding the cathodic reaction.

Keywords: Magnesium, Corrosion, Arsenic, Cathodic poison, Polarisation

Introduction

The specific strength of Mg, coupled with other favourable properties, has seen technologies such as consumer electronics adopt Mg alloys in low corrosivity environments due to their lightweight and mass production capability. There is major interest in the utility of Mg deployment in many more forms, such as automotive sheet, powertrains, laptop casings, and anywhere that significant energy reductions can be realised. From a corrosion perspective, Mg is highly reactive in aqueous environments. This is due in part to the highly negative potential of Mg (~ $-2.38V_{NHE}$) [1], and also because the attendant cathodic reaction is the reduction of water ($2H_2O + 2e^- \rightarrow H_2 + 2OH^-$) – with no rate limitation from the requirement of oxygen, allowing corrosion to freely occur in the whole pH range below about 11 [2].

The susceptibility to corrosion of Mg has been documented for nearly a century [3], and to date, alloying additions and impurities have increased the corrosion of Mg [4–7]. The principal reasons include the formation of second phases that serve as intense local cathodes, driving anodic dissolution. In spite of the high reactivity of Mg, one salient feature of Mg is that it is an inherently poor cathode, with one of the lowest exchange current densities of all metals [8,9]. As such, even in the pure form, Mg is fortunate that its sluggish cathodic ability limits what could be significantly more rapid corrosion (which is indeed what occurs when Mg is alloyed or when impurities elements such as Cu, Fe and Ni exist). Limited solubility of most elements in Mg [10,11] makes it difficult to reach a critical alloying content to impart a stainless character such as that in stainless steels, whereby the native oxide is replaced by that of a passive oxide (such as one based on Cr). Of the elements with a thermodynamic tendency to form oxides in preference to Mg, such elements are even more reactive and have equally wide pH windows of instability (such as Ca and Y) [12,13].

Recent work studying the corrosion of Mg in electrolytes containing soluble As species (arsenate) indicates an inhibition character capable of slowing the rate of Mg corrosion [14]. This was related to the ability of arsenate to serve as a poison for the cathodic reaction by inhibiting hydrogen atom recombination through the electrode position of elemental arsenic, As(0) at cathodic sites. This, in turn, retarded the dissolution of Mg significantly. Remarkably, the efficiency of arsenate was greatest at low pH, consistent with conditions favouring the deposition of As (0), while under neutral conditions, a mechanism of inhibition involving the formation of insoluble Mg-arsenate compounds predominated.

Overall however, the remarkable corrosion inhibition from dissolved As was clear.

To date, the influence of metallic As upon the electrochemical and corrosion response of Mg remains unstudied. The work herein was designed to explore the ability of metallic As to impart corrosion protection to Mg similar to that of the case of As-species in solution.

Materials and methods

Pure metals were sourced from Alfa-Aeser (USA). The composition of the pure Mg and the Mg–As alloy were independently analysed using ICP-AES (Spectrometer Services, Australia).

The Mg–As alloy was produced by encapsulating Mg and As in a quartz tube. The tube was backfilled with high purity argon to avoid any reaction of the Mg with the atmosphere. As an extra precaution, to avoid reaction of any molten metal with the quartz itself, the tube was internally coated with graphite. The charge was held molten at 700 °C for 3 min, and periodically agitated to ensure mixing. The alloy was then left to cool in air, removed from the encapsulation, and tested in this condition.

Electrochemical testing was conducted using a Bio-logic VMP potentiostat. A three-electrode setup was employed using a PAR Flat Cell incorporating a saturated calomel reference electrode and Pt-mesh counter electrode. In all cases, the electrolyte was 0.1 M NaCl (pH 6). Potentiodynamic polarization was carried out at a scan rate of 0.5 mV/s. Hydrogen collection was executed via an inverted funnel and burette assembly above the mass loss specimens. Nuances related to this method were outlined by Kirkland [15]. All reported tests were repeated a minimum of six times. SEM was conducted using a JEOL 7001 F.

Results and Discussion

a)

wt. %	Pure Mg	Mg-As
As	0	0.37
Fe	0.004	0.003
Mn	0.01	0.032
Al	0.01	0.033
Mg	Bal.	Bal.

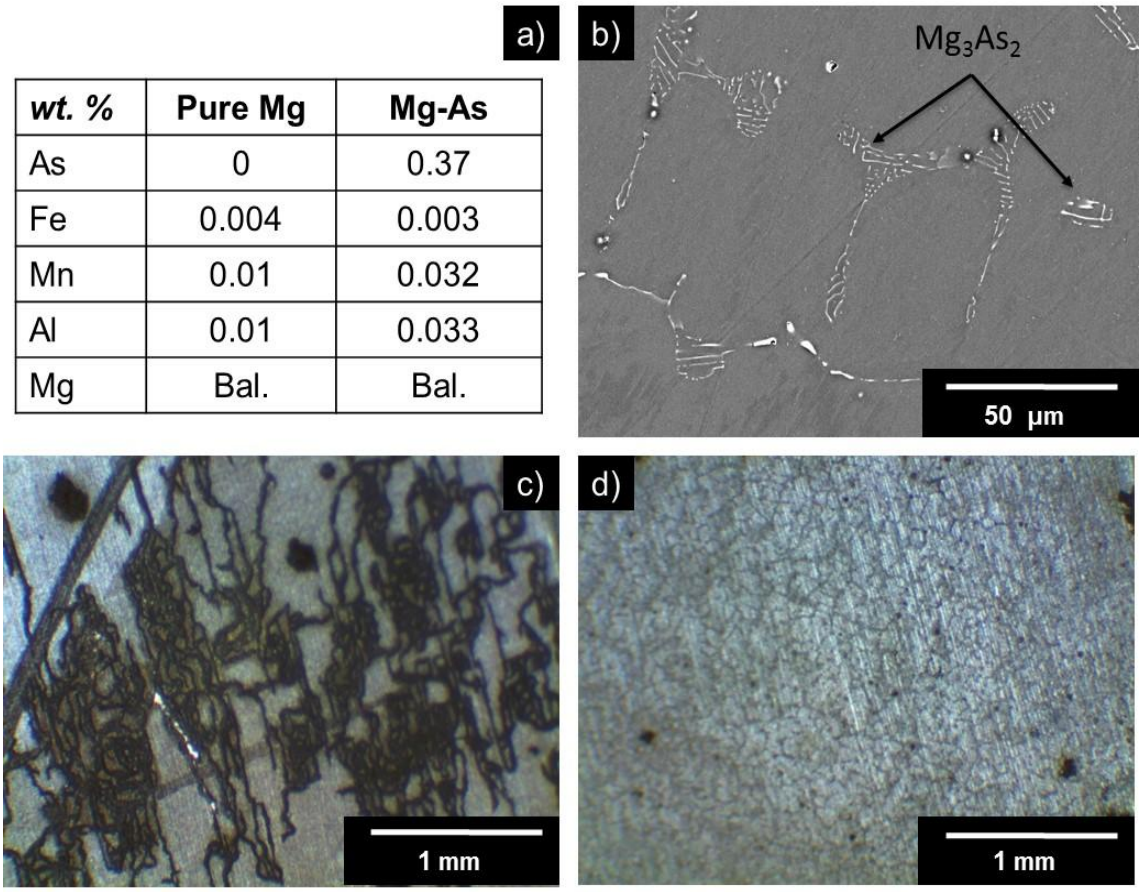

Fig. 1. *a) Composition of alloys tested herein as measured using ICP-AES. b) Backscattered SEM image ofMg-0.37 wt.% As. c) Optical micrograph of pure Mg following 24h immersion in 0.1 M NaCl. Filiform-like corrosion morphology is observed. d) Optical micrograph of Mg- 0.37 wt.% As following 24 h immersion in 0.1 M NaCl. Discrete corrosion sites observed with a substantial portion of the surface left un-attacked.*

The custom Mg–As alloy preparation methodology resulted in the successful formation of anMg-0.37 wt.% As alloy (Fig. 1a). The alloy microstructure was comprised of the α-Mg matrix, and the presence of the Mg3As2 phase. This phase is the only intermetallic that forms between Mg and As for levels of As up to ~65 wt.% [10], and confirmed via EDX analysis. Potentidynamic polarisation results contrasting pure Mg and Mg–As

alloy reveal significant features that are atypical from all other reported polarisation data from Mg-alloys compared with pure Mg (Fig. 2). There are two significant features to note from the Fig. 2. The first is that cathodic reaction kinetics for Mg–As are lower than those of pure Mg. This feature is remarkable given that Mg is already a sluggish

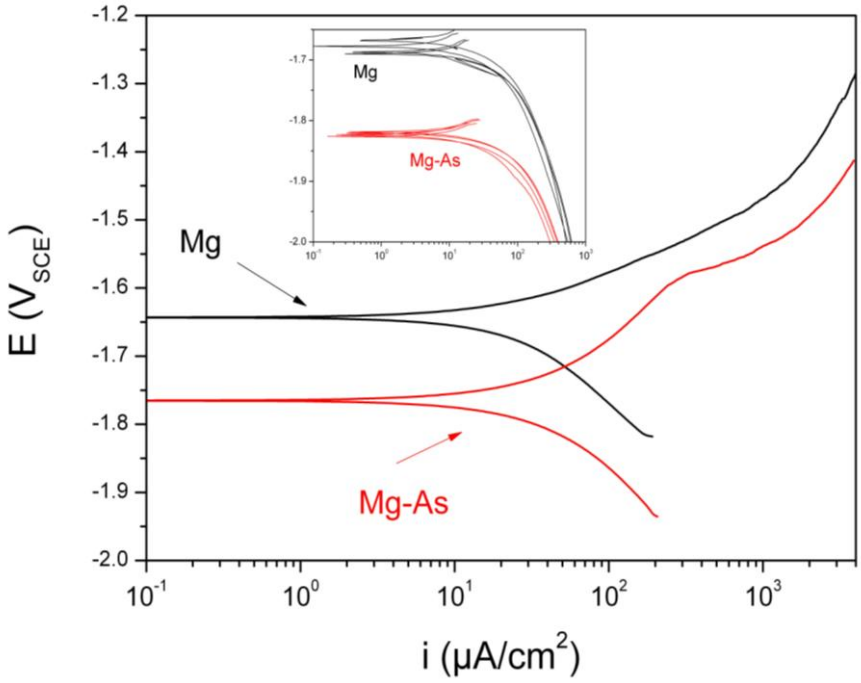

***Figure 2**: Potentiodynamic polarisation curves for Mg and Mg - 0.37 wt.% As (inset: Replicate cathodic polarisation curves).*

cathode, however the presence of alloyed As was able to effectively reduce the cathodic reaction rates. The corrosion potential of the Mg–As alloy is ~150 mV less noble than that of pure Mg, owing to the reduction in the rate of the cathodic reaction. To ensure that this finding was highly reproducible, a significant number of duplicate cathodic polarization tests were conducted and shown in the inset of Fig. 2. It is therefore revealed that metallic As has a significant influence on the electrochemical response of Mg. The other feature of note in Fig. 2 is that the Mg–As alloy reveals somewhat of an inflexion in the current density at potential values of about −1.65VSCE. This inflexion appears to be of the form of what is typically termed a breakdown potential, however such breakdown is usually reserved for passive system signalling the passive to active transition. In the case of Mg, any surface films are nominally only partially protective. In the case of Mg–As where the corrosion potential of the alloy has been suppressed, the revelation of a breakdown in the vicinity of the corrosion potential of pure Mg has not been previously reported. This effect was not necessarily anticipated as a functional step for As providing corrosion protection, however is an apparent coincidence of the suppression of the cathodic reaction (which for Mg is not able to be artificially achieved by deaeration given that the cathodic reaction rate is independent of oxygen concentration). A concomitantly lower level of surface attack together with a differing corrosion morphology, was observed following immersion of the pure Mg and Mg–As in 0.1 M NaCl for 24 h. For pure Mg, a relatively widespread surface coverage of what

is the typically observed filiform-like corrosion morphology [16] was observed for pure Mg (Fig. 1c), whereas for Mg–As, discrete corrosion sites were observed (Fig. 1d). This difference in morphology for minor alloying additions is rather marked, indicating that As is able to halt the filiform-like attack that spreads across Mg, noted to be cathodically controlled [16]. Of major interest is also the notion that a large proportion of the Mg–As surface remains completely unattacked, even after 24 h in 0.1 M NaCl, suggestive that passive-like dissolution rates can prevail upon the majority of the alloy surface (in spite of purported thermodynamic instability [2]). Longer term (7 day) mass loss tests coupled with simultaneous hydrogen collection indicate that the corrosion of the Mg–As alloy was ~5 times lower than pure Mg, with pure Mg being traditionally regarded as the most corrosion resistant form of Mg and its alloys [7]. It is also noted that the attendant hydrogen evolved was, for a 0.37wt.% As addition, an order of magnitude lower on average compared with pure Mg. The variations observed are deemed to be statistically significant, since they are outside the range of scatter for each material and test type (Fig. 3).

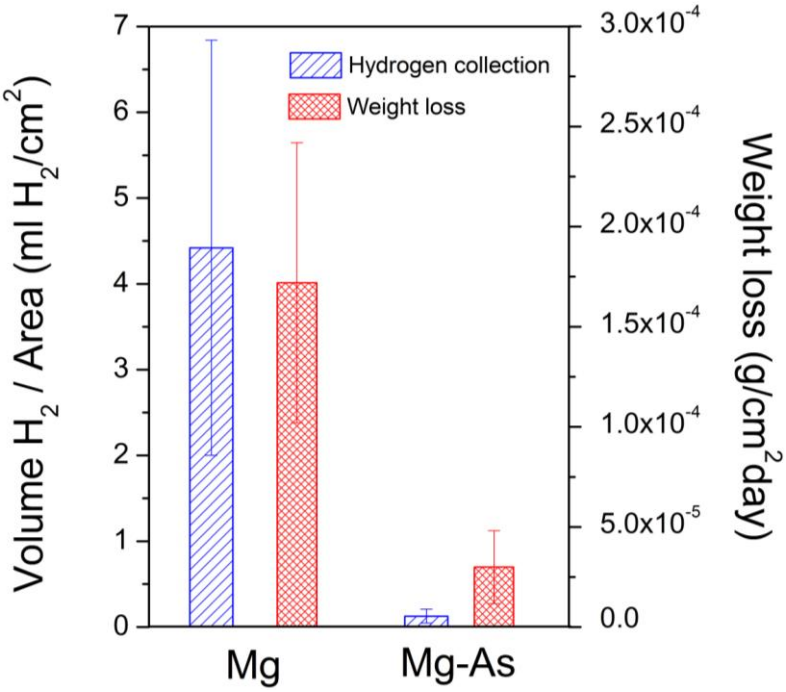

***Figure 3**: Mass loss and hydrogen evolved following 7 days of immersion in 0.1M NaCl for pure Mg and Mg - 0.37 wt.% As.*

It is proposed that the action of the As alloying addition is to stifle hydrogen evolution by poisoning the principal cathodic sites on Mg. McNulty and Hanawalt, in their seminal paper, following the foundational work of Boyer [3], argued that iron-rich second-phase particles constitute the principal cathodic hydrogen evolution reaction

(HER) site on Mg [17]. They also demonstrated a 'tolerance limit' for iron of 100–320 ppm, above which second-phase particles became too large to be covered over by any surface film and steady-state HER rate increased dramatically. Recent thermodynamic calculations of the Mg- Fe phase diagram have predicted a Fe tolerance limit of 180 ppm, above which a discrete iron-rich BCC phase exists [18]. However, the same predictions depend on thermal history and the limit falls to 5– 10 ppm for samples heat treated at 550oC. McNulty and Hanawalt similarly concluded that "the corrosion behaviour of the highest purity specimens (10 ppm Fe) is still a function of the trace impurities contained" [17]. It is therefore reasonable to assume that Fe or a Fe-rich second phase will be an important site of cathodic HER in our experimental samples. The kinetics of the HER are known to be strongly influenced by adsorption of cathodic poisons such as arsenic, antimony, thiourea, for example, [19–21] which decrease surface coverage by the adsorbed H atom intermediate and hence the rate of the H atom recombination. Arsenic is the most powerful of the cathodic poisons [22]. It is therefore reasonable to hypothesise that low-level alloying additions of As might produce a similar effect in cast Mg if this resulted in As(0) being (or becoming) present at the surface of any iron (rich) phase.

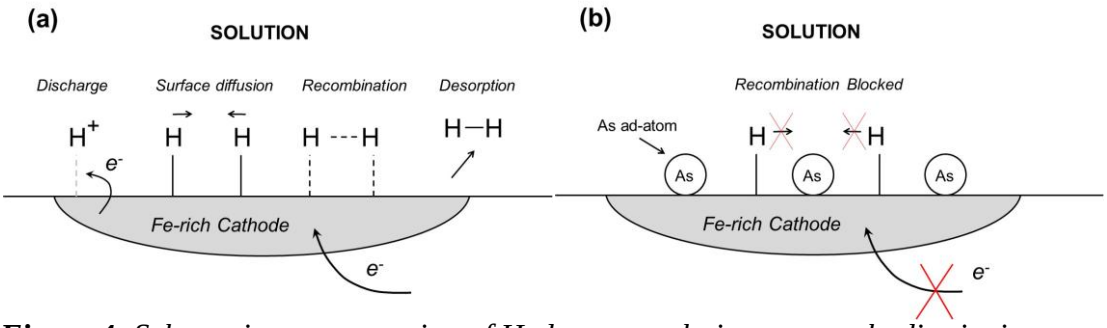

***Figure 4**: Schematic representation of Hydrogen evolution on a cathodic site in the absence (a) and presence (b) of arsenic.*

The mechanism by which this is achieved is summarised in Fig. 4, with As(0) surface deposits or ad-atoms to effectively block H atom recombination. This hypothesised mechanism will require future work to further validate. The approach of imparting functionality via a cathodic poison is uniquely suited to Mg, since of the engineering metals,Mg and its alloys are the only metals in which water reduction (and hence hydrogen evolution) is the sole cathodic reaction.

Of all elements ever studied as additions to Mg to date, only As has the ability to significantly reduce the rate of corrosion of Mg; which is an important finding in the development of next generation Mg-alloys.

Conclusions

1. Kinetics of the hydrogen evolution (cathodic) reaction upon Mg were strongly influenced by the presence of alloyed As.

2. The reduction in corrosion rates arising from metallurgically alloyed As was clearly evident beyond any statistical variation from all of hydrogen collection, mass loss, and polarisation testing.

3. The decreased cathodic kinetics are posited to arise from interfering with the H atom recombination by a cathodic poisoning mechanism.

4. The presence of alloyed As also modifies the resultant corrosion morphology upon Mg, mitigating the typically observed filiform like corrosion.

Acknowledgements

We acknowledge the Australian Research Council Centre of Excellence for Design in Light Metals and use of facilities in the Monash Centre for Electron Microscopy.

References

[1] G.L. Makar, J. Kruger, International Materials Reviews 38 (3) (1993) 138.
[2] M. Pourbaix, Atlas of electrochemical equilibria in aqueous solutions, National Association of Corrosion Engineers, Houston, TX, USA, 1974.
[3] J.A. Boyer, The corrosion of magnesiumand of themagnesiumaluminum alloys containing manganese, Report-248, American Magnesium Corporation, Niagara Falls, NY, USA, 1927.
[4] G.L. Makar, J. Kruger, Journal of the Electrochemical Society 137 (1990) 414.
[5] N.T. Kirkland, J. Lespagnol, N. Birbilis, M.P. Staiger, Corrosion Science 52 (2010) 287.
[6] A.D. Sudholz, N. Birbilis, C.J. Bettles, M.A. Gibson, Journal of Alloys and Compounds 471 (2009) 109.
[7] F. Cao, Z. Shi, G.-L. Song,M. Liu, A. Atrens, Corrosion Science (2013), http://dx.doi.org/ 10.1016/j.corsci.2013.06.030, (in press).
[8] J.O'.M. Bockris, A.K.N. Reddy,Modern Electrochemistry 2B: Electrodics in Chemistry, Engineering, Biology and Environmental Science, Springer, NY, USA, 2001.
[9] G.S. Frankel, A. Samaniego, N. Birbilis, Corrosion Science 70 (2013) 104.
[10] I.J. Polmear, Light Alloys: Metallurgy of the light metals, 3rd edn Edward Arnold, London, UK, 1995.
[11] T.B. Massalski, O. Hiroaki, P.R. Subramanian, L. Kacprzak, Binary alloy phase diagrams, ASM International, OH, USA, 1990.

[12] N.T. Kirkland, N. Birbilis, J.Walker, T.B.Woodfield, G.J. Dias,M.P. Staiger, In-vitro dissolution of magnesium–calcium binary alloys: Clarifying the unique role of calcium additions in bioresorbablemagnesium implant alloys, Journal of BiomedicalMaterials Part B: Applied Biomaterials 95B (1) (2010) 91.
[13] A.D. Sudholz, K. Gusieva, X.B. Chen, B.C. Muddle, M.A. Gibson, N. Birbilis, Corrosion Science 53 (2011) 2277.
[14] D. Eaves, G. Williams, H.N. McMurray, Electrochimica Acta 79 (2012) 1.
[15] N.T. Kirkland, N. Birbilis, M.P. Staiger, Acta Biomaterialia 8 (2012) 925.
[16] G. Williams, H.N. McMurray, Journal of the Electrochemical Society 155 (7) (2008) C340.
[17] R.E. McNulty, J.D. Hanawalt, Journal of the Electrochemical Society 81 (1) (1942) 423.
[18] M. Liu, P.J. Uggowitzer, A.V. Nagasekhar, P. Schmutz, M. Easton, G.-L. Song, A. Atrens, Corrosion Science 51 (2009) 602.
[19] P. Stonehart, G. Kohlmayr, Electrochimica Acta 17 (1972) 369.
[20] J.O'.M. Bockris, B.E. Conway, Studies in hydrogen overpotential, Transactions of the Faraday Society 45 (1949) 989.
[21] J. Barbier, E. Lamy-Pitara, P. Marecot, J.P. Boitiaux, J. Cosyns, F. Verna, in: D.D.
Eley, H. Pines, P.B. Weisz (Eds.), Advances in Catalysis, 37, Academic Press, NY, 1990, p. 279.
[22] B.E. Conway, B.V. Tilak, Advances in Catalysis 38 (1992) 1.

Exploring the Possibility of Protective Surface Oxides Upon Mg alloy AZ31 via Lutetium Additions

A. Samaniego[a,b,], K. Gusieva[a], I. Llorente[b], S. Feliu Jr[b]. and N. Birbilis[a]

[a]Department of Materials Engineering, Monash University, Clayton, VIC 3800. Australia
[b]National Centre for Metallurgical Research (CENIM-CSIC). Department of Materials Engineering, Corrosion and Durability, Madrid, 828040, Spain.

Abstract

In the present study, Mg-alloy AZ31 was alloyed with low-level lutetium (Lu) additions, with the aim of generating a more protective surface oxide/film. To stimulate Lu-rich surface films, AZ31 + Lu specimens were heat treated at 400ºC for up to 300 minutes. Lu was not detected in the α-Mg matrix by EDXS; instead it was incorporated in Al-Mn-Lu particles. Micro-additions of Lu promoted a significant reduction of corrosion rates of as-cast AZ31, although Lu was not detected in the surface oxide as determined by XPS. The subsequent heat treatment of as-cast AZ31+ Lu had a negative impact upon corrosion.

Keywords: Magnesium alloy, lutetium, AZ31, corrosion, alloying

En revisión en Corrosion Science

1. Introduction

Magnesium (Mg) alloys posses a combination of low density, high specific strength and good castability, which makes them promising lightweight structural materials [1]. Currently, magnesium usage has risen to make it the third most used structural metal behind iron and aluminium based alloys [1-3]. However magnesium is prone to corrosion in atmospheric conditions, which currently limits its wider use. Among the Mg alloys, AZ31 (nominal Mg- 3 wt. % Al - 1 wt. % Zn) presents a balance of properties and price and hence nowadays commonly used industrially [4]. However the corrosion rate of AZ31 is still too rapid for numerous engineering applications and its durability must still be improved [4], which is nominally achieved by surface coatings [5]; however the study herein is an effort to improve the corrosion properties of this alloy in the cast condition.

Although magnesium is a very active metal with a reduction potential of -2.4V_{SHE} [6], any oxides which form on the surface do not kinetically passivate the surface owing to a combination of, i) a low Pilling-Bedworth coefficient of <1 leading to incomplete surface oxide coverage, ii) the solubility of surface oxide/hydroxides in atmospheric conditions. Generally, magnesium hydroxide ($Mg(OH)_2$) is soluble in environments below pH ~11 and does not provide corrosion protection [7-10]. The presence of aluminium in the alloy has been reported to influence the corrosion rate of Mg-alloys, and perhaps the protective ability of any surface film [11-14]. These issues are obviously further influenced by the % Al added, since additions > ~3 wt.% Al in the AZ class of alloys lead to a discrete second phase ($Mg_{17}Al_{12}$) which can localise the corrosion reactions and accelerate corrosion. Recent studies using focused ion beam (FIB) prepared specimens for subsequent scanning TEM and x-ray microanalysis (STEM-EDX) suggested that some Al enrichment was developed at the surface of Mg [14]. More specifically, a recent study by Danaie et al. [15] which employed the FIB-STEM approach, revealed the enrichment of metallic Al at the surface of the Mg alloy AM50 (nominal Mg- 5 wt. % Al – 0.5 wt. % Mn). Independent studies employing XPS [13] have also noted a segregation of Al in the case AZ Mg alloys where moderate increases in the level of Al just beneath the native oxide film were detected. All in all however, as clearly obvious from the empirically determined corrosion rates of Al containing Mg-alloys, the surface layers formed still provide insufficient protection from corrosion; therefore the surface film compositions need to be further altered to impart protective properties and promote a reduction in corrosion rate.

The influence of rare earth (RE) elements (i.e. Ce, La, Nd, Y, etc.) on the corrosion properties of Mg, although studied [16-18], has not been extensively interpreted in the context of the surface films developed. It is known that the presence of RE concentrations above their respective solubility limit increases alloy corrosion rate, and that the corrosion rate increases monotonically with subsequent increases in RE content [17, 19, 20]. This is attributed to the ability of RE-rich intermetallics to support the reduction reaction at enhanced rates [21], whilst at lower concentrations (<<1%), REs may not be detrimental for corrosion [22], however the effect is likely to depend on the specific RE element added. Studies focused on the addition of RE elements into AZ (Mg–Al–Zn) or AM (Mg–Al–Mn) series Mg alloys have indicated that that RE alloying additions can result in moderation of corrosion rate in those alloys [23-27]. Some of these studies also purport an influence of the RE element on the nature of the surface film formed upon the respective Mg alloys [16, 26, 27]. Based on such empirical findings, further insights into the possibilities for specific alloying elements to influence corrosion protection via modified surface films appear a worthy avenue of work. To this end, from a theoretical standpoint, modifying Mg (oxide) surface films via alloying would require an alloying element with a higher tendency to combine with oxygen than the tendency of Mg. Given the reactivity of Mg and its tendency to form MgO ($\Delta G_{f\ MgO}^{o}$= -569.3 kJ/mol) [28], there are only finite options of the known elements.

Of the elements, X, which could thermodynamically replace Mg-oxide on the surface of an Mg-X alloy, a criterion would be that any X-oxide be less soluble than Mg-oxides/hydroxides at neutral pH. As such, elements such as calcium (Ca) which do not passivate below ~pH ~12, are less desirable than Mg itself.

Of candidate elements, those potentially effective (in order) include Th, Sc, Be, Lu, Er, Tm and Ho. Based on practicalities that include toxicity, price and radioactivity, the (presently) most practical selection is therefore lutetium (Lu). The influence of Lu on Mg or Mg-alloys has not previously been reported, with no other documented use of Lu as an alloying element for Mg, other than the work herein.

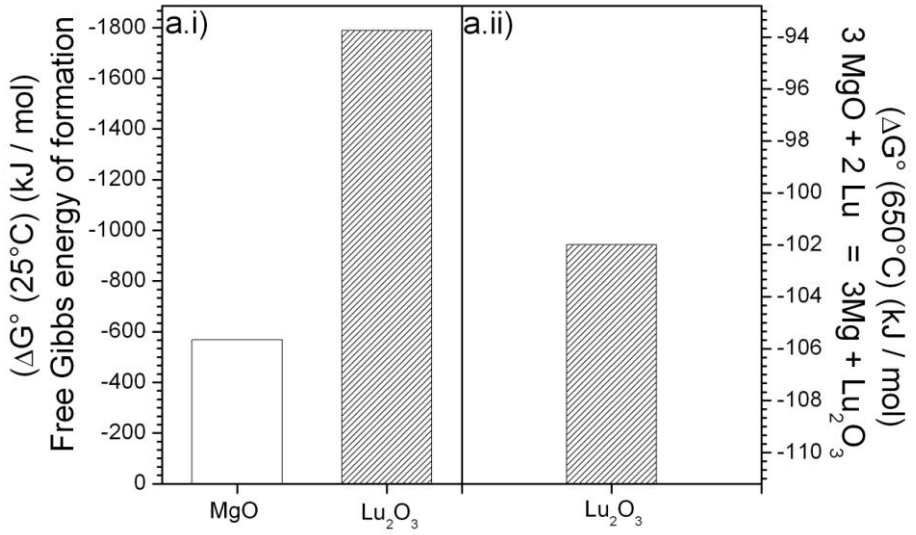

Figure 1a. *Thermodynamic data for Mg/MgO and Lu/Lu2O3 a.i) Standard Gibbs free energy of formation of MgO and Lu2O3 (25ºC). a.ii). Standard Gibbs free energy of the following equation: (Lutetium replacing Mg in the oxide): 3 MgO + 2 Lu = 3Mg + Lu2O3 at 650 ºC [28]. b) Evolution of ionic species concentration with pH. [7]*

Theoretically, Lu replacing Mg in the surface oxide is possible due to the free energy of formation, $\Delta G^{o}_{Lu_2O_3}$, being -1789.1 kJ/mol (25ºC) [28]. Lu also presents a high tendency to replace Mg at high temperature as the $\Delta G^{o}_{(650ºC)}$ = -102 kJ/mol $_{Lu_2O_3}$ (Reaction 1, Figure 1(a)).

$$3\ MgO + 2\ Lu \rightarrow 3\ Mg + Lu_2O_3 \quad \Delta G^{o}_{(650ºC)} = -102\ kJ \quad (1)$$

Furthermore, some potential benefits are that Lu_2O_3 has a Pilling-Bedworth coefficient value of 1.093 [29], and $Lu(OH)_3$ is stable over the pH window above pH as low as ~7, whilst $Mg(OH)_2$ is stable > ~11.5 [7]. This stability region is seen in Figure 1(b) and also elaborated in Figure 2, which provides a more obvious visual representation whilst also indicating the location of other RE metal hydroxides. As such, if Lu_2O_3 is able to

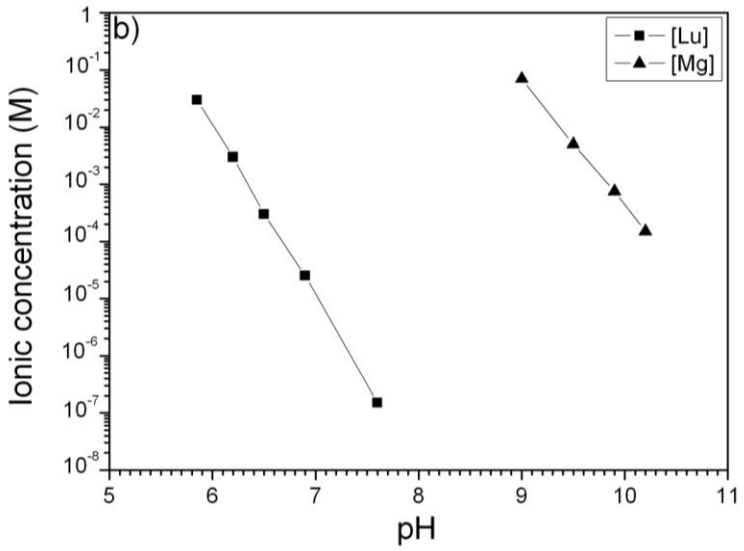

Figure 1b. *Thermodynamic data for Mg/MgO and Lu/Lu_2O_3. Saturation concentration of ionic species with pH.*

preferentially form as the surface film if Lu is alloyed with Mg, it could provide increased protection at lower pH - which could expand the range of potential applications for Mg alloys. The present work is an initial exploration, based on theoretical considerations and without prior empirical knowledge on critical concentrations, or kinetic effects. It is noted that Lu is comparatively heavy with respect to Mg, somewhat rare (the 60th most abundant element on Earth) and the most difficult to extract of the lanthanide series elements, which also makes it relatively expensive [30]. Considering, the previous reported studies which reported RE contents of ~0.5 wt% [22], it was also deemed logical to study similarly low additions of Lu (i.e. ≤0.5 wt%) in this first instance, since, i) low levels of Lu additions were determined to be the safest in the development of melting and casting protocols for a previously un-investigated (and reactive) element; ii) given the additional cost, the study of low Lu levels could practically be most important, similarly, given the density penalty, low levels are again practically most important.

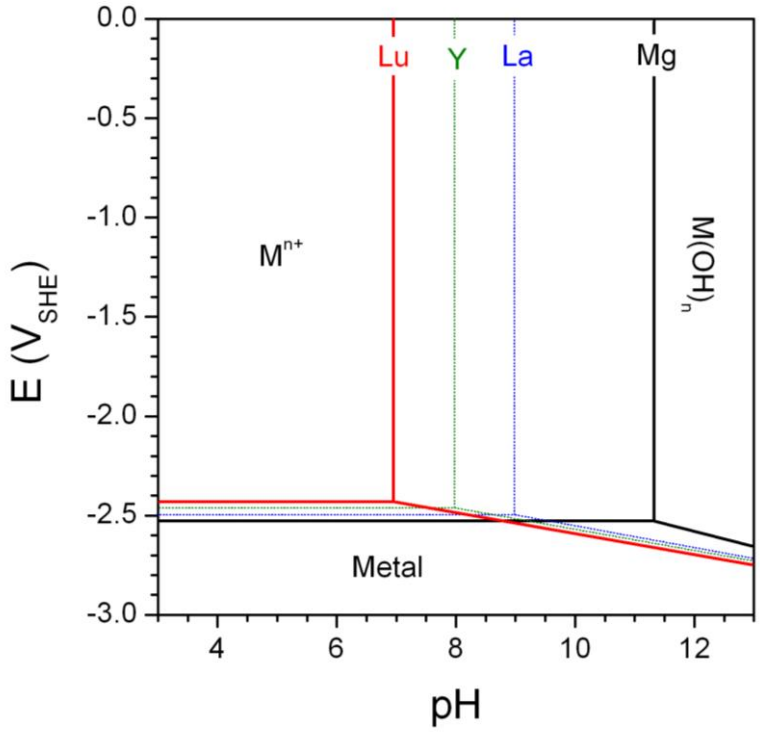

Figure 2. *Simplified Potential (E) - pH diagram showing the domains of thermodynamic stability for various metals (at a metal ion concentration of 10-6 M, 25°C). The vertical lines are of most relevance in the context of this study, as the domains of stability of the metals shown have very similar forms, with a single transition in pH defining the 'active' to 'passive' state. The value of this pH differs for the different metals; Lu(OH)3 shows a wider domain of passivity compared to that of magnesium and other metal hydroxides [7].*

Herein we report the changes in surface oxide, microstructure and corrosion properties of commercial AZ31 alloyed with low-level additions of Lu (0.21 wt.%).

2. Experimental.

2.1 Alloys.

Samples used in this work were prepared from commercially available AZ31(B) ingot. Because of the different physical properties of Mg and Lu (pure Mg melts at about 650 ºC while Lu melts around 1663ºC [31], pure Lu was finely cut and placed into an orifice made inside an AZ31 block to facilitate liquid-solid diffusion and subsequent melting of Lu into the AZ31. The alloys were melted in an induction furnace (Leybold-Heraeus) under an argon atmosphere. The melt was maintained at a temperature of 730 ºC within a mild steel crucible coated with graphite. After three cycles of vigorous stirring over

the course of approximately one hour, the melt was then poured into a pre-heated (to 250 ºC) steel mold and left to cool to room temperature inside the chamber.

The compositions of alloys tested are given in Table 1. The precise composition was confirmed via inductively coupled plasma atomic emission spectrometry (ICP-AES), carried out by Spectrometer Services (Coburg, Victoria, Australia).

Table 1. *Composition of alloys tested herein as measured by ICP-AES.*

(wt.%)	%Mg	%Al	%Zn	%Mn	%Lu	%Fe
AZ31	95.48	3.28	0.86	0.38	-	0.010
AZ31-Lu	95.5	3.05	0.91	0.36	0.21	0.002

To potentially stimulate Lu-rich surface films, samples were also subsequently heat treated in air at 400 ºC for times ranging from 0 to 300 minutes. According to the Mg-Lu phase diagram (Figure 3), there are no phases in the alloy that would melt at 400 ºC. We also note that the phase diagram for AZ31+Lu could not be produced on the basis that Lu does not populate the commercially available CALPHAD databases. Longer heat treatment times were not used so as to avoid the potential growth of undesired globular oxides [32]. Three types of heat treatment were performed: (a) from room temperature to 400 ºC at a rate of 20 ºC/min; denoted as "Ramp"; (b) Ramp + 100 min at 400 ºC; and, (c) Ramp + 300 min at 400 ºC. After heat treatment specimens were air-cooled.

2.2 Microstructural characterisation

For metallographic characterisation, specimens were polished according to standard metallographic procedures and then given an additional polishing step using non-crystalline colloidal silica suspension (0.05μm). For general microstructural characterisation, samples were examined by scanning electron microscopy (SEM) using a JEOL JSM-6400 electron microscope in back-scattered electron mode (BSE), equipped with an Oxford Link energy dispersive X-ray spectrometer.

Grain size was determined by optical microscopy; specimens were etched for ~5 s in a solution of 225 mL ethanol / 12.5 mL picric acid / 40 mL acetic acid / 40 mL water.

Surface potential maps were obtained using an atomic force microscope (AFM, 5100, Agilent Technologies) working in acoustic AC Mode (tapping mode). AppNano tips made of n-type Si coated with Pt were used. The tip length was 225 μm and resonant frequency between 50–70 kHz. A dual scan mode was used to record a potential signal as well as the surface topography signal. The topography of the sample surface was obtained in the first pass. In the second pass, the cantilever was lifted up 100 nm to avoid the influence of topographic features on the potential mapping.

The potential values obtained were done so using the so-called Scanning Kelvin probe Force Microscopy (SKPFM) method [33, 34] and were referenced against the potential of the tip used. In this study, all AFM and SKPFM measurements were performed in air at room temperature.

2.3 Surface characterisation.

2.3.1 X-ray photoelectron spectroscopy (XPS)

Photoelectron spectra were acquired using a Fisons MT500 spectrometer equipped with a hemispherical electron analyser (CLAM 2) and non-monochromatic magnesium Kα X-ray source operated at 300 W. The specimens were mechanically fixed on small flat discs supported on an XYZ manipulator placed in the analysis chamber. The residual pressure in this ion-pumped analysis chamber was maintained below 10^{-8} Torr during data acquisition. Spectra were collected for 20–90 minutes, depending on the peak intensities, at a pass energy of 20 eV, which is typical for high-resolution conditions. The intensities were estimated by calculating the areas under each peak after smoothing and subtraction of the S-shaped background and fitting the experimental curves to several combined Lorentzian and Gaussian lines; the Lorentzian/Gaussian ratio was not fixed in the fits. Although specimen charging was observed, it was possible to determine accurate binding energies (BE) by referencing to the adventitious C1s peak at 285.0 eV. Atomic ratios were computed from peak intensity ratios and reported atomic sensitivity factors [35]. The sampled areas were 1×1 mm^2. The energy resolution was about 0.8 eV. Bombardment was performed using an EXO5 ion gun incorporated in the equipment, provided with a scanning unit to track the beam and operating at a voltage of 5 kV, an intensity of 10 mA and a pressure of 1×10^{-7} Torr. The sample current was 1 μA during bombardment.

2.3.2 Surface conductivity

Surface conductivity was measured using a Jandel Model RM3 four-point probe. The test was performed five times on each sample at different locations and the mean values were calculated.

2.4 Corrosion tests.

2.4.1 Electrochemical Testing.

Potentiodynamic polarisation tests were carried out in quiescent 0.1M NaCl using a standard electrochemical "flat-cell" (PAR) including a saturated calomel reference electrode (SCE), and a Pt-mesh counter electrode. A VMP 3Z potentiostat was used, under the control of EC-Lab software. The open circuit potential was measured for 10 minutes prior to polarisation in order to establish an approximately stable potential. Potentiodynamic polarisation was performed using a sweep rate of 1 mV/s and tests were carried out at least 3 times. The polarisation curves were also used to determine i_{corr} (via a Tafel-type fit) using EC-Lab software. Such fitting is inherently difficult and it was performed using the EC-lab manual control. Fits were executed by selecting a portion of the curve that commenced > 50 mV from E_{corr} and i_{Corr} was subsequently estimated from the value where the fit intercepted the potential value of the true E_{corr}. [17, 18]. The Tafel slopes for this work are not tabulated, however the raw data is given. It is evident that the cathodic Tafel slopes in all cases were close to ~200mV/decade, whilst values for the anodic Tafel slope were in the vicinity of ~200mV/decade, for this alloy system. We don't emphasise the Tafel analysis, since the slopes are subject to change with time, and the long-term corrosion analysis is derived from exposure tests. The purpose of the polarization tests is not a definitive i_{corr}, but a qualitative inspection of relative anodic and cathodic reactions rates, and their variation in processing and composition. To this end, polarization testing is essential.

2.4.2 Hydrogen collection and mass loss testing.

Hydrogen collection and mass loss tests were performed using an inverted burette system [36, 37]. The experimental difficulties and limitations of such tests have recently been documented [38]. Prior to testing, specimens were ground to 2000 grit finish via successive grades of silicon carbide papers, cleaned and weighed. The exposed area was approximately 2.5 cm^2 and specimens were immersed in approximately 200 mL of quiescent 0.1M NaCl at laboratory temperature (20°C) for a period of 7 days. Experiments were performed at least in duplicate. At the end of the exposure test, corrosion products were removed using a chromic acid solution (200 g chromium trioxide (CrO_3), 10 g silver nitrate ($AgNO_3$), 20 g barium nitrate ($Ba(NO_3)_2$) and water to make up to 1000 mL) and the specimens were weighed.

3. Results and Discussion

3.1 Microstructural analysis

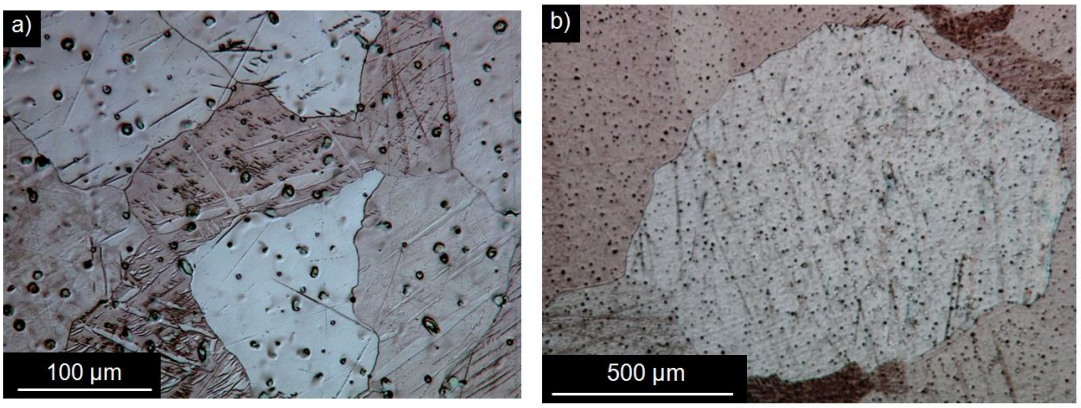

Figure 3. *Typical optical micrographs showing grain structures of as-cast a) AZ31 b) AZ31+0.21% Lu. Specimens were etched in a solution of 225 mL ethanol / 12.5 mL picric acid / 40 mL acetic acid / 40 mL water.*

Optical micrographs (Figure 3) illustrate the typical microstructures of the as-cast alloys prepared herein and formed upon cooling, with uniformly distributed second phase particles evident. The microstructure of the baseline AZ31 consists principally of an α-magnesium matrix (which is a solid solution of Mg-Al-Zn). Particle precipitation in the classical sense does not occur in AZ31, as the alloy composition is such that the Al and Zn content are close to, but not in excess, of the respective solubility limits. As is common with many Mg alloys, Mn is added in small quantities (<0.5 wt. %) and this does result in Al_xMn_y constituent particles, which are common to AZ series of Mg-alloys [39]. A distinction is made that the particles (and indeed constituent type particles by definition) do not have a strong (or often any) response to heat treatment, and are nominally on the size range of >1µm in diameter. This is distinct from precipitates, which respond to thermal treatment and hence vary in size from the nm scale and upwards. The grains of the baseline AZ31 alloy are comparatively small, on average ~100 µm in diameter. On the other hand, although the AZ31+0.21% Lu alloy has similar microstructure to AZ31, it shows a much coarser grain structure, with an average grain diameter of ~700 µm. Whilst not the focus of this study, we also believe it merits comment that further heat-treatment of the AZ31+0.21% Lu alloy (as described below) stimulates the grain growth at a rate greater than any grain growth in the baseline AZ31.

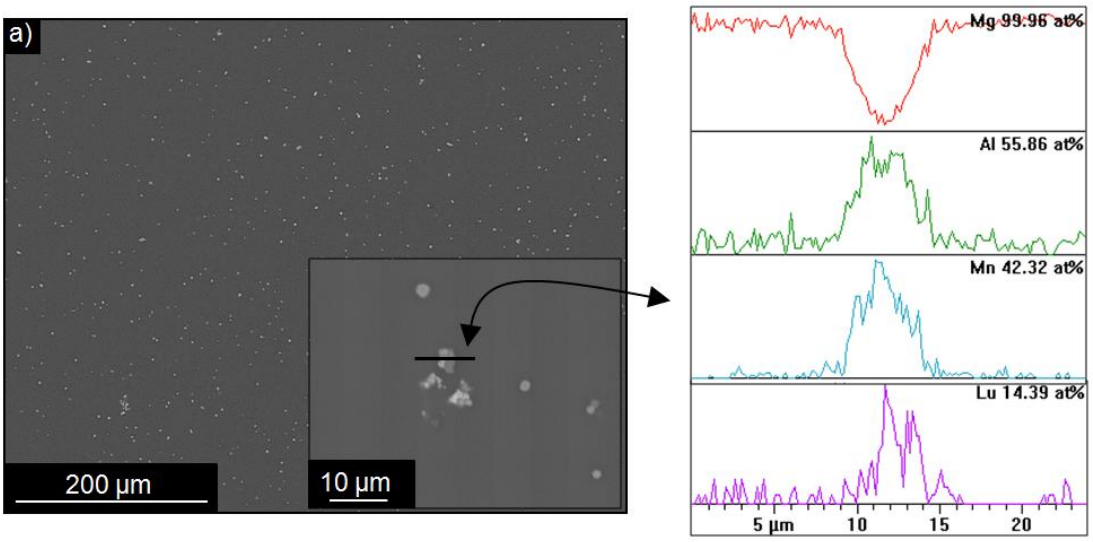

Figure 4a. *Typical SEM images collected in backscattered electron mode of as cast AZ31+0.21% Lu. a) Image, along with the composition profile in the vicinity of a MnAlLu particle (the values given with the line profiles of each element are the peak value for the given element in the scan).*

The backscattered electron SEM image in Figure 4 shows the morphology of the AZ31+0.21% Lu alloy to contain uniformly distributed particles within the α-Mg matrix; which EDXS analysis identified as Mn-Al-Lu (constituent) particles. The amount of Lu detected in the Mn-Al-Lu particles was ~15–30 wt.% (Table 2). As previously mentioned, the prediction a prior was not possible due to the absence of Lu on thermodynamic databases and no published data on the system being studied. When viewed in the context of Lu alloyed with pure Mg, the result is in contrast to the predictions that Lu would dissolve into the α-Mg solid solution (viz. the solid solubility of Lu in Mg is ~3 wt.% at room temperature, [31]). What is empirically observed is that the Lu (added in pure form) was instead segregated to, and became incorporated with, the Al_xMn_y constituent particles. Similar observations from adding other RE elements (although not Lu) where reported by Nordlien [40] who noted no RE elements detectable either in the solid solution matrix or in the oxides of AE alloys since the RE elements segregated to Al and formed Al-Mn-RE. These particles tend to be distributed

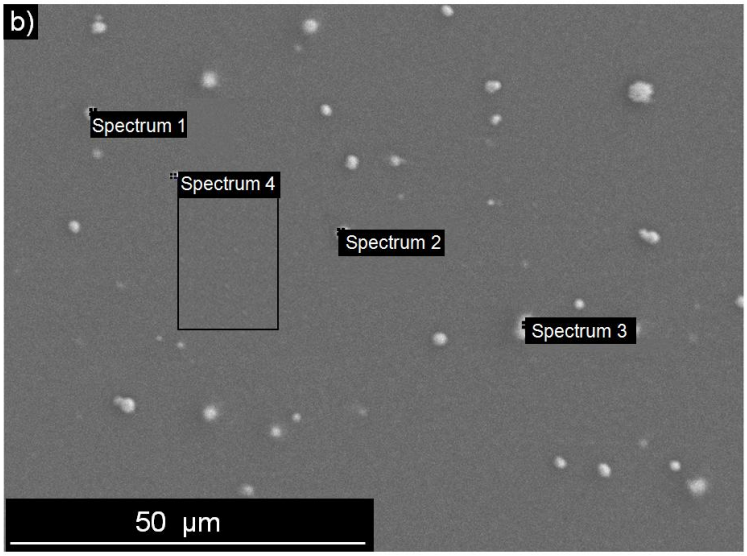

Figure 4b. *Typical SEM images collected in backscattered electron mode of as cast AZ31+0.21% Lu. b) Image showing locations where EDX spectra were measured. Spectra 1–3 were taken from MnAlLu particles, while Spectrum 4 was from the α matrix.*

The backscattered electron SEM image in Figure 4 shows the morphology of the AZ31+0.21% Lu alloy to contain uniformly distributed particles within the α-Mg matrix; which EDXS analysis identified as Mn-Al-Lu (constituent) particles. The amount of Lu detected in the Mn-Al-Lu particles was ~15–30 wt.% (Table 2). As previously mentioned, the prediction a prior was not possible due to the absence of Lu on thermodynamic databases and no published data on the system being studied. When viewed in the context of Lu alloyed with pure Mg, the result is in contrast to the predictions that Lu would dissolve into the α-Mg solid solution (viz. the solid solubility of Lu in Mg is ~3 wt.% at room temperature, [31]). What is empirically observed is that the Lu (added in pure form) was instead segregated to, and became incorporated with, the Al_xMn_y constituent particles. Similar observations from adding other RE elements (although not Lu) where reported by Nordlien [40] who noted no RE elements detectable either in the solid solution matrix or in the oxides of AE alloys since the RE elements segregated to Al and formed Al-Mn-RE. These particles tend to be distributed throughout the alloy matrix, with a size if ~1–3 µm (Figure 4). As per the characteristic thermal response of constituent particles (independent of the alloy system) the constituents in the AZ31+0.21% Lu alloy were not affected by subsequent heat treatment (reported below) with regards to either their volume fraction, number density or distribution.

Table 2. *Spot EDX analysis on AZ31+0.21% Lu, as observed in Figure 6(b). Spectra 1–3 were taken at the surfaces of selected intermetallic particles, while Spectrum 4 was from the α matrix.*

wt.%	%Mg	%Al	%Mn	%Zn	%Lu	Total %
Spectrum 1	45.18	19.91	15.69	-	19.23	100
Spectrum 2	8.30	27.19	34.12	-	30.38	100
Spectrum 3	46.58	18.60	18.56	-	16.26	100
Spectrum 4	96.20	2.60	-	1.20	-	100

A surface potential image (and corresponding topographical image) as determined using SKPFM, along with a Volta potential profile of the AZ31+0.21% Lu alloy show that AlMnLu particles are ~260 mV more noble than the surrounding α-Mg matrix (Figure 5). These values are similar to those observed for the Al_xMn_y particles in AZ31 (~250 mV more noble than the surrounding magnesium matrix), which were reported and observed in previous studies for Mg–Al alloys [41-43]. Therefore, as a first approximation, the electrochemical characteristics may be expected to similar in AZ31+0.21% Lu and in AZ31; whereby in both the case of AZ31 and AZ31+0.21% Lu, the Al_xMn_y and AlMnLu constituent particles are expected to support the cathodic reaction with respect to the α-Mg matrix at open circuit. An obvious caveat is that the Volta potential differences, as measured in air, provide no estimation of the relative electrochemical kinetics.

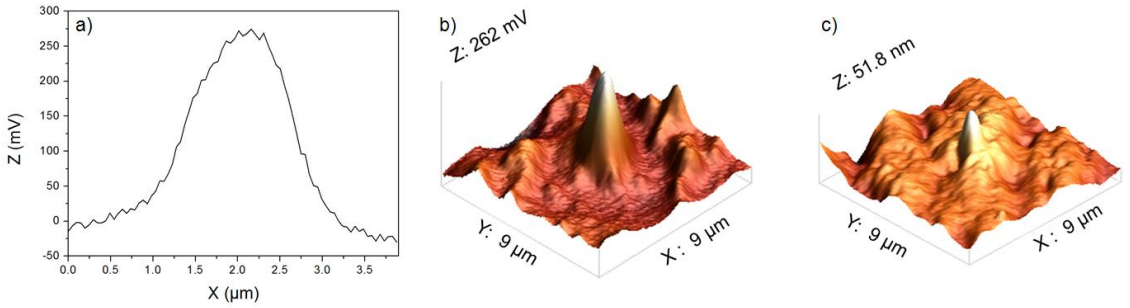

Figure 5. *Scanning Kelvin Probe Force microscopy (SKPFM) measurements on AZ31-0.21%Lu alloy. a) Volta potential profile. b) Volta potential difference image of MnAlLu particle. c) Topographic image of MnAlLu particle.*

3.2 Surface characterisation.

The surface oxide was characterised by XPS in the present study, as we have previously done for Mg-Al alloys [9, 11]. Of the alloys studied, Lu was only detected in small quantities on the surface of the AZ31+0.21% Lu sample heat treated from room temperature to 400ºC (RAMP), as noted in the abridged tabulated values (Table 3). We note that whilst the most intense Lu signal is the Lu4f peak [44, 45], this unfortunately overlaps with the O2s peak and the associated signal corresponding to the valence bands. As such, the presence of Lu was determined by analysing the Lu4d peak, which however has lower intensity. Taking into account that the alloy only contains 0.21 wt.% Lu, and that the intensity of Lu4d is comparatively low, Lu, if in the surface oxide, is below the detection limit of the method / equipment. In all, Lu was not detected in appreciable quantities by the XPS technique.

No significant differences in surface conductivity were observed between alloys and/or heat treatment, so these data are not shown.

Table 3. *Atomic percentage observed by XPS at the outer surface of alloy AZ31+0.21% Lu following different heat treatment durations at 400ºC. Samples were sputtered for different periods of time to yield a concentration profile.*

Sample	Sputtering Time (min)	% C	% O	% Mg	%Al	% Lu
AZ31-Lu	0	37	41	21	1	0
	5	12	49	37	2	0
	10	12	42	43	3	0
AZ31-Lu+RAMP	0	25	51	23	1	0.13
	5	10	48	37	5	0
	10	5	36	56	3	0
AZ31-Lu+100	0	19	51	28	2	0
	5	5	57	36	2	0
	10	5	55	38	2	0
AZ31-Lu+300	0	22	51	25	2	0
	5	4	57	38	1	0
	10	4	56	38	2	0

3.3 Electrochemical and Corrosion testing

The surface of as-cast AZ31+0.21% Lu after 3 hours of immersion in 0.1 M NaCl is shown in Figure 7. Filiform-like corrosion is seen in Figure 6(a); this is consistent with previous studies, where corrosion that resembles the nature of filiform attack was observed in uncoated Mg in chloride-containing environments [46-48]. The nature of this corrosion morphology is not dictated by corrosion under coatings or by the concentration of oxygen, typical of the common definition of filiform attack [6]. Prior studies have employed the scanning vibrating electrode technique (SVET) and reveal that the leading edge of the filament is a focal anode while the active corroded track behind the advancing filament is an activated cathode [21, 48].

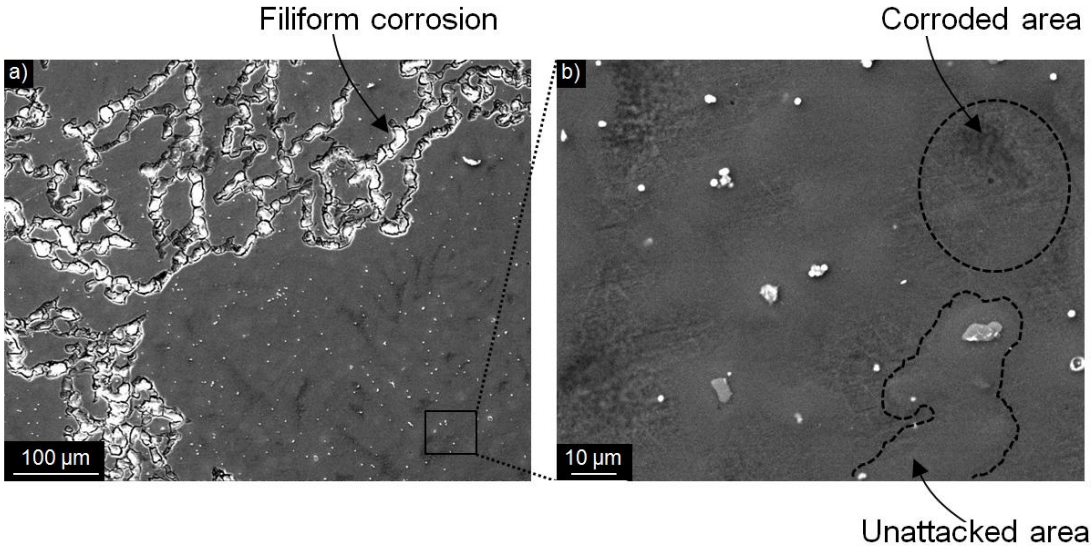

Figure 6. *Backscattered electron SEM images of as cast AZ31-0.21% after 3 hours of immersion in 0.1 M NaCl. a) Lower magnification image, showing filiform-like corrosion; b) higher magnification image showing unattacked areas surrounding intermetallic particles (MnAlLu). The area adjacent to the AlMnLu particles appears uncorroded, whereas corrosion has initiated in the areas farther from the AlMnLu particles.*

The magnified area in Figure 6(b) shows the influence of AlMnLu particles supporting the cathodic reaction locally during the initial stages of corrosion (3 hours of immersion). As a result of the cathodic reaction occurring on such particles, areas of the α–Mg matrix surrounding the AlMnLu particles are less corroded than areas of α matrix some distance away from the particles. In supporting the cathodic reaction, AlMnLu particles (due to hydroxyl ion generation) increase the local pH and contribute to an alkaline, and hence less aggressive, environment surrounding them during the initial

stages of of corrosion. Based on these observations, it seems that the α-Mg matrix is more affected by the local increase of pH due from a localised cathodic reaction than by a localised attack form arising from the micro-galvanic couple.

3.3.1. Instantaneous corrosion rate measurements. Potentiodynamic polarization

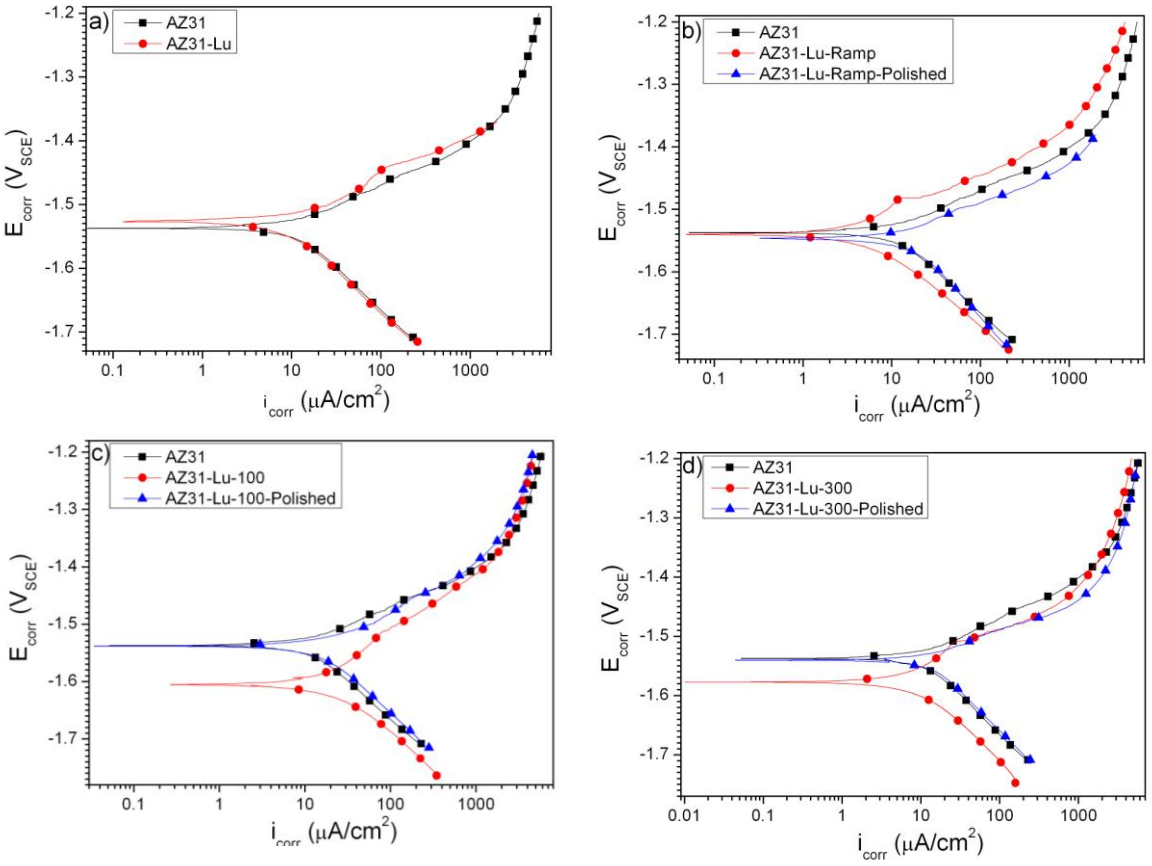

Figure 7. *Comparison between typical polarisation curves of alloys AZ31 and AZ31+0.21% Lu in 0.1 M NaCl following different heat treatments. a) No thermal treatment. b) Ramp (From room temperature to 400 ºC; 20 ºC/min) c) 100 min at 400 ºC. d) 300 min at 400 ºC. Curves represented by triangles were performed on samples heat treated where surface films formed during heat treatment were removed by polishing before the potentiodynamic test*

One characteristic of Mg is an inherently poor ability to support the cathodic reaction, owing to a low exchange current density [37, 46, 49]. The corrosion of Mg is controlled by its cathodic reaction that can accelerate if Mg is alloyed (for example, as in [50]) or dissolved [51]. Mg is affected by impurities or alloying elements with high exchange current densities, which usually serve as potent cathodes and increase corrosion rate [6,

52]. The addition of Lu to AZ31, indicates that Lu tended to combine with Al and Mn without increasing the inherent cathodic characteristics of AZ31. Moreover, although Lu was not detected on the surface of the alloys by XPS, when AZ31+0.21% Lu was heat treated at 400 ºC, the cathodic kinetics tended to decrease (Figure 7 (a–d)). Larger reduction in the cathodic reaction where achieved after longer heat-treatments and as a consequence the instant corrosion current density measured decreased. For instance, AZ31+0.21% Lu samples heat treated at 400ºC during 300 minutes exhibited lower corrosion current densities than specimens heat treated for 100 minutes (Figure 8). After both thermal-treatments, AZ31+0.21% Lu samples exhibited similar anodic curves but cathodic kinetics were lower after 300 minutes of heat treatment.

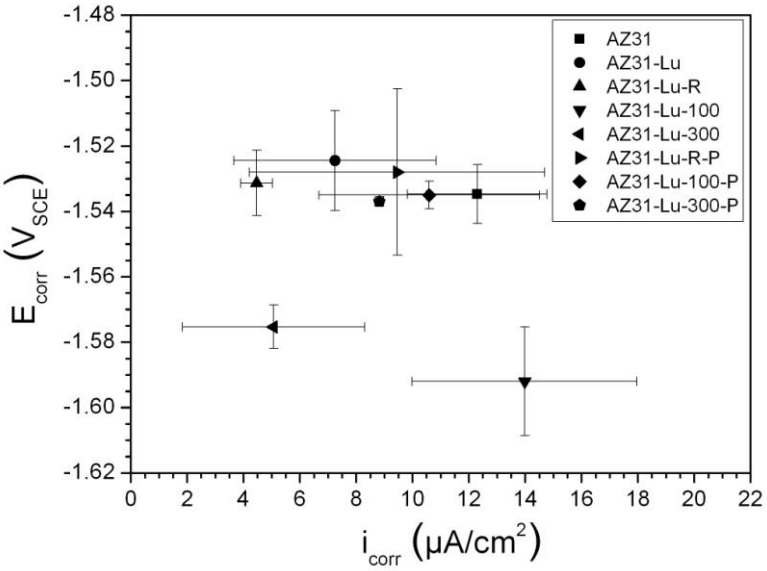

Figure 8. *Corrosion potential (E_{corr}) - Corrosion current density (i_{corr}) plot for all the specimens studied in this work, collected in 0.1 M NaC.l*

A reduction of the cathodic kinetics is usually accompanied by a decrease of the corrosion potential. Figure 8 shows that micro-additions of lutetium did not lead to significant changes in the OCP of the alloy. However, when AZ31+0.21% Lu samples were heat treated during 100 and 300 minutes at 400 ºC the corrosion potential decreased (-1.59 V_{SCE} and -1.575 V_{SCE} respectively) compared with the average value for the rest of the alloys/conditions (~ -1.54 V_{SCE}). This reduction of the cathodic kinetics and the corrosion potential after heat-treatment was only observed when Lu was present in the alloy; therefore we relate this effect with Lu. Moreover, these reductions disappeared when the surface films that evolved during heat treatment were removed by subsequent polishing of specimens.

Concomitantly, if AZ31+0.21% Lu was not heat-treated or just briefly heat-treated (ramping from room temperature to 400 ºC), the anodic kinetics slightly decreased in comparison with those of AZ31 (Figure 7 (a, b)). Some curves (Figure 7 (a, b) exhibited a breakdown in the anodic region, but AZ31-Lu did not present passive behavior under the conditions studied. This reduction in the anodic kinetics completely disappeared after 100 and 300 minutes of heat treatment where both anodic curves were similar (Figure 7 (c, d)).

3.3.3. Long term exposure: Hydrogen collection and mass loss.

All specimens/treatments studied herein were immersed in quiescent 0.1 M NaCl for 7 days in order to determine the associated corrosion over a longer period and from physical means. The results from mass loss testing are seen in Figure 9.

It is observed that rather significant reductions in corrosion rate were observed when low-level additions of Lu were incorporated into the base alloy. This reduction in corrosion rate was seen to deteriorate with the thermal exposure of the AZ31+0.21% Lu alloy. The RAMP specimen having mass loss rates similar to that of the base AZ31, whilst a recovery of some corrosion resistance was achieved on further heat treatment, however not to the low levels of the as-cast AZ31+0.21% Lu.

Figure 10 reveals the data from hydrogen collection experiments. In Figure 10a, the hydrogen evolved over the duration of the experiment is shown for one data set. The trends are obvious, however the average values of hydrogen evolution converted to a rate are presented in Figure 10b. The ranking of the specimens again reveals that the low level additions of Lu were beneficial in reducing the rate of corrosion as determined from evolved hydrogen.

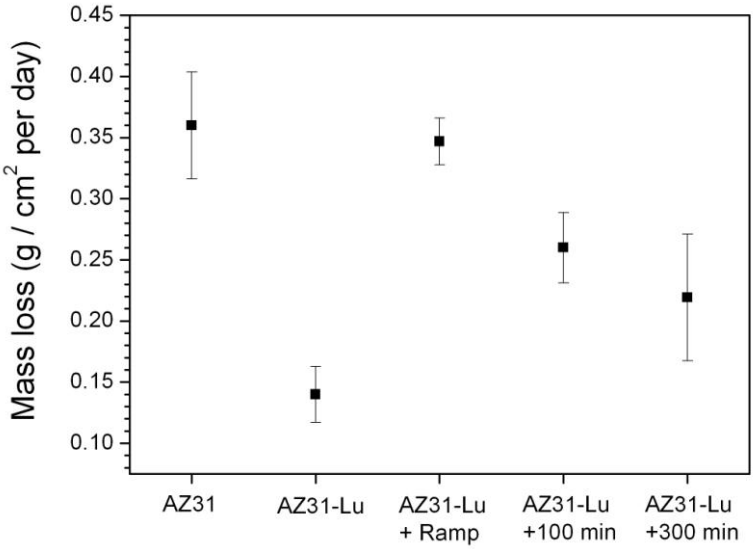

Figure 9. *Average corrosion rate values based on weight loss after 7 days immersion in 0.1 M NaCl for AZ31 and AZ31+0.21% Lu following different heat treatments. To remove corrosion products, samples were cleaned using a chromic acid solution.*

The rates obtained by mass loss and hydrogen collection are compiled in Figure 11, revealing a strong correlation between corrosion rates obtained by mass loss and hydrogen collection, corroborating the data. Figures 9–11 show that as-cast AZ31+0.21% Lu presents the lowest corrosion rate, with rates ~80% lower than that of the base AZ31. Although heat treatment decreased corrosion for short immersion times, the influences of surface oxide tended to disappear when samples were immersed for a week in 0.1 M NaCl solution, likely due to any protective effects from surface films reduced upon extended exposure to Cl^- ions.

What was seen is that heat treatment increases corrosion rate of the as-cast AZ31+0.21% Lu. However, values still remain (albeing marginally in the case of the RAMP specimen) below those AZ31. It is interesting that the RAMP treatment from room temperature to 400ºC produces a greater increase in corrosion rate that than found with longer heat treatments, where samples were exposed at 400 ºC for 100 or 300 minutes. Figure 9 shows that after this initial heat-treatment period, which increases corrosion rate, corrosion rate tends to decrease with increasing heat-treatment time, reaching values only slightly higher than that of the non-heat-treated AZ31-Lu after 300 minutes at 400 ºC. This is in agreement with conclusions from electrochemical techniques, where a reduction in the cathodic kinetics was observed after longer thermal-treatments (100 and 300 minutes), than after shorter ones (RAMP) (Figure

7b,c,d)). A reduction of the open circuit potential (OCP) was observed following 100 minutes of heat-treatment (HT), whilst a reductios of cathodic kinetics was higher following 300 minutes rather than after 100 minutes of heat treatment (Figure 7c,d)); with the average instantaneous corrosion current density being 14 and 5 $\mu A/cm^2$ respectively (Figure 8).

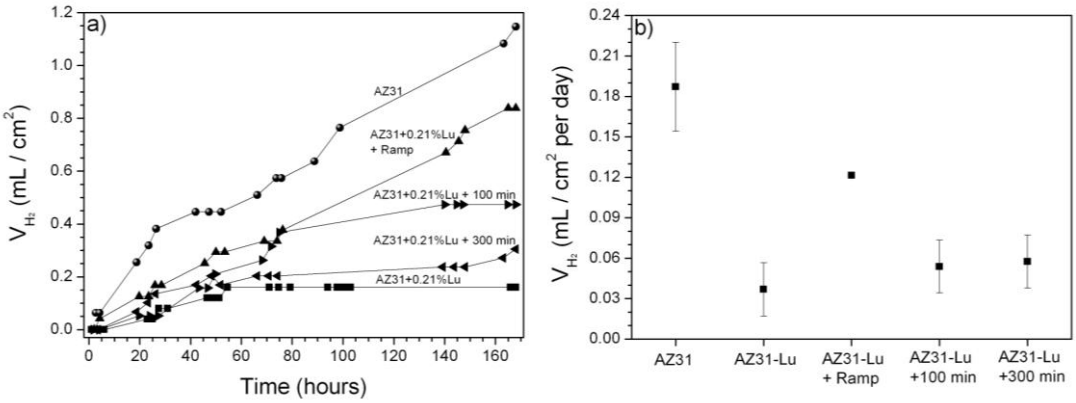

Figure 10. *The influence of low level Lu additions and heat treatment on hydrogen volume collected after 7 days immersion in 0.1M NaCl for AZ31 and AZ31+0.21%Lu. a) Volume of hydrogen collected with time b) Average values converted to a rate.*

We recall that the average grain size in the as-cast AZ31+0.21% Lu (~700 µm) is larger than the average grain size of as-cast AZ31 (~100 µm); however we don't believe that the different in corrosion rates reported herein are principally associated with this difference in grain size. The influence of grain size on the corrosion of Mg alloys depends on several factors, including the chloride concentration of the environment and the pH. Previous studies performed in 0.1 M NaCl reported that finer grain size leads to oxide/hydroxide surface films which can resist breakdown more effectively than the films formed on specimens with larger grain size [48]. Moreover, the heat-treated AZ31+0.21% Lu samples have larger average grain sizes than the untreated AZ31+0.21% Lu, but corrode faster; thus, although grain size may have some influence on corrosion, it is not the principal cause of the difference in corrosion rate described in this work.

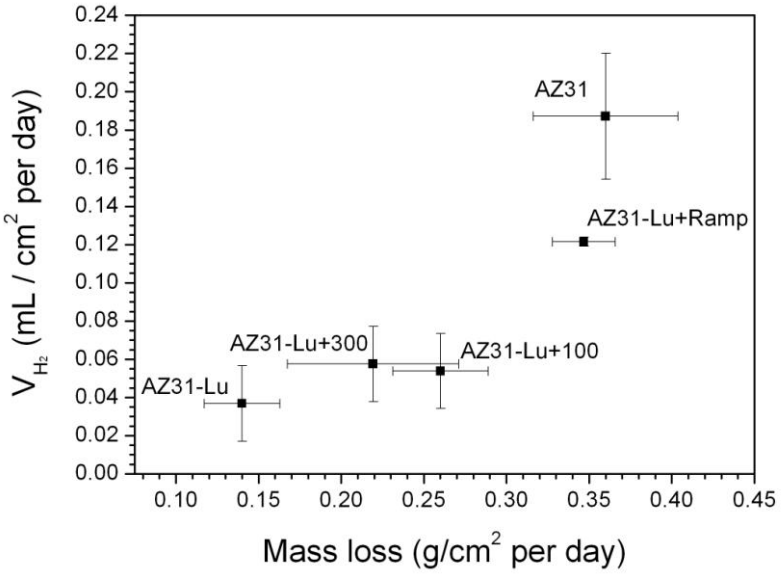

Figure 11. *Comparison of corrosion rates measured by weight loss and hydrogen evolution for specimens immersed in quiescent 0.1M NaCl.*

3.4 General discussion

The work herein, from a variety of tests, indicates that micro-additions of Lu decrease the extent of corrosion realised by AZ31. The precise atomic scale mechanism for this was difficult to elucidate, however mechanistic interpretation from polarisation data coupled with XPS indicate that oxide doping was not excessive, although kinetics of the corrosion reactions were altered. Other works studying RE additions to AZ alloys have suggested an additional stabilization of the surface oxide layer, improving the corrosion resistance of the alloy – however the definitive mechanisms in such work were not defined [16, 26, 27]. What is however apparent, is that the presence of aluminium in the alloy is crucial to obtain a beneficial effect [40]. This can be rationalised on the basis of the notion that RE additions including Ce, La, Nd and Y, have all been shown to deteriorate the corrosion performance of Mg when added as binary additions [17]. If such rationale can be translated to Lu, albeit with caution given, then the combined presence of the Al may be a requirement for the improvement in corrosion resistance.

Although short time heat-treatments had a negative impact on the corrosion of AZ31+0.21% Lu, longer heat-treatment led to a more protective surface film. In order to explore the development of a more resistant passive layer, future work involving longer heat treatment times may be performed, along with differing loadings of Lu.

4. Conclusions

1. The safe production of AZ31 + 0.21 wt. % Lu was achieved, with XPS results indicating that the addition of 0.21 wt. % Lu in AZ31 does not lead to replacement of magnesium in the developed surface oxide/hydroxide. However, when added to AZ31, Lu promotes the change of reducing cathodic kinetics during the initial stages of corrosion, for alloys in the as-cast condition. The work herein did not explore a wider range (and hence did not determine a critical content) of Lu additions in this first instance – however heat treatments were investigated. It was seen that heat treatments at elevated temperatures (at 400 ºC for up to 300 minutes), intended to stimulate Lu-rich surface films, had a negative impact on the corrosion of AZ31+ 0.21% Lu.
2. The corrosion rate of AZ31 in the as-cast condition (which is the nominally used condition for AZ31 commercially) decreased when 0.21 wt. % Lu was added. This was observed both electrochemically (from the average values of 12.3 to 7.25 $\mu A/cm^2$), from mass loss (from the average values of 0.36 to 0.14 mg/cm^2 per day) and also from hydrogen collection tests (from the average values of 0.187 to 0.037 mL/cm^2 per day). The combination of the methods, and replicate tests, make the reduction in corrosion rate statistically relevant.
3. We did not detect any appreciable amount of Lu in the matrix solid solution; however it was noted that Lu tends to combine with Al and Mn to form Al-Mn-Lu particles (~2 µm in diameter).
4. Additions of Lu to Al-Mn particles do not significantly change the cathodic activity of these particles relative to the magnesium matrix. Al-Mn-Lu particles are ~260 mV more cathodic than the surrounding magnesium matrix – based on the measured Volta potentials in air. Micro-additions of Lu were found to increase the as-cast grain size of AZ31 magnesium alloy (from 100 to 700 µm).

Acknowledgments

We gratefully acknowledge the financial support of the Spanish Ministry of Economy and Competitiveness (MAT 2009-13530) and the Australian Research Council. A special thanks is extended to Leslie Bland at the University of Virginia for her assistance with Scanning Electron Microscopy, and Colleen Bettles of Monash University for her advice.

References

[1] B.L. Mordike, T. Ebert, Magnesium-Properties-applications-potential, Materials Science and Engineering a-Structural Materials Properties Microstructure and Processing, 302 (2001) 37-45.
[2] T. Ruden, Lightweight Magnesium Technology 2001–2005, Society of Automotive Engineers, Warrendale, 2006.
[3] A.A. Luo, Magnesium casting technology for structural applications, Journal of Magnesium and Alloys, 1 (2013) 2-22.
[4] I. J. Polmear,Light Alloys, Fourth ed., Butterworth-Heinemann, United kingdom, 2005.
[5] X.B. Chen, H.Y. Yang, T.B. Abbott, M.A. Easton, N. Birbilis, Magnesium: Engineering the Surface, JOM, 64 (2012) 650-656.
[6] G.L. Makar, J. Kruger, Corrosion of magnesium, International Materials Reviews, 38 (1993) 138-153.
[7] M. Pourbaix, Atlas déquilibre electrochimiques, Gauthiers-Villars, Paris, 1963.
[8] J.D. Hanawalt, C.E. Nelson, J.A. Peloubet, Corrosion studies of magnesium and its alloys, Transactions of the American Institute of Mining and Metallurgical Engineers, 147 (1942) 273-298.
[9] S. Feliu, Jr., C. Maffiotte, A. Samaniego, J. Carlos Galvan, V. Barranco, Effect of the chemistry and structure of the native oxide surface film on the corrosion properties of commercial AZ31 and AZ61 alloys, Applied Surface Science, 257 (2011) 8558-8568.
[10] M. Taheri, R.C. Phillips, J.R. Kish, G.A. Botton, Analysis of the surface film formed on Mg by exposure to water using a FIB cross-section and STEM-EDS, Corrosion Science, 59 (2012) 222-228.
[11] S. Feliu, Jr., C. Maffiotte, A. Samaniego, J. Carlos Galvan, V. Barranco, Effect of naturally formed oxide films and other variables in the early stages of Mg-alloy corrosion in NaCl solution, Electrochimica Acta, 56 (2011) 4554-4565.
[12] J.H. Nordlien, K. Nisancioglu, S. Ono, N. Masuko, Morphology and structure of oxide films formed on MgAl alloys by exposure to air and water, Journal of the Electrochemical Society, 143 (1996) 2564-2572.
[13] S. Feliu Jr., J.C. Galván, A. Pardo, M.C. Merino, R. Arrabal, Native Air-Formed Oxide Film and its Effect on Magnesium Alloys Corrosion, The Open Corrosion Journal, 3 (2010) 80-91.
[14] R.C. Phillips, J.R. Kish, Nature of Surface Film on Matrix Phase of Mg Alloy AZ80 Formed in Water, Corrosion, 69 (2013) 813-820.
[15] M. Danaie, R.M. Asmussen, P. Jakupi, D.W. Shoesmith, G.A. Botton, The role of aluminum distribution on the local corrosion resistance of the microstructure in a sand-cast AM50 alloy, Corrosion Science, 77 (2013) 151-163.
[16] F. Zucchi, V. Grassi, A. Frignani, C. Monticelli, G. Trabanelli, Electrochemical behaviour of a magnesium alloy containing rare earth elements, Journal of Applied Electrochemistry, 36 (2006) 195-204.
[17] N. Birbilis, M.A. Easton, A.D. Sudholz, S.M. Zhu, M.A. Gibson, On the corrosion of binary magnesium-rare earth alloys, Corrosion Science, 51 (2009) 683-689.
[18] N. Birbilis, M.K. Cavanaugh, A.D. Sudholz, S.M. Zhu, M.A. Easton, M.A. Gibson, A combined neural network and mechanistic approach for the prediction of corrosion rate and yield strength of magnesium-rare earth alloys, Corrosion Science, 53 (2011) 168-176.
[19] L.L. Rokhlin, Magnesium alloys containing rare earth metals. Structure and Properties, J. N. Fridlyander & D. G. Eskin, London, 2003.
[20] M.A. Timonova, Magnievye Splavy. Sprovochnik (Magnesium alloys. A reference Book), Metallurgiya, Moscow, 1978.
[21] G. Williams, K. Gusieva, N. Birbilis, Localized Corrosion of Binary Mg-Nd Alloys in Chloride-Containing Electrolyte Using a Scanning Vibrating Electrode Technique, Corrosion, 68 (2012) 489-498.
[22] T. Takenaka, T. Ono, Y. Narazaki, Y. Naka, M. Kawakami, Improvement of corrosion resistance of magnesium metal by rare earth elements, Electrochimica Acta, 53 (2007) 117-121.
[23] Y.L. Song, Y.H. Liu, S.H. Wang, S.R. Yu, X.Y. Zhu, Effect of cerium addition on microstructure and corrosion resistance of die cast AZ91 magnesium alloy, Materials and Corrosion-Werkstoffe Und Korrosion, 58 (2007) 189-192.
[24] Y.L. Song, Y.H. Liu, S.R. Yu, X.Y. Zhu, S.H. Wang, Effect of neodymium on microstructure and corrosion resistance of AZ91 magnesium alloy, Journal of Materials Science, 42 (2007) 4435-4440.
[25] F. Rosalbino, E. Angelini, S. De Negri, A. Saccone, S. Delfino, Electrochemical behaviour assessment of novel Mg-rich Mg-Al-RE alloys (RE = Ce, Er), Intermetallics, 14 (2006) 1487-1492.

[26] R. Arrabal, A. Pardo, M.C. Merino, M. Mohedano, P. Casajus, K. Paucar, G. Garces, Effect of Nd on the corrosion behaviour of AM50 and AZ91D magnesium alloys in 3.5 wt.% NaCl solution, Corrosion Science, 55 (2012) 301-312.
[27] N.D. Nam, J.G. Kim, K.S. Shin, H.C. Jung, The effect of rare earth additions on the electrochemical properties of Mg-5Al-based alloys, Scripta Materialia, 63 (2010) 625-628.
[28] J. Speight, Lange´s Handbook of Chemistry 16 ed., McGraw Hill, New York, 2005.
[29] C.L. Yaws, Yaws´Hasndbook of properties of the chemical elements, Knovel, Texas, 2011.
[30] R.E. Krebs, The History and Use of Our Earth's Chemical Elements: A Reference Guide, second ed., Greenwood Press, London, 2006.
[31] A.A. Nayeb-Hashemi, J. B. Clark, Phase diagrams of binary magnesium alloys, ASM Interntional, Ohio, 1988.
[32] F. Czerwinski, The oxidation behaviour of an AZ91D magnesium alloy at high temperatures, Acta Materialia, 50 (2002) 2639-2654.
[33] M. Nonnenmacher, M.P. Oboyle, H.K. Wickramasinghe, Kelvin probe force microscopy, Applied Physics Letters, 58 (1991) 2921-2923.
[34] V. Guillaumin, P. Schmutz, G.S. Frankel, Characterization of corrosion interfaces by the scanning Kelvin probe force microscopy technique, Journal of the Electrochemical Society, 148 (2001) B163-B173.
[35] D. Briggs, M.P. Seah, Practical Surface Analysis (Auger and X-ray Photoelectron Spectroscopy), second ed., Wiley Interscience., New York, 1990.
[36] J.W. Turrentine, Reversed electrolysis, Journal of Physical Chemistry, 12 (1908) 448-467.
[37] G.S. Frankel, A. Samaniego, N. Birbilis, Evolution of hydrogen at dissolving magnesium surfaces, Corrosion Science, 70 (2013) 104-111.
[38] N.T. Kirkland, N. Birbilis, M.P. Staiger, Assessing the corrosion of biodegradable magnesium implants: A critical review of current methodologies and their limitations, Acta Biomaterialia, 8 (2012) 925-936.
[39] H.E. Friedrich, B.L. Mordike, Magnesium Technology, Springer, Germany, 2006.
[40] J.H. Nordlien, K. Nisancioglu, S. Ono, N. Masuko, Morphology and structure of water-formed oxides on ternary MgAl alloys, Journal of the Electrochemical Society, 144 (1997) 461-466.
[41] F. Andreatta, I. Apachitei, A.A. Kodentsov, J. Dzwonczyk, J. Duszczyk, Volta potential of second phase particles in extruded AZ80 magnesium alloy, Electrochimica Acta, 51 (2006) 3551-3557.
[42] S. Feliu, Jr., A. Pardo, M.C. Merino, A.E. Coy, F. Viejo, R. Arrabal, Correlation between the surface chemistry and the atmospheric corrosion of AZ31, AZ80 and AZ91D magnesium alloys, Applied Surface Science, 255 (2009) 4102-4108.
[43] R. Arrabal, E. Matykina, A. Pardo, M.C. Merino, K. Paucar, M. Mohedano, P. Casajus, Corrosion behaviour of AZ91D and AM50 magnesium alloys with Nd and Gd additions in humid environments, Corrosion Science, 55 (2012) 351-362.
[44] J.P. Espinós, A.R. González-Elipe, J.A. Odriozola, XPS study of lutetium oxide samples with different hydration/carbonation degrees as a function of the preparation method, Applied Surface Science, 29 (1987) 40-48.
[45] W.C. Lang, B.D. Padalia, D.J. Fabian, L.M. Watson, X-Ray photoelectron studies of pure and oxided ytterbium and lutetium, Journal of Electron Spectroscopy and Related Phenomena, 5 (1974) 207-215.
[46] N. Birbilis, G. Williams, K. Gusieva, A. Samaniego, M.A. Gibson, H.N. McMurray, Poisoning the corrosion of magnesium, Electrochemistry Communications, 34 (2013) 295-298.
[47] A. Samaniego, I. Llorente, S. Feliu, Jr., Combined effect of composition and surface condition on corrosion behaviour of magnesium alloys AZ31 and AZ61, Corrosion Science, 68 (2013) 66-71.
[48] K.D. Ralston, G. Williams, N. Birbilis, Effect of pH on the Grain Size Dependence of Magnesium Corrosion, Corrosion, 68 (2012) 507-517.
[49] J.O.M. Bockris, A.K.N. Reddy, Modern Electrochemistry 2B: Electrodics in Chemistry, Engineering, Biology and Environmental Science, Springer, New York, 2001.
[50] A.D. Sudholz, K. Gusieva, X.B. Chen, B.C. Muddle, M.A. Gibson, N. Birbilis, Electrochemical behaviour and corrosion of Mg-Y alloys, Corrosion Science, 53 (2011) 2277-2282.
[51] M. Taheri, J.R. Kish, N. Birbilis, M. Danaie, E.A. McNally, J.R. McDermid, Towards a Physical Description for the Origin of Enhanced Catalytic Activity of Corroding Magnesium Surfaces, Electrochimica Acta, 116 (2014) 396-403.
[52] N.T. Kirkland, J. Lespagnol, N. Birbilis, M.P. Staiger, A survey of bio-corrosion rates of magnesium alloys, Corrosion Science, 52 (2010) 287-291.

Discusión Capítulo III

Estrategias para reducir la velocidad de corrosión del magnesio y sus aleaciones.

1. Tratamiento térmico a bajas temperaturas y tiempos cortos.

- **Influencia del tratamiento sobre las aleaciones en estado pulido:** con el fin de potenciar el efecto protector de la fina capa de óxidos superficiales anteriormente descrito, se realizó un tratamiento térmico a 200ºC durante tiempos inferiores a una hora. Para las aleaciones en estado pulido, se observó que estos tratamientos térmicos no produjeron ningún cambio en la uniformidad, homogeneidad y compactación de los óxidos espontáneamente formados tras el pulido. A estas temperaturas, no se observó la aparición de óxidos globulares sin carácter protector. En la aleación AZ61, se detectó un notable enriquecimiento en el contenido de aluminio metálico superficial, dos o tres veces superior a la concentración de aluminio en la aleación base. Este enriquecimiento en aluminio, se asoció al significativo incremento de la resistencia a la transferencia de carga observada experimentalmente incluso para los tiempos más cortos de tratamiento térmico. Este efecto fue mucho menos notable en la aleación AZ31.

- **Influencia del tratamiento sobre las aleaciones en estado de recepción:** para las aleaciones en estado de recepción se detectaron notables diferencias en las capas de óxidos superficiales tras el tratamiento térmico. Las aleaciones estaban cubiertas de precipitados que, mediante la combinación de XPS y SEM, se identificaron como una mezcla de Al_2O_3 y ZnO. La cantidad de estos precipitados se determinó muy superior en el caso de la aleación AZ31, donde se observó un enriquecimiento superficial de aluminio en forma de óxido, no detectado en la aleación AZ61. Esta diferencia en la proporción de Al_2O_3 y ZnO fue asociada al efecto de la fase β en los límites de grano, presente en la aleación AZ61, que dificulta la difusión de aluminio hacia la superficie, evitando el enriquecimiento superficial de aluminio observado en la aleación AZ31. Respecto a la influencia de los tratamientos térmicos sobre la corrosión, no se observaron cambios significativos en la aleación AZ61 mientras que estos tratamientos aumentaron la velocidad de corrosión de la aleación AZ31.

2. Modificación de los óxidos superficiales de la aleación AZ31 mediante micro-adiciones de lutecio (Lu).

Con el fin de modificar los óxidos superficiales de la aleación AZ31 y crear una película superficial con un mayor poder protector, se realizó un profundo análisis sobre posibles elementos capaces de reemplazar al magnesio en los óxidos superficiales de esta aleación. De este análisis se concluyó que el lutecio (Lu) es un buen candidato, ya que su reactividad frente al oxígeno es mayor que la del magnesio y su óxido es estable en un intervalo mayor de pH. Pese a sus buenas propiedades, el Lu es un elemento pesado y caro, por lo que únicamente se adicionó un 0,27 % en peso en la aleación.

- **Caracterización de la microestructura:** se realizó un análisis de la microestructura de la aleación obtenida por fundición y se observó la presencia de Lu combinado con Al y Mn en partículas homogéneamente distribuidas de unos 2 µm de diámetro. Sin embargo, no se detectó su presencia en la matriz de magnesio. El potencial de volta de las partículas Al-Mn-Lu fue medido mediante una sonda Kelvin acoplada a un microscopio de fuerza atómica (SKPFM), observando que la presencia de Lu no alteró de forma significativa el carácter catódico de las partículas frente a la matriz de magnesio cuyo valor fue ~260 mV, muy similar al obtenido para las partículas Mn-Al presentes en la aleación base AZ31. La presencia de Lu en la aleación, aumentó de manera significativa al tamaño de grano de la misma.

- **Caracterización de las capas superficiales:** mediante XPS, se realizó un análisis composicional de los óxidos superficiales formados sobre la aleación AZ31 con un 0.27 % en peso, donde no se detectaron cantidades significativas de Lu en estos óxidos. Con el fin de provocar un enriquecimiento superficial de este elemento, se realizaron varios tratamientos térmicos a 400ºC durante tiempos de exposición de hasta 300 minutos. Sin embargo no se consiguió el objetivo deseado y no se observó un incremento significativo del contenido de lutecio superficial.

- **Influencia de Lu sobre la corrosión:** la influencia de Lu sobre la corrosión de la aleación fue estudiada y analizada mediante técnicas electroquímicas (curvas de polarización) y mediante técnicas de desprendimiento de hidrógeno (DH) y pérdida de peso (PP). Los resultados de estas tres técnicas revelaron un efecto positivo del lutecio en la velocidad de corrosión de la aleación. En este sentido se observó que la aleación AZ31 con un 0,27 % en peso de Lu, presentó una reducción de la velocidad de corrosión de hasta un 80% respecto a la velocidad de corrosión de la aleación base

AZ31. El mecanismo por el cual la presencia de lutecio disminuye la velocidad de corrosión de la aleación no pudo ser clarificado en este estudio. Sin embargo, parece razonable pensar que la presencia de este elemento en la aleación produce una estabilización adicional de la capa de óxidos superficial que aumenta la resistencia a la corrosión de la aleación.

- **Influencia de los tratamiento térmicos sobre la corrosión:** los tratamientos térmicos realizados sobre la aleación AZ31-Lu tuvieron un impacto negativo en la velocidad de corrosión ya que las aleaciones tratadas térmicamente presentaron una velocidad de corrosión mayor que la aleación AZ31-Lu sin tratar. Pese a todo, ninguna de las aleaciones tratadas térmicamente presentó una velocidad de corrosión mayor que la aleación base AZ31. Aunque el efecto global de los tratamientos térmicos estudiados mediante los ensayos de larga duración (PP y DH) fue negativo, durante los ensayos electroquímicos, se detectó un efecto positivo de Lu sobre los óxidos superficiales, que desapareció al aumentar el tiempo de exposición debido a la acción de los cloruros en el medio.

3. Tratamiento de conversión superficial en AZ31 y AZ61: Carbonatación

Con el fin de producir una capa protectora sobre las aleaciones, se realizó un tratamiento de conversión superficial sobre las aleaciones AZ31 y AZ61 en estado de recepción, utilizando un baño de bicarbonato sódico saturado. Los tiempos de inmersión de los distintos tratamientos variaron entre 10 y 360 minutos. Estos tratamientos no tuvieron un efecto positivo sobre la aleación AZ31, sin embargo, para tiempos de carbonatación de 10 y 60 minutos sobre la aleación AZ61, el tratamiento presentó mejoras significativas en la resistencia a la corrosión debido a la formación de una capa superficial interna con menos defectos y micro-grietas que los observados sobre la aleación AZ31.

- **Caracterización de las películas de conversión:** gracias al microscopio electrónico de barrido (SEM), se observó la presencia de dos capas superficiales derivadas del tratamiento de conversión superficial. Mediante XPS se analizó la evolución de la concentración de aluminio, carbonatos y sodio con el tiempo de carbonatación. Tras el tratamiento de conversión, se observó un fuerte incremento en la concentración de aluminio respecto al contenido de este metal en la aleación de partida. Cabe destacar, que este enriquecimiento superficial en aluminio, sufrió una fuerte disminución,

acompañado por un aumento en el contenido de carbonatos para tiempos de tratamiento de 30 minutos. Esta diferente composición para este tiempo de conversión, fue relacionada con los cambios de pH sufridos durante el proceso de conversión superficial.

- **Influencia sobre la corrosión:** la protección aportada por las capas superficiales formadas durante estos tratamientos, fueron analizadas mediante espectroscopia de impedancia electroquímica y medidas de desprendimiento de hidrógeno. Se observó un efecto positivo de este tratamiento sobre la aleación AZ61 para tiempos de inmersión de 10 y 60 minutos, asociados al incremento de los contenidos de hidróxido de aluminios sobre la superficie junto con la ausencia de micro-grietas observada en la capa más interna de las películas formadas.

4. Adición de As sobre Magnesio puro.

Estudios anteriores mostraron una importante influencia de aniones arseniato (AsO_4^{3-}) sobre la reacción catódica del magnesio, por lo que se elaboró una aleación de magnesio con un pequeño porcentaje de arsénico (0,37 % en peso). Mediante el microscopio electrónico de barrido se observó la presencia de la fase secundaria Mg_3As_2, rica en arsénico. El efecto del arsénico sobre la corrosión fue analizado por técnicas electroquímicas y ensayos de larga duración (pérdida de peso y desprendimiento de hidrógeno).

Se observó una fuerte influencia del arsénico en la morfología de la corrosión, al disminuir la tendencia a la formación de corrosión filiforme.

Mediante las curvas de polarización pudo observarse una fuerte disminución de la reacción catódica debido a la presencia de arsénico en la aleación, siendo el As el único elemento, encontrado hasta la fecha, capaz de disminuir esta reacción al formar una aleación binaria con magnesio.

Las medidas de larga duración confirmaron el efecto positivo del arsénico sobre la corrosión del magnesio que fue disminuida en más de un 400%. Esta disminución en la velocidad de corrosión se asoció al efecto del arsénico en la recombinación del hidrógeno molecular sobre la superficie de la aleación.

Conclusiones

Conclusiones

A partir de los estudios realizados durante esta tesis, se ha concluido lo siguiente:

1. Se pudo esclarecer que no existen evidencias sobre la presencia de Mg^{+} durante el proceso de corrosión, por lo que es muy improbable que esta especie sea la responsable del efecto diferencial negativo (NDE). Se propuso un mecanismo alternativo para explicar este efecto, en el que sugiere la variación de la corriente de intercambio para la reacción de hidrógeno al polarizar el magnesio.

2. Se observó un efecto importante del aluminio sobre los óxidos superficiales espontáneamente formados sobre las aleaciones del sistema Mg-Al-Zn. Para la aleación con mayor contenido de aluminio (AZ61), el pulido mecánico indujo la formación de una capa de óxido de mayor espesor, libre de defectos, con un carácter protector muy superior al observado sobre la aleación AZ31. Este efecto protector desapareció tras ~ 4 días de exposición en NaCl 0.6 M.

3. Se observó un enriquecimiento de carbonatos de magnesio en los productos de corrosión formados sobre la aleación AZ31 respecto a los formados sobre la aleación AZ61 en una solución de cloruro sódico 0.6 M. Se concluyó que este enriquecimiento en carbonatos incrementa el carácter protector de los productos de corrosión, lo que disminuye la velocidad de corrosión de la aleación con el tiempo de exposición.

4. Tratamiento térmicos a bajas temperaturas (200ºC) durante tiempos cortos (hasta 60 minutos), ejercieron una influencia positiva sobre la aleación AZ61 en condiciones de pulido, provocando un enriquecimiento superficial de aluminio que aumentó significativamente la resistencia a la transferencia de carga de esta aleación. El efecto sobre la aleación AZ31 fue menos importante. En las aleaciones en estado de recepción, estos tratamientos provocaron la formación de una mezcla de Al_2O_3 y ZnO, cuya cantidad se determinó muy superior en el caso de la aleación AZ31. Su influencia en la corrosión tuvo un impacto negativo sobre la aleación AZ31 mientras que no se observaron cambios importantes sobre la aleación AZ61.

5. Micro-adiciones de un 0.27% en peso de lutecio (Lu) no provocaron la formación de una capa superficial de óxido de lutecio sobre la aleación AZ31, sin embargo, la presencia de este elemento en la aleación tuvo un impacto positivo, disminuyendo la velocidad de corrosión hasta un 80% en soluciones de NaCl al 0.1 M. Tratamiento térmicos a 400ºC de hasta 300 minutos de duración tuvieron un impacto negativo sobre la resistencia a la corrosión de esta aleación.

6. Al formar una aleación de magnesio con una pequeña cantidad de arsénico (As), se observó un fuerte efecto sobre la reacción de reducción de hidrógeno. Un 0.37% en peso de As originó un fuerte impedimento en esta reacción, lo que originó una reducción mayor de un 400% en la velocidad de corrosión de la aleación y un cambio en la morfología del ataque en soluciones de NaCl 0.1M..

Bibliografía

[1] B.L. Mordike, T. Ebert, Materials Science and Engineering a-Structural Materials Properties Microstructure and Processing, 302 (2001) 37-45.
[2] I. Polmear, Light Alloys, Fourth ed., Butterworth-Heinemann, United kingdom, 2005.
[3] A.A. Luo, Journal of Magnesium and Alloys, 1 (2013) 2-22.
[4] G. Williams, N. Birbilis, H.N. McMurray, Electrochemistry Communications, 36 (2013) 1-5.
[5] F.J.G. Mur, Aleaciones ligeras, UPC, barcelona, 2001.
[6] H.E. Friedrich, B.L. Mordike, Magnesium Technology, Springer, Germany, 2006.
[7] H. Friedrich, S. Schumann, Conference Paper at Second Israeli International Conference on Mg Science and Technology 2000.
[8] E.L. Bray, Magnesium metall survey 2014, February 2014.
[9] D.A. Kramer, Magnesium metall survey U.S. Geological Survey, Mineral Commodity Summaries, 2001.
[10] D.A. Kramer, in: M.C. Summaries (Ed.) Magnesium metall survey. U.S. Geological Survey, 2009.
[11] D.A. Kramer, Magnesium metall survey, U.S. Geological Survey, 2010.
[12] D.M. Behrens, Magnesium metall survey, U.S. Geological Survey, 2007.
[13] Z. Yang, J.P. Li, J.X. Zhang, G.W. Lorimer, J. Robson, Acta Metallurgica Sinica (English Letters), 21 (2008) 313-328.
[14] E.W. Kelley, W.F. Hosford, Transactions of the Metallurgical Society of Aime, 242 (1968) 5-&.
[15] W.F. Smith, Ciencia e Ingeniería de Materiales, 3ª ed., McGraw Hill, Madrid, 2004.
[16] D.A. Kramer, U.S. Geological Year Book 2011.
[17] R.E. Brown, Presentation at Materials Science & Technology Conference
Pittsburgh, USA.
[18] H. Friedrich, S. Schumann, Journal of Materials Processing Technology, 117 (2001) 276-281.
[19] O. Pashkova, I. Ostrovsky, Y. Henn, Presentation at New Challenges in Aeronautics, Moscow. 2007.
[20] G.D. Wardlow, 64th Annual World Magnesium Conference, Vancouver, Canada 2007.
[21] Magnesium's Tough Strength. Endures Abuse to Protect Portable Electronic Devices, International Magnesium Association, Wauconda, IL, USA, 2008.
[22] International Magnesium Association, Lighter Magnesium Improves
Power Tool Performance I.M. Association Ed, Wauconda, IL, USA, 2008.
[23] X.B. Chen, H.Y. Yang, T.B. Abbott, M.A. Easton, N. Birbilis, Jom, 64 (2012) 650-656.
[24] N. Birbilis, G. Williams, K. Gusieva, A. Samaniego, M.A. Gibson, H.N. McMurray, Electrochemistry Communications, 34 (2013) 295-298.
[25] G.L. Makar, J. Kruger, International Materials Reviews, 38 (1993) 138-153.
[26] J.A. Juárez-Islas, J. Genesca, R. Pérez, JOM, 45 (1993) 42-44.
[27] S. Feliu, Jr., M.C. Merino, R. Arrabal, A.E. Coy, E. Matykina, Surface and Interface Analysis, 41 (2009) 143-150.
[28] S. Feliu, Jr., A. Pardo, M.C. Merino, A.E. Coy, F. Viejo, R. Arrabal, Applied Surface Science, 255 (2009) 4102-4108.
[29] K. Asami, S. Ono, Journal of the Electrochemical Society, 147 (2000) 1408-1413.
[30] M. Santamaria, F. Di Quarto, S. Zanna, P. Marcus, Electrochimica Acta, 53 (2007) 1314-1324.
[31] K. Huber, Journal of the Electrochemical Society, 100 (1953) 376-382.
[32] O. Fruhwirth, G.W. Herzog, I. Hollerer, A. Rachetti, Surface Technology, 24 (1985) 301-317.
[33] M. Pourbaix, Atlas déquilibre electrochimiques, Gauthiers-Villars, Paris., 1963.
[34] G.L. Makar, J. Kruger, Journal of the Electrochemical Society, 137 (1990) 414-421.
[35] J.D. Hanawalt, C.E. Nelson, J.A. Peloubet, Transactions of the American Institute of Mining and Metallurgical Engineers, 147 (1942) 273-298.
[36] Y. Mikhailovskii, A. Skurikhin, M. Czerny, R. Wellesz, M. Zaydel, Protection of Metals, 15 (1979) 419-426.
[37] N. LeBozec, M. Jonsson, D. Thierry, Corrosion, 60 (2004) 356-361.
[38] M. Jonsson, D. Persson, D. Thierry, Corrosion Science, 49 (2007) 1540-1558.
[39] M. Jonsson, D. Persson, C. Leygraf, Corrosion Science, 50 (2008) 1406-1413.

[40] M. Jonsson, D. Persson, R. Gubner, Journal of the Electrochemical Society, 154 (2007) C684-C691.
[41] G. Song, A. Atrens, D. Stjohn, J. Nairn, Y. Li, Corrosion Science, 39 (1997) 855-875.
[42] D.A. Jones, Principles and Prevention of Corrosion, Prentice Hall, 1996.
[43] J.A.G. Fernández, control de la corrosión. Estudio y medida por técnicas electroquímicas, CSIC, Madrid, 1989.
[44] J.E. Hillis, R.W. Murray, in Metals Handbook, 9th ed. 13 (1987) 740-754.
[45] E. Ghali, W. Dietzel, K.U. Kainer, Journal of Materials Engineering and Performance, 13 (2004) 7-23.
[46] K.D. Ralston, G. Williams, N. Birbilis, Corrosion, 68 (2012) 507-517.
[47] G.L. Dunlop, W.P. Sequeira, M.S. Dargusch, G. Song, A. Atrens, T. Kittel, D. St. John, A.K. Dahle, a.M. Murray, Annual World Magnesium, A Global Vision for Magnesium, 55th meeting of the International Magnesium Association, ed., International Magnesium Association, Coronado, CA, , 1998, pp. 68-73.
[48] G.L. Song, A. Atrens, M. Dargusch, Corrosion Science, 41 (1999) 249-273.
[49] A. Pardo, M.C. Merino, A.E. Coy, F. Viejo, R. Arrabal, S. Feliu, Jr., Electrochimica Acta, 53 (2008) 7890-7902.
[50] M.-C. Zhao, P. Schmutz, S. Brunner, M. Liu, G.-l. Song, A. Atrens, Corrosion Science, 51 (2009) 1277-1292.
[51] O. Lunder, J.E. Lein, T.K. Aune, K. Nisancioglu, Corrosion, 45 (1989) 741-748.
[52] G.L. Song, A. Atrens, Advanced Engineering Materials, 5 (2003) 837-858.
[53] N.T. Kirkland, J. Lespagnol, N. Birbilis, M.P. Staiger, Corrosion Science, 52 (2010) 287-291.
[54] A.D. Sudholz, N. Birbilis, C.J. Bettles, M.A. Gibson, Journal of Alloys and Compounds, 471 (2009) 109-115.
[55] J.O.M. Bockris, A.K.N. Reddy, Modern Electrochemistry 2B: Electrodics in Chemistry, Engineering, Biology and Environmental Science, Springer, New York, 2001.
[56] N.D. Tomashov, Theory and Protection of Metals: The Science of Corrosion, The Macmillan Company, New York, 1966.
[57] A. Froats, T.K. Aune, W. Unsworth, J. Hillis., Metals Handbook 13th ed., Ohio.1987
[58] R. Arrabal, A. Pardo, M.C. Merino, S. Merino, M. Mohedano, P. Casajus, Materials and Corrosion-Werkstoffe Und Korrosion, 62 (2011) 326-334.
[59] N. Cabrera, N.F. Mott, Reports on Progress in Physics, 12 (1948) 163-184.
[60] R. Lindstrom, J.E. Svensson, L.G. Johansson, Journal of the Electrochemical Society, 149 (2002) B103-B107.
[61] R. Lindstrom, L.G. Johansson, G.E. Thompson, P. Skeldon, J.E. Svensson, Corrosion Science, 46 (2004) 1141-1158.
[62] R. Lindstrom, L.G. Johansson, J.E. Svensson, Materials and Corrosion-Werkstoffe Und Korrosion, 54 (2003) 587-594.
[63] A. Samaniego, I. Llorente, S. Feliu, Jr., Corrosion Science, 68 (2013) 66-71.
[64] G. Song, A. Atrens, Advanced Engineering Materials, 9 (2007) 177-183.
[65] G.S. Frankel, Journal of the Electrochemical Society, 145 (1998) 2970-2970.
[66] G.S. Frankel, Journal of the Electrochemical Society, 145 (1998) 2186-2198.
[67] J.F. Li, B. Maier, G.S. Frankel, Corrosion Science, 53 (2011) 2142-2151.
[68] G. Williams, K. Gusieva, N. Birbilis, Corrosion, 68 (2012) 489-498.
[69] A.A. Nayeb-Hashemi, J. B. Clark, Phase diagrams of binary magnesium alloys, ASM Interntional, Ohio, 1988.
[70] J.H. Nordlien, K. Nisancioglu, S. Ono, N. Masuko, Journal of the Electrochemical Society, 143 (1996) 2564-2572.
[71] G.L. Song, A. Atrens, Advanced Engineering Materials, 1 (1999) 11-33.
[72] A.M. Lafront, W. Zhang, S. Jin, R. Tremblay, D. Dubé, E. Ghali, Electrochimica Acta, 51 (2005) 489-501.
[73] S. Mathieu, C. Rapin, J. Steinmetz, P. Steinmetz, Corrosion Science, 45 (2003) 2741-2755.
[74] O. Lunder, J.E. Lein, T.K. Aune, K. Nisancioglu, Corrosion, 45 (1989) 741-748.
[75] G. Song, International Conference on Magnesium. 488 (2005) 649-652.
[76] T. Beldjoudi, C. Fiaud, L. Robbiola, Corrosion, 49 (1993) 738-745.
[77] S. Feliu, Jr., C. Maffiotte, A. Samaniego, J. Carlos Galvan, V. Barranco, Electrochimica Acta, 56 (2011) 4554-4565.
[78] S. Feliu, Jr., C. Maffiotte, A. Samaniego, J. Carlos Galvan, V. Barranco, Applied Surface Science, 257 (2011) 8558-8568.

[79] D. Eliezer, P. Uzan, E. Aghion, Effect of second phases on the corrosion behavior of magnesium alloys, in: Y. Kojima, T. Aizawa, K. Higashi, S. Kamado (Eds.) Magnesium Alloys 2003, Pts 1 and 2, 2003, pp. 857-865.
[80] R. Ambat, N.N. Aung, W. Zhou, Corrosion Science, 42 (2000) 1433-1455.
[81] R.N. Reichek, K.J. Clark, J.E. Hillis, Controlling the salt water corrosion performance of magnesium AZ91 alloy (1985).
[82] M. Liu, G.-L. Song, Corrosion Science, 77 (2013) 143-150.
[83] D. Briggs, M.P. Seah, Practical Surface Analysis (Auger and X-ray Photoelectron Spectroscopy), second ed.,Wiley Interscience, New York, 1990.
[84] C.D. Wagner, W.M. Riggs, L.E. Davies, J.F. Moulder, G.E. Muilenberg, Handbook of X-ray Photoelectron Spectroscopy, Perkin-Elmer Corporation, Minnesota, 1979.
[85] J.A.G. Fernández, Control de la Corrosión. Estudio y medida por técnicas electroquímicas., CENIM-CSIC, Madrid, 1989.
[86] W. Beetz, Philosophical Magazine, (1866) 216 -269.
[87] J.W. Turrentine, Journal of Physical Chemistry, 12 (1908) 448-467.
[88] R.L. Petty, A.W. Davidson, J. Kleinberg, Journal of the American Chemical Society, 76 (1954) 363-366.
[89] M.E. Straumanis, B.K. Bhatia, Journal of the Electrochemical Society, 110 (1963) 357-360.
[90] P.F. King, Journal of the Electrochemical Society, 113 (1966) 536-&.
[91] P.F. King, Journal of the Electrochemical Society, 110 (1963) 1113-1116.
[92] J.L. Robinson, P.F. King, Journal of the electrochemical society, 108 (1961) 36.
[93] G.G. Perrault, Journal of Electroanalytical Chemistry and Interfacial Electrochemistry, 27 (1970) 47-58.
[94] G.G. Perrault, Journal of Electroanalytical Chemistry, 51 (1974) 107-119.
[95] G.R. Hoey, M. Cohen, Journal of the Electrochemical Society, 105 (1958) 245-250.
[96] M.N. Hull, Journal of Electroanalytical Chemistry and Interfacial Electrochemistry, 38 (1972) A1-A4.
[97] G. Song, A. Atrens, D. St John, X. Wu, J. Nairn, Corrosion Science, 39 (1997) 1981-2004.
[98] G. Lee, J. Park, Geochimica Et Cosmochimica Acta, 102 (2013) 162-174.
[99] S. Bender, J. Goellner, A. Heyn, S. Schmigalla, Materials and Corrosion-Werkstoffe Und Korrosion, 63 (2012) 707-712.
[100] M. Taheri, R.C. Phillips, J.R. Kish, G.A. Botton, Corrosion Science, 59 (2012) 222-228.
[101] M. Taheri, J.R. Kish, N. Birbilis, M. Danaie, E.A. McNally, J.R. McDermid, Electrochimica Acta, 116 (2014) 396-403.
[102] N. Birbilis, A.D. King, S. Thomas, G.S. Frankel, J.R. Scully, Electrochimica Acta. In press (2014).
[103] R.M. Souto, A. Kiss, J. Izquierdo, L. Nagy, I. Bitter, G. Nagy, Electrochemistry Communications, 26 (2013) 25-28.
[104] G. Williams, H.N. McMurray, Journal of the Electrochemical Society, 155 (2008) C340-C349.
[105] J. Swiatowska, P. Volovitch, K. Ogle, Corrosion Science, 52 (2010) 2372-2378.
[106] R. L. Petty. Thesis submitted in partial fulfillment of the requirements for the degree of Doctor of Philosophy, University of Kansas, (1953).
[107] J.E. Gray, B. Luan, Journal of Alloys and Compounds, 336 (2002) 88-113.
[108] H.J. Zhang, D.F. Zhang, C.H. Ma, S.F. Guo, Materials Letters, 92 (2013) 45-48.
[109] X.B. Chen, D.R. Nisbet, R.W. Li, P.N. Smith, T.B. Abbott, M.A. Easton, D.H. Zhang, N. Birbilis, Acta Biomaterialia, 10 (2014) 1463-1474.
[110] H. Yang, X. Guo, G. Wu, W. Ding, N. Birbilis, Corrosion Science, 53 (2011) 381-387.
[111] E. Georgiza, J. Novakovic, P. Vassiliou, Surface and Coatings Technology, 232 (2013) 432-439.